DECIPHERING AND OPTIMIZING THE PROCESS OF REMOVAL AND RECOVERY OF Pb(II) AND CD(II) FROM WASTEWATER BY BIOSORBENT DERIVED FROM FRUIT WASTE

WANG QIAN

PhD

The Hong Kong Polytechnic University

2019

The Hong Kong Polytechnic University

Department of Applied Biology and Chemical Technology

Deciphering and Optimizing the Process of Removal and Recovery of Pb(II) and Cd(II) from Wastewater by Biosorbent Derived from Fruit Waste

WANG Qian

A thesis submitted in partial fulfillment of the requirements for the degree of

DOCTOR OF PHILOSOPHY

February, 2019

Certificate of Originality

I hereby declare that this thesis is my own work and that, to the best of my knowledge and belief, it reproduces no material previously published or written, nor material that has been accepted for the award of any other degree or diploma, except where due acknowledgement has been made in the text.

WANG Qian

Abstract

Lead (Pb) and cadmium (Cd) are the two most hazardous heavy metals in consideration of their prevalence in industries and high toxicity to living organisms. Biosorption by using abundant fruit waste is an environmentally benign and cost-effective approach for heavy metal removal from wastewater. In this study, the rind of *Citrullus lanatus* (watermelon rind, shorten as WR) and the seed of *Mangifera indica* (mango seed, shorten as MS) were employed for Pb(II) and Cd(II) biosorption in aqueous solutions. For comprehensive mechanistic elucidation, which is crucial for process control and commercial (bio)sorbent development, a hybrid methodology of surface and structure analysis, spectroscopic techniques, chemical methods and quantum chemistry simulation (QCS) was established in combination with macroscopic biosorption studies.

In batch studies, the maximum biosorption capacities of 231.57 ± 1.09 mg-Pb/g-WR at pH 5.0 and 98.51 ± 1.15 mg-Cd/g-WR at pH 7.0 were achieved by WR. The Redlich-Peterson (R-P) and Dubinin-Radushkevich (D-R) isotherms provided the best description to the equilibrium data of Pb(II) and Cd(II), respectively, suggesting the heterogeneous surface of WR. Besides, Pb(II) and Cd(II) were rapidly sequestered by WR, with the kinetic processes well described by the pseudo-first-order and pseudo-second-order equations, respectively. For MS, the maximum biosorption capacities were determined to be 263.63 ± 0.06 mg-Pb/g-MS at pH 5.0 and 93.53 ± 1.43 mg-Cd/g-MS at pH 7.5. The R-P isotherm provided the best description to Pb(II) and Cd(II) biosorption by MS, implying multilayer

loadings of Pb(II) and Cd(II) on the heterogeneous surface of MS. Rapid biosorption of Pb(II) and Cd(II) was observed in the kinetic studies with the pseudo-first-order and pseudo-second-order equations as the best fitting models, respectively. The sequestered Pb(II) and Cd(II) were easily eluted from MS by dilute acids including HNO_3 and citric acid with a good biosorption capacity remained in the regenerated MS. Unlike WR, the biosorption capacity of MS dramatically decreased as its particle size increased. In the continuous mode, the WR-packed bed column reactor maintained superior performance of Pb(II) biosorption over 10 cycles with a breakthrough time ranging from 8.3 h to13.0 h, and 95% of the sequestered Pb(II) was desorbed in 1.3-2.3 h by 0.05 M HCl. To the best of my knowledge, advanced solid-state nuclear magnetic resonance (NMR) spectroscopy was employed for the first time to investigate the interactions between heavy metals and biosorbents in this study. Coupling with conventional spectroscopic techniques such as Fourier-transform infrared (FTIR) spectroscopy and X-ray photoelectron spectroscopy (XPS), carboxyl, hydroxyl, amine and ether groups from cellulose, pectin and hemicellulose in WR, and cellulose, hemicellulose and tannins in MS, were distinguished as the binding sites for Pb(II) and Cd(II) sequestration. Together with analytical methods such as zeta potential measurement, scanning electron microscopy equipped with energy dispersive X-ray spectroscopy (SEM-EDX), powder X-ray diffraction (PXRD) and ion exchange experiments, the underlying mechanisms were identified as complexation, electrostatic attraction, ion exchange (with Ca^{2+} and Mg^{2+}) and microprecipitation. The QCS at a molecular level verified the feasibility of heavy metal complexation with the identified binding sites and indicated the preference of heavy metal binding

to carboxyl groups. The mechanistic studies reveal that pectin, hemicellulose and amorphous cellulose are promising matrices for developing commercial (bio)sorbents for heavy metal sequestration.

Compared with other fruit-waste-derived biosorbents in the literature, WR and MS in this study exhibited much higher Pb(II) biosorption capacities and comparable Cd(II) biosorption capacities. In particular, the high selectivity of WR towards Pb(II), the stability of the biosorption process, and the excellent column performance reveal the great practicability of WR in scale-up treatment of Pb(II)-bearing wastewater. Moreover, the hybrid mechanistic methodology established in this study can comprehensively decipher biosorption processes at both macroscopic and microscopic scales. It also provides important insights into other environmental studies, as most environmental processes are related to interactions between adsorbates and biological surfaces with varying degrees.

Acknowledgements

This thesis presents the research work of my PhD study in the past four years at the Department of Applied Biology and Chemical Technology, The Hong Kong Polytechnic University. The work could not have been finished without the valuable assistance of several people and research funding provided by the Research Grants Council (RGC) of Hong Kong SAR (China).

I would like to express my great gratitude to my chief supervisor, Dr. LO Wai-hung, Thomas, for his patient guidance and constructive advice throughout the entire period of my PhD study.

I am very grateful for Dr. LAM Yan Yan, who carefully instructed me in the biosorption studies. Academic discussion with her gave me a lot inspiration in the experimental design and result analysis. I also appreciate the continuous help from my research colleagues Mr. HO Kwok Pan, Mr. CHAN Kwan Shing, Mr. KIM Chi-fai and Mr. CHUNG Sai Fung. I want to thank Ms. CHENG Siu Yim and Ms. WONG Ka Ki, who performed their final year projects in our lab, for their contribution to parts of experiments in Pb(II) and Cd(II) biosorption by mango seed. Mr. HO Chi-man, Jimmy, is acknowledged for his assistance with recording elemental information of serval biosorbent samples and the use of the ICP-OES instrument.

The research studies relevant to solid-state NMR spectroscopy, PXRD and SEM-EDX were performed in a collaboration program with Prof. Ulla Gro Nielsen's research group at the Department of Physics, Chemistry, and Pharmacy, University of Southern Denmark. I would like to thank Prof. Nielsen and Mr.

Anders Bruhn Arndal Andersen, who helped me record the solid-state NMR spectra of my samples and patiently instructed me to access the solid-state NMR instruments. Besides, the PXRD and SEM-EDX information of my samples was collected with the kind help from Dr. KIM Tae-Hyun; he also assisted with the analysis of the SEM-EDX results of mango seed. The quantum chemistry simulation via Gaussian modelling was performed with the assistance of Dr. WANG Jian, who is an expert in structural chemistry. The discussion with her gave me a better understanding on the heavy metal interaction with functional groups in a molecular level.

I want to give my sincere thanks to Dr. LEE Po-Heng, Henry. As my previous supervisor and also collaborator in some parts of my PhD study, he continuously provided me with constructive advice on both academic and non-academic aspects. Dr. HUANG Xiao Wu and Dr. TAN Giin-Yu, Amy also shared a lot of their research experience with me and gave me extensive encouragement during my PhD study. Their passion and persistency on research inspire me a lot. Besides, I would like to thank Ms. LEUNG Hong-man, Josephine, who carefully proofread this thesis and gave corrections on the writing of some parts.

Finally, I want to thank my dear family and friends, especially my best friend, WANG Yun Long, for their continuous support and encouragement to me to pursue my dreams. I am always on my way with their solid support.

Table of Contents

List of Abbreviations

1/n: Heterogeneity factor in the Sips isotherm (0-1)

AC: Activated carbon

ANOVA: Analysis of variance

a_R: R-P isotherm constant (L/mmol)

A_T: Temkin isotherm equilibrium binding constant (L/g)

b: Sips equilibrium constant (L/mg)

BET: Brunauer-Emmett-Teller

b_R: R-P isotherm constant ($0<b_R \leqq 1$)

B_T: Temkin isotherm constant related to heat of adsorption (J/mol)

BV: Bed volume

C: Intercept related to thickness of boundary layer in intraparticle diffusion equation

C_0: Adsorbate concentration in column influent (mg/L)

$C_{ad,e}$: Concentration of adsorbate on adsorbent in equilibrium (mg/L)

CCD: Central composite design

C_e: Concentration of adsorbate remaining in solution in equilibrium (mg/L)

Cel: Cellulose

Cit: Citrulline

CP: Cross polarization

CPCM: Conductor-like polarizable continuum model

CSA: Chemical shift anisotropy

C_t: Adsorbate concentration in column effluent (mg/L)

DAF: Dissolved air flotation

DD: Dipolar dephasing

DDI: Distilled deionized water

DE: Desorption efficiency

D-R: Dubinin-Radushkevich

E. coli: Escherichia coli

EDTA: Ethylenediaminetetraacetic acid

EDX: Energy dispersive X-ray spectroscopy

EPS: Extracellular polymeric substance

EXAFS: Extended X-ray absorption fine structure

FTIR: Fourier-transform infrared spectroscopy

HRT: Hydraulic retention time

HSAB: Hard and soft acids and bases

IARC: International Agency for Research on Cancer

ICP-MS: Inductively coupled plasma mass spectrometer

ICP-OES: Inductively coupled plasma optical emission spectrometer

k: Fractional power kinetics constant

k: Thomas rate constant (mL/min·mg)

k_0: Temperature independent factor (g/mg·min)

k_1: Lagergren equilibrium rate constant (min^{-1})

k_2: Equilibrium rate constant of the pseudo-second-order equation (g/mg·min)

k_{BA}: Bohart-Adams rate constant (L/h/mg)

K_D: Equilibrium constant

K_F: Freundlich isotherm constant related to adsorption capacity (L/g)

k_{int}: Intraparticle diffusion rate constant

K_L: Langmuir isotherm constant related to affinity of binding sites (L/mg)

K_R: R-P isotherm constant (L/g)

k_{YN}: Yoon and Nelson's proportionality constant (min^{-1})

M: Mass of adsorbent in column (g)

M^{2+}: Divalent heavy metal ions

MAS: Magic angle spinning

MF: Microfiltration

MS: Mango seed

N_0: Equilibrium volumetric sorption capacity in the Bohart-Adams model (mg/L),

NA: Not applicable

N_F: Freundlich isotherm constant related to adsorption intensity

NF: Nanofiltration

NMR: Nuclear magnetic resonance

Pec: Pectin

pK_a: Acid dissociation constant

ppb: Unit of concentration, μg/L

ppm: Unit of concentration, mg/L

PXRD: Powder X-ray diffraction

Q: Volumetric flow rate in column (mL/min)

q_0: Maximum loading capacity of adsorbate on adsorbent in column (mg/g)

QCS: Quantum chemistry simulation

Q_e: Amount of adsorbate bound to adsorbent in equilibrium, namely equilibrium biosorption capacity (mg/g)

Q_{exp}: Experimental biosorption capacity (mg/g)

Q_m: Maximum biosorption capacity (mg/g)

Q_{pre}: Predicted biosorption capacity by modeling (mg/g)

Q_t: Amount of adsorbate adsorbed at time t (mg/g)

R: Universal gas constant, 8.314 J/mol·K

R^2: Coefficient of determination

RMSD: Root-mean-square deviation

RO: Reverse osmosis

R-P: Redlich-Peterson

RSM: Response surface methodology

S/L: Solid/liquid ratio

SDS: Sodium dodecyl sulfate

SEM: Scanning electron microscopy

SPIDER: Saturation-pulse induced dipolar exchange with recoupling

T: Absolute temperature (K)

t: time (min)

$t^{1/2}$: Square root of time ($min^{1/2}$)

t_b: Breakthrough time

TMS: Tetramethylsilane

TOC: Total organic carbon

u: Linear flow velocity in column (cm/h)

UF: Ultrafiltration

v: Fractional power kinetic constants

V: Throughput volume in column (mL)

WHO: World Health Organization

WR: Watermelon rind

X_0: Value of X_i at the center point

XANES: X-ray absorption near edge structure

x_i: Dimensionless coded value of the variable X_i

X_i: Experimental variable

XPS: X-ray photoelectron spectroscopy

Z: Bed height of column (cm)

α: Dose-Response constant

β: D-R isotherm constant related to adsorption energy (mol^2/kJ^2)

γ: Dose-Response constant representing the time when effluent concentration reached 50% of influent concentration

ΔG^0: Gibbs free energy change at standard condition (kJ/mol)

ΔH^0: Enthalpy change at standard condition (kJ/mol)

ΔS^0: Entropy change at standard condition (kJ/mol·K)

ΔX: Step change

τ: Time required for retaining 50% of the initial adsorbates in the Yoon and Nelson model (min)

List of Figures

List of Tables

1. Introduction

1.1. Motivations

Water is the most essential substance for life on Earth and also an indispensable resource for human civilization. Population growth, urbanization and industrialization have resulted in water scarcity and contamination, rendering the reliable access to clear water a major global challenge (Qu et al., 2013). The prevalent use of heavy metals in industries (e.g., electroplating, mining, battery and plastic factories) produces increasing amounts of heavy-metal-bearing wastewater. Inappropriate treatment of this type of wastewater before discharge results in heavy metal contamination in the receiving water bodies, which poses hazards to ecosystems and humans due to the highly toxic and bioaccumulative properties of heavy metals (Kurniawan et al., 2006b, Wei et al., 2018). In recent years, rice containing high amounts of cadmium (Cd) caused by Cd(II)-polluted irrigation (Ok et al., 2011), drinking water contaminated by lead (Pb) leaked from pipe systems (Khan et al., 2013), and other heavy metal related accidents have been reported (Li et al., 2014). The ever-growing demand for clean water resource and the increasingly strict legislation make it imperative to apply efficient approaches for the treatment of heavy-metal-bearing wastewater. Meanwhile, solid waste has become another global challenge as a result of population growth and urbanization (Greene and Tonjes, 2014). Fruit waste, which includes peels, rinds, shells and seeds of fruits, comprises a large part of solid waste. It always makes solid waste management intractable due to its highly hydrous and perishable nature. Biosorption, a technology using inexpensive non-living biomaterials to sequester heavy metals or other contaminants in aqueous solutions (Volesky, 1990), has attracted considerable attention due to its low cost, high efficiency, easy operation

and lack of toxic sludge compared with conventional physicochemical methods, e.g., precipitation, ionic exchange and membrane processes (Fu and Wang, 2011, Kurniawan et al., 2006a, b). It is strategically promising to utilize fruit waste materials for the treatment of heavy-metal-bearing wastewater, so as to simultaneously relieve the two environmental issues, i.e., heavy metal contamination and fruit waste disposal.

The rind of *Citrullus lanatus* (watermelon rind, shorten as WR) and the seed of *Mangifera indica* (mango seed, shorten as MS) are both abundant fruit waste materials given the huge consumption of the two fruits in the world, with 117 million tons of watermelon and 40 million tons of mango produced per year (FAOSTAT, 2016). Being natural sources of cellulose, hemicellulose, pectin, protein and other biopolymers, WR and MS are found capable of effective entrapment of heavy metals and organic pollutants (Alencar et al., 2012, Bhatnagar et al., 2009, Lakshmipathy and Sarada, 2013, Liu et al., 2012b). However, their biosorption performance on Pb(II) and Cd(II), two of the most toxic heavy metals, has not been well-addressed, especially the biosorption-desorption operation in a continuous mode and the underlying mechanisms governing the biosorption processes (Lakshmipathy and Sarada, 2016, Liu et al., 2012a, Nadeem et al., 2016). The former is crucial for evaluating the practicability of the biosorbents, and the latter is highly important for better control of the biosorption processes and development of commercial (bio)sorbents.

In the early literature, most biosorption studies focused on the fundamental adsorption studies at the macroscopic scale, such as optimization of operational

conditions, biosorption isotherms, kinetics and thermodynamics (Banerjee et al., 2012, Choinska-Pulit et al., 2018, Liu et al., 2012a, Reddy et al., 2014). For mechanistic elucidation, the research efforts are limited and usually restricted to several conventional analytical methods (Lakshmipathy et al., 2013, Lalhmunsiama et al., 2017, Li et al., 2018, Oliveira et al., 2014, Schiewer and Balaria, 2009), resulting in vague and incomplete elucidation of the underlying biosorption mechanisms (Ramrakhiani et al., 2017). It is noteworthy that a variety of complicated interactions could be concurrently involved in a biosorption process, given that a biomaterial often has a complex composition with barely defined constituents. A hybrid mechanistic methodology that combines diverse complementary analytical methods is indispensable to comprehensively decipher a biosorption process, so as to facilitate the better control of biosorption and the development of commercial (bio)sorbents. To this end, this study established a methodology for mechanistic elucidation at both macroscopic and microscopic scales. Solid-state nuclear magnetic resonance (NMR) spectroscopy, to the best of my knowledge, was employed for the first time to investigate the interactions between heavy metal ions and the surface of biosorbents. A variety of conventional analytical tools, including scanning electron microscopy equipped with energy dispersive X-ray spectroscopy (SEM-EDX), powder X-ray diffraction (PXRD), Fourier-transform infrared (FTIR) spectroscopy and X-ray photoelectron spectroscopy (XPS), were combined to disclose the underlying biosorption mechanisms from different perspectives. In addition, chemical methods and quantum chemistry simulation (QCS) were applied to complement the mechanistic elucidation. Beyond biosorption studies, the methodology established in this study

will also be helpful to other environmental studies as biosorption is a prevalent and important process that occurs in nature and in environmental studies (e.g., biofilm, sorption in soil, and adsorption onto the host cell as the first step for uptake or invasion), which are related to interactions between biological surfaces and adsorbates as involved in a biosorption process (Fomina and Gadd, 2014).

1.2. Objectives

In order to fill the research gaps in the literature as aforementioned, the present study aimed to:

(1) Investigate the biosorption performance of WR and MS on Pb(II) and Cd(II) at varying operational parameters, including pH, biosorbent particle size, biosorbent dosage, initial metal concentration, ionic strength, and presence of co-metal ions.

(2) Examine the biosorption isotherms, kinetics and thermodynamics to unveil the intrinsic nature of the biosorption processes.

(3) Screen superior desorbing agents for Pb(II) and Cd(II) desorption and biosorbents regeneration.

(4) Develop a packed bed column reactor for continuous biosorption-desorption of Pb(II) and Cd(II).

(5) Employ and integrate a variety of complementary analytical methods for comprehensive mechanistic elucidation of Pb(II) and Cd(II) biosorption by WR and MS so as to establish a hybrid methodology that can thoroughly decipher a biosorption process.

1.3. Organization of this dissertation

There are seven chapters in this dissertation. The chapters are listed as follows:

Chapter 1 Introduction

Chapter 2 Literature Review

Chapter 3 Materials and Methods

Chapter 4 Biosorption of Pb(II) and Cd(II) by Watermelon Rind

Chapter 5 Biosorption of Pb(II) and Cd(II) by Mango Seed

Chapter 6 Comprehensive Elucidation of Biosorption Mechanisms

Chapter 7 Conclusions and Future Perspectives

2. Literature Review

2.1. Heavy metal pollution and hazards

Although there is not yet an unambiguous definition of a "heavy metal" in consensus, density is most frequently used as the defining criterion. It is commonly thought that a heavy metal is a naturally occurring element with a specific density greater than 5 g/cm^3. Given the general toxic properties of heavy metals, a number of metalloids (e.g., arsenic) are also categorized as heavy metals (Järup, 2003). Pb and Cd, being the "big two" when considering the environmental impact of heavy metals, pose serious health and environmental concerns due to their widespread uses in industries, bioaccumulative properties, and high toxicity to living organisms (see Table 2.1) (Volesky, 1994). They are categorized as the first-level pollutants in "Discharge standard of pollutants for municipal wastewater treatment plant" of China (GB 18918-2002), and also specifically listed among the top three of European Restriction of Hazardous Substances (RoHS3, 2015). Pb(II) and Cd(II) may occur in substantial concentrations in the hydrosphere due to the improper discharge of heavy-metal-bearing wastewater. The characteristics of Pb and Cd are summarized in Table 2.1.

2.1.1. Lead

Lead is a natural constitute of Earth's crust with a crustal abundance of 13 mg/kg (WHO, 2011c). The occurrence of Pb contamination in the environment, however, mainly results from anthropogenic activities such as mining, smelting, refining, soldering, manufacturing of batteries and paints, and use of leaded gasoline (WHO, 2010). Despite the banning of Pb additives in gasoline since the mid-1970s and their reduced use in paints and solders (Cheng and Hu, 2010),

significant sources of Pb exposure still remain due to the technological importance of Pb in industries. Once Pb is released into the environment, it can be bioaccumulated and biomagnified along with the food chain/net, resulting in high health risks to living organisms in high trophic levels, e.g., humans. Pb can affect body functions in neurological, haematological, gastrointestinal, cardiovascular and renal systems. In particular, children are much more susceptible to the neurotoxic effect of Pb than adults; a low level of exposure can cause irreversible neurological damage (WHO, 2010). Besides, Pb has been categorized as a possible human carcinogen in Group 2B of the International Agency for Research on Cancer (IARC) classification, and its inorganic compounds have been placed in Group 2A, i.e., probable human carcinogens. The discharge limit of Pb in municipal wastewater is 0.1 ppm (i.e., mg/L) in China (GB 18918-2002), and its guideline value in drinking water is 0.01 ppm according to the World Health Organization (WHO) (WHO, 2011b). The speciation of Pb in 0.48 mM $Pb(NO_3)_2$ solution at varying pH indicates that Pb exists in the form of free cation (i.e., Pb^{2+}) when the pH is lower than 6.0 (Figure 2.1a). Hydroxides will be generated as the pH gradually increases. Hence, the Pb(II) biosorption in this study was investigated at pH lower than 6.0 to avoid precipitation.

2.1.2. Cadmium

Cadmium is chemically similar to zinc (Zn), and naturally occurs with Zn and Pb in sulfide ores. Similar to Pb, it is also widely employed in industrial activities such as coal combustion, electroplating, manufacturing of glass, plastics, and batteries (WHO, 2011a). Cadmium is a cumulative element along with the food

chain/net and poses serious health risks to humans. Once it enters the human body, it will adversely affect the functions of the kidneys, lung and bones. Particularly, it can form a strong bond with sulfur and displace essential metals, e.g., Zn^{2+} and Ca^{2+}, from the binding sites of certain enzymes. There are evidences that Cd is carcinogenic by inhalation (Group 2A in the IARC classification) (WHO, 2011b). The discharge limit of Cd in municipal wastewater is 0.01 ppm in China (GB 18918-2002), and its guideline value in drinking water is 0.003 ppm (WHO, 2011b). In solution, Cd hydroxides will not form until the pH increases over 8.0 (Figure 2.1b); this provides a wider pH range in investigating Cd(II) biosorption in this study (pH < 8.0) as compared with that of Pb(II) biosorption (pH < 6.0).

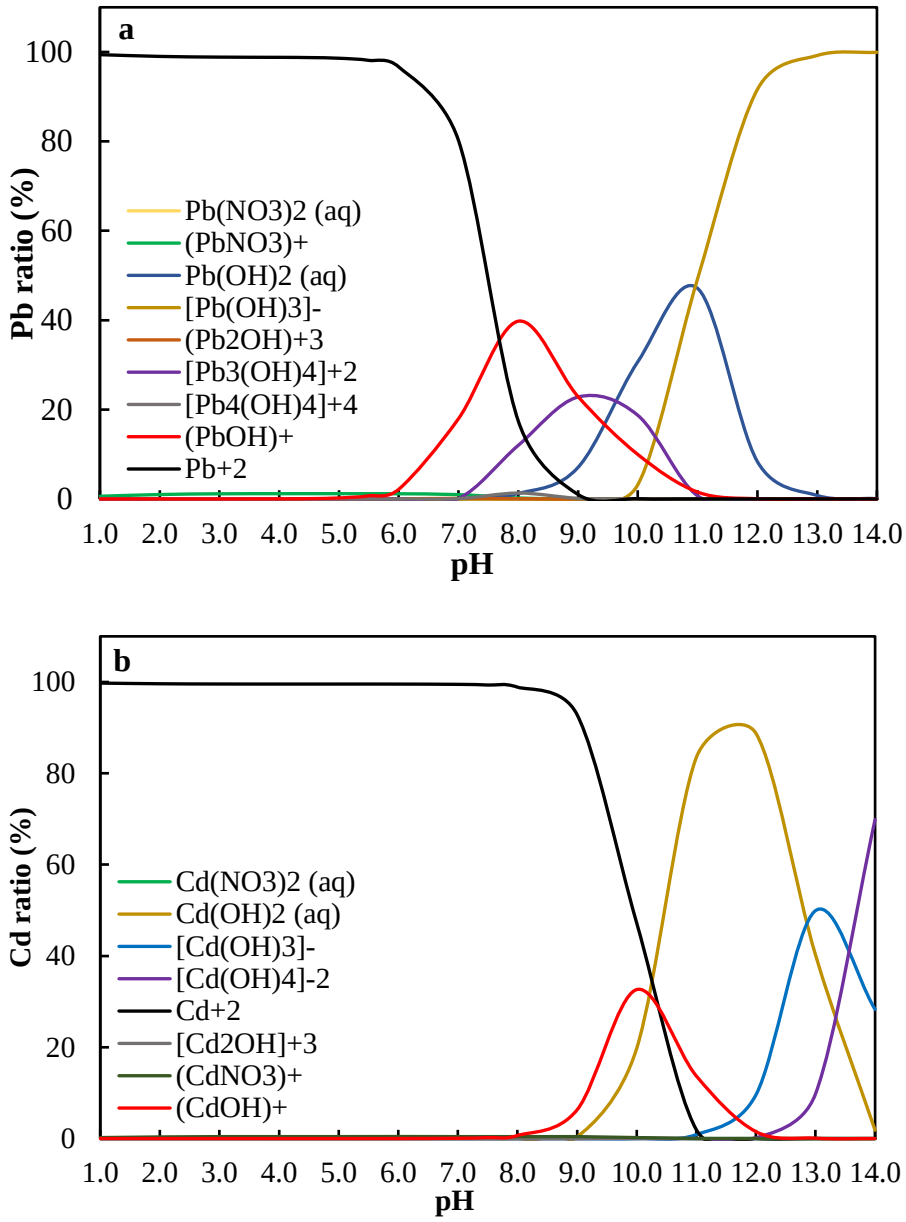

Figure 2.1 Speciation of (a) Pb and (b) Cd at different pH.

[Simulated by *Visual MINTEQ* 3.1 with 0.48 mM $Pb(NO_3)_2$ solution and 0.89 mM $Cd(NO_3)_2$ solution, namely 100 ppm Pb/Cd.]

Table 2.1 Important properties of Pb and Cd.

	Pb	Cd
Atomic number	82	48
Atomic weight	207.2	112.4
Density (g/cm^3)	11.34	8.65
Electronegativity[a]	1.854	1.521
Ionic radius (pm)	133	109
Ionic potential[b]	0.0150	0.0183
Hydration energy (kJ/mol)	-1480	-1806
HSAB behavior[c]	Borderline acid	Soft acid
Discharge limit (mg/L)[d]	0.1	0.01
Guideline value (mg/L)[e]	0.01	0.003
Carcinogenesis	Group 2B; Inorganic compounds in Group 2A	Group 2A
Toxicity to human	Cardiovascular effects, kidney damage, premature birth, damage on nervous system, especially for children	Kidney disease, lung damage, and fragile bones

(**Notes:** a - Allen electronegativity of the element in the oxidation state (Allen, 1989); b - The ratio of electric charge to ionic radius; c - Pearson's HSAB principle (Pearson, 1963); d - Discharge limit in municipal wastewater in China, GB 18918-2002; e - Guideline value in drinking water (WHO, 2011b); Data of ionic radius and hydration energy from (Wulfsberg, 2000).)

2.2. Conventional treatment

The traditional methods to remove heavy metal contaminants from (waste)water systems mainly include chemical precipitation, ion exchange, adsorption, membrane filtration, coagulation-flocculation, flotation, and electrochemical methods (Fu and Wang, 2011, Kurniawan et al., 2006b). The details of these physico-chemical methods, their advantages and limitations are discussed below.

2.2.1. Chemical precipitation

Chemical precipitation is the most widely applied method in industries given its simplicity and low cost. It is a process in which precipitant reagents react with heavy metal ions to form insoluble precipitates at basic conditions (usually pH 8.0-11.0), and the precipitates are separated from aqueous solutions by sedimentation or filtration. Lime, i.e., CaO or $Ca(OH)_2$, is the most frequently used precipitant because it is easily available in most countries (Charerntanyarak, 1999, Kurniawan et al., 2006b). During chemical precipitation, heavy metal ions are precipitated in the form of hydroxides through the reaction shown in Eq. 2.1:

$$M^{2+} + 2OH^- \rightarrow M(OH)_2 \downarrow \quad (2.1)$$

where M^{2+} denotes divalent heavy metal ions, and OH^- is the hydroxyl ions from the precipitant, e.g., $Ca(OH)_2$. To facilitate heavy metal precipitation, fly ash has been used as a seed material. Chen et al. (2009) reported that the fly ash-lime-carbonation treatment, in which fly ash was added as a seed material to enhance lime precipitation, and the suspension was exposed to CO_2, significantly increasing

the particle size of the precipitate and improving the heavy metal removal efficiency and sludge sedimentation. The concentrations of Cr(III), Cu(II), Pb(II) and Zn(II) were found to be reduced to 0.08, 0.14, 0.03, and 0.45 ppm, respectively, from the initial concentrations of 100 ppm. Moreover, addition of coagulants such as alum and iron salts can enhance heavy metal removal via chemical precipitation (Charerntanyarak, 1999). Sulfide precipitation is also an effective alternative, as the solubility of metal sulfide precipitates is significantly lower than that of hydroxide precipitates, making heavy metal removal possible over a broader pH range compared with hydroxide precipitation. Pyrite and synthetic iron sulfide (Özverdi and Erdem, 2006), and even the hydrogen sulfide produced by sulfate-reducing bacteria (Kousi et al., 2007), have been used for the precipitation of heavy metals. The underlying principle is illustrated in Eq. 2.2:

$$M^{2+} + H_2S \rightarrow MS \downarrow + 2H^{+} \qquad (2.2)$$

where M^{2+} denotes divalent heavy metal ions. Yet, sulfide precipitation can result in emission of toxic H_2S gas as heavy metal ions usually exist in acidic conditions. Besides, the colloidal precipitates generated can cause difficulties in separation. These drawbacks somehow restrict the application of sulfide precipitation in practice (Fu and Wang, 2011). Overall, chemical precipitation is effective for wastewater bearing high concentrations of heavy metal ions, e.g., industrial effluents. Still, the processed wastewater usually requires further treatment such as adsorption, filtration, and ion exchange to fulfill the increasingly stringent environmental regulations (Gonzalez-Munoz et al., 2006, Papadopoulos et al., 2004). Besides, chemical precipitation is chemical-intensive, and the produced

toxic sludge is a big concern due to the high cost of sludge disposal and the potential second pollution in the environment.

2.2.2. Ion exchange

Ion exchange is widely used for the removal and recovery of heavy metal ions from aqueous solutions due to its high efficiency, selectivity on specific metal ions, and lack of sludge generation. An ion-exchange resin removes metal ions from the liquid phase and releases a chemically equivalent amount of ions from itself (Vigneswaran et al., 2005). This exchange process is reversible without any structural change of the resin: the entrapped metal ions can be recovered in a concentrated form by appropriate eluants, and the ion-exchange resin will be simultaneously regenerated. The most prevalent cation exchangers are strongly acidic resins with sulfonic acid groups (-SO_3H) and weakly acidic resins with carboxylic acid groups (-COOH). Protons (H^+) in these two types of groups exchange with metal cations and finally separate the metal ions from the liquid phase, as shown in Eqs. 2.3 and 2.4:

$$nR\text{-}SO_3H + M^{n+} \rightarrow (R\text{-}SO_3^-)_nM^{n+} + nH^+ \quad (2.3)$$

$$nR\text{-}COOH + M^{n+} \rightarrow (R\text{-}COO^-)_nM^{n+} + nH^+ \quad (2.4)$$

where M^{n+} represents metal cations. In addition to the operational parameters (e.g., pH, initial metal concentration and temperature), the charge of the metal ion also influences its removal efficiency via ion exchange. Abo-Farha et al. (2009) observed that more positively charged metals achieved higher removal efficiencies in ion exchange processes. In the market, there are a variety of synthetic ion-

exchange resins, including Amberlite IR-120, Dowex 2-X4, IRN77, SKN1, Amberjet series and other types. Natural zeolites (especially clinoptilolite) have also been frequently used as ion-exchangers for heavy metal removal because of their high abundance and low cost. The nature and capabilities of these synthetic and natural ion-exchange resins have been reviewed and discussed by Kurniawan et al. (2006b). It was observed that ion-exchange resins were effective for the removal of heavy metal ions in concentrations lower than 10 ppm, within the range of 10-100 ppm, and even higher than 100 ppm (Kurniawan et al., 2006b). Furthermore, synthetic ion-exchange resins usually exhibited high removal efficiencies close to 100%, whereas lower effiencies (60%-90%) were generally achieved by natural ones (Kurniawan et al., 2006b). This should be attributed to the complicated and non-well defined components of natural ion-exchangers compared with synthetic resins. In spite of the aforementioned advantages of ion exchange processes, the drawbacks such as the high capital and operational cost and the requirement of pretreatment of wastewater have restricted the application of ion-exchangers in a large scale.

2.2.3. Adsorption

Adsorption has been widely used as a cost-effective technology for the treatment of heavy-metal-bearing wastewater (Jusoh et al., 2007, Kang et al., 2008). Conventional adsorption processes mostly employ granular activated carbon (AC) as the adsorbent given its large surface area provided by micropore and mesopore. The reversibility of adsorption processes makes heavy metal recovery and adsorbent regeneration achievable; successive adsorption-desorption cycles can be

implemented in practice for sustainable wastewater treatment. Hence, adsorption was thought better than other technologies for heavy metal removal from wastewater in consideration of the low capital and operational cost, simple design, easy operation, and insensibility to toxic or suspended substances (Jusoh et al., 2007). Nowadays, however, the limited remaining source of coal results in an increasing price of the coal-based AC. Converting carbonaceous materials, e.g., coconut shells, palm shells and other agro-waste materials, into AC has become a sustainable measure to produce AC, especially in Southeast Asian countries (e.g., Malaysia and Thailand) (Dias et al., 2007, Yang et al., 2010). Yet, the high energy required for the carbonization of raw materials at high temperatures (700-1100 ºC), and the use of the gases (e.g., steam and CO_2) or chemical agents (e.g., $ZnCl_2$, H_3PO_4 and KOH) for activation substantially increases the cost of adsorption processes using AC converted from carbonaceous materials.

2.2.4. Membrane filtration

Membrane filtration is a promising technique for treatment of heavy-metal-bearing wastewater due to its high efficiency and low space requirement. Apart from heavy metal contaminants, it can remove suspended substances and organic pollutants from wastewater at the same time. Membrane filtration is mainly categorized into microfiltration (MF), ultrafiltration (UF), nanofiltration (NF) and reverse osmosis (RO) depending on the characteristics of the membrane applied for filtration. UF utilizes a permeable membrane at a low transmembrane pressure to separate dissolved, colloidal and suspended pollutants larger than the pore size of the membrane (5-20 nm). For dissolved heavy metal ions, either in the form of

hydrated ions or complexes, the pore size of UF membrane is usually too large to separate them from the liquid phase. Micellar enhanced and polymer enhanced UF techniques have been proposed for the efficient removal of heavy metal ions (Camarillo et al., 2010, Landaburu-Aguirre et al., 2010). Landaburu-Aguirre et al. (2010) reported that retention of 98% of Zn(II) and 99% of Cd(II) (initial metal concentrations of 0.5 mM) were achieved by the micellar enhanced UF with sodium dodecyl sulfate (SDS) as the surfactant. NF is an intermediate process between UF and RO. It has the unique property of separating contaminants based on steric (sieving) and electrical (Donnan) effects. That is to say, the NF membrane has small pores and surface charge, through which the charged ions/molecules smaller than the membrane pore can be retained together with the larger neutral ions/molecules (Kurniawan et al., 2006b). RO is a pressure-driven membrane process in which the water molecules can pass through the membrane. Under a hydrostatic pressure higher than the osmotic pressure of the feeding solution, cationic ions/molecules (e.g., heavy metal ions) can be removed from the aqueous solution. To fulfill the increasingly stringent environmental standards, the RO membrane has been developed with a particle size as small as 10 nm (Xie et al., 2015). As reviewed by Kurniawan et al. (2006b), RO exhibited a higher capacity of heavy metal removal with rejection efficiencies over 97% (initial metal concentrations of 21-200 ppm) in comparison with UF and NF.

Taken together, the heavy metal removal capabilities of the aforementioned membrane techniques are in an ascending order of UF < NF < RO, in which the requirement for the membrane material and consumption of energy are increasing. How to select a suitable membrane technique for the treatment of heavy-metal-

bearing wastewater? This question is answered by taking into account the discharging standards and the characteristics of the target wastewater (e.g., properties of the co-pollutants and metal concentrations). In a nutshell, there is a trade-off between efficiency and cost. Notably, membrane fouling is a common problem in membrane filtration processes. It will cause a high transmembrane pressure and even biodegradation of the membrane material, resulting in impairment of the membrane performance and a high cost for operation and maintenance of the membrane system.

2.2.5. Coagulation-flocculation

Coagulation is a process of adding coagulants, e.g., ferric or alum salts, to destabilize colloidal particles in wastewater via neutralizing the repulsive force between particles. It is followed by flocculation, which employs polymers (e.g., polyanionic cellulose, polyferric sulfate and polyacrylamide) to form bridges between the generated flocs and aggregate them into large clumps, for easy sedimentation or filtration (Kurniawan et al., 2006b). Given that the main targets of coagulation-flocculation are hydrophobic colloids and suspended particles, there are intensive efforts to invent new coagulants and flocculants and to modify the conventional ones to remove soluble heavy metal ions together with turbidity (Chang and Wang, 2007, Chang et al., 2009b, Duan et al., 2010). In general, application of coagulation-flocculation alone on heavy-metal-bearing wastewater cannot meet the stringent environmental legislations. Other techniques such as adsorption and filtration are usually necessary (Fu and Wang, 2011). It is noteworthy that pH plays a very important role in the efficiency of coagulation-

flocculation. Chang and Wang (2007) found that the colloidal substances with negative charges were coagulated at lower pH with a poor removal of Ni(II), whereas the removal of Ni(II) was improved with impaired turbidity treatment at higher pH. However, intensive chemical consumption and sludge generation render coagulation-flocculation far from an environmentally benign measure for the treatment of heavy-metal-bearing wastewater.

2.2.6. Flotation

Flotation is a process to separate solids or dispersed liquids from a liquid phase through bubble attachment. It has been employed to separate heavy metals that originate from mineral processing in aqueous solutions (Fu and Wang, 2011). Among the various types of flotation, dissolved air flotation (DAF), ion flotation, and precipitation flotation are mainly used in the treatment of heavy-metal-bearing wastewater. DAF utilizes micro air bubbles to attach to impurities and separated the floated substances from the bulk solution in a foaming phase. Ion flotation removes heavy metal ions in wastewater by using surfactants (e.g., SDS and biosurfactants) and subsequent separation of the generated hydrophobic species by air bubbles. It was reported that 90%, 81% and 71% of Pb(II), Cu(II) and Cd(II), respectively, were removed by ion flotation with a tea-derived biosurfactant (Yuan et al., 2008). Precipitation flotation is more like a combination of metal precipitation and flotation, which generates metal precipitates and then separates them by the attachment to air bubbles. Although flotation has the potential for industrial application due to the low cost and short hydraulic retention time (HRT), it is

usually not as efficient as other physio-chemical techniques for heavy metal removal from aqueous solutions (Kurniawan et al., 2006b).

2.2.7. Electrochemical methods

Electrochemical methods refer to concentrating metal ions on a cathode surface with the possibility to recover metals in the elemental state. There are a variety of electrochemical techniques that have been investigated for heavy metal removal from aqueous solutions, such as electrodialysis, electrocoagulation and electrodeposition. Electrodialysis denotes a membrane separation process in which ionized species pass through an ion exchange membrane (usually plastic materials with either anionic or cationic properties) by the driving force of the applied electric potential. It is generally effective for metal ions at concentrations less than 20 ppm (Kurniawan et al., 2006b). Electrocoagulation is a process in which coagulants are generated *in situ* by electrically dissolving aluminum or ferric ions from aluminum or iron electrodes. The coagulants can coagulate heavy metal species in the liquid phase and the H_2 gas produced in the cathode can help float the flocs out of water (Heidmann and Calmano, 2008). Electrodeposition, also known as electroplating, is a process of depositing heavy metal ions from the liquid phase onto a conducting surface. It was reported as a potential method for recovery of metals under certain operational conditions (Chang et al., 2009a, Oztekin and Yazicigil, 2006). Yet, the requirements of qualified feed solutions, high capital investment and high operational cost (e.g., electricity consumption and system maintenance) have restricted a wider application of electrochemical methods.

2.3. Fruit waste

2.3.1. Fruit waste disposal

Fruit waste refers to discarded or leftover parts of fruits such as peel, rind, seed and shell. A huge amount of fruit waste is produced from the food processing industries. *Citrullus lanatus* (i.e., watermelon), which has the highest yield (117 million tons/year) among fruits in the world (FAOSTAT, 2016), leaves almost 50% of its weight as waste in the form of rind. *Mangifera indica* (i.e., mango), which is one of the most prized tropical fruits marketed in the world with a global production around 40 million tons/year (FAOSTAT, 2016), generates plenty of fruit waste as seed and peel from industrial processing. The mango seed alone corresponds to 30-45% of the fruit weight (Meireles et al., 2010). For the treatment of fruit waste like watermelon rind (WR) and mango seed (MS), composting has been frequently employed in some developed countries. For instance, the city of Toronto offers curbside collection of organic materials (e.g., fruit and vegetables scraps) to divert waste from landfill to more environmentally benign compost (Assamoi and Lawryshyn, 2012). Yet, in most countries, fruit waste produced from food processing industries is directly disposed of with municipal solid waste in landfill and/or incinerator, posing a heavy burden on waste management with nuisance due to the high water content and perishable nature of fruit waste (USDA, 2004).

2.3.2. Components of fruit waste materials

Fruit waste materials have been widely studied as the precursors of biosorbents for the removal of heavy metals. Their capability of sequestering heavy metal ions is mainly due to their high contents of polysaccharides such as cellulose,

hemicellulose, pectin and lignin, which contain abundant organic functional groups capable of binding heavy metal ions. It was determined that WR comprised 20% of cellulose, 23% of hemicellulose, 13% of pectin and 10% of lignin (Singh et al., 1975), while MS consisted of 55% of cellulose, 24% of lignin and 21% of hemicellulose (based on dry weight) (Henrique et al., 2013). The major components of fruit waste materials are introduced as follows.

Cellulose

Being the most abundant organic polymer on Earth, cellulose is a very important skeletal component in plants. It is a straight chain polymer that consists of hundreds to thousands of β(1→4) linked D-glucose units without branching or coiling. However, the hydroxyl groups in glucose units from one chain can form hydrogen bonds with oxygen atoms in the same or an adjacent chain, holding the chains firmly with high tensile strength. This ordered structure leads to much higher crystallinity of cellulose than other polysaccharides (e.g., hemicellulose, pectin and lignin) (Habets et al., 2013). A variety of crystalline structures have been found in cellulose as a result of different locations of hydrogen bonds. It is noteworthy that most natural cellulose is cellulose I, which is metastable.

Hemicellulose

Hemicellulose is also an important natural polymer which contributes to about 20% of most plant biomass. In addition to glucose, xylose, mannose, galactose, rhamnose and arabinose are usually included in hemicellulose. Unlike cellulose which has a linear and crystalline structure, hemicellulose has a random, branched and amorphous structure with weak strength. Hence it can be easily

hydrolyzed by dilute acids or bases. Given the variety of monomers and the random organization, hemicelluloses have different chemical structures including xylan, glucuronoxylan, arabinoxylan, glucomannan and xyloglucan. Furthermore, sugars in the acidified forms such as glucuronic acid and galacturonic acid can be found in hemicellulose, providing a variety of potential functional groups for the binding of heavy metals.

Pectin

Pectin is a structural material of heteropolysaccharide in the primary cell walls of terrestrial plants, especially abundant in the non-woody parts. It is mainly composed of β(1→4) linked D-galacturonic acid, in which the uronic acid carboxyl groups are either fully or partially methyl esterified. Apart from galacturonic acid, pectin comprises a complex set of polysaccharides such as galacturonans and rhamnogalacturonan. In nature, about 80% of the carboxyl groups in galacturonic acid are esterified with methanol (methyl esters), while the non-esterified ones can be either free acids or salts with Na^+, K^+, Mg^{2+} or Ca^{2+} (known as "pectinate").

Lignin

Lignin, as a cross-linked phenolic polymer, is a crucial structural material in the supporting tissues of vascular plants. It fills up the empty space between cellulose and hemicellulose polymers, leading to more rigid cell wall structures (Habets et al., 2013). The structure of lignin presents significant quantities of methoxy and free hydroxyl groups, which can interact with various metal ions (Farinella et al., 2007). There are mainly three types of lignols, i.e., 4-hydroxy-3-

methoxyphenylpropane, 3,5-dimethoxy-4-hydroxyphenylpropane and 4-hydroxyphenylpropane.

Beyond the four commonly found polysaccharides, a number of characteristic macromolecules may exist in certain types of fruit waste materials. For example, cutin, which is a waxy polyester functionalized as a cuticular component covering all aerial surfaces of plants, was extracted from WR (Chaudhari and Singhal, 2015). In MS, which denotes a mix of mango seed shell and kernel in this study, there is an unneglectable content of tannins, starch and lipids from the kernel (Widsten et al., 2014). The functional groups such as hydroxyl, carboxyl, carbonyl and ether groups in these macromolecules can contribute to the sequestration of heavy metal ions from aqueous solutions.

2.4. Biosorption

2.4.1. Conception of biosorption

"Biosorption" has become a more and more common concept in environmental science since the 1980s (Friis and Myerskeith, 1986, Kuyucak and Volesky, 1989, Tsezos and Volesky, 1981, Tsezos and Volesky, 1982). However, the development of its relevant studies over the past few decades results in difficulties in giving "biosorption" a sound definition, mainly due to the complicated mechanisms involved and the types of biosorbents used. In the literature, this term has been used for a diverse range of processes including bioadsorption, bioabsorption, bioaccumulation and biosorption by living and dead biomass (Fomina and Gadd, 2014). The prefix "bio" indicates the utilization of biological matrices such as fungal biomass, agro-waste and fruit waste materials. However, "sorption" is a polysemous term that refers to both adsorption and absorption. The former denotes physical adherence or bonding of ions/molecules onto the surface of another substance, e.g., entrapment of precious metal ions by ion-exchange resin. The latter, absorption, is a process of incorporation of a substance in one phase into another substance in a different phase (e.g., gases being absorbed by liquids) (Fomina and Gadd, 2014). In the research area of biosorption, most researchers consider biosorption as a subcategory of adsorption with biomaterials as adsorbents (Michalak et al., 2013), since adsorption is the most common form involved in a biosorption process for environmental remediation. Another ambiguous aspect of the conception of biosorption is whether this process is passive or not. Such ambiguity is the result of the utilization of different types of

biosorbents. For example, the removal of heavy metal ions from wastewater by a microbial consortium can be attributed to active intake into the cell, and/or passive adsorption onto the cell wall and extracellular polymeric substance (EPS) secreted by microorganisms (Li et al., 2018). To circumvent the complex metabolically dependent process of active intake, biosorption has been defined by most researchers as a passive and metabolically independent process by non-living biomass. Accordingly, biosorption in the present study is based on the conception of passive adsorption of adsorbates by non-living biomass.

Notably, biosorption is not only a promising technology applied for removing pollutants in environmental remediation, but also a prevalent and important process occurring in nature, e.g., adsorption in soil and adsorption onto the host cell as the first step for uptake or invasion. Similar to biosorption processes, almost all life phenomena and natural processes are related to the interactions between biological surfaces and adsorbates with different degrees (Fomina and Gadd, 2014).

2.4.2. Biosorption of heavy metal by using fruit waste

In addition to fungal biomass and agro-waste, fruit waste is also an abundant, reproducible and low-cost resource for biosorbents used in biosorption processes. Among all the contaminants which have been investigated in biosorption studies, heavy metals are the most widely targeted ones (He and Chen, 2014, Nguyen et al., 2013). Park et al. (2008) investigated the Cr(VI) biosorption capacities of abundant biowastes including banana skin and several agricultural wastes (e.g., oak leaf and rice husk), and it was observed that the highest Cr(VI) biosorption capacity, 249.6

mg/g, was achieved by banana skin. The highest reported biosorption capacities on various heavy metals are summarized in Table 2.2 based on the plentiful studies of heavy metal biosorption by using fruit waste materials in the literature. In the present study, only native fruit waste materials without any pretreatment were considered, given that any physical or chemical pretreatment may contradict the low cost of using fruit waste materials as biosorbents. Table 2.2 indicates that almost all heavy metal ions have been studied in biosorption for their removals from aqueous solutions by fruit-waste-derived biosorbents. A variety of fruit waste materials, including different types of citrus peels, mango seed, yellow passion fruit shell, banana peel and durian husk, have been explored as potential biosorbents.

Table 2.2 Highest reported heavy metal uptakes by fruit waste materials.

Adsorbent	Heavy metal	Q_{max} (mg/g)	Reference
Citrus maxima peel	Cd(II)	135.2[a]	(Chao and Chang, 2012)
Mango seed (shell)	Pb(II)	183	(Nadeem et al., 2016)
Ponkan mandarin peels	Ni(II)	75	(Pavan et al., 2006)
Citrus maxima peel	Cu(II)	84	(Chao and Chang, 2012)
Grapefruit peel	Zn(II)	49.4	(Iqbal et al., 2009b)
Yellow passion fruit shell	Cr(III)	80	(Jacques et al., 2007)
Banana skin	Cr(VI)	249.6[b]	(Park et al., 2008)
Fresh *Garcinia cambogia*	As(III)	116	(Kamala et al., 2005)
Orange waste peel	As(V)	36.81[a]	(Khaskheli et al., 2011)
Citrus grandis waste	U(VI)	38.97	(Saleem and Bhatti, 2011)
Citrus reticulate (tangerine) peel	La(III)	88	(Torab-Mostaedi, 2013)
Citrus reticulate (tangerine) peel	Ce(III)	95	(Torab-Mostaedi, 2013)
Durio zibethinus (durian) husk	Au(III)	339.6[a]	(Abidin et al., 2011)

(**Notes:** a - Simulated from the Langmuir isotherm model; b - Reduction capacity.)

2.5. Important operational parameters in biosorption

Investigation of the effects of different operational parameters is indispensable in fundamental biosorption studies, as the information is crucial for the process optimization and control. The important operational parameters, including pH, particle size of biosorbent, ionic strength, presence of co-metal ions, and temperature, are discussed as follows.

2.5.1. pH

pH plays a crucial role in a biosorption process, as it can influence the protonation/deprotonation of functional groups on biosorbents, the release of naturally occurring ions/molecules from biosorbents, and the speciation of adsorbates (e.g., heavy metals in this study) in the liquid phase. For biosorption of a cationic heavy metal, it was usually found that the biosorption capacity was augmented with increasing pH due to less competition from H^+ at higher pH (Ahmad et al., 2018, Deniz and Karabulut, 2017). In addition, some functional groups such as carboxyl and hydroxyl groups become deprotonated as pH increases, providing more negative binding sites on the biosorbent surface for cationic heavy metal ions. It is worth noting that precipitation of heavy metal ions may occur when pH increases to a certain value (Vafajoo et al., 2018).

2.5.2. Particle size of biosorbent

Particle size of biosorbent may affect the biosorption performance of a biosorbent in consideration of the surface area, the exposure of binding sites, and the intraparticle diffusion (pore diffusion). It is frequently observed that biosorbents

in smaller particle sizes exhibit higher biosorption capacities due to the larger surface area, which increases the availability of binding sites to adsorbates (Ali et al., 2016, Krika et al., 2016, Liu et al., 2012b, Tarley and Arruda, 2004). Moreover, smaller biosorbents may benefit the biosorption kinetics given the rapid transport of adsorbates from the bulk solution to the surface of biosorbents, whereas larger particle size may impede the biosorption rate because pore diffusion within the solid particle is relatively slow (Leusch and Volesky, 1995). However, the preparation of biosorbents in smaller particle sizes may increase the energy and time input since more intense grinding work is required. Besides, biosorbents that are too small can cause difficulties in the biosorption operation, e.g., poor separation of solids from solutions and blocking of packed bed column reactors. The aforementioned factors should be comprehensively considered when selecting a suitable particle size for a biosorbent.

2.5.3. Ionic strength

Heavy-metal-bearing wastewater generally contains a mass of salt ions, which may impact the biosorption capacity of the employed biosorbent by weakening its electrostatic interaction with the targeted heavy metal ions. For example, Na^+ can occupy the negatively charged binding sites on the surface of biosorbents and thus reduce the heavy metal uptake. In this sense, investigating the effect of ionic strength on a biosorption process is necessary to evaluate the practicality of the biosorbent. On the other hand, the effect of ionic strength is capable of clarifying the roles of physical sorption and chemisorption in a biosorption process. An insignificant effect of ionic strength may imply that the

binding of heavy metal ions to the biosorbent surface is mainly via chemisorption rather than non-specific physical sorption (Albadarin et al., 2011).

2.5.4. Presence of co-metal ions

In general, there are various types of heavy metal ions that exist in industrial wastewater. From the effect of co-existing heavy metal ions (shorten as co-metal ions), it is possible to evaluate the selectivity of a biosorbent on the target heavy metal ion. This is especially important when heavy metal recovery is expected.

The affinities of heavy metal ions to the binding sites mainly depend on four respects: (1) Electronegativity. A metal ion with a higher electronegativity would pose stronger attraction for the shared pair of electrons and forms stronger coordination bonds with ligands (Chong and Volesky, 1996, Mahamadi and Nharingo, 2010). (2) Ionic potential (i.e., charge/radius ratio). A metal ion with a higher ionic potential can be electrostatically attracted by oppositely charged ions more easily and strongly (Kalmykova et al., 2008). (3) Hydration energy. Metal ions are generally hydrated in aqueous solutions. With lower hydration energies, they would more readily dehydrate and bind to ligands, whereas those with higher hydration energies prefer to remain in ionic forms (Hui et al., 2005). (4) Hard and soft acids and bases (HSAB) characteristic. HSAB denotes a concept that rapid reactions and strong bonds occur between hard acids and hard bases or between soft acids and soft bases (Pearson, 1963). Accordingly, the discriminating factors of heavy metal affinities to biosorbents can vary with the underlying biosorption mechanisms. For example, the electronegativity of a heavy metal would be important for a complexation-based biosorption process.

2.5.5. Temperature

Generally, a biosorption process is more rapid at a higher temperature given that the faster movement of the adsorbate facilitates its entrapment by the biosorbent. Yet, the effect of temperature on the equilibrium biosorption capacity is more closely related to the thermodynamic nature of the adsorption process. For an exothermic biosorption, there should be a negative correlation between the biosorption capacity and temperature (Sari and Tuzen, 2008), whereas the biosorption capacity of an endothermic biosorption process is usually positively correlated to temperature (Ali et al., 2016, Khambhaty et al., 2009). Furthermore, a higher temperature may enlarge the pore size of biosorbents and increase the availability of binding sites by breaking some internal bonds on biosorbents, leading to a higher biosorption capacity (Saeed et al., 2010).

2.6. Important properties of biosorption

2.6.1. Biosorption isotherms

Biosorption isotherm studies (also known as equilibrium studies) explore the relationship between the concentration of adsorbate remaining in the solution (C_e, ppm) and the amount of adsorbate bound to the biosorbent (Q_e, mg/g) in equilibrium. The maximum biosorption capacity (Q_m, mg/g), which is an important parameter to evaluate the performance of a biosorbent, can be obtained through biosorption isotherm studies. Besides, different adsorption isotherm models, including the Langmuir, Freundlich, Temkin, Dubinin-Radushkevich (D-R), Redlich-Peterson (R-P) and Sips models, are frequently used to simulate equilibrium data linearly or non-linearly. The most applicable model and the values of the model constants can provide insights into the biosorption mechanism, surface properties, adsorbate-biosorbent affinity and thermodynamics.

Langmuir isotherm

The Langmuir isotherm model was first presented to correlate the amount of a gas adsorbed on a solid surface to the gas pressure by Langmuir (Langmuir, 1918). As a widely used adsorption isotherm having good agreement with a wide variety of experimental data, the Langmuir model is based on the following principles: (1) adsorbates are chemically adsorbed at a fixed amount of well-defined surface sites; (2) each site binds with one adsorbate molecule; (3) all sites are structurally homogenous and energetically equivalent; (4) adsorption is limited to a monolayer; and (5) no interaction exists between adsorbates adsorbed on neighboring sites (Ruthven, 1984). Accordingly, this model describes

quantitatively about monolayer adsorption of an adsorbate on the outer surface of an adsorbent, and it can be represented as

$$Q_e = \frac{Q_m K_L C_e}{1 + K_L C_e},$$

where Q_m (mg/g) is the amount of adsorbate at complete monolayer coverage; K_L (L/mg), which is derived from the rate constant of adsorption to desorption, is related to the affinity of binding sites (molar heat of adsorption); Q_e (mg/g) denotes the amount of adsorbate adsorbed by per unit weight of adsorbent, and C_e (mg/L) is the concentration of adsorbate remaining in the solution in equilibrium. The Langmuir model effectively reduces to Henry's law at low concentrations.

Freundlich isotherm

Freundlich (1906) developed the earliest known empirical adsorption isotherm to illustrate the non-ideal adsorption on a heterogeneous surface as well as multilayer adsorption with non-uniform distribution energy. The Freundlich model is expressed as

$$Q_e = K_F C_e^{1/N_F},$$

where K_F (L/g) and N_F are Freundlich constants respectively representing adsorption capacity and intensity; Q_e (mg/g) denotes the amount of adsorbate adsorbed by per unit weight of adsorbent, and C_e (mg/L) is the concentration of adsorbate remaining in the solution in equilibrium. As the original equation is exponential, it can only be adequately applied in low and intermediate concentrations (Liu and Liu, 2008).

Temkin isotherm

The Temkin isotherm, which was proposed to depict adsorption of hydrogen on platinum electrodes in acidic solutions, considers the effect of indirect adsorbate-adsorbate interactions on adsorption isotherms. Due to these interactions, the heat of adsorption of all molecules in the layer decreases with coverage linearly rather than logarithmically as in the Freundlich model (Aharoni and Sparks, 1991, Aharoni and Ungarish, 1977). In a word, the heat of adsorption of all molecules in the layer decreases linearly with coverage due to adsorbate-adsorbent interactions. The Temkin model is given as

$$Q_e = \frac{RT}{B_T} Ln(A_T C_e),$$

where A_T (L/g) is the Temkin isotherm equilibrium binding constant; Q_e (mg/g) is the amount of adsorbate adsorbed by per unit weight of adsorbent; C_e (mg/L) refers to the concentration of adsorbate remaining in the solution in equilibrium; R (8.314 J/mol·K) is the universal gas constant, and T (K) is the absolute temperature. RT/B_T is also expressed as B (J/mol), which is a constant related to the heat of adsorption.

D-R isotherm

Assuming that binding sites on the surface of a biosorbent are non-identical instead of being homogenous as in the Langmuir isotherm, Dubinin and Radushkevich (1947) presented the D-R equation as

$$Q_e = Q_m \exp(-\beta[RTLn(1+\frac{1}{C_e})]^2),$$

where Q_m (mg/g) represents the theoretical monolayer saturation capacity; Q_e (mg/g) is the amount of adsorbate adsorbed by per unit weight of adsorbent; C_e (mg/L) is the concentration of adsorbate remaining in the solution in equilibrium; R (8.314 J/mol·K) is the universal gas constant, and β (mol^2/kJ^2) is the D-R isotherm constant related to adsorption energy.

R-P isotherm

The three-parameter R-P model first developed by Redlich and Peterson (1959) was modified to incorporate characteristics of the Langmuir and Freundlich isotherms (Jossens et al., 1978). It can be depicted as

$$Q_e = \frac{K_R C_e}{1 + a_R C_e^{b_R}},$$

where K_R (L/g), a_R (L/mmol), and b_R ($0 < b_R \leqq 1$) are R-P isotherm constants; Q_e (mg/g) is the amount of adsorbate adsorbed by per unit weight of adsorbent, and C_e (mg/L) is the concentration of adsorbate remaining in the solution in equilibrium. This equation reduces to Henry's law at low concentrations ($b_R = 0$), and to the Langmuir model when b_R equals to 1. In the case where the value of $a_R C_e^{bR}$ is much bigger than 1, the R-P isotherm approaches the Freundlich isotherm.

Sips isotherm

The Sips isotherm (as known as the Langmuir-Freundlich isotherm) is a combination of the Langmuir and Freundlich isotherms (Sips, 1948). It describes heterogeneous adsorption surface and circumvents the limitation of the Freundlich equation for increasing adsorbate concentrations (Gunay et al., 2007). It is expressed as

$$Q_e = \frac{Q_m b C_e^{1/n}}{1 + b C_e^{1/n}},$$

where b (L/mg) is the Sips equilibrium constant; $1/n$ (0-1) is the heterogeneity factor; Q_e (mg/g) refers to the amount of adsorbate adsorbed by per unit weight of adsorbent, and C_e (mg/L) is the concentration of adsorbate remaining in the solution in equilibrium. Values of $1/n$ close to 0 reveal heterogeneous adsorbents, whereas values close to 1 indicate homogenous surfaces of adsorbents. The Sips isotherm effectively reduces to the Freundlich isotherm at low adsorbate concentrations and thus does not obey Henry's law. At high concentrations, it predicts a monolayer adsorption capacity characteristic of the Langmuir isotherm (Ho et al., 2002).

2.6.2. Biosorption kinetics

The kinetic aspect of a biosorption process plays an important role in its scaling-up and the design of biosorption systems. In general, a biosorption process consists of four stages: (1) adsorbate transfers from the bulk solution to the boundary film bordering the biosorbent surface; (2) adsorbate transports from the boundary film to the biosorbent surface; (3) adsorbate transfers from the biosorbent surface to the intraparticle binding sites; and (4) interactions of the adsorbate with the available binding sites (McKay, 1984). Determination of the time course of heavy metal biosorption in kinetic studies can provide a window to the steps of heavy metal sequestration. Besides, biosorption kinetic studies are always carried out at different temperatures for thermodynamic insights (Ben-Ali et al., 2017). A number of kinetic equations, including the pseudo-first-order, pseudo-second-order,

intraparticle diffusion and fractional power equations, are usually used to simulate kinetic data for a better understanding of biosorption behaviors.

Pseudo-first-order kinetics

The pseudo-first-order kinetic equation, also known as the Lagergren's rate equation, illustrates that the rate of adsorption is proportional to the quantity of unoccupied sites on an adsorbent (Lagergren, 1898). It can be written as

$$Q_t = Q_e(1 - e^{-k_1 t}),$$

where Q_e and Q_t (mg/g) are respectively the amounts of adsorbate adsorbed in equilibrium and at time t (min), and k_1 (min^{-1}) is the Lagergren equilibrium rate constant.

Pseudo-second-order kinetics

The pseudo-second-order kinetic equation is based on the assumption that adsorption rate is positively correlated to the square of the number of unoccupied sites upon an adsorbent (Schiewer and Patil, 2008). It is expressed as

$$Q_t = \frac{Q_e^{\,2} k_2 t}{1 + Q_e k_2 t},$$

where Q_e and Q_t (mg/g) are respectively the amounts of adsorbate adsorbed in equilibrium and at time t (min), and k_2 (g/mg·min) is the equilibrium rate constant of the pseudo-second-order equation (Ho and McKay, 1999).

Intraparticle diffusion kinetics

The intraparticle diffusion model proposed by Weber and Morris (Weber and Morris, 1963) was applied for the modeling of kinetic data to predict steps of diffusion in an adsorption process. It is given as

$$Q_t = k_{int} t^{1/2} + C ,$$

where Q_t (mg/g) is the amount of adsorbate adsorbed at time t (min); k_{int} is the intraparticle diffusion rate constant, and C is the intercept related to the thickness of the boundary layer. If an adsorption process only follows intraparticle diffusion, the plot of Q_t versus $t^{1/2}$ will be a straight line. In an adsorption process comprising two or more steps, however, multi-linear plots will be obtained.

Fractional power kinetics

The fractional power model, which is modified from the Freundlich equation (Dalal, 1974), is expressed as

$$Q_t = kt^{v} ,$$

where Q_t (mg/g) is the amount of adsorbate adsorbed at time t (min); k and v (< 1) are fractional power kinetic constants, and kv is a constant representing the specific adsorption rate at unit time (Ho and McKay, 2002).

2.6.3. Biosorption thermodynamics

An adsorption process, taking biosorption of heavy metal ions as an example, can be regarded as a reversible reaction as

Heavy metal ions in solution ⇌ Heavy metal ions bound on biosorbent

The thermodynamic study of a biosorption process is to estimate the values of the Gibbs free energy change (ΔG^0), enthalpy change (ΔH^0) and entropy change (ΔS^0), and such that to disclose the thermodynamic nature of biosorption. The thermodynamic analysis of a biosorption process is usually based on the values of the equilibrium constant, K_D (also known as the distribution coefficient), which is a constant describing the adsorption/desorption equilibrium for each reactant in contact with a surface, at different temperatures (Khani et al., 2008, Sari and Tuzen, 2008). On the basis of the equilibrium biosorption capacities at 293, 303, 313 and 323 K, Sari and Tuzen (2008) computed that Pb(II) and Cd(II) biosorption on *Ulva lactuca* biomass was spontaneous and exothermic (enthalpy-driven) under the examined conditions, with a more negative value of ΔG^0 at a lower temperature. Given that the Langmuir isotherm describes the fraction of surface that is covered by adsorbate molecules at a particular temperature and pressure, the Langmuir isotherm constant (K_L) is considered analogous to K_D and used for thermodynamic calculations in some biosorption studies (Gupta and Rastogi, 2008, Padmavathy, 2008). The negative ΔG^0, positive ΔH^0 and positive ΔS^0 estimated in the Pb(II) biosorption by green algae *Spirogyra* biomass revealed that the biosorption process was spontaneous and endothermic, and the randomness at the solid-liquid interface increased after Pb(II) fixation on the biosorbent surface (Gupta and Rastogi, 2008).

2.7. Biosorption mechanism

2.7.1. Potential underlying mechanism

In a biosorption process, an adsorbate is usually sequestered by a biosorbent via a variety of forces, making complete elucidation of the biosorption mechanism challengeable. To date, electrostatic attraction, ion exchange, complexation and microprecipitation have been identified as the common underlying mechanisms that govern the processes of heavy metal biosorption.

Electrostatic attraction

Electrostatic attraction is a non-specific force that weakly attracts the target ions/molecules. A biosorbent with a negatively charged surface is capable of binding heavy metal cations and other positively charged contaminants. The surface charge of a biosorbent is associated to the organic functional groups it possesses. For instance, deprotonation of functional groups such as carboxyl and hydroxyl groups will lead to a negative surface charge, whereas the protonation of amine groups may result in a positive surface charge. Therefore, the characteristics and strength of the surface charge of a biosorbent are dependent on the biosorbent composition and the pH of the biosorption system. Ogi et al. (2016) reported that the positively charged *Escherichia coli* (*E. coli*) biomass efficiently removed tungsten anions, and the biosorption performance was improved when the zeta potential of *E. coli* was increased by heat treatment. Moubarik et al. (2015) observed that the zeta potential of olive stone and bagasse changed from positive to negative and became more negative when the pH increased from 2.0 to 12.0. Along with this change, the biomass exhibited higher and higher affinity to Cd(II) ions.

Ion exchange

Ion exchange is a process in which the binding of one or several ionic species onto a material is accompanied by the simultaneous desorption/displacement of an equivalent amount of one or more ionic species. It is the fundamental principle on which the commercial ion-exchange resins are based. The ion-exchange characteristics of most biological materials, including microbial biomass, agro-waste and fruit waste materials, have been intensively investigated and confirmed (Hackbarth et al., 2015, Liu et al., 2012a, Pozdniakova et al., 2016, Reddy et al., 2014). It has been well established that divalent metal ions (shown as M^{2+}) exchange with counter-ions, e.g., naturally occurring alkali and alkali earth metal ions like Na^+, K^+, Ca^{2+} and Mg^{2+} (termed as "light metal ions" in this study), from functional groups of polysaccharides. The reaction is shown in Eq. 2.5 with alginic acid (ALG) as an example (Volesky, 2003).

$$2NaALG + M^{2+} \rightarrow M(ALG)_2 + 2Na^+ \quad (2.5)$$

To investigate whether ion exchange is involved in a biosorption process, the release of light metal ions such as Na^+, K^+, Ca^{2+} and Mg^{2+} during the biosorption process is required to be monitored. Some studies reported the participation of a light metal ion in the ion exchange based on its loss from the biosorbent surface by spectroscopic measurements (Maresova et al., 2011, Panda et al., 2006), or its release into the liquid phase during the biosorption process (Girardi et al., 2014). However, the spontaneous dissolution of light metal ions from biosorbents into aqueous solutions might be overlooked; their natural release other than the repulsion from adsorbates must be considered.

Complexation

Complexation and coordination, which refer to the formation of a covalent bond in which the two shared electrons are from only one of the two atoms linked by it, are frequently used as synonyms. Strictly speaking, however, they are not identical since the latter also involves metal-free compounds (e.g., the combination of trimethylamine with phosphorous fluoride) (Volesky, 2003). In this sense, complexation is used instead of coordination to describe the interactions between heavy metals and biosorbents in the present study. It is an important underlying mechanism in heavy metal biosorption, as heavy metal ions can contribute unoccupied orbitals to the lone pairs of electrons of O, N or S in the functional groups on the biosorbent surface. Liang et al. (2010) found that the removal of Cu(II), Cd(II), Pb(II), Zn(II) and Ni(II) by orange peel xanthate was attributed to the formation of complexes between the empty orbitals of the heavy metals and the lone pairs of electrons of S or N in the orange peel xanthate.

Microprecipitation

Microprecipitation of heavy metal ions can occur due to the deviation of the local conditions (e.g., changes in pH or presence of certain substances) on the biosorbent surface. Microprecipitation can significantly contribute to heavy metal removal, as metal microprecipitates are collected by biosorbents and thus immobilized and separated from aqueous solutions (Volesky, 2003). In a Cr K-edge X-ray absorption near edge structure (XANES) spectroscopic study on Cr(VI) biosorption by coconut coir, a portion of Cr(III) reduced by the biomass was found to be precipitated as Cr(III) hydroxides on the biomass surface (Shen et al., 2010).

Table 2.3 lists a number of mechanistic studies of heavy metal biosorption in the literature. Accordingly, biosorption of heavy metal ions by fruit waste materials is usually governed by ion exchange, electrostatic attraction, and/or complexation. This should be ascribed to the presence of charge and unoccupied orbitals in heavy metal ions. Reduction is also likely to be involved in Cr(VI) biosorption, in which a part of Cr(VI) is first reduced to Cr(III) and then sequestered by biosorbents through the aforementioned biosorption mechanisms (Chand et al., 2009, Park et al., 2008, Pehlivan and Kahraman, 2012). Notably, carboxyl and hydroxyl groups were frequently identified as the active functional groups providing binding sites to heavy metal ions.

Table 2.3 Proposed mechanisms of heavy metal biosorption by fruit waste materials.

Biosorbent	Heavy metal	Proposed mechanism	Active functional group	Reference
Grapefruit peel	Cd(II)	Ion exchange	Carboxyl, amine, hydroxyl	(Schiewer and Iqbal, 2014)
Banana peel	Cd(II)	Ion exchange	Carboxyl	(Memon et al., 2008)
Citrus maxima peel Passion fruit shell	Cu(II), Cd(II), Ni(II), Pb(II)	Complexation, ion exchange	Carboxyl, hydroxyl	(Chao et al., 2014)
Garcinia mangostana L. shell	Pb(II), Cd(II), Co(II)	Ion exchange	Carboxyl, amino, hydroxyl, ester	(Zein et al., 2010)
Mango peel	Cd(II), Pb(II)	Ion exchange	Carboxyl, hydroxyl	(Iqbal et al., 2009a)
Cucumis melo seed	Pb(II)	Electrostatic attraction, ion exchange	Carboxyl	(Akar et al., 2012)
Ponkan peel	Pb(II)	Electrostatic attraction, coordination	Carboxyl	(Pavan et al., 2008)
Sour orange residue	Cu(II)	Complexation, ion exchange, electrostatic attraction	Carboxyl, hydroxyl	(Khormaei et al., 2007)
Grapefruit peel	Ni(II), Zn(II)	Ion exchange	Carboxyl, hydroxyl	(Iqbal et al., 2009b)
Orange waste	Zn(II)	Ion exchange	Carboxyl, hydroxyl	(Perez Marin et al., 2010a)

Banana peel	Cr(VI)	Reduction, complexation	Amino, carboxyl, sulfonate, thiol, phenolic	(Park et al., 2008)
Osage orange peel	Cr(VI)	Electrostatic attraction, ion exchange, complexation, reduction	Polyphenyl, carboxyl, alcoholic, carbonyl	(Pehlivan and Kahraman, 2012)
Garcinia cambogia rind	As(III)	Complexation	Carboxyl	(Kamala et al., 2005)

2.7.2. Techniques for mechanistic studies

To elucidate the underlying mechanism of a biosorption process, characterization of the biosorbent is indispensable. Generally, the characterization includes structural analysis, elemental analysis and phase analysis (a phase is a specific chemistry and atomic arrangement). A variety of analytical tools, including SEM-EDX for structural and elemental analysis, PXRD for structural analysis, FTIR and solid-state NMR spectroscopy for phase analysis, and XPS for elemental and phase analysis, have been used in the characterization of biomaterials. In general, the characterization of a biosorbent before and after heavy metal biosorption can examine the changes in structure, elemental composition, and phase of the biosorbent caused by the interaction with heavy metal ions. This will provide important insights into the binding sites and mechanisms involved in the biosorption process.

SEM-EDX

SEM-EDX has been widely used in the surface analysis of biosorbents since it can visualize morphological structure, determine elemental composition and trace elemental distribution through a rapid, inexpensive and non-destructive approach (Fontana et al., 2018, Mende et al., 2016, Oliveira et al., 2014, Pugazhendhi et al., 2018, Remenarova et al., 2012). High resolution images of surface morphology are produced by scanning the sample surface with a highly focused electron beam, which enters the surface and interacts with the atoms in the sample. The excited atoms emit low-energy secondary electrons, whose intensity is correlated to the surface morphology (Stokes, 2008). In this way, images displaying the sample

surface can be created by scanning the sample and collecting the emitted secondary electrons. Backscattered electrons, namely beam electrons back-scattered out of the sample by elastic scattering interactions with atoms in the sample, are also used to reflect the contrast between areas with distinct chemical compositions since heavy elements can backscatter electrons more strongly than light elements. Its intensity, which is dependent on the atomic number of the element from which the beam electrons are back-scattered, can provide qualitative elemental information of the sample. Quantitative elemental information can be obtained via EDX analysis of characteristic X-rays, which are emitted from the sample surface as the electron beam removes an inner shell electron in the sample, and a higher-energy electron subsequently fills the shell and releases energy (Goldstein et al., 2017). Fontana et al. (2018) observed a rigid structure of brewing waste with an irregular surface by using SEM, and they found regular pores in the cross-section of the biomass. The EDX spectra showed reduced amounts of light metals (i.e., Na, Ca and Mg) in the biomass after Fe and Mn biosorption. Mende et al. (2016) reported the formation of crystal-like structures in needle shape on the chitosan surface after exposing chitosan to $CuSO_4$ and $FeSO_4$ solutions. The uneven distribution of Fe on the chitosan surface detected by X-ray mapping implied partially adsorbed iron oxide due to the rapid oxidation of Fe(II) in the air. SEM-EDX analysis revealed the simultaneous entrapment of metal cations and sulfate anions by chitosan (Mende et al., 2016).

PXRD

PXRD is a non-destructive and rapid analytical technique used for phase identification and crystallinity measurement of materials. When an X-ray is targeted on a crystalline material, it diffracts in a pattern characteristic of the structure of the material. By scanning the material through a range of 2θ (the angle of the detector), all possible diffraction directions can be attained given the random orientation of powdered materials (Jenkins and Snyder, 1996). Unlike single-crystal XRD that focuses on an individual crystal, PXRD looks at a powder material as a bulk characterization method. The PXRD pattern, which plots the intensity of the diffracted X-ray against 2θ, is a sum of the diffraction patterns produced by each individual phase in a mixture. Given that most materials have unique diffraction patterns, compounds can be identified by referring to the database of diffraction patterns. Hence, the PXRD pattern is considered a fingerprint that helps figure out what is in a given sample, and also the phase and crystallinity. Le Troedec et al. (2008) employed PXRD to assess the effect of various chemical treatments on the crystallinity of hemp fibers. The wide applications of PXRD in the characterization of biomaterials, e.g., eggplant leaves (Yuvaraja et al., 2014), wheat straw (Tian et al., 2011), grape bagasse (Farinella et al., 2007), and tree bark (Reddy et al., 2011), indicated the amorphous nature of most biomaterials with broad reflections in their diffraction patterns.

FTIR spectroscopy

FTIR spectroscopy, which collects the infrared spectrum of absorption of a material over a wide spectral range, is widely employed for qualitative characterization of functional groups in biosorbents (Fontana et al., 2018, Oliveira

et al., 2014). The term Fourier-transform refers to the mathematical process of Fourier transform used in this analytical technique to convert raw data into a final spectrum. The spectrum is formed based on how much of the light is absorbed at each wavelength. Given that the wavelength at which absorption occurs is characteristic to a functional group, the functional groups contained in a sample can be recognized accordingly. Furthermore, the active ones involved in the biosorption process can be inferred by collecting the FTIR spectra of the biosorbent before and after exposure to the adsorbate. For instance, FTIR analysis of an apple pomace-derived biosorbent with and without Cd(II) loading suggested the involvement of ester, carboxyl, and amine groups in Cd(II) biosorption (Chand et al., 2014). The participation of carboxyl and hydroxyl groups in the entrapment of crystal violet by grapefruit peels (Saeed et al., 2010), and that of C=O groups in azo dye biosorption by *Citrus sinensis* were also reported based on FTIR analysis (Asgher and Bhatti, 2010). Due to its easy operation and low cost, FTIR spectroscopy is the most widely used spectroscopic method in biosorbent characterization in the literature. However, it is very difficult to determine a detailed biosorption mechanism by using FTIR analysis alone (Lalhmunsiama et al., 2017).

XPS

XPS is a versatile and sensitive surface analysis technique for compositional and chemical states analysis (Oliveira et al., 2014). A sample is irradiated by a beam of X-rays, and the quantity and kinetic energy of electrons ejected from the sample surface (0-10 nm) are analyzed to determine the binding energy, which is element-specific and allows chemical characterization of the sample. After spectral

collection, deconvolution of an XPS spectrum is performed to categorize the diverse functional groups of a specific element, e.g., ligands of C 1s, O1s, or N 1s. Not only being capable of examining the elemental composition and functional groups of a biosorbent qualitatively and quantitatively, XPS can also provide useful insights into the biosorption mechanism (Chen and Yang, 2006, Lim et al., 2008, Oliveira et al., 2014). Oliveira et al. (2014) employed XPS to characterize the *Sargassum* sp. biomass before and after La(III) biosorption, and a variety of C groups (e.g., C-C, C-O, C=O/O-C-O, and COO^-), O groups (e.g., La-O and C=O), and N groups (e.g., NH_2 and NH_3^+) were identified. The significant reduction of the amount of Ca after La(III) biosorption suggested the occurrence of ion exchange between Ca(II) and La(III) for the binding sites during the biosorption process (Oliveira et al., 2014).

Solid-state NMR spectroscopy

Despite the well-established technology of liquid-state NMR spectroscopy, the most appropriate samples for the analysis of molecular structure are solid in many situations, especially in environmental studies. Solid-state NMR spectroscopy provides a means to analyze a sample in its natural state via a noninvasive manner. In liquid-state NMR spectroscopy, the spectral lines are sharp given that the anisotropic NMR interactions are averaged by rapid random tumbling. In contrast, solid-state NMR spectra are very broad due to the effect of anisotropic (orientation-dependent) interactions in solid samples (Pavia et al., 2008). Despite the challenges in spectral analysis, the broad lines produced in solid-state NMR spectroscopy conceal crucial information on the chemistry, structure, and dynamics

of the targeted sample. A variety of techniques, e.g., cross polarization (CP) and magic angle spinning (MAS), are frequently employed in solid-state NMR spectroscopy for better resolution and higher signal/noise ratio. Superior to the common spectroscopic techniques (e.g., FTIR spectroscopy and XPS), solid-state NMR spectroscopy can provide information on the magnetically distinct atoms of the functional group being studied. In the literature, it has been used for profiling pollens and planktonic biomass (Komatsu et al., 2015, Zhang et al., 2016). Furthermore, Habets et al. (2013) investigated the effects of thermochemical treatments on the composition of wheat straw using ^{13}C and ^{1}H solid-state NMR spectroscopy, and they found that hemicellulose, acetyl groups, and ash minerals were removed via aquathermolysis. It is noteworthy that the limitations of solid-state NMR spectroscopy (e.g., chemical shift anisotropy and dipole-dipole coupling) often lead to the overlap of isotropic chemical shifts, making it difficult to distinguish the magnetically distinct atoms (e.g., C atoms in pectin and cellulose) (Ren et al., 2016). Also, the high cost and complexity of operation and spectral analysis restrict the wide application of solid-state NMR spectroscopy in biosorption studies.

The aforementioned techniques are always complementary in biosorbent characterization and mechanistic elucidation. Although solid-state NMR spectroscopy has emerged as a robust tool to provide unprecedented information regarding molecular structures and interactions, it is not yet powerful enough to take the place of FTIR spectroscopy and XPS. For instance, most of the solid-state NMR studies on biomaterials only collect the ^{13}C spectra because of the stringent requirements on the element being studied. In this case, FTIR spectroscopy and

XPS can supplement information about the functional groups based on O and N atoms. Beyond the aforementioned techniques, there are also some other methods that can be helpful in disclosing biosorption mechanisms. For example, zeta potential measurement can examine the surface electric properties of biosorbents and provide insights into the contribution of electrostatic interaction in biosorption processes. Besides, chemical methods, e.g., ion exchange experiment, are crucial to investigate the role of the ion exchange with naturally occurring light metal ions (e.g., Na^+, K^+, Mg^{2+} and Ca^{2+}) in heavy metal biosorption. The utilization of diverse techniques and methods makes the complete elucidation of a biosorption process possible.

2.8. Desorption of heavy metal

Efficient desorption of the sequestered adsorbate is essential to improve the cost-effectiveness of a biosorption process via adsorbate recovery and biosorbent regeneration. A desirable desorption process should be able to recover the adsorbates and regenerate the adsorbents to conditions similar to the original forms (Volesky, 2001). This is highly dependent on the selection of desorbing agents, which are expected to be non-destructive, mild and efficient. As summarized in Table 2.4, dilute acids and alkalis, mineral salt solutions, and complexing agents are the most frequently employed desorbing agents in the desorption of heavy metals from fruit-waste-derived biosorbents.

As the most common desorbing agents with easy access and low cost, mineral acids, e.g., HCl, HNO_3 and H_2SO_4, desorb sequestered adsorbates via proton exchange (Abdolali et al., 2015). Yet, mineral acids may destroy the biosorbent surface to some extent, resulting in the often-observed impaired biosorption capacities of regenerated biosorbents. Organic acids such as acetic acid and citric acid are usually biocompatible and environmentally friendly alternatives without deteriorating the surface structure of biosorbents to allow subsequent reuse. This merit makes organic acids irreplaceable in some desorption situations in spite of the relatively high cost (Jing et al., 2007). Mineral salt solutions, including $CaCl_2$, $Ca(NO_3)_2$, NaCl, $NaHCO_3$ and other salt solutions, are also used as desorbing agents through supplying competing cations for ion exchange with the bound adsorbates. Meanwhile, anions present in salt solutions, e.g., HCO_3^-, CO_3^{2-}, Cl^- and SO_4^{2-}, can form metal complexes with heavy metal ions, and such that they can destabilize the biosorbent-metal complex and entrap the bound heavy metal ions

(Stirk and van Staden, 2002). Still, this type of desorbing agents seems not suitable when recovery of adsorbates (e.g., precious metals and radioactive elements) is expected. A number of strong metal complexing agents, e.g., ethylenediaminetetraacetic acid (EDTA), are also employed to capture the sequestered heavy metals from biosorbents through complexation (Koduru et al., 2013, Njikam and Schiewer, 2012). However, the higher cost of complexing agents than mineral acids and salts limits their applications in desorption studies.

Taken together, mineral acids are the most popular desorbing agents for desorption of heavy metals (Table 2.4). One hundred percent of Cd(II) was recovered by using 0.1 M HCl, 0.1 M H_2SO_4 or 0.05 M HNO_3 from Cd(II)-loaded banana peels (Memon et al., 2008). Besides, two adsorption-desorption cycles were achieved by using 0.1 M HCl as the desorbing agent to recover Pb(II) from Pb(II)-loaded passion fruit peels (Gerola et al., 2013). There was even an increase in the Cu(II) uptake by a regenerated gooseberry fruit with 0.1 M HCl as the desorbing agent; the increase could be due to the activation of more surface sites after contact with 0.1 M HCl (Rao and Ikram, 2011). Njikam and Schiewer (2012) observed more efficient Cd(II) desorption from citrus peels by using $Ca(NO_3)_2$ than HNO_3, but the Cd(II) biosorption capacity of the regenerated biosorbent treated by HNO_3 was similar to that of the original biosorbent and considerably higher than that of the $Ca(NO_3)_2$-treated one. This implies that both the desorption efficiency and the regeneration ability of the biosorbent should be considered when selecting a suitable desorbing agent. Occasionally, desorption of adsorbates and regeneration of biosorbents require different agents. Abdolali et al. (2015) used $CaCl_2$ after the desorption process (HCl as the desorbing agent) to improve the stability and

reusability of a multi-metal binding biosorbent, which was a mixture of mandarin peels, tea waste and maple leaves. The use of $CaCl_2$ could repair the damage caused by HCl and exchange the protons to provide accessible binding sites to heavy metal cations in the subsequent biosorption cycles (Abdolali et al., 2015).

Table 2.4 Desorbing agents used for heavy metals desorption from fruit waste materials.

Heavy metal	Biosorbent	Desorbing agent	S/L (g/L)	Time (h)	DE (%)	Reference
Cd(II)	Banana peel	0.005 M HNO_3	20	0.5	100	(Memon et al., 2008)
		0.01 M HCl			100	
		0.01 M H_2SO_4			100	
Cd(II)	Grapefruit peel	0.01 M HNO_3	1	1.67	100	(Njikam and Schiewer, 2012)
		0.1 M $Ca(NO_3)_2$	1	24	90	
	Orange peel	0.001 M Na_2EDTA	1	24	100	
		0.001 M S,S-EDDS	1	1.67	100	
Cd(II)	Mango peel	0.1 M HCl	20	1	98.2	(Iqbal et al., 2009a)
Pb(II)					99.1	
Ni(II)					95.8	
Cu(II)	Gooseberry fruit residue	0.1 M HCl	10	24	>80	(Rao and Ikram, 2011)
Cu(II)	*Prunus persica* L. stone	0.1 M HCl	10	2	98.64	(Lopicic et al., 2017)
		0.1 M HNO_3	10	2	96.96	
		0.1 M CH_3COOH	10	2	77.70	
Cu(II)	Sour orange residue	0.1 M HCl	2	1	99	(Khormaei et al., 2007)
Pb(II)	Passion fruit peel	0.1 M HCl	NA	NA	91.1	(Gerola et al., 2013)
Ni(II)	*Citrus limetta* peel	0.05 M HCl	8	1	96.56	(Singh and Shukla, 2017)

(**Notes:** DE - Desorption efficiency; NA - Not available.)

2.9. Biosorption in a continuous mode

In the literature, a sizable portion of biosorption studies was based on the batch mode for optimization of operational conditions and desorption. Yet, a packed bed column reactor is more practically and commercially viable as this type of reactor has been widely used in industries which employ ion exchange resins or other commercial adsorbents (Chatterjee and Schiewer, 2011). The setting up of a laboratory-scale packed bed column reactor is an indispensable procedure to evaluate the practicability of the biosorbent being studied. Glass (Castro et al., 2011, Long et al., 2014, Lopez-Garcia et al., 2013, Martin-Lara et al., 2012, Sivasankara et al., 2010) and clear acrylic columns (Chatterjee and Schiewer, 2011, Perez Marin et al., 2010a) are usually used for establishing continuous biosorption systems. To avoid column blocking caused by the swelling of biosorbents, "wet packing" is usually employed to pack already wet biosorbents inside the column reactor. Both upward flow (Chatterjee and Schiewer, 2011, Martin-Lara et al., 2012) and downward flow (Jin et al., 2018, Long et al., 2014) are adopted in continuous biosorption experiments in column reactors. A number of studies on the effects of operational parameters on the performance of column reactors have found that higher bed height, lower flow rate and influent concentration can lead to longer breakthrough and exhaustion time in packed bed column reactors (Chatterjee and Schiewer, 2011, Jin et al., 2018, Long et al., 2014). To achieve a high biosorption efficiency and ensure the effluent can meet the discharge limit, several identical packed bed column reactors can be connected for a high enough bed height (Chatterjee and Schiewer, 2011).

In column studies, a breakthrough curve, which corresponds to the plot of the adsorbate concentration in effluent against time, is examined to evaluate the adsorption performance of a packed bed column reactor. Sometimes it is also expressed as a plot of the relative concentration (the ratio of the adsorbate concentration in effluent to that in influent) against bed volume (BV). To predict the dynamic behavior occurring in a column and allow some kinetic coefficients to be estimated, the Thomas, Bohart-Adams, Dose-Response and Yoon and Nelson models are frequently used to simulate breakthrough curves (Calero et al., 2009).

Thomas model

The Thomas model is the most widely applied model in column studies (Thomas, 1948). It has the following form of

$$\frac{C_t}{C_0} = \frac{1}{1+\exp[\frac{k}{Q}(q_0 M - C_0 V)]},$$

where C_t and C_0 (mg/L) refer to the adsorbate concentrations in effluent and influent, respectively; k (mL/min·mg) is the Thomas rate constant; q_0 (mg/g) is the maximum loading capacity of adsorbate on adsorbent; M (g) is the mass of adsorbent in the column reactor; V (mL) is the throughput volume, and Q (mL/min) is the volumetric flow rate. The Thomas model assumes that the adsorption process follows the pseudo-second-order rate law, fits to the Langmuir isotherm in equilibrium, and holds a plug flow without dispersion in the column reactor being studied (Thomas, 1948).

Bohart-Adams model

The Bohart-Adams model was developed based on the surface reaction theory to describe the relationship between C_t/C_0 and t in a continuous system for gas adsorption onto solids (Bohart and Adams, 1920). However, it has been extensively used in other types of adsorption systems. This model assumes that equilibrium is not instantaneous, and thus the rate of an adsorption process is proportional to the adsorption capacity that still remains on the adsorbent (Goel et al., 2005). The Bohart-Adams model is expressed as

$$\frac{C_t}{C_0} = \frac{1}{1+\exp(\frac{k_{BA}N_0Z}{\mu} k_{BA}C_0t)} ,$$

where C_t and C_0 (mg/L) refer to the adsorbate concentrations in effluent and influent, respectively; N_0 (mg/L) is the equilibrium volumetric sorption capacity; k_{BA} (L/h/mg) is the Bohart-Adams rate constant; Z (cm) refers to the bed height, and u (cm/h) is the linear flow velocity. It assumes an irreversible adsorption process and an ideal plug flow in the column reactor being studied.

Dose-Response model

The Dose-Response model, which is commonly used in pharmacology, has been frequently applied to illustrate adsorption in column reactors (Calero et al., 2009). This model is presented as follows,

$$\frac{C_t}{C_0} = 1 - \frac{1}{1+(\frac{t}{\gamma})^{\alpha}} ,$$

where C_t and C_0 (mg/L) refer to the adsorbate concentrations in effluent and influent, respectively; α is the constant of the Dose-Response model, and γ is the constant

representing the time when the adsorbate concentration in effluent reached 50% of that in influent (C_t/C_0 = 50%). The Dose-Response model is an empirical model with a zero value of C_t/C_0 at time zero (Yan et al., 2001).

Yoon and Nelson model

The Yoon and Nelson model was initially developed for adsorption of gases or vapors into activated coal (Calero et al., 2009). It is in the form of

$$\frac{C_t}{C_0} = \frac{1}{1+\exp(k_{YN}(\tau - t)}\ ,$$

where C_t and C_0 (mg/L) are the adsorbate concentrations in effluent and influent, respectively; k_{YN} (min^{-1}) is the Yoon and Nelson's proportionality constant, and τ (min) is the time required for retaining 50% of the initial adsorbates.

3. Materials and Methods

3.1. Chemicals

The Pb(II) and Cd(II) solutions were respectively prepared by dissolving metal salts, i.e., $Pb(NO_3)_2$ and $Cd(NO_3)_2 \cdot 4H_2O$, in distilled deionized (DDI) water in the desirable concentrations. Other solutions of cationic heavy metal ions (e.g., Cu(II), Zn(II), Ni(II) and Cr(III)) used in this study were also prepared in DDI water using the corresponding metal nitrate salts. Solutions of HCl and NaOH at 0.5 M and 1.0 M were used for pH adjustment. Sodium nitrate was employed to adjust the ionic strength of the biosorption systems to investigate the effect of ionic strength. In determination of metal concentrations, the standard solutions and samples were diluted to the desirable concentrations by using 1% HNO_3 (trace metal grade) prepared in Milli Q water. All chemicals and reagents used in this study were of analytical grade.

3.2. Preparation of biosorbents

A number of abundant fruit waste materials, including green pomelo peel, yellow pomelo peel, dragon fruit peel, watermelon rind (WR), and mango seed (MS), were tested for Pb(II) and Cd(II) removal in the preliminary studies (results not shown). WR and MS were screened out for subsequent biosorption studies because of their superior Pb(II) and Cd(II) biosorption capacities as compared with other fruit waste materials.

Native WR and MS without any pretreatment were prepared as biosorbents in this study for easy operation and low cost. As shown in Figure 3.1, WR and MS (including the mango seed shell and kernel) collected from a local market were first washed by tap water to remove the flesh residues and dusts. Then they were cut into small pieces and washed by DDI water before drying in a laboratory-scale oven at 333 K for 24 h. Subsequently, the dried biomaterials were ground using an electronic blender. Particles in the size distributions of < 180 μm, 180-500 μm and 500-1000 μm were collected by using sieves with the corresponding particle sizes and stocked in sealed polypropylene containers at 277 K. WR and MS smaller than 180 μm were used in the biosorption studies in the batch mode and mechanistic studies unless otherwise stated.

Figure 3.1 Preparation of WR and MS biosorbents from raw fruit waste materials.

3.3. Instrumentations

The biosorption operations in a batch mode are schematically described in Figure 3.2. Biosorbents were dispersed in Pb(II)/Cd(II) solutions in biosorption reactors made of polypropylene, and the reactors were placed in a thermostat orbital shaker at 250 rpm (at room temperature for 24 h unless otherwise stated). The pH of the biosorption systems was periodically measured and adjusted using a HCl or NaOH solution to maintain constant pH. When the biosorption equilibrium was reached, the suspensions were centrifuged at 4000 rpm for 10 min. The supernatants were acidified and subjected to determination of the concentrations of the residual Pb(II)/Cd(II) ions by inductively coupled plasma optical emission spectrometer (ICP-OES, Agilent 700 Series, USA). Inductively coupled plasma mass spectrometer (ICP-MS, Agilent 7500ce, USA) was used for the measurement of metal ions at lower concentrations (0-100 ppb). The quantity of Pb(II)/Cd(II) adsorbed was computed based on the mass balance between the initial and equilibrium concentrations of the heavy metal ions.

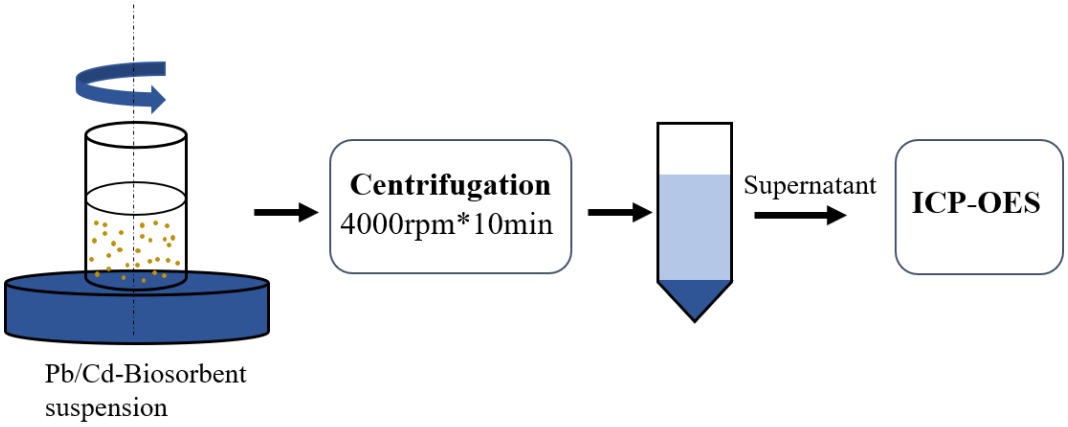

Figure 3.2 Schematic diagram of Pb(II)/Cd(II) biosorption operations in a batch mode.

3.4. Biosorption of Pb(II) and Cd(II) by WR

3.4.1. Effect of pH

A 0.015 g portion of WR was added into 50-mL polypropylene tubes containing 15 mL of Pb(II)/Cd(II) solutions at varying pH, i.e., 2.0-5.5 in Pb(II) biosorption and 3.0-7.5 in Cd(II) biosorption, to investigate the effect of pH. Two initial metal concentrations, 100 ppm and 500 ppm, were used in this study.

3.4.2. Effect of WR dosage

The effect of WR dosage was examined by applying 0.5, 1, 2, 3 and 5 g/L of WR into 15 mL of 500 ppm Pb(II)/Cd(II) solutions in 50-mL polypropylene tubes. The pH was maintained at 5.0 in the Pb(II) biosorption systems and 7.0 in the Cd(II) ones.

3.4.3. Effect of initial metal concentration

To unravel the effect of initial metal concentration, 0.015 g of WR was respectively dispersed into 50-mL polypropylene tubes containing 15 mL of Pb(II) solutions at 50, 100, 150, 250, 500, 750, 1000, 1250 and 1500 ppm, and 15 mL of Cd(II) solutions at 25, 100, 200, 300, 500, 750 and 1000 ppm. The pH was maintained at 5.0 in the Pb(II) biosorption systems and 7.0 in the Cd(II) ones.

3.4.4. Effect of ionic strength

By applying 0-0.2 M $NaNO_3$ into 15 mL of 500 ppm Pb(II)/Cd(II) solutions with 1.0 g/L WR in 50-mL polypropylene tubes, the Pb(II)/Cd(II) biosorption capacities of WR at different ionic strength were examined. The pH was maintained at 5.0 in the Pb(II) biosorption systems and 7.0 in the Cd(II) ones.

3.4.5. Effect of co-metal ions

Given that heavy-metal-bearing wastewater usually contains various types of heavy metal ions, the effect of co-metal ions, including Cu(II), Zn(II), Ni(II) and Cr(III) on Pb(II) and Cd(II) biosorption, was investigated in binary systems. A 0.015 g portion of WR was dispersed into 15 mL of metal solution containing Pb(II) and a co-metal ion, i.e., Cd(II), Cu(II), Zn(II), Ni(II) or Cr(III), at pH 5.0 (initial concentration of each heavy metal at 1 mM). In consideration of the optimal pH of 7.0 for Cd(II) biosorption by WR (see Section 4.1), at which Pb(II), Cu(II) and Cr(III) would be remarkably precipitated, only the effect of Zn(II) and Ni(II) on Cd(II) biosorption by WR at pH 7.0 was examined. The speciation of these types of heavy metals at a pH range of 5.0-7.5 was simulated by *Visual MINTEQ* 3.1 and shown in Figure A1 in Appendices.

3.4.6. Biosorption isotherms

The biosorption isotherm studies were carried out by respectively adding 0.015 g of WR into 50-mL polypropylene tubes containing 15 mL of Pb(II) solutions at 100-1500 ppm, and Cd(II) solutions at 25-1000 ppm. The pH was maintained at 5.0 in the Pb(II) biosorption systems and at 7.0 in the Cd(II) ones. Given the frequently reported bias in linear regression (Ho, 2006, Ho et al., 2005, Kumar, 2007, Vasanth Kumar, 2006), the six frequently used adsorption isotherm models, namely the Langmuir, Freundlich, Temkin, D-R, R-P and Sips equations, were non-linearly fitted to the equilibrium data to identify the best-fitting isotherm.

3.4.7. Biosorption kinetics

The kinetic information of a biosorption process is crucial for the design of the biosorption system. Pilot studies showed that Pb(II) and Cd(II) were entrapped by WR at a substantially high speed, with 94.4% of Pb(II) and 92.1% of Cd(II) biosorption finished in the first 5 min at an initial metal concentration of 500 ppm and a WR dosage of 1.0 g/L (Figure A2). Although the high biosorption speed is beneficial for practical applications, it makes the monitoring and analysis of the biosorption process as a function of time very difficult. Hence, a lower initial metal concentration (50 ppm) and WR dosage (0.5 g/L) were applied in the kinetic studies. Namely, 70 mL of WR solution at 1.5 g/L was mixed with 140 mL of 75 ppm Pb(II)/Cd(II) solution in a 500-mL polypropylene bottle, obtaining a biosorption system with an initial Pb(II)/Cd(II) concentration of 50 ppm and a WR dosage of 0.5 g/L. NaOH was constantly added to maintain the pH at around 5.0 in Pb(II) biosorption and 7.0 in Cd(II) biosorption. Besides, a magnetic stirrer, instead of an orbital shaker (as used in other biosorption studies), was applied for convenient sampling in short time intervals. In order to investigate the effects of temperature and biosorbent particle size on kinetics, Pb(II) and Cd(II) uptakes by WR were determined as a function of time at different temperatures (i.e., 278 K, 298 K and 310 K) and different particle sizes of WR (i.e., < 180 μm, 180-500 μm and 500-1000 μm). To examine the significance of constant pH to the biosorption processes, Pb(II) biosorption by WR at different temperatures were also carried out at initial pH of 5.0 without further pH adjustment as a comparison. The kinetic data were non-linearly simulated by the pseudo-first-order, pseudo-second-order, and fractional power equations. In addition, the intraparticle diffusion curves of the

Pb(II) and Cd(II) biosorption processes were also analyzed to disclose the different steps involved in the biosorption.

3.4.8. Desorption of Pb(II) and Cd(II) from WR

Desorption of the sequestered adsorbate is of crucial importance for concentrating the adsorbate as well as regenerating the biosorbent. To this end, HCl, HNO_3 and citric acid at 0.05 M and 0.1 M were tested as potential desorbing agents for Pb(II) and Cd(II) desorption from WR. Pb- and Cd-loaded WR were added to 15 mL acid solutions with a solid/liquid (S/L) ratio of 1.0 g/L. The flasks containing the suspensions were shaken at 250 rpm and 298 K for 3 h, and then centrifuged at 4000 rpm for 10 min to obtain the supernatants, which were subjected to the determination of the quantity of Pb(II)/Cd(II) desorbed by ICP-OES. The suspensions of Pb- and Cd-loaded WR in DDI water were used as the control groups. Additionally, the separated WR after centrifugation was washed by DDI water 3 times and used for resorption of Pb(II)/Cd(II) after drying in a laboratory oven at 333 K for 12 h.

In order to evaluate the relative significance of the different experimental factors and their possible interactions, and to optimize the desorption process, response surface methodology (RSM) with central composite design (CCD), was used for modeling and analyzing Pb(II) desorption by HCl from WR. *Design-Expert* (Version 10) was utilized in the experimental design and data analysis. In this study, desorption efficiency was the response variable, and S/L ratio, acid concentration, and time were the independent variables. The levels of factors are shown in Table 3.1. In the CCD, the total number of experiments is 2^k+2k+n_0, where

k is the number of independent variables, and n_0 is the number of repetitions of experiments at the center point. For statistical calculations, the experimental variables X_i have been coded as x_i according to the following transformation equation:

$$x_i = \frac{X_i - X_0}{\Delta X}$$

where x_i is the dimensionless coded value of the variable X_i; X_0 is the value of X_i at the center point, and ΔX is the step change (Muralidhar et al., 2001).

Table 3.1 Levels of factors used in CCD for optimization of desorption efficiency.

Variable	Label	Level					Δx
		-1.682 (-α)	-1	0	1	1.682 (+α)	
x1	S/L ratio (g/L)	2.64	4	6	8	9.36	2
x2	Acid concentration (M)	0.064	0.2	0.4	0.6	0.74	0.2
x3	Time (h)	0.32	1	2	3	3.68	1

3.4.9. Potential of WR for Pb(II) removal from drinking water

Given the disturbing Pb contamination in drinking water that occurred at Hong Kong in 2015 (HK, 2015), the potential of WR for Pb(II) removal to fulfill the stringent standard of drinking water was investigated. Different dosages of WR, i.e., 0.01, 0.02, 0.05 and 0.1 g/L, were dispersed in 15 mL of 400 ppb Pb(II) solutions in 50-mL polypropylene tubes. After agitation at 250 rpm and 298 K for 24 h, the Pb-WR suspensions were centrifuged at 4000 rpm for 10 min and the supernatants were subjected to the determination of the residual Pb(II) concentrations by ICP-MS.

3.4.10. Biosorption-desorption in a continuous mode

Biosorption in a continuous mode is essential in practical applications for an easy and efficient operation. In the preliminary studies, it was found that WR smaller than 180 μm, which were used in the batch studies, exerted high pressure drops in the column reactors due to the blocking of fine particles. Given that the effect of particle size on the biosorption capacity of WR was slight (as observed in the batch studies), WR in 500-1000 μm was used in the packed bed column reactors to reduce the pressure drop. The packed bed column reactors were established by filling WR in polystyrene columns with internal diameters of 6 mm. As shown in Figure 3.3., glass wool was placed in the two terminals of the column reactor to confine the biosorbent particles inside, and glass beads were used for an even distribution of flows. The flows were injected in an upward mode at 1 mL/min using a peristaltic pump (Masterflex, Cole-Parmer, USA). A fraction collector (Model 2110, Bio-Rad, USA) was used to automatically collect the effluent samples, which

were subjected to the determination of the Pb(II)/Cd(II) concentrations by ICP-OES. Before biosorption, DDI water was injected for 20 h to wet the column reactor and establish an equilibrium between the biosorbent and water.

For Pb(II) biosorption, a bed column reactor packed with 0.68 g of WR to a bed height of 19 cm (the ratio of bed height to internal diameter was 32:1) was employed. A Pb(II) solution at 50 ppm and pH 5.0 was used as the influent. For Cd(II) biosorption, however, the WR-packed bed column reactor showed undesirable biosorption performance in the preliminary study with breakthrough time (at which C_t/C_0 = 5%) of 30.3 BV and 15.9 BV in the first and second cycles, respectively. This was probably due to the low pH condition inside the column during biosorption (below 6.0 as measured in the effluent); it was observed that the Cd(II) biosorption capacity of WR at pH 6.0 was only 34% of that at pH 7.0 in the batch study (Section 4.1). The dissolution of CO_2 from the air into the column system and the existence of acidic substances in WR could be the causes for the dropped pH, even though a Cd(II) solution at pH 7.5-8.0 was used as the influent and the column was washed by DDI water to a pH of 7.0 before Cd(II) biosorption started. Therefore, WR was pretreated by soaking in 0.05 M NaOH for 3 h to remove the acidic substances, and also help break down the inter- and intra-molecular hydrogen bonds to increase the number of free hydroxyl groups (Sostaric et al., 2018). The pretreated WR was then washed by DDI water to a pH of 7.5-8.0 before column packing. The column reactor packed with NaOH-treated WR was fed with a 50 ppm Cd(II) solution at pH 7.5-8.0. This pH was higher than the optimal pH for Cd(II) biosorption (pH 7.0 as observed in the batch study, Section

4.1) considering that pH would decrease when the Cd(II) solution came in contact with the WR particles packed in the column reactor.

A biosorption-desorption cycle in the column reactor comprised successive injections of: (1) Pb(II)/Cd(II) solution for a sufficient time to saturate the WR packed in the column reactor; (2) DDI water to remove the residue metal ions that had not bound to WR; (3) 0.05 M HCl (selected based on the desorption studies in batch systems) to desorb the metal ions sequestered by WR and to regenerate the column reactor; (4) DDI water for a sufficient time to wash off any excess acid and clean the column reactor for the subsequent cycles. The changes in pH and total organic carbon (TOC) release (Shimadzu TOC-LCSN, Japan) during the biosorption-desorption cycles were monitored. To understand the biosorption behaviors in the column reactor, the Thomas, Bohart-Adams, Dose-Response and Yoon and Nelson models were applied to simulate the breakthrough curves.

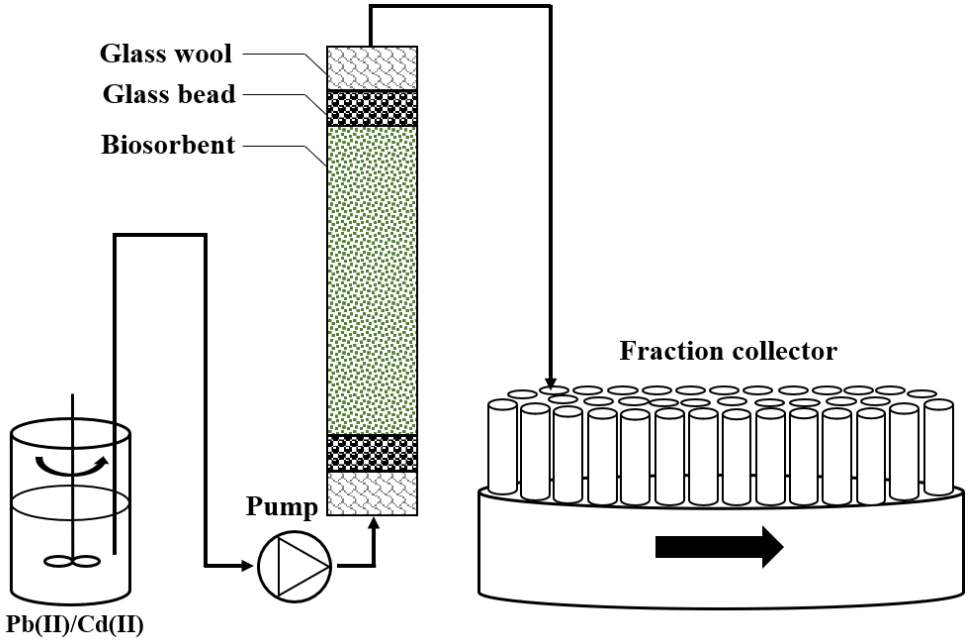

Figure 3.3 Schematic diagram of the WR-packed bed column reactor.

3.5. Biosorption of Pb(II) and Cd(II) by MS

3.5.1. Effect of particle size

The effect of MS particle size on Pb(II) and Cd(II) biosorption was investigated. A 0.015 g portion of MS in the particle size distributions of < 180 μm, 180-500 μm, and 500-1000 μm were respectively dispersed into 15 mL of 500 ppm Pb(II)/Cd(II) solutions. The pH was maintained at 5.0 in the Pb(II) biosorption systems and 7.5 in the Cd(II) ones.

3.5.2. Effect of pH

To examine the pH effect and identify the optimal pH condition, 0.015 g of MS was added into 50-mL polypropylene tubes containing 15 mL of 100 ppm Pb(II) solutions at pH of 2.0-7.0, and Cd(II) solutions at pH of 4.0-8.5. The pH of the biosorption systems was consistently adjusted and maintained at the desirable values.

3.5.3. Effect of MS dosage

The effect of MS dosage was investigated by respectively adding 0.5, 1, 2, 3 and 5 g/L of MS into 15 mL of 500 ppm Pb(II)/Cd(II) solutions in 50-mL polypropylene tubes. The pH was maintained at 5.0 in the Pb(II) biosorption systems and 7.5 in the Cd(II) ones.

3.5.4. Effect of initial metal concentration

To examine the effect of the initial concentration of Pb(II)/Cd(II) on the biosorption performance, 0.015 g of MS was dispersed into 50-mL polypropylene tubes containing 15 mL of Pb(II) solutions at 50, 100, 150, 200, 300, 400, 500, 600,

800, 1000 and 1500 ppm, and Cd(II) solutions at 50, 100, 150, 200, 300, 400, 500, 800 and 1000 ppm. The pH was maintained at 5.0 in the Pb(II) biosorption systems and 7.5 in the Cd(II) ones.

3.5.5. Effect of ionic strength

The effect of ionic strength on Pb(II)/Cd(II) biosorption by MS was studied by adding 0-0.2 M $NaNO_3$ into 50-mL polypropylene tubes containing 15 mL of 500 ppm Pb(II)/Cd(II) solutions with 1.0 g/L MS. The pH was maintained at 5.0 in the Pb(II) biosorption systems and 7.5 in the Cd(II) ones.

3.5.6. Effect of co-metal ions

To explore the selectivity of MS on Pb(II) and Cd(II), the effect of co-metal ions, including Cu(II), Zn(II), Ni(II) and Cr(III), on Pb(II) and Cd(II) biosorption by MS was investigated. In binary systems, 0.015 g of MS was added into 15 mL of metal solutions comprising Pb(II) and a co-metal ion, i.e., Cd(II), Cu(II), Zn(II), Ni(II) or Cr(III), at pH 5.0 (initial concentration of each heavy metal at 1 mM). Due to the optimal operational pH of 7.5 for Cd(II) biosorption by MS, at which Pb(II), Cu(II) and Cr(III) would be significantly precipitated, only the effect of the presence of Zn(II) and Ni(II) on Cd(II) biosorption was examined at pH 7.5.

3.5.7. Biosorption isotherms

In the biosorption isotherm studies of Pb(II) and Cd(II) biosorption by MS, 0.015 g of MS was added into 15 mL of Pb(II) solutions at 50-1500 ppm, and Cd(II) solutions at 50-1000 ppm. The pH was adjusted to 5.0 in the Pb(II) biosorption systems and 7.5 in the Cd(II) ones. Six adsorption isotherm models, namely the

Langmuir, Freundlich, Temkin, D-R, R-P and Sips equations, were used to non-linearly simulate the equilibrium data.

3.5.8. Biosorption kinetics

The Pb(II) and Cd(II) uptakes by MS were determined as a function of time in kinetic studies. In the 250-mL biosorption flasks, 0.15 g of MS was dispersed into 150 mL of 100 ppm Pb(II) solution and also 150 mL of 100 ppm Cd(II) solution. The pH was kept constant at 5.0 in the Pb(II) biosorption systems and 7.5 in the Cd(II) ones. The flasks were placed on magnetic stirrers at 250 rpm and 298 K. At predetermined time intervals, 2 mL of sample suspensions were collected and centrifuged for ICP-OES analysis. The kinetic data were non-linearly simulated by the pseudo-first-order, pseudo-second-order and fractional power equations.

3.5.9. Biosorption thermodynamics

The equilibrium constant (K_D) of the biosorption process is defined as Eq. 3.1. ΔG^0 can be calculated through Eq. 3.2, and the values of ΔH^0 and ΔS^0 can be estimated from the slope and intercept of the plot of ln K_D versus 1/T, respectively, via Eq. 3.3.

$$K_D = \frac{C_{\mathrm{ad,e}}}{C_{\mathrm{e}}} \tag{3.1}$$

$$\Delta G^0 = -RT \ln K_D \tag{3.2}$$

$$\ln K_D = \frac{\Delta S^0}{R} - \frac{\Delta H^0}{RT} \tag{3.3}$$

where $C_{ad,e}$ (mg/L) is the concentration of metal ions on the biosorbent in equilibrium; C_e (mg/L) refers to the concentration of metal ions remaining in

solution in equilibrium; R (8.314 J/mol·K) is the universe gas constant, and T (K) is the absolute temperature. To obtain the values of K_D at different temperatures, Pb(II) biosorption was performed by applying 15 mL of 50 ppm Pb(II) solutions with 0.5 g/L of MS at 288, 298 and 308 K, respectively. Cd(II) biosorption was carried out at the same conditions as Pb(II) biosorption but with 1.0 g/L of MS to assure a high enough distribution of Cd(II) on the solid phase (i.e., MS) in equilibrium. The pH was adjusted to 5.0 in the Pb(II) biosorption systems and 7.5 in the Cd(II) ones.

3.5.10. Desorption of Pb(II) and Cd(II) from MS

Different desorbing agents, including 0.2 M HCl, 0.2 M HNO_3, 0.2 M citric acid and 0.1 M sodium EDTA, were used to elute the bound Pb(II) and Cd(II) from MS. Desorption was performed at a S/L ratio of 2 g/L for 3 h. The suspensions were centrifuged at 4000 rpm for 10 min, and the concentrations of the desorbed Pb(II)/Cd(II) ions in the supernatants were determined by ICP-OES. The suspensions of Pb- and Cd-loaded MS in DDI water were used as the control groups. Besides, the separated MS after centrifugation was washed by DDI water 3 times and used for resorption of Pb(II)/Cd(II) after drying in a laboratory oven at 333 K for 12 h.

3.6. Mechanistic studies

3.6.1. Basic characterization of WR and MS

Elemental analysis

The elemental compositions of WR and MS were examined by an elemental analyzer (Elementar vario MICRO, Germany). The atomic concentrations of C, H, N and S were determined, while the concentration of O was estimated based on mass difference by neglecting the presence of other elements (Li et al., 2010).

Zeta potential measurement

In order to examine the surface charging characteristics of WR and MS, a WR solution and a MS solution at 0.15 g/L were prepared in 1 mM KCl, and the zeta potential was measured at pH ranging from 2.0 to 8.0 by a Malvern Zetasizer (Nano Series, UK). The measurement was performed in triplicate with the averaged value reported.

PXRD

PXRD can provide important information of the crystalline structure and even the composition of the solid sample being studied. The wide-angle PXRD patterns of pristine WR and MS in different particle sizes (i.e., < 180 μm, 180-500 μm and 500-1000 μm), as well as the metal-loaded biosorbents (i.e., Pb- and Cd-loaded WR, Pb- and Cd-loaded MS) were recorded by a Rigaku MiniFlex 600 diffractometer (Rigaku, Japan) with CuKα radiation (λ = 1.54060 Å) at 40 kV and 15 mA in the range of 2θ from 3° to 90°. The biomass samples were first ground

into even powders and then pressed into thin tablets onto the sample holders for PXRD measurement.

SEM-EDX

A SEM (Hitachi S-4800, Japan) coupled with an EDX tool (XFlash® 6, Bruker, Germany) was employed to investigate the morphological properties of WR and MS before and after Pb(II)/Cd(II) biosorption. In addition to SEM micrographs, X-ray elemental mappings were performed to examine the element distribution, especially that of Pb and Cd after biosorption, on the surface of WR and MS. The EDX spectra were also collected for investigating the elemental characteristics of the biosorbents.

3.6.2. Spectroscopic techniques

FTIR spectroscopy

The functional groups on WR and MS were examined by FTIR spectroscopy before and after Pb(II)/Cd(II) biosorption (AVATAR 330, Thermo Nicolet, USA). To prepare sample tablets for FTIR analysis, the biomass samples were ground and evenly mixed with dry KBr salts.

XPS

An XPS (Axis Ultra DLD, Kratos, Japan) was used to examine the elemental and structural characteristics of the surface of WR and MS before and after Pb(II)/Cd(II) biosorption. The different forms of the same element and their interactions with the adsorbed heavy metals were identified based on the obtained high-resolution XPS spectra. The binding energy for C 1s at 285 eV was applied as

the internal reference for all binding energies. The XPS spectra were deconvoluted and analyzed by the software *Vision Processing*.

Solid-state NMR spectroscopy

The CP-MAS (CP contact time of 1 ms) ^{13}C solid-state NMR spectra of WR and MS before and after Pb(II)/Cd(II) biosorption were recorded using a 3.2-mm ZrO_2 rotor at a spinning speed of 15 kHz with 4900 scans (JEOL 500 MHz, Japan). The ^{13}C chemical shifts were referenced to tetramethylsilane (TMS) with adamantane as the secondary reference. The radiation frequency was 125 MHz for ^{13}C and 500 MHz for ^{1}H. Spectral editing and analysis were performed in *MestReNova* 12. In consideration of the sensitivity of solid-state NMR spectroscopy, the ^{13}C solid-state NMR spectra of cellulose, pectin, and lignin (model biopolymers) were collected at the same operation conditions to set references for line assignment (Figures A3-5). Hemicellulose was not used as a model biopolymer due to its random chemical structure which is difficult to be standardized. The characteristic resonances of the ^{13}C NMR spectra of the three model biopolymers are summarized in Table A1 in Appendices.

3.6.3. Ion exchange experiment

In order to verify the involvement of ion exchange and to identify the responsible light metal ions (e.g., Na^+, Mg^{2+}, K^+ and Ca^{2+}) in biosorption, the release of light metal ions during the Pb(II) and Cd(II) biosorption processes was determined by respectively adding 0.125 g of WR into 250 mL of 50 ppm Pb(II) solution and 250 mL of 50 ppm Cd(II) solution. WR suspensions with the same dosage of WR in DDI water were set as the blank groups. The release of light metal

ions from MS during Pb(II) and Cd(II) biosorption was measured through the same procedures.

3.6.4. Quantum chemistry simulation

To further disclose the biosorption mechanisms and verify the proposed ones from the aforementioned spectroscopic methods, the microscopic interactions between Pb(II)/Cd(II) and the identified binding sites (e.g., hydroxyl and carboxyl) were simulated by quantum chemistry simulation (QCS). The structures and thermodynamic properties of the potential heavy metal complexes formed in biosorption were analyzed through M06 method with the 6-311+G (d,p) basis set in water solvent at 298 K. Chemical modelling was conducted by performing ab initio electronic structure calculations using Gaussian 09 program package (Frisch, 2009). The calculations were carried out in an implicit water solvent (ε=78.3553) using the conductor-like polarizable continuum model (CPCM) combined with Bondi radii. The structural optimizations were obtained using the B3LYP hybrid density functional with D3 dispersion correction. The def2tzvp was for Pb as basis set and effective core potential, and 6-311++G (d,p) was for the other atoms, i.e., N, C, H and O. Frequency calculations at the same level were performed to check whether the obtained stationary point is an isomer. All reported energy values are free energies (in kcal/mol) at 298 K.

3.7. Data processing and analysis

All the batch biosorption experiments were performed in duplicate and the averaged results were reported in this study. The Microsoft Excel 2007 program was applied for data processing, and the software *Prism* 5.0 was used for non-linear simulation of adsorption isotherms, kinetics, and breakthrough curves. In addition to the frequently used coefficient of determination (R^2), the fitting of the applied models was also evaluated by the root-mean-square deviation (RMSD), which is a widely used statistical parameter for evaluating the predictive power of a model. RMSD is expressed as

$$RMSD = \frac{\sqrt{\sum_{i=1}^{n} (Q_{exp} - Q_{pre})^2}}{n-1},$$

where Q_{exp} (mg/g) is the experimental biosorption capacity, and Q_{pre} (mg/g) is the predicted biosorption capacity from modeling (Jalil et al., 2012).

4. Biosorption of Pb(II) and Cd(II) by Watermelon Rind

4.1. Effect of pH

The Pb(II) and Cd(II) biosorption capacities of WR at varying pH are shown in Figure 4.1. It can be concluded that the biosorption capacities of WR (Q, mg/g) were augmented with increasing pH to the maximum values, namely 203.82 ± 2.85 mg/g for Pb(II) at pH 5.0 and 87.03 ± 0.47 mg/g for Cd(II) at pH 7.5. This positive correlation was attributed to the presence of less H^+ competition for the binding sites and the deprotonation of the weakly acidic functional groups (e.g., carboxyl groups) as pH increased (Ahmad et al., 2018, Jin et al., 2018). At the initial Pb(II) concentration of 100 ppm, Pb(II) uptake was scarcely influenced at pH 4.0-5.5 (Figure 4.1a). This could be due to the presence of sufficient binding sites on WR for entrapping the low amount of Pb(II) ions at this pH condition, implying that WR has a wide applicable pH range for Pb(II) removal as the Pb(II) concentration in industrial wastewater is usually below 100 ppm (Wang and Ren, 2014). Notably, Cd(II) precipitation was observed at pH 7.5 in the control group (i.e., Cd(II) solution without WR). Hence, pH 5.0 and 7.0 were respectively chosen as the optimal pH for Pb(II) and Cd(II) biosorption by WR in the subsequent studies.

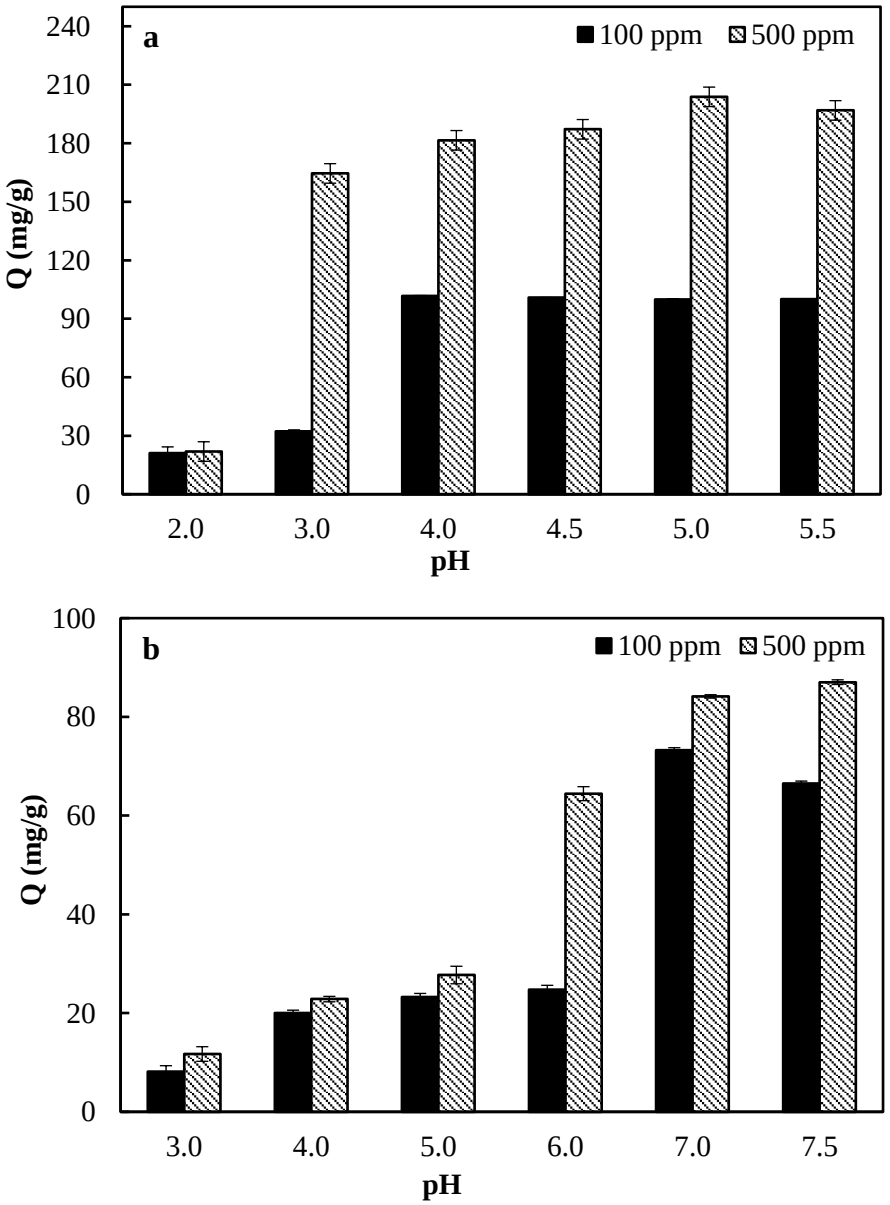

Figure 4.1 Effect of pH on (a) Pb(II) and (b) Cd(II) biosorption by WR.

[Initial metal concentrations of 100 and 500 ppm, 1.0 g/L WR, 250 rpm, 298 K, 24 h.]

4.2. Effect of WR dosage

As Figure 4.2a illustrates, the highest Pb(II) biosorption capacity was achieved at the WR dosage of 1.0 g/L. The Pb(II) biosorption capacity of WR gradually reduced as its dosage increased in the biosorption system. This was a consequence of the redundant binding sites supplied by a high dosage of WR. The number of binding sites was beyond the demand of Pb(II) ions in the system, resulting in a lower biosorption capacity per gram of WR. A similar result was observed in the Cd(II) biosorption system (Figure 4.2b). Although the removal efficiencies of Pb(II) and Cd(II) increased along with increasing WR dosage, 1.0 g/L was used in the subsequent biosorption studies to make the best use of the WR biosorbent.

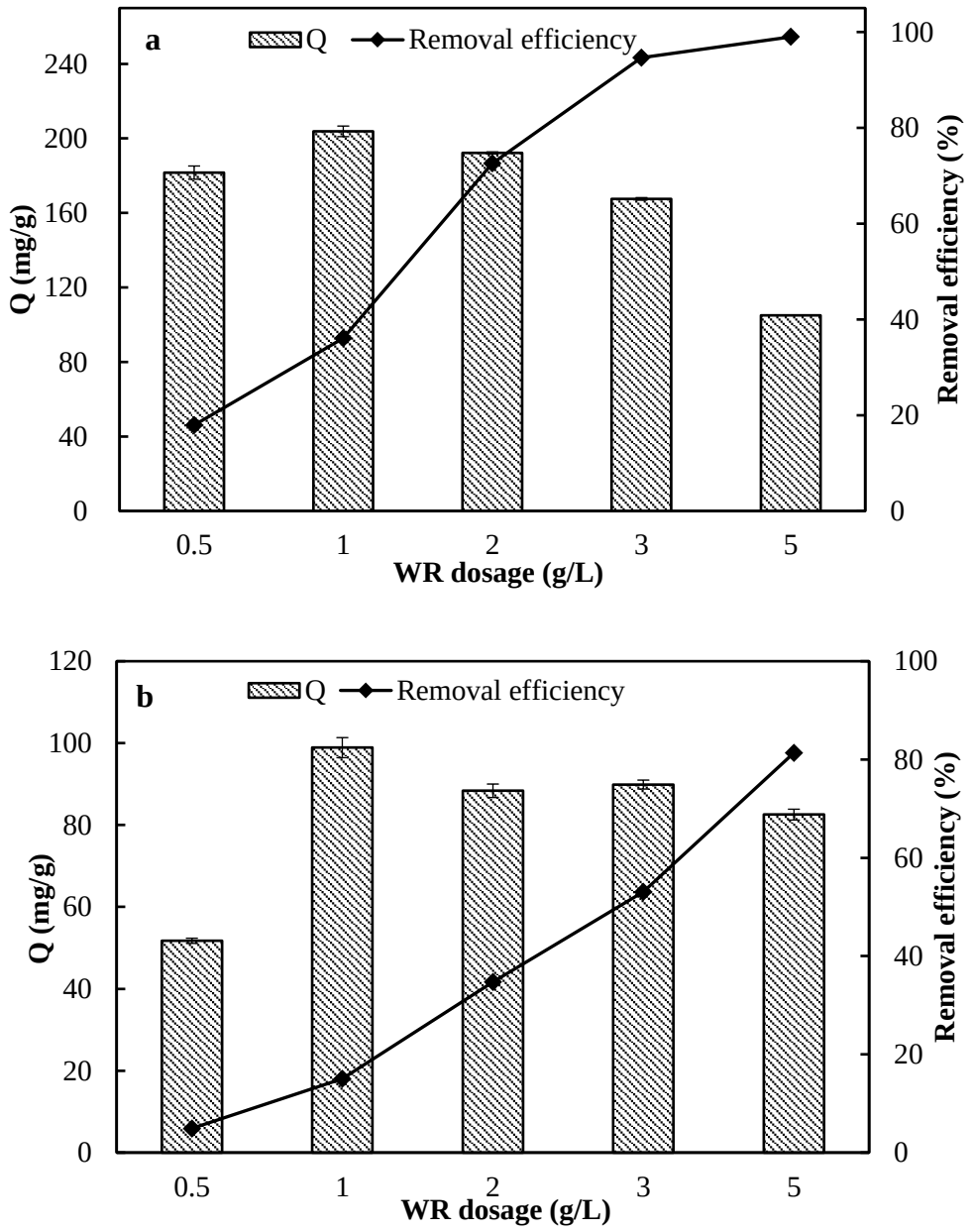

Figure 4.2 Effect of WR dosage on (a) Pb(II) and (b) Cd(II) biosorption.

[Initial metal concentration of 500 ppm, pH 5.0 for Pb(II) and 7.0 for Cd(II) biosorption, 250 rpm, 298 K, 24 h.]

4.3. Effect of initial metal concentration

Figure 4.3 indicates that the Pb(II) and Cd(II) biosorption capacities of WR were positively correlated to the initial concentrations of Pb(II) and Cd(II) in the biosorption systems. This was because heavy metal ions at a high concentration would exert a high driving force to overcome the mass transfer resistance between liquid and solid phases, leading to enhanced loadings of Pb(II) and Cd(II) on WR. Due to the limited binding sites provided by the fixed dosage of WR in the biosorption systems, the Pb(II) and Cd(II) uptakes gradually became steady as the initial metal concentrations increased (Duan et al., 2010). Besides, descending removal efficiencies were observed along with increasing initial metal concentrations. This was due to the lack of sufficient number of binding sites on WR for binding the increasing amounts of Pb(II)/Cd(II) ions. Accordingly, a higher initial metal concentration can lead to a higher biosorption capacity of the biosorbent. However, the removal efficiency of the heavy metal from the system would be impaired.

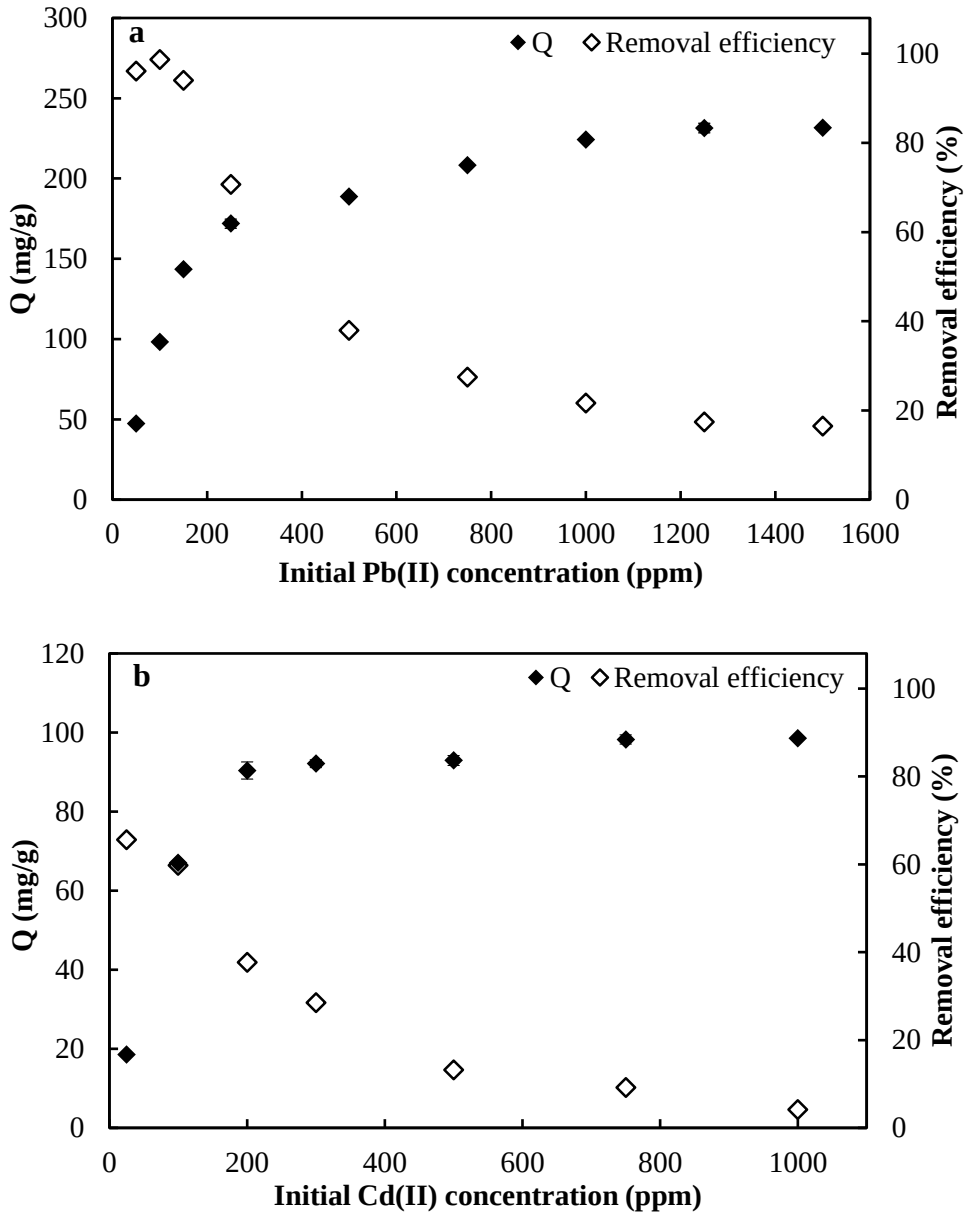

Figure 4.3 Effect of initial metal concentration on (a) Pb(II) and (b) Cd(II) biosorption by WR.

[pH 5.0 for Pb(II) and 7.0 for Cd(II) biosorption, 1.0 g/L WR, 250 rpm, 298 K, 24 h.]

4.4. Effect of ionic strength

The effect of ionic strength on Pb(II) and Cd(II) biosorption by WR is illustrated in Figure 4.4. It shows that the Pb(II) uptake was slightly impaired by the increasing ionic strength, with a decrease of 13.8% in *Q* at the ionic strength as high as 0.2 M $NaNO_3$ compared with the control group without $NaNO_3$. Comparatively, the Cd(II) biosorption by WR was influenced by the ionic strength to a greater extent, with 42% of *Q* reduced at 0.2 M $NaNO_3$. At higher ionic strength, the surface sites on WR were surrounded by more counter ions, i.e., Na^+, which weakened the binding force of Pb(II)/Cd(II) to WR by electrostatic attraction (Lv et al., 2012, Wang et al., 2013). Therefore, electrostatic attraction was one of the underlying mechanisms responsible for Pb(II) and Cd(II) biosorption by WR, and it was inferred that electrostatic attraction played a more important role in Cd(II) biosorption than in Pb(II) biosorption by WR.

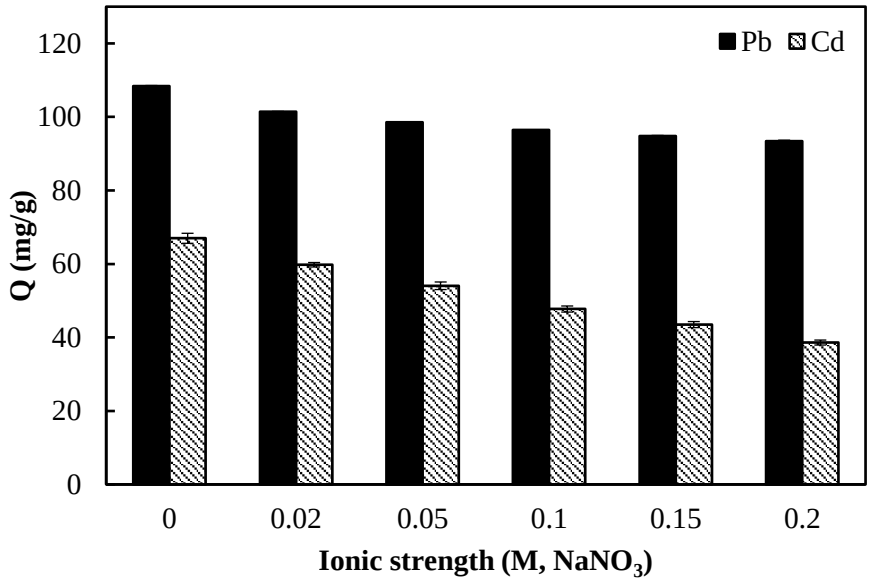

Figure 4.4 Effect of ionic strength on Pb(II) and Cd(II) biosorption by WR.

[Initial metal concentration of 100 ppm, pH 5.0 for Pb(II) and 7.0 for Cd(II) biosorption, 1.0 g/L WR, 250 rpm, 298 K, 24 h.]

4.5. Effect of co-metal ions

As Figure 4.5a indicates, the Pb(II) biosorption capacity of WR was not remarkably impeded by the presence of Cd(II), Ni(II) or Zn(II) at the same concentration (i.e., 1.0 mM), whereas relatively intensive impact was exerted by Cu(II) and Cr(III), which respectively reduced the Pb(II) uptake by 13.1% and 17.3% (compared with the single system). For Cd(II) biosorption, only the effect of Zn(II) and Ni(II) was examined given the dramatic precipitation of other heavy metal ions at pH 7.0. It was observed that the presence of Zn(II) and Ni(II) reduced the Cd(II) biosorption capacity of WR to 63.3% and 85.8% of that in the single system, respectively (Figure 4.5b). The results revealed that WR had a much higher selectivity on Pb(II) than Cd(II) under the studied conditions, and it also exhibited great potential in the removal of Zn(II) and Cr(III) from heavy-metal-bearing wastewater. As aforementioned in Section 2.5.4, the affinity of a cationic heavy metal ion to the binding site is theoretically dependent on four major factors, namely, electronegativity, ionic potential, hydration energy, and HSAB property. Referring to the characteristics of Pb(II) and Cd(II) as shown in Table 2.1, the higher selectivity of WR on Pb(II) over Cd(II) could be attributed to the higher electronegativity and lower hydration energy of Pb(II). Also, Pb(II) is categorized as a borderline acid, and such that it can react more rapidly and form stronger bonds with the functional groups (e.g., hydroxyl and carboxyl groups, categorized as hard bases) on the WR surface than Cd(II) (categorized as a soft acid) can (Unuabonah et al., 2008). The lower ionic potential of Pb(II) than that of Cd(II) suggested that electrostatic attraction played a less important role in Pb(II) biosorption than in

Cd(II) biosorption by WR. This was consistent with the effect of ionic strength on Pb(II) and Cd(II) biosorption by WR as observed in Section 4.4.

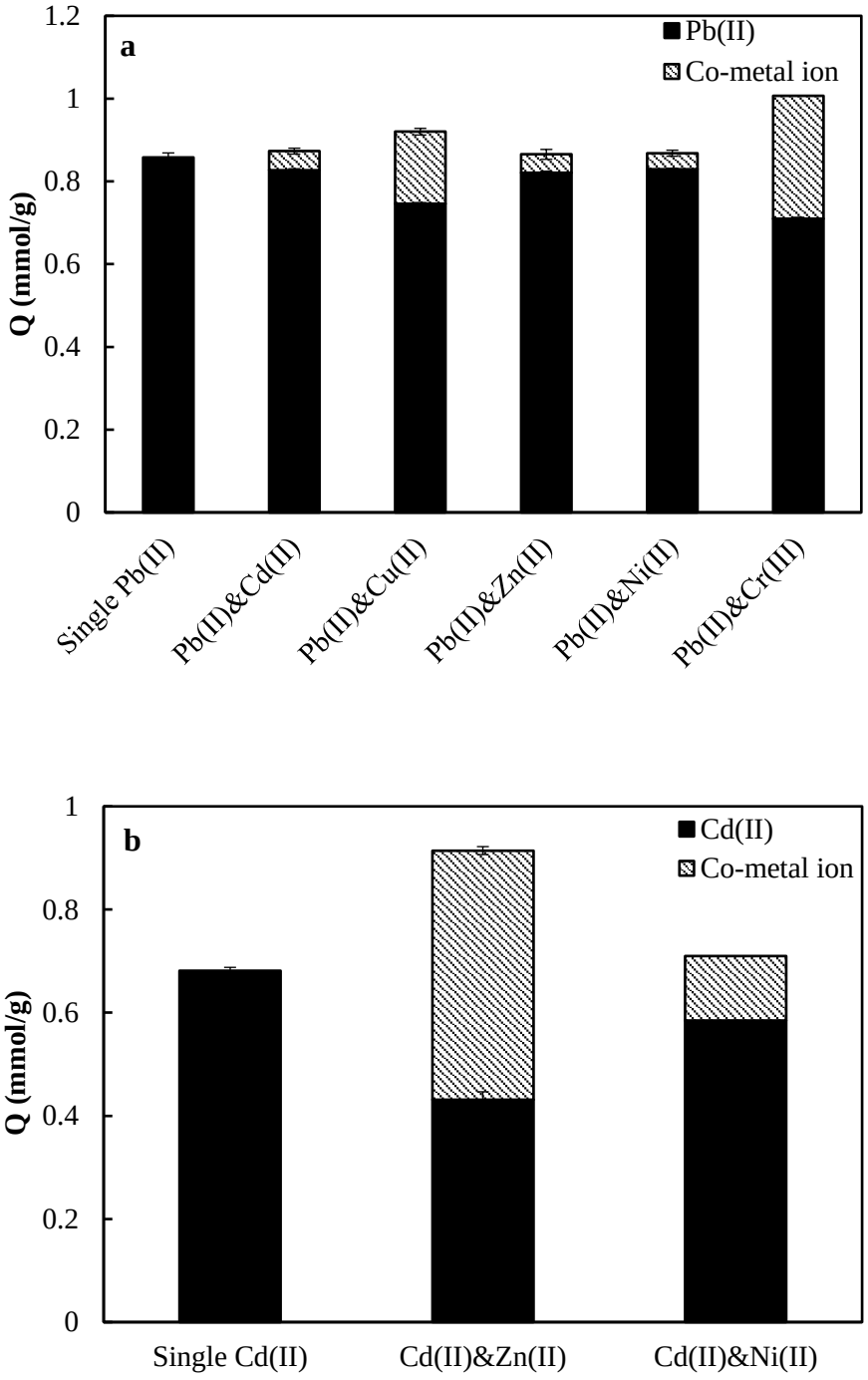

Figure 4.5 Effect of co-metal ions on (a) Pb(II) and (b) Cd(II) biosorption by WR in binary systems.

[Initial metal concentrations of 1.0 mM, pH 5.0 for Pb(II) and 7.0 for Cd(II) biosorption, 1.0 g/L WR, 250 rpm, 298 K, 24 h.]

4.6. Biosorption isotherms of Pb(II) and Cd(II) biosorption by WR

The equilibrium data of Pb(II) and Cd(II) biosorption by WR are described in Figure 4.6 with non-linear regression to the Langmuir, Freundlich, Temkin, D-R, R-P and Sips models. The constants of the adsorption isotherm models are summarized in Table 4.1. Figure 4.6a indicates that the maximum Pb(II) biosorption capacity, 231.57 ± 1.09 mg/g (1.12 ± 0.005 mmol/g), was achieved by WR with the R-P isotherm as the best fitting model (the highest R^2 of 0.995 and the lowest RMSE of 2.219, Table 4.1). The R-P isotherm is similar to the Freundlich isotherm when the term of $a_R C_e^{bR}$ is much larger than 1.0. In this study, the value of $a_R C_e^{bR}$ ranged from 6.61 to 3187.56, implying that the Pb(II) biosorption by WR could be interpreted by the Freundlich isotherm as well. This observation was consistent with the high R^2 (0.993) and low RMSE (2.586) of the Freundlich isotherm, suggesting multilayer biosorption of Pb(II) on the heterogeneous surface of WR with non-uniform distribution energy. The surface heterogeneity of WR was also supported by the low value of 1/n (0.149) in the Sips equation, which suggests a heterogeneous surface when approaching 0 (Papageorgiou et al., 2006). According to Figure 4.6b, the maximum Cd(II) biosorption capacity, 98.51 ± 1.15 mg/g (0.88 ± 0.01 mmol/g), was achieved by WR. The values of R^2 and RMSE revealed the fitness of the adsorption isotherm models in a descending order of Sips > R-P > D-R > Langmuir > Temkin > Freundlich (Table 4.1). However, the value of 1/*n* (the heterogeneity factor) in the Sips model was 1.669, which was beyond the defined range of 0-1. Moreover, the constant, b_R, in the R-P model was 1.105, which exceeded its range defined as 0-1. The disagreements observed in these

isotherm constants revealed the inapplicability of the Sips and R-P isotherms for simulating the Cd(II) biosorption by WR regardless of the values of R^2 and RMSE. Consequently, the D-R model was the most appropriate isotherm for modeling the Cd(II) biosorption by WR, suggesting heterogeneous binding sites on the WR surface as inferred in the equilibrium study of Pb(II) biosorption (Dubinin and Radushkevich, 1947).

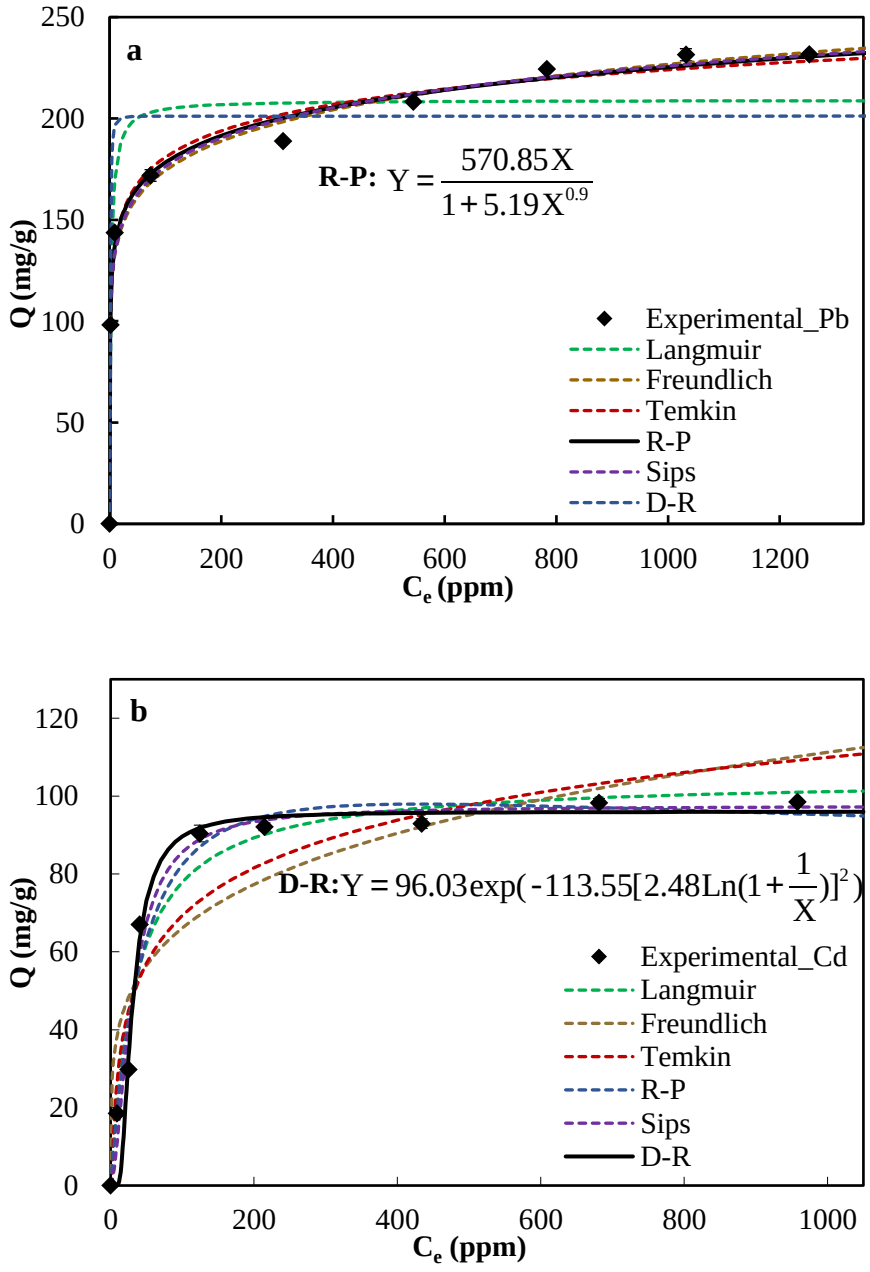

Figure 4.6 Non-linear regression of the equilibrium data of (a) Pb(II) and (b) Cd(II) biosorption by WR.

[pH 5.0 for Pb(II) and 7.0 for Cd(II) biosorption, 1.0 g/L WR, 250 rpm, 298 K, 24 h.]

Table 4.1 Adsorption isotherm constants of Pb(II) and Cd(II) biosorption by WR.

	Parameter	Pb(II)	Cd(II)
Langmuir	Q_m (mg/g)	204.900 ± 1.838	104.650 ± 1.485
	K_L (L/mg)	0.458 ± 0.052	0.029 ± 0.001
	R^2	0.922 ± 0.008	0.965 ± 0.001
	RMSE	8.449 ± 0.376	2.917 ± 0.007
Freundlich	K_F	101.250 ± 0.212	23.355 ± 0.049
	N_F	8.791 ± 0.030	4.426 ± 0.033
	R^2	0.993 ± 0.002	0.861 ± 0.001
	RMSE	2.586 ± 0.332	5.830 ± 0.062
Temkin	A_T (L/mg)	157.200 ± 16.829	0.505 ± 0.014
	B_T (J/mol)	18.360 ± 0.269	17.675 ± 0.304
	R^2	0.992 ± 0.001	0.917 ± 0.002
	RMSE	2.656 ± 0.161	4.510 ± 0.023
D-R	Q_m (mg/g)	197.150 ± 1.202	96.025 ± 1.209
	β (mol^2/kJ^2)	0.384 ± 0.072	113.550 ± 2.192
	R^2	0.868 ± 0.004	**0.967** ± 0.001
	RMSE	11.025 ± 0.100	**2.841** ± 0.000
R-P	K_r (L/g)	570.850 ± 2.539	2.368 ± 0.023
	a_R (L/mg)	5.191 ± 1.732	0.012 ± 0.001
	b_R	0.900 ± 0.003	1.105 ± 0.003
	R^2	**0.995** ± 0.001	0.974 ± 0.001
	RMSE	**2.219** ± 0.212	2.533 ± 0.033
Sips	Q_m (mg/g)	744.400 ± 1.986	97.480 ± 1.414
	b (L/mg)	0.160 ± 0.0450	0.003 ± 0.000
	$1/n$	0.149 ± 0.012	1.669 ± 0.025
	R^2	0.993 ± 0.002	0.979 ± 0.001
	RMSE	2.564 ± 0.307	2.270 ± 0.001

4.7. Kinetics of Pb(II) and Cd(II) biosorption by WR

4.7.1. Kinetic studies at different temperatures

The Pb(II) and Cd(II) biosorption capacities of WR are plotted against time at different temperatures in Figure 4.7. It shows that the Pb(II) and Cd(II) biosorption processes were faster at higher temperature in the initial periods (0-7 min in Pb(II) biosorption and 0-10 min in Cd(II) biosorption). This should result from the higher kinetic energies and thus faster diffusions of Pb(II) and Cd(II) to the binding sites on WR at higher temperature. In the following stages, the biosorption processes of Pb(II) and Cd(II) gradually reached equilibrium, with an insignificant effect of temperature on the biosorption kinetics. Intriguingly, the Pb(II) biosorption capacity of WR in equilibrium was slightly lower at higher temperature (Figure 4.7a), whereas the Cd(II) biosorption capacity of WR in equilibrium augmented from 15.53 ± 0.31 mg/g to 29.47 ± 0.67 mg/g when the temperature increased from 278 K to 310 K. This observation could be ascribed to the different thermodynamic properties of Pb(II) and Cd(II) biosorption by WR. Beneficial to the practical removal/recovery of Pb(II) and Cd(II) in aqueous solutions by WR, the biosorption processes were very rapid. Take the biosorption at 298 K as an example, 94.3% of Pb(II) biosorption and 88.4% of Cd(II) biosorption were completed in the first 10 min.

Figure 4.8 illustrates the non-linear simulation of the kinetics of Pb(II) and Cd(II) biosorption by WR at 298 K using the pseudo-first-order, pseudo-second-order and fractional power kinetic equations. The modeling results revealed that the pseudo-first-order kinetics provided the best description to the Pb(II) biosorption

process, whereas the pseudo-second-order kinetics fitted best to the Cd(II) biosorption process with the highest R^2 and lowest RMSE (details in Table 4.2).

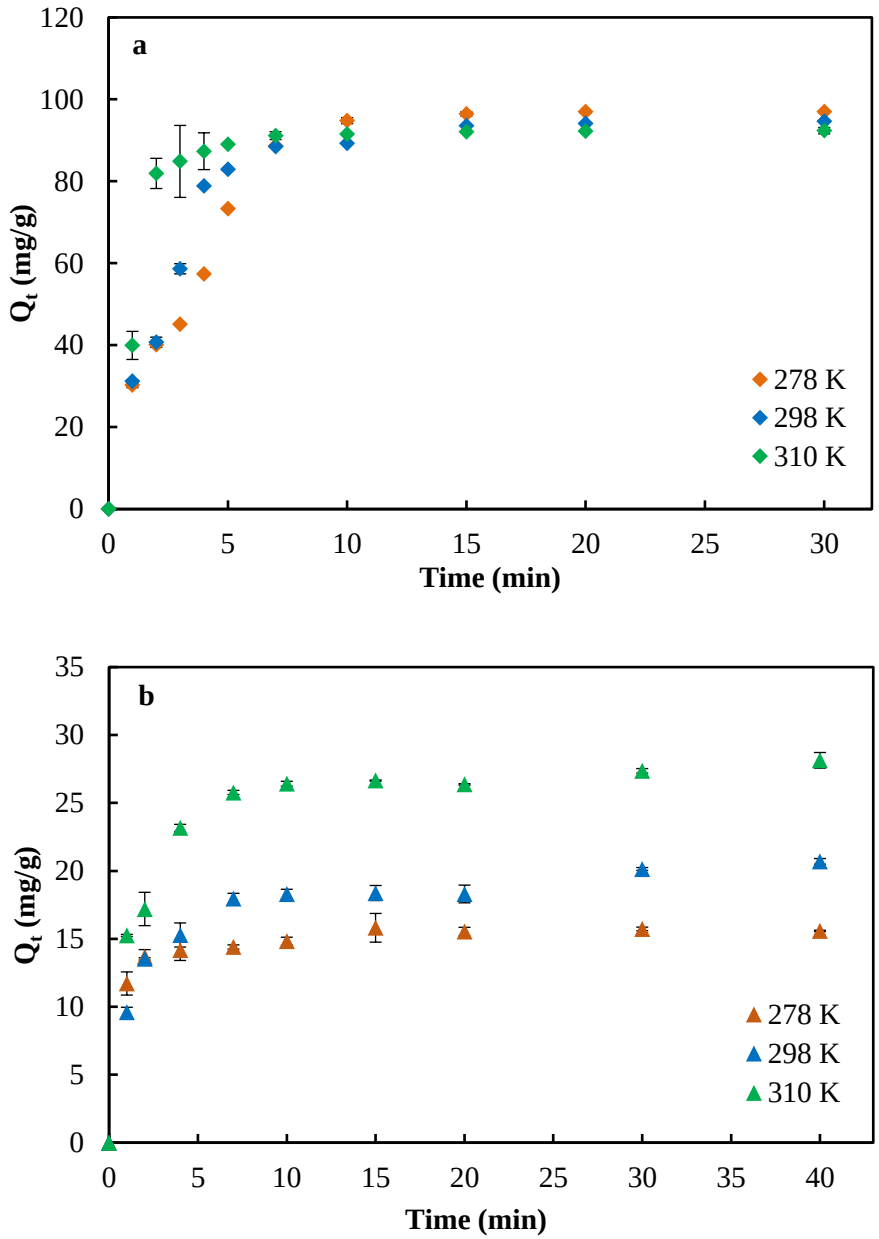

Figure 4.7 (a) Pb(II) and (b) Cd(II) uptakes by WR versus time at different temperatures.

[Initial metal concentrations of 50 ppm, pH 5.0 for Pb(II) and 7.0 for Cd(II) biosorption, 0.5 g/L WR, WR < 180 µm, 250 rpm.]

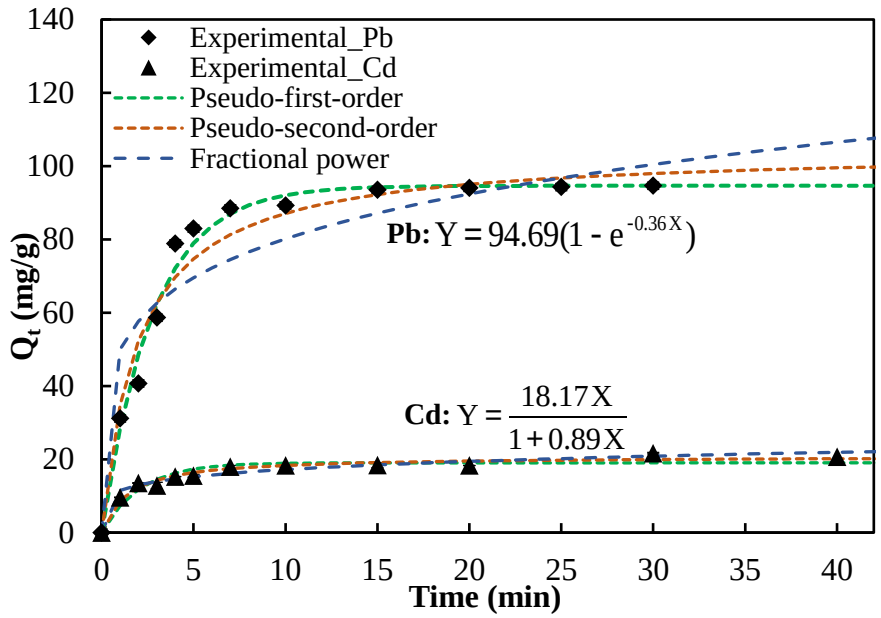

Figure 4.8 Non-linear regression of the kinetics of Pb(II) and Cd(II) biosorption by WR at 298 K.

[Initial metal concentrations of 50 ppm, pH 5.0 for Pb(II) and 7.0 for Cd(II) biosorption, 0.5 g/L WR, WR < 180 µm, 250 rpm.]

Table 4.2 Kinetic constants of Pb(II) and Cd(II) biosorption by WR at 298 K.

	Parameter	Pb(II)	Cd(II)
Pseudo-first-order	Q_e (mg/g)	94.695 ± 0.007	18.840 ± 0.467
	k_1 (min^{-1})	0.359 ± 0.001	0.608 ± 0.032
	R^2	**0.985** ± 0.002	0.968 ± 0.016
	RMSD	**1.382** ± 0.069	0.416 ± 0.097
Pseudo-second-order	Q_e (mg/g)	107.600 ± 0.000	20.375 ± 0.530
	k_2 (g/mg/min)	0.004 ± 0.000	0.044 ± 0.004
	R^2	0.963 ± 0.002	**0.990** ± 0.007
	RMSD	2.917 ± 0.060	**0.229** ± 0.080
Fractional power	k	49.005 ± 0.078	11.830 ± 0.141
	v	0.229 ± 0.000	0.161 ± 0.003
	R^2	0.915 ± 0.001	0.968 ± 0.008
	RMSD	3.918 ± 0.036	0.425 ± 0.062

(**Notes:** WR < 180 μm was used.)

4.7.2. Kinetic studies with WR in different particle sizes

Kinetics of the biosorption processes

The profiles of Pb(II) and Cd(II) biosorption capacities versus time by using WR in different particle sizes are illustrated in Figure 4.9. Figure 4.9a indicates that the Pb(II) biosorption process became faster, especially in the first 20 min, when the particle size of WR decreased. Similarly, the biosorption rate of Cd(II) also increased with decreasing particle size of WR in the initial periods (0-7 min, Figure 4.9b). Over time, WR in different particle sizes obtained similar Pb(II) biosorption capacities in equilibrium (89.6-92.0 mg/g, Figure 4.9a). The Cd(II) biosorption process by WR < 180 µm gradually reached equilibrium after 10 min with the Cd(II) biosorption capacity of 20.96 ± 0.40 mg/g in equilibrium, whereas those of WR in 180-500 µm and in 500-1000 µm approached equilibrium after 40 min and 60 min, respectively, achieving higher Cd(II) equilibrium biosorption capacities of 25.11 ± 0.62 and 26.45 ± 0.08, respectively (Figure 4.9b). The observation of the faster biosorption with smaller WR is explained by the shorter distance that the lead and cadmium ions need to diffuse from the external surface to the interior of the smaller particles compared with larger particles. Additionally, the larger external surface area provided by the smaller particles allow a faster access of lead and cadmium ions to the surface and pores of WR particles. To evaluate the effect of pore size distribution on the biosorption rate of Pb(II) and Cd(II), the N_2 adsorption-desorption isotherms of WR at 77 K were determined by an ASAP 2020 Physisorption Analyzer (Micromeritics, USA). The Barrett-Joyner-Halenda method and the Horvath-Kawazoe method were used to determine the size

distributions of macropores and mesopores, and micropores, respectively. It was found that the different sized WR particles were dominated with mesopores with a total pore volume of 0.02 cm^3/g (80%-85% in mesopores), and the mesopore surface areas were calculated to be 10.58-11.63 m^2/g by the Barrett-Joyner-Halenda method (BET surface area of 20.07-39.25 m^2/g). It was observed that the total pore volumes of different sized WR were statistically similar with slightly different mesopore volumes and areas, showing that the pore volume and size distribution did not significantly influence the Pb(II) and Cd(II) biosorption rate. Furthermore, to evaluate the contribution of ion exchange to biosorption, the amount of naturally occurring light metal ions on WR was examined by soaking WR in different particle sizes into 0.05 M HNO_3 for 3 h. It was determined that the content of Ca^{2+} and Mg^{2+} in WR < 180 μm (0.307 ± 0.00368 mmol/g) was lower as compared with those of larger WR in 180-500 μm (0.332 ± 0.00917 mmol/g) and 500-1000 μm (0.377 ± 0.00870 mmol/g) (details in Figure A6). This observation could explain why the larger WR particles exhibited a higher Cd(II) equilibrium biosorption capacities, given that ion exchange with light metal ions (i.e., Ca^{2+} and Mg^{2+}) played a dominant role in Cd(II) biosorption by WR (see Section 6.1.8). It was estimated that Ca^{2+} and Mg^{2+} on WR could exchange with Cd(II) in solution and provide binding sites to 81.5% of the sequestered Cd(II); in contrast, this value was only 18.5% in Pb(II) biosorption by WR.

Intraparticle diffusion curves

The intraparticle diffusion model developed by Weber and Morris (1962) was employed to further analyze the kinetics of Pb(II) and Cd(II) biosorption by

WR in different particle sizes. Figure 4.10 shows the plots of the Pb(II) and Cd(II) biosorption capacities against the square root of time ($t^{1/2}$, $min^{1/2}$). No curves shown in Figures 4.10a and 4.10b have a prominent initial straight-line section passing through the origin, showing that the rate of external mass transfer (film diffusion) was not significantly faster compared with the rate of intraparticle diffusion. This observation was consistent with the pore size distribution of the WR material, which suggested that diffusion through the fluid-filled mesopores was expected to be quite efficient during the biosorption of lead and cadmium ions, with a rate not much different from the rate of film diffusion. On the other hand, the multi-linearity observed in each biosorption process indicated that different steps were involved in Pb(II) and Cd(II) biosorption by WR in three different ranges of particle size. The first steep linear section of the curves should be attributed to the external mass transfer of Pb(II) and Cd(II) from the bulk solution across the boundary layer to the external surface of WR. The second linear section was the gradual biosorption stage, in which the biosorption was limited by intraparticle diffusion of Pb(II) and Cd(II) through the mesoporous WR solid matrix. The third linear section was the final equilibrium stage with slow biosorption due to the decreased concentrations of Pb(II) and Cd(II) in solution and the oncoming saturation of the binding sites on the WR surface (Ofomaja, 2010, Wu et al., 2009). Comparison of the linearity of the three steps shows that the WR in a larger particle size exhibited a longer stage of rate-limiting intraparticle diffusion (i.e., the second step) in both Pb(II) and Cd(II) biosorption processes. The lead and cadmium ions took longer time to diffuse from the external surface to the interior of the larger particles compared with smaller particles.

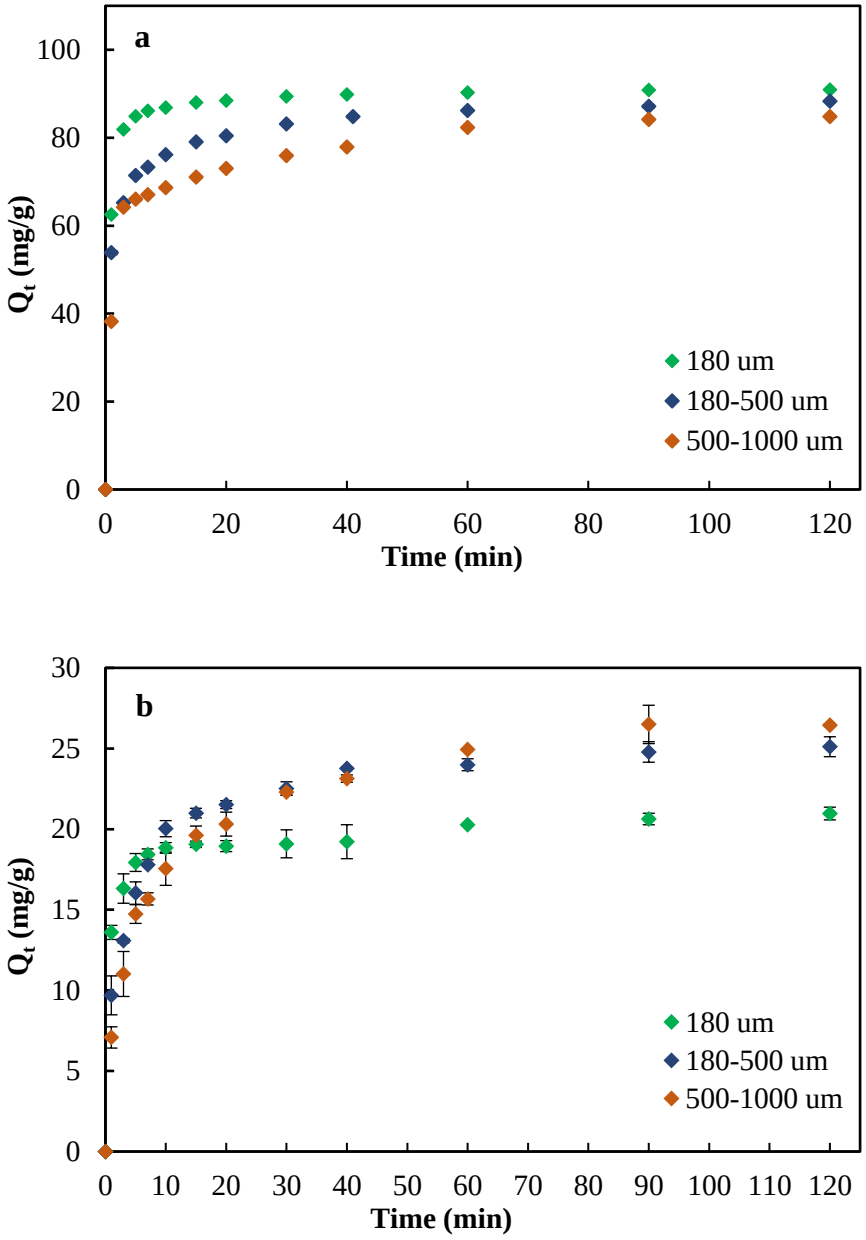

Figure 4.9 (a) Pb(II) and (b) Cd(II) uptakes versus time by using WR in different particle sizes.

[Initial metal concentrations of 50 ppm, pH 5.0 for Pb(II) and 7.0 for Cd(II) biosorption, 0.5 g/L WR, 250 rpm, 298 K.]

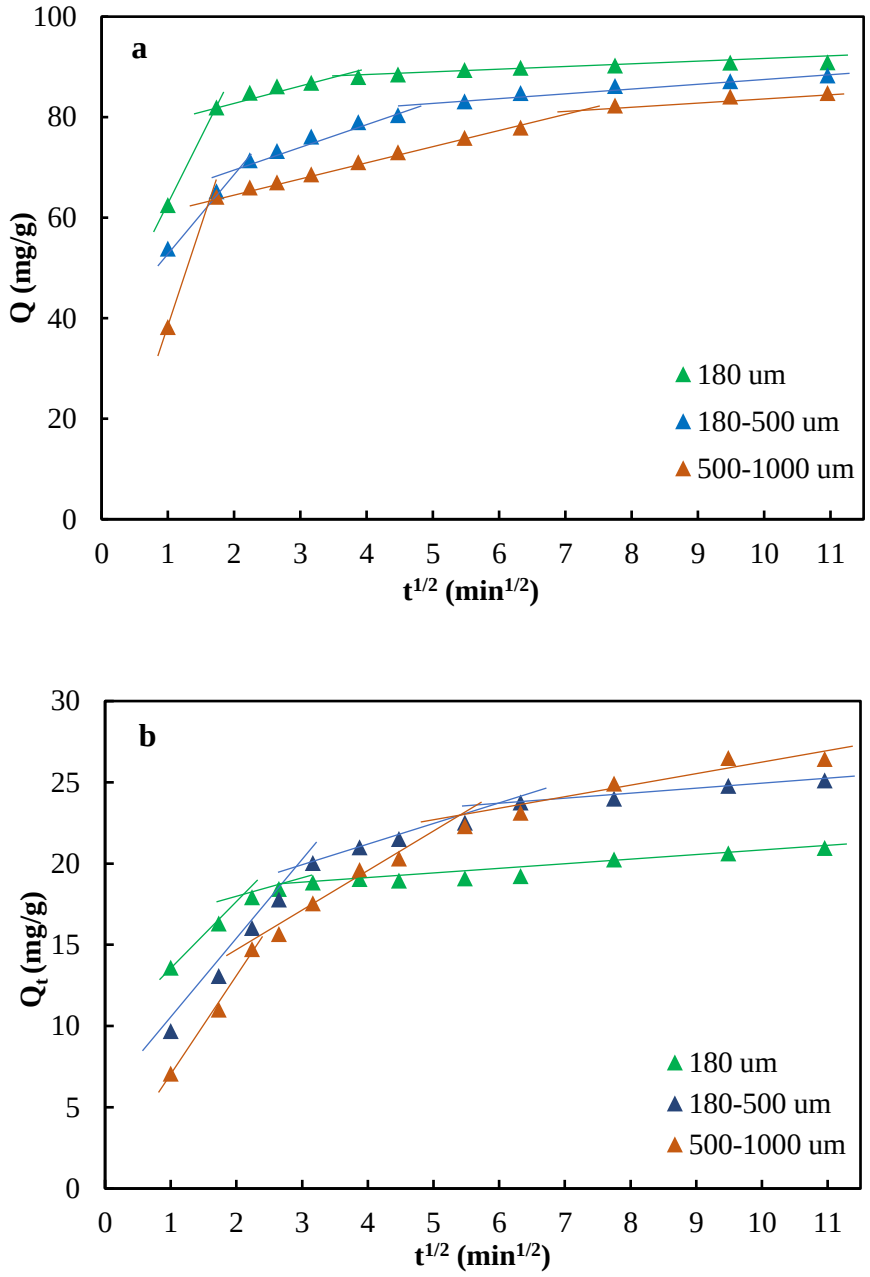

Figure 4.10 Intraparticle diffusion curves of the (a) Pb(II) and (b) Cd(II) biosorption processes.

[Initial metal concentrations of 50 ppm, pH 5.0 for Pb(II) and 7.0 for Cd(II) biosorption, 0.5 g/L WR, 250 rpm, 298 K.]

4.7.3. Pb(II) biosorption without continuous pH adjustment

Figure 4.11 depicts the kinetics of Pb(II) biosorption by WR at 298, 310 and 319 K without continuous pH adjustment (the initial pH of the biosorption systems was adjusted to 5.0). Similar to Pb(II) biosorption by WR with constant pH (Figure 4.7a), faster biosorption was observed at higher temperature in the initial periods (0-15 min), and similar Pb(II) biosorption capacities in equilibrium (92.16-96.97 mg/g) were obtained. It is interesting to note that Pb(II) biosorption without continuous pH adjustment dramatically slowed down as compared with Pb(II) biosorption with constant pH (equilibrium time 9-14 h versus 15-30 min). Why did Pb(II) biosorption by WR was much slower without continuous pH adjustment, but achieve similar equilibrium biosorption capacities in comparison with Pb(II) biosorption by WR with constant pH?

The decrease of pH in the Pb(II) biosorption systems indicated the release of H^+ from the binding sites (e.g., -COOH and $-NH_3^+$, see Section 6.1) when Pb(II) bound to them (Eqs. 4.1-4.4, M^{2+} refers to Pb(II) in this study). To maintain constant pH during Pb(II) biosorption, NaOH was continuously added into the biosorption systems. The introduction of OH^- instantly consumed the released H^+ according to Eqs. 4.1 & 4.3 and facilitated the deprotonation of the active functional groups (Eqs. 4.1 & 4.3). This rendered the binding sites on WR more accessible for Pb(II) in solution (Eqs. 4.2 & 4.4), leading to a faster Pb(II) biosorption process in the biosorption system with constant pH. Without continuous pH adjustment (namely, without NaOH addition), H^+ produced according to Eqs. 4.1 & 4.3 would not be instantly consumed by OH^-, resulting in slower deprotonation of the active

functional groups and thus slower binding of Pb(II) to the WR surface. However, similar reaction equilibrium could be eventually reached because Pb(II) in solution continuously reacted with the deprotonated functional groups (e.g., R-COO^- in Eq. 4.1 and R-NH_2 in Eq. 4.3) according to Eqs. 4.2 & 4.4. Besides, the final pH in the Pb(II) biosorption systems without continuous pH adjustment was about 4.10, at which the equilibrium Pb(II) biosorption capacity of WR was observed to be similar to that at pH 5.0 (see Figure 4.1a with initial Pb(II) concentration of 100 ppm).

$$\text{R-COOH} \leftrightarrow \text{R-COO}^- + \text{H}^+ \tag{4.1}$$

$$2\text{R-COO}^- + \text{M}^{2+} \rightarrow (\text{R-COO}^-)_2\text{M} \tag{4.2}$$

$$\text{R-NH}_3^+ \leftrightarrow \text{R-NH}_2 + \text{H}^+ \tag{4.3}$$

$$\text{R-NH}_2 + \text{M}^{2+} \leftrightarrow \text{R-NH}_2\text{M}^{2+} \tag{4.4}$$

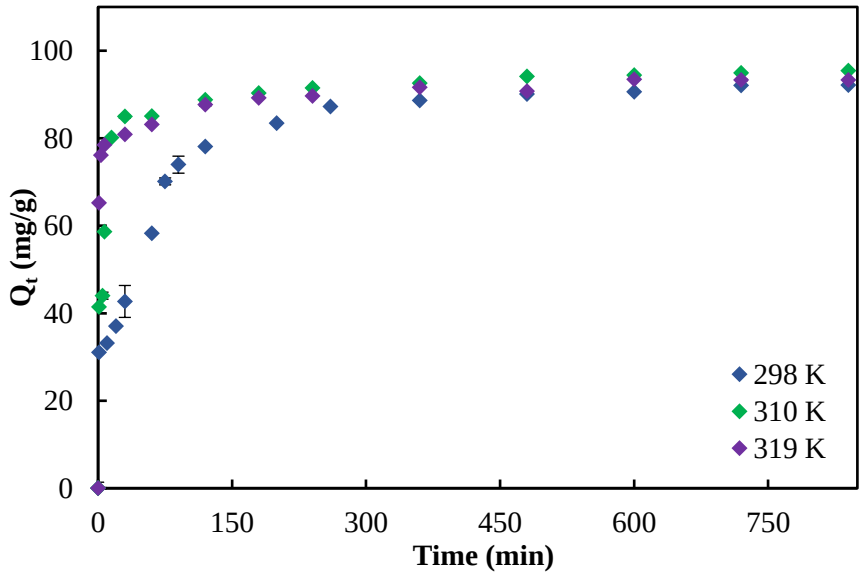

Figure 4.11 Pb(II) uptake by WR versus time at different temperatures without continuous pH adjustment.

[50 ppm Pb(II), initial pH 5.0, 0.5 g/L WR, WR < 180 µm, 250 rpm; Pb(II) biosorption was also studied at 278 K, but the result was not shown given the extremely long equilibrium time of 54 h.]

4.8. Desorption of Pb(II) and Cd(II) from WR

4.8.1. Optimal desorbing agents for desorption of Pb(II) and Cd(II)

The desorption efficiencies of Pb(II) and Cd(II) from WR by different desorbing agents, i.e., HCl, HNO_3 and citric acid, are described in Figure 4.12. Pb(II) was readily eluted with high desorption efficiencies (91%-99%) achieved by all types of desorbing agents; the highest desorption efficiency of Pb(II), i.e., 99%, was obtained by 0.1 M HCl. In the case of Cd(II) desorption, 78%-93% was recovered with the highest desorption efficiency of 93% attained by 0.1 M HNO_3. The underlying mechanism of Pb(II)/Cd(II) desorption by acids should be the competition from H^+ with the loaded metal ions for the binding sites; H^+ either neutralized the negatively charged sites to release the electrostatically bound Pb(II)/Cd(II) or occupied around the lone pairs of electrons of N and O atoms to break the metal complexes. It is noteworthy that as high as 12% of Cd(II) loaded on WR was desorbed by DDI water (only 1% of Pb(II)), suggesting that a part of Cd(II) was weakly bound to WR. This could explain why Cd(II) desorption efficiencies obtained were lower than the Pb(II) desorption efficiencies; a part of adsorbed Cd(II) ions was removed from WR by DDI water during the washing operation before desorption (the metal-loaded WR was washed by DDI water before suspending in the desorbing agents to remove the metal residues that were not attached to the binding sites). The resorption performance of the regenerated WR after desorption was investigated, and it was observed that more than 90% of the Pb(II) and Cd(II) biosorption capacities of WR (compared with pristine WR)

were maintained after desorption using 0.1 M HCl, HNO_3 or citric acid, indicating the sustainability of WR in biosorption.

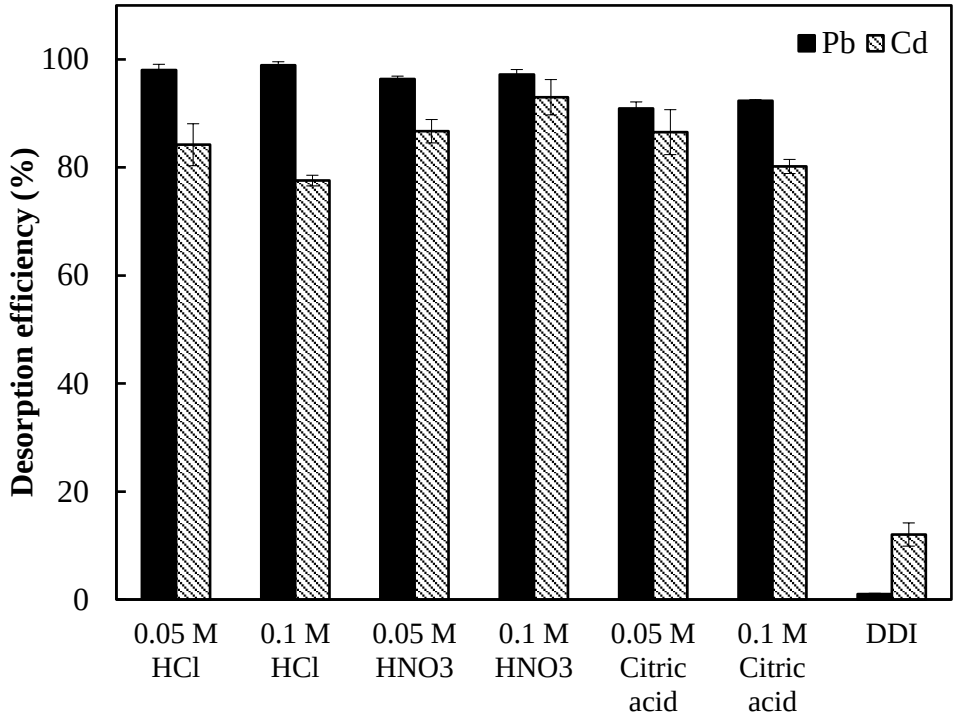

Figure 4.12 Desorption efficiencies of Pb(II) and Cd(II) from WR by various desorbing agents.

[S/L ratio 1.0 g/L, desorption time 3 h, 250 rpm, 298 K.]

4.8.2. Response surface methodology analysis

Taking Pb(II) desorption from WR as an example, RSM was used to evaluate the impact of three important desorption parameters, namely, S/L ratio, acid concentration, and desorption time, on the desorption of Pb(II). HCl, which had been proven as an efficient desorbing agent for Pb(II) elution, was used in the RSM analysis. The experiments designed by CCD of RSM are listed in Table A2. Based on the desorption efficiencies determined from the designed experiments, a quadratic equation in coded factors (Eq. 4.5) and actual factors (Eq. 4.6) were obtained to express the relationship between the response and independent variables. In the equations, *Y* refers to desorption efficiency (%), and *A*, *B*, *C* are S/L ratio (g/L), acid concentration (M), and desorption time (h), respectively. The coded equation is useful for identifying the relative impact of the factors by comparing their coefficients. Thus, the impact of the three factors on the desorption efficiency was in a descending order of acid concentration > S/L ratio > desorption time according to Eq. 4.5. Also, the interaction between acid concentration and desorption time was relatively significant. Specifically, the impact of the acid concentration on desorption efficiency became more significant at higher S/L ratios, as shown in Figure 4.13. Likewise, desorption time played a more and more important role as the S/L ratio increased (Figure 4.14). Figure 4.15 indicates that time only exerted obvious influence on desorption efficiency at low acid concentrations (e.g., 0.2-0.4 M HCl).

$$Y=95.20-2.63*A+3.65*B+2.28*C+2.00*AB+2.02*AC-2.69*BC-0.18*A^2-1.38*B^2-1.49*C^2 \quad (4.5)$$

$$Y=91.55-4.80*A+42.69*B+7.54*C+4.99*AB+1.01*AC-13.45*BC-0.044*A^2-34.39*B^2-1.49*C^2 \quad (4.6)$$

Furthermore, the reliability of Eq. 4.6 for describing the relationship among desorption efficiency, S/L ratio, acid concentration, and desorption time in Pb(II) desorption from WR by HCl was evaluated by comparing the predicted and experimental desorption efficiencies (Table 4.3). It was predicted that the desorption efficiency would be the highest (98.92%) with S/L of 4 g/L, 0.6 M HCl, and desorption time of 1.182 h. The experimental result was 97.14% at the recommended conditions, indicating a good predictability of Eq. 4.6. The Analysis of Variance (ANOVA) revealed that Eq. 4.6 derived from RSM analysis was significant and its lack of fit for the experimental data was not significant. In addition, the high value of R^2 (0.89) supported the applicability of Eq. 4.6 for describing the desorption data. However, the low value of the Prediction R^2 suggested its weak predictability (details in Table A3). Despite the extensive applications of RSM, especially on optimization of fermentation media (Desai et al., 2008), some biases were observed when applying this method to desorb heavy metal ions in this study. For example, with the same S/L ratio (6 g/L) and acid concentration (0.2 M), the desorption efficiency of Pb(II) was supposed to increase as the desorption time increased from 2 to 5 h. However, the highest desorption efficiency was predicted at 3.42 h rather than 5 h by RSM (runs 11-13 in Table 4.3). This was probably caused by the intrinsic limitation of RSM. RSM was mostly used in the optimization of growth conditions and compositions of media/feed for organisms, in which the response (e.g., growth rate of bacteria) would augment along with the increase of an important factor (e.g., concentration of mineral ions

in the medium) and start to decline due to inhabitation/toxicity when the factor was larger than a certain value. However, this was not the case in heavy metal desorption from biosorbents. Despite this limitation, this study suggests that RSM is still a great tool for investigating the significance of various factors (e.g., S/L ratio, concentration of the desorbing agent, and desorption time) on desorption performance, as well as the interactive effect of any two factors in a system.

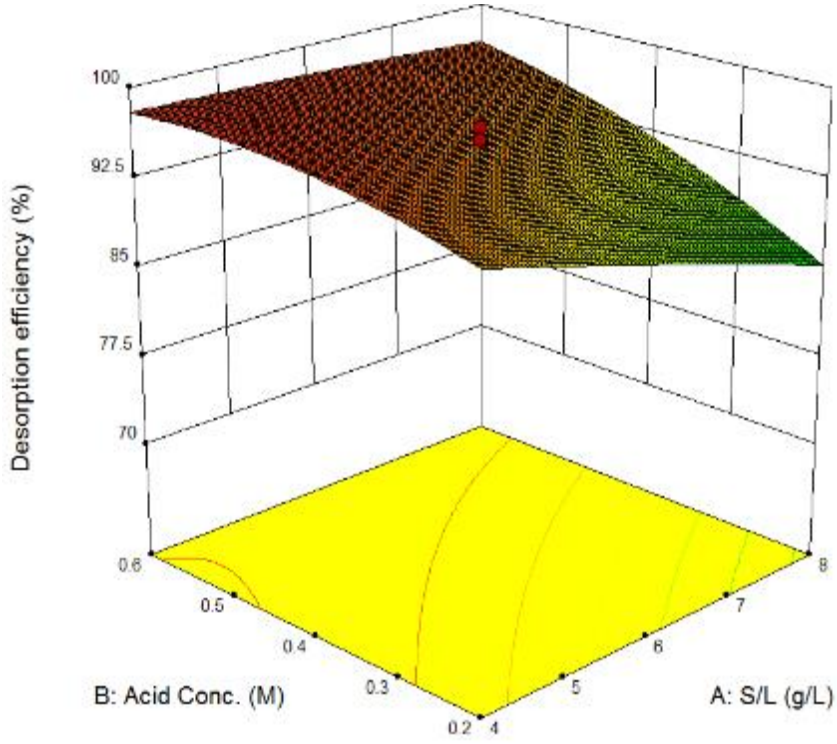

Figure 4.13 Three-dimensional plot showing the effect of S/L ratio and acid concentration on desorption efficiency.

[Desorption time 2 h.]

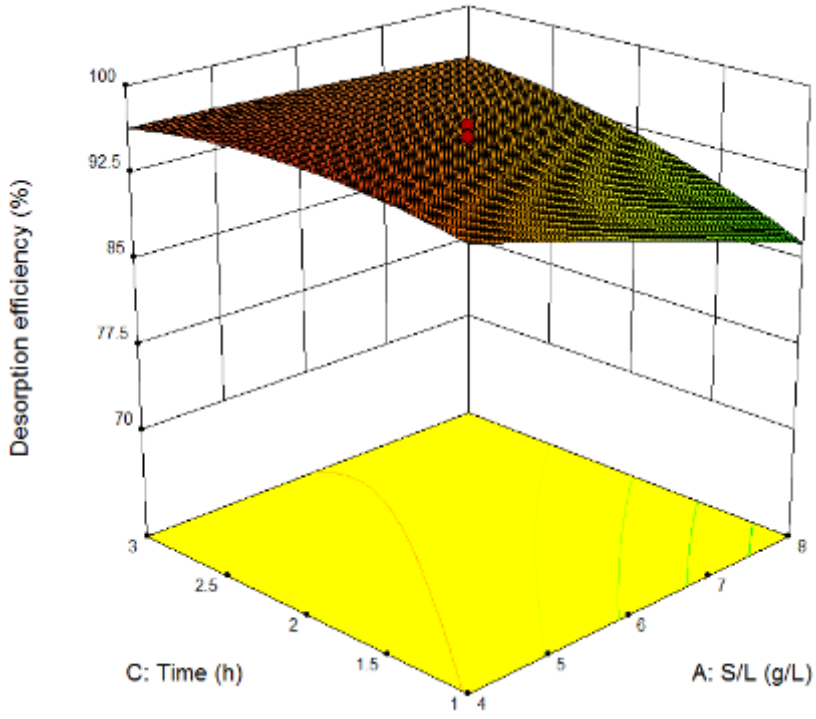

Figure 4.14 Three-dimensional plot showing the effect of S/L ratio and time on desorption efficiency.

[Acid concentration 0.4 M.]

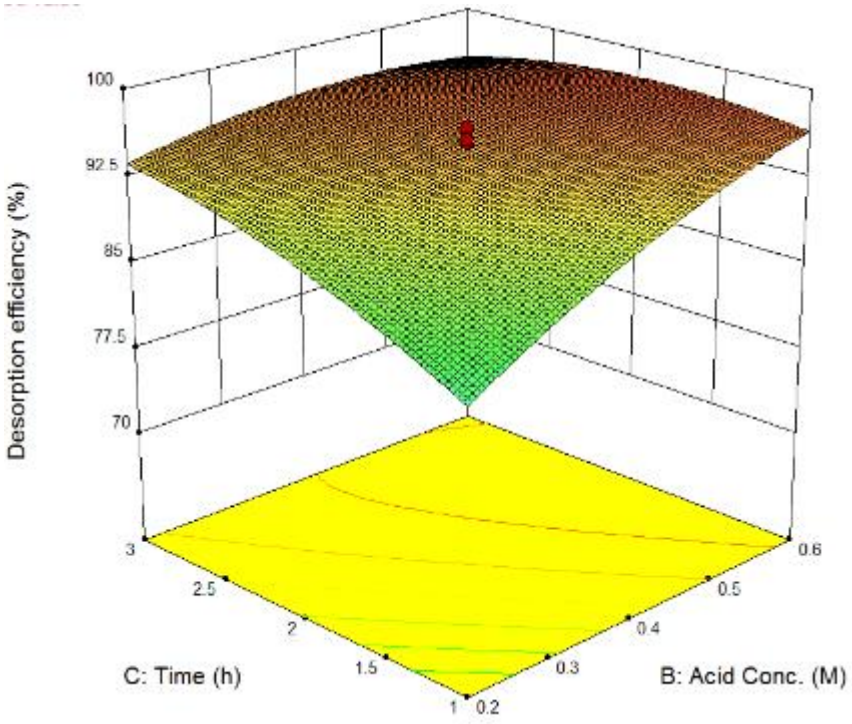

Figure 4.15 Three-dimensional plot showing the effect of acid concentration and time on desorption efficiency.

[S/L ratio 6 g/L.]

Table 4.3 Confirmation of the predicted model by desorption experiments.

Run	S/L (g/L)	Acid (M)	Time (h)	DE_p (%)	DE_e (%)	Residual
1[a]	4	0.6	1.182	98.92	97.14	-1.78
2	4.098	0.575	0.191	96.77	95.57	-1.20
3	5.323	0.6	0.05	94.15	92.27	-1.88
4	5.323	0.6	0.1	94.38	92.94	-1.44
5	4	0.359	0.191	90.93	93.68	2.75
6	4	0.359	1	94.96	94.24	-0.72
7	4	0.359	3	96.57	93.99	-2.58
8	2	0.2	0.5	93.99	95.05	1.06
9	2	0.2	1	96.31	94.56	-1.75
10	2	0.2	3	98.15	94.47	-3.68
11	6	0.2	2	90.17	89.75	-0.42
12	6	0.2	3.41	94.21	89.52	-4.69
13	6	0.2	5	91.68	94.54	2.86
14	6	0.4	0.083	85.37	89.36	3.99
15	6	0.4	0.1667	86.02	89.25	3.23
16	6	0.4	0.5	88.43	91.24	2.81
17	6	0.4	1	91.43	91.61	0.18
18	6	0.4	2	95.19	92.31	-2.88
19	6	0.4	3.41	95.44	92.7	-2.74
20	6	0.6	0.083	92.80	91	-1.80
21	6	0.6	0.1667	93.23	91.72	-1.51
22	6	0.6	0.5	94.74	91.83	-2.91
23	6	0.6	1	96.40	92	-4.40
24	6	0.6	2	97.47	92.75	-4.72
25	6	0.6	3.41	93.93	92.38	-1.55

(**Notes**: a - The predicted optimal group of experiment; DE_p - Predicted desorption efficiency; DE_e - Experimental desorption efficiency.)

4.9. Pb(II) removal from drinking water by using WR

In consideration of the frequent outbreaks of Pb contamination in drinking water all over the world, the potential of WR for Pb(II) removal from drinking water was investigated to examine if the stringent standard of drinking water can be met. Different dosages of WR were employed to treat a Pb(II) solution at 400 ppb. The results showed that the Pb(II) concentrations of the WR-treated solutions were as low as 5.21 ± 0.55 ppb and 1.97 ± 0.09 ppb with WR dosages of 0.05 g/L and 0.1 g/L, respectively. These values were lower than the WHO guideline value of Pb in drinking water, namely, 10 ppb (WHO, 2011b), revealing the great potential of WR in treating Pb(II) contaminated drinking water to safeguard the health of humans.

4.10. Biosorption-desorption in WR-packed bed column reactors

4.10.1. Pb(II) biosorption-desorption cycles

Biosorption

The breakthrough curves of Pb(II) biosorption in a WR-packed bed column reactor are illustrated in Figure 4.16. It was observed that the column reactor achieved excellent performance over 10 biosorption-desorption cycles (0.05 M HCl as the desorbing agent) with a long breakthrough time (t_b, time at which C_t/C_0=5%) of 8.3-13.0 h (i.e., 93-144 BV), revealing its high durability and repeatability for Pb(II) sequestration. As shown in Table 4.4, there were even increasing trends in t_b and the equilibrium biosorption capacity (q_0). Non-linear simulation of the breakthrough curves by a variety of models, including the Thomas, Bohart-Adams, Dose-Response, and Yoon and Nelson models, indicated that the Thomas model was the best fitting one to Pb(II) biosorption in the WR-packed bed column reactor (see details in Figure A7) with extremely high values of R^2 (0.992-0.999, Table 4.4), implying that Pb(II) biosorption in the column reactor had a plug flow and followed the Langmuir isotherm and the pseudo-second-order kinetics.

Desorption

Figure 4.17 describes the desorption curves at the 1st, 3rd, 5th and 10th cycles (for unambiguous plotting, other cycles were not shown due to the high similarity). It can be seen that most of the bound Pb(II) in the column reactor was rapidly eluted by the desorbing agent (i.e., 0.05 M HCl). As high as 95% of the sequestered Pb(II) was rapidly desorbed within 1.3-2.3 h, achieving high concentration factors (i.e., ratio of Pb(II) concentration in desorption effluent to that in influent) of 5.8-11.6.

In addition to the profoundly efficient desorption, the biosorption performance of the packed bed column reactor remained very well after the acidic treatment in desorption and became even better in the subsequent cycles. The improvement could be ascribed to the release of organic substances (i.e., colored materials and reducing sugars) from WR, which led to a more porous WR structure with larger exposure of active sites for Pb(II) sequestration (Gupta and Rastogi, 2009). In addition, the methylester group (-$COOCH_3$) of galacturonic acid in pectin could be hydrolyzed to carboxylic groups, which would favor Pb(II) biosorption as carboxyl groups were identified as preferred active functional groups for heavy metal binding (see Section 6.3).

Monitoring of the column effluent

The change in pH and total organic carbon (TOC) release were monitored in the effluent of the WR-packed bed column reactor during the 10 Pb(II) biosorption-desorption cycles. As shown in Figure 4.18, the pH of the effluent at the beginning (0-230 min) of the biosorption process in the first cycle was higher than 5.0 (i.e., the pH of the Pb(II) influent). This could be due to the release of organic components from WR in the first cycle (evidenced by the high TOC release in the first cycle, data not shown), which dissolved in the Pb(II) solution that passed through the column reactor and resulted in the effluent with pH values higher than 5.0. In addition, light metal ions (i.e., Mg^{2+} and Ca^{2+}) bound to the binding sites on WR exchanged with Pb(II) in solution during the biosorption process of the first cycle (see Section 6.1.8). The release of Mg^{2+} and Ca^{2+} from WR could barely cause acidification of the Pb(II) solution that passed through the column reactor in

comparison with the release of H^+, which was responsible for the ion exchange with Pb(II) in solution in the subsequent cycles due to the consumption of naturally occurring light metal ions on WR in the first biosorption-desorption cycle. The WR packed in the bed column reactor was regenerated by using 0.05 M HCl after Pb(II) biosorption in the first cycle, and the binding sites on its surface would be protonated. In the biosorption of the subsequent cycles (2^{nd}-10^{th} cycles), however, the pH values of the column effluent were lower than 5.0 (i.e., the pH of Pb(II) influent) at the beginning of the biosorption processes; it slowly approached 5.0 as the column reactor gradually became saturated. The dropped pH of the effluent (compared with that of the Pb(II) influent) should be caused by the release of H^+ from the binding sites (e.g., carboxyl and hydroxyl groups) when Pb(II) loaded upon them, and this interaction gradually weakened as the WR packed in the column reactor became more and more saturated, resulting in less pH drops in the Pb(II) effluent in the late phase of the biosorption processes. Determination of TOC in the effluent of the WR-packed bed column reactor showed that there was leaching of organic components from the WR in the column reactor during the 10 Pb(II) biosorption-desorption cycles (*ca.* 10% of the original WR biomass was released in total); the TOC release from WR mainly occurred in the first biosorption-desorption cycle.

The high durability, excellent repeatability, and efficient desorption observed in the WR-packed bed column reactor indicate that WR was competitive to those commercial adsorbents or ion-exchangers used in Pb(II) removal/recovery, not to mention its low cost as a fruit waste material.

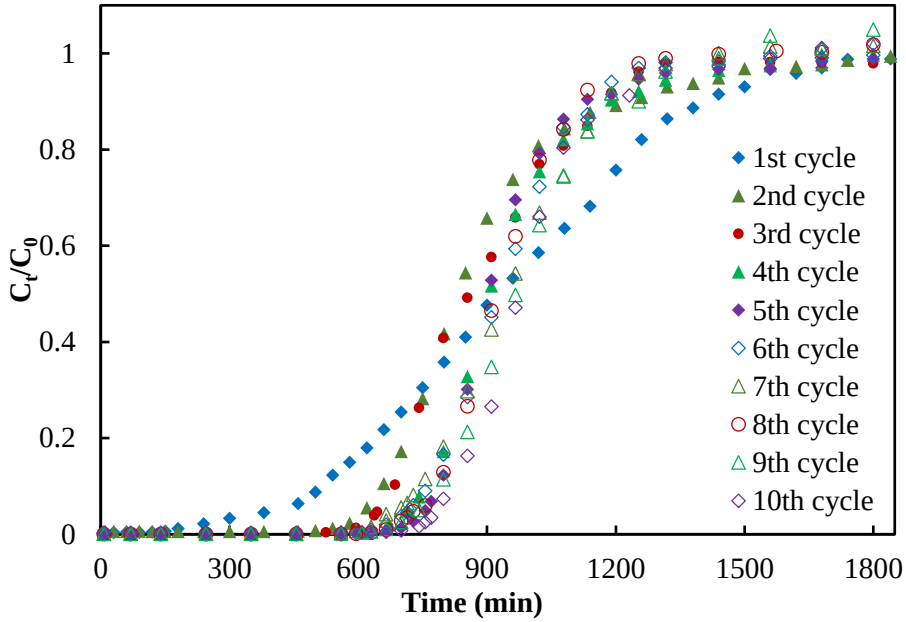

Figure 4.16 Breakthrough curves of Pb(II) biosorption in the WR-packed bed column reactor.

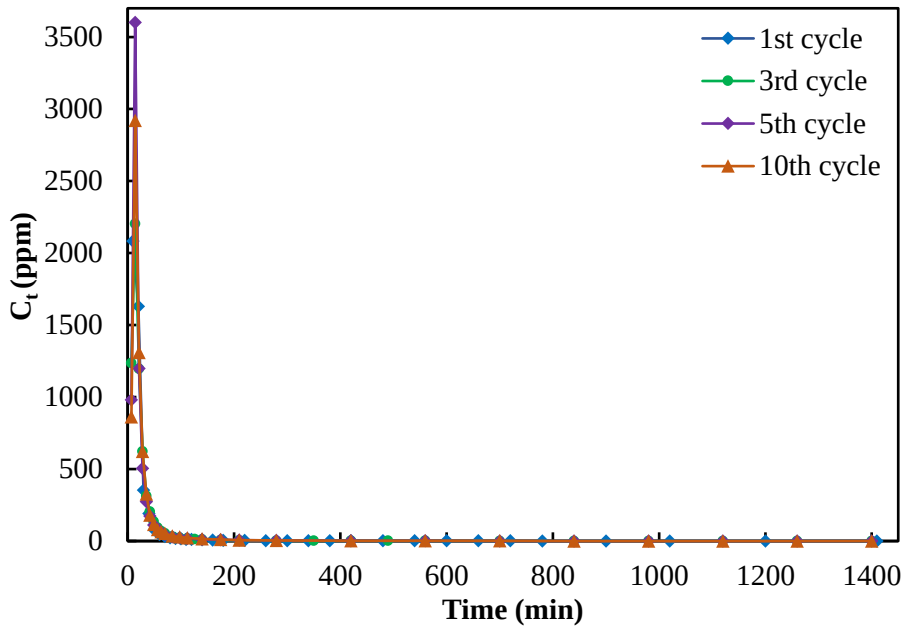

Figure 4.17 Pb(II) desorption in the WR-packed bed column reactor.

[Desorbing agent 0.05 M HCl was used; Four cycles shown as the representatives.]

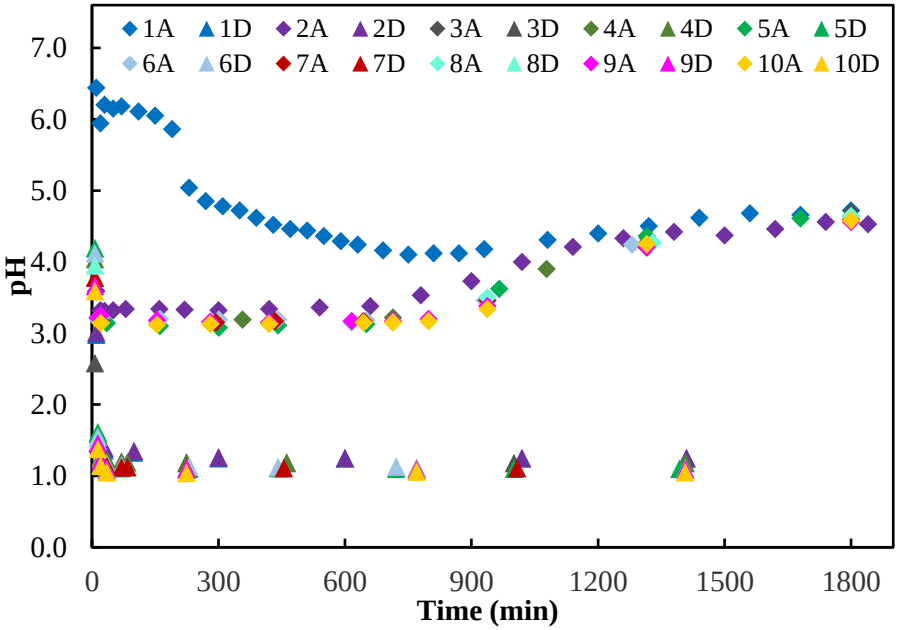

Figure 4.18 Change in pH of the effluent from the WR-packed bed column reactor in 10 cycles of Pb(II) biosorption-desorption.

[A: Adsorption; D: Desorption.]

Table 4.4 Column performance and parameters of the Thomas model in Pb(II) biosorption.

Cycle	1	2	3	4	5	6	7	8	9	10
t_b (h)	8.3	10.3	10.8	12.0	12.6	12.0	11.7	12.1	12.4	13.0
q_e (mg/g)	73.37	77.76	75.54	78.86	77.88	80.17	79.97	79.36	75.89	76.31
q_0 (mg/g)[a]	71.96	74.68	74.30	76.25	75.48	79.65	79.80	78.77	79.86	81.19
k^b	0.142	0.173	0.171	0.221	0.282	0.232	0.196	0.256	0.213	0.277
R^2	0.999	0.993	0.992	0.995	0.995	0.999	0.999	0.999	0.998	0.998

(**Notes:** a - Maximum Pb(II) biosorption capacity predicted by the Thomas model; b -Thomas rate constant with unit of mL/min/mg; Modeling results of the Bohart-Adams, Dose-Response, and Yoon and Nelson models were not shown due to the poor fitness.)

4.10.2. Cd(II) biosorption-desorption cycles

As mentioned in Section 3.4.10, the column reactor packed with native WR exhibited a poor performance on Cd(II) biosorption in the preliminary study (Figure A8). It was observed that the Cd(II) biosorption capacity of WR at pH 6.0 was only 34% of that at pH 7.0 in the batch study (see Section 4.1). The poor Cd(II) biosorption performance of the column reactor packed with native WR should be caused by the low pH condition inside the column during biosorption, i.e., below pH 6.0 as measured in the effluent. The dissolution of CO_2 from the air into the column reactor and the release of acidic substances from WR could be the causes for the dropped pH, even though a Cd(II) solution at pH 7.5-8.0 was used as the influent. To solve the pH problem, WR was pretreated by 0.05 M NaOH for 3 h to remove the acidic substances and break down the inter- and intra-molecular hydrogen bonds to increase the number of free hydroxyl groups. The NaOH-treated WR was washed by DDI water to remove the residual Na^+ and OH^- before packing inside the column reactor for Cd(II) biosorption. HCl at 0.05 M were used as the desorbing agent to elute the sequestered Cd(II) and regenerate the column reactor. After one biosorption-desorption cycle, the column reactor was thoroughly washed by DDI water to remove the residual acid before the next biosorption-desorption started. As shown in Figure 4.19, the breakthrough time (t_b, time at which C_t/C_0=5%) of the column reactor packed with NaOH-treated WR was 4.8 h and 2.6 h (i.e., 42.3 BV and 27.3 BV) in the first and second cycles, respectively, increasing by 40% and 72% in comparison with those of the native WR column reactor without any NaOH treatment (details in Figure A8). Besides, the biosorption capacities significantly increased to 93.9 mg/g in the first cycle and 76.3 mg/g in the second

cycle, which were much higher than those of the native WR column reactor (22.9 mg/g and 24.7 mg/g, respectively). The great improvement should be attributed to: (1) the removal of acidic substances from WR by NaOH, creating a neutral or even slightly alkaline condition which was preferable for Cd(II) biosorption, and (2) the more porous structure of WR with increased swelling resulted after pretreatment, leading to exposure of more binding sites and better contact with Cd(II). In the literature, NaOH was also used for pretreatment of *Agaricus bisporus* biomass for better Pb(II) biosorption in a packed bed column reactor (Long et al., 2014). The reduction of biosorption capacity observed in the second cycle could be caused by the acidic treatment in desorption, which totally protonated the functional groups (e.g., -COOH, -OH, and $-NH_3^+$) on the surface of WR, making Cd(II) binding to WR difficult. Besides, the pH was still be slightly acidic inside the column reactor even after a long time of washing by DDI water; the acidic condition impaired the Cd(II) biosorption performance of the column reactor in the second cycle. In addition, the successive treatment of WR by alkali in pretreatment and acid in desorption could impair the structure of WR, resulting in a weakened biosorption performance of WR. Pretreatment and regeneration of WR by proper reagents for the biosorption of Cd(II) should be considered in future studies. As shown in Figure 4.20, most Cd(II) was rapidly eluted in 60 min, at which 95% and 97% of the entrapped Cd(II) were eluted (concentration factors of 8.4 and 7.0) in the first and second cycles, respectively.

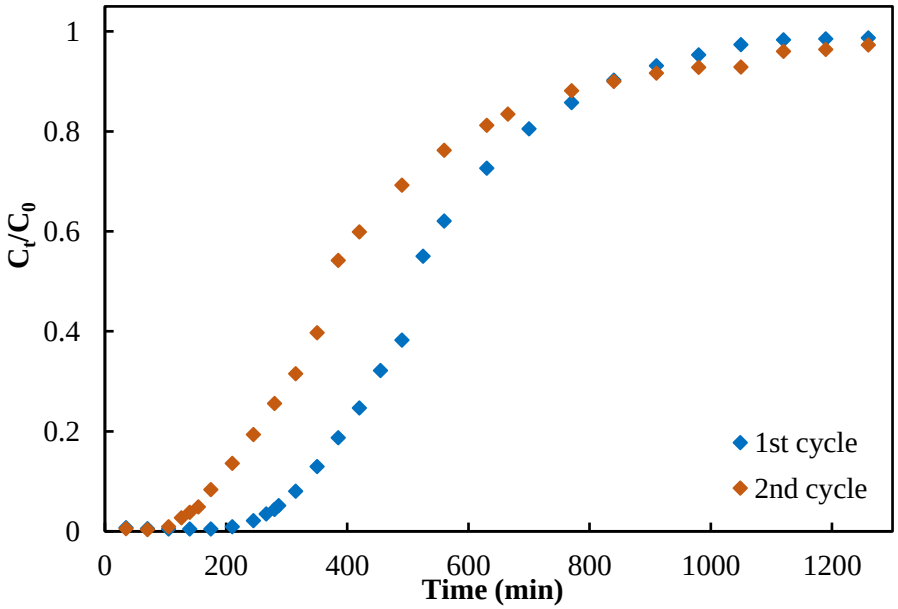

Figure 4.19 Breakthrough curves of Cd(II) biosorption in the column reactor packed with NaOH-treated WR.

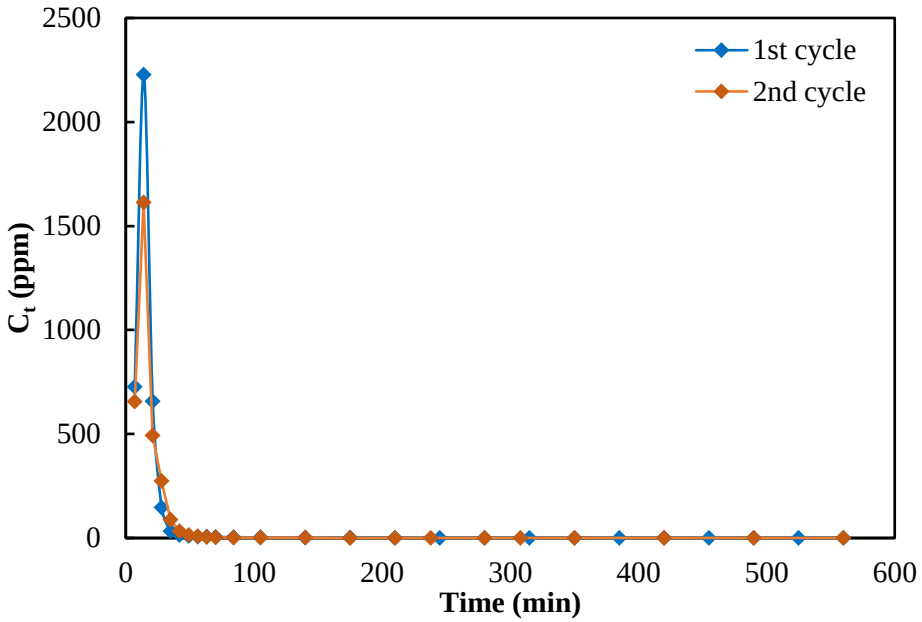

Figure 4.20 Cd(II) desorption in the column reactor packed with NaOH-treated WR.

[Desorbing agent 0.05 M HCl was used.]

4.11. Summary

This chapter presents the results obtained in the macroscopic biosorption studies of Pb(II) and Cd(II) using WR as the biosorbent, both in batch and continuous modes. The main findings are summarized as follows.

(1) The biosorption capacities of WR augmented with increasing pH, with optimal pH 5.0 for Pb(II) biosorption and 7.0 for Cd(II) biosorption.

(2) Both Pb(II) and Cd(II) biosorption by WR were partially influenced by ionic strength, implying electrostatic attraction as one of the underlying binding mechanisms.

(3) WR had a high selectivity on Pb(II) in the presence of co-metal ions. Using WR for biosorption of multiple heavy metal ions can make better use of the biosorbents, as it was observed that a higher amount of heavy metal ions (in mmol) was sequestered by a unit mass of biosorbent (in gram) in binary systems than that of the single system.

(4) The maximum biosorption capacities, 231.57 ± 1.09 mg-Pb/g (1.12 ± 0.005 mmol/g) and 98.51 ± 1.15 mg-Cd/g (0.88 ± 0.01 mmol/g), were achieved by WR at pH 5.0 and 7.0, respectively.

(5) The equilibrium data of Pb(II) biosorption were best described by the R-P isotherm, suggesting multilayer loading of Pb(II) on the heterogeneous surface of WR. The equilibrium data of Cd(II) biosorption were best fitted by the D-R isotherm, which implied Cd(II) binding to non-identical sites on the WR surface.

(6) Pb(II) and Cd(II) biosorption became faster as the particle size of WR decreased. The equilibrium Pb(II) biosorption capacities of WR in different particle sizes remained similar, whereas the equilibrium Cd(II) biosorption capacity augmented as the particle size increased. This should be caused by the higher content of light metal ions in larger WR as ion exchange played a more important role in Cd(II) biosorption than in Pb(II) biosorption by WR (see Section 6.1.8).

(7) The sequestered Cd(II) on WR was more easily eluted by DDI water than the sequestered Pb(II), suggesting that ion exchange and/or electrostatic attraction (weaker force than complexation) played a more important role in Cd(II) biosorption than in Pb(II) biosorption by WR.

(8) The WR-packed bed column reactor showed high durability, excellent repeatability, and efficient desorption in Pb(II) biosorption-desorption operations. However, the column performance for Cd(II) biosorption-desorption operations was not as good as that for Pb(II) biosorption-desorption operations, even after pretreatment of WR by using NaOH.

Taken together, WR is a promising biosorbent for Pb(II) and Cd(II) removal from wastewater. In particular, the wide range of appropriate operational pH, the slight effects of particle size, ionic strength, and co-metal ions, and the excellent performance of the packed bed column reactor reflect that WR is competitive to those commercial adsorbents and ion-exchangers for Pb(II) removal/recovery from wastewater (and even drinking water), not to mention its low cost as a fruit waste material.

5. Biosorption of Pb(II) and Cd(II) by Mango Seed

5.1. Effect of particle size

The Pb(II) and Cd(II) biosorption capacities of MS in different particle sizes are shown in Figure 5.1. MS smaller than 180 µm exhibited much higher Pb(II) and Cd(II) uptakes than MS at 180-500 µm and at 500-1000 µm. The remarkably different biosorption capacities could be caused by the different compositions of MS in different particle sizes. Various characterization methods were employed to further investigate the cause of the significant effect of particle size on the biosorption capacity of MS as reported in Section 6.2.9. MS smaller than 180 µm was used in the subsequent biosorption studies.

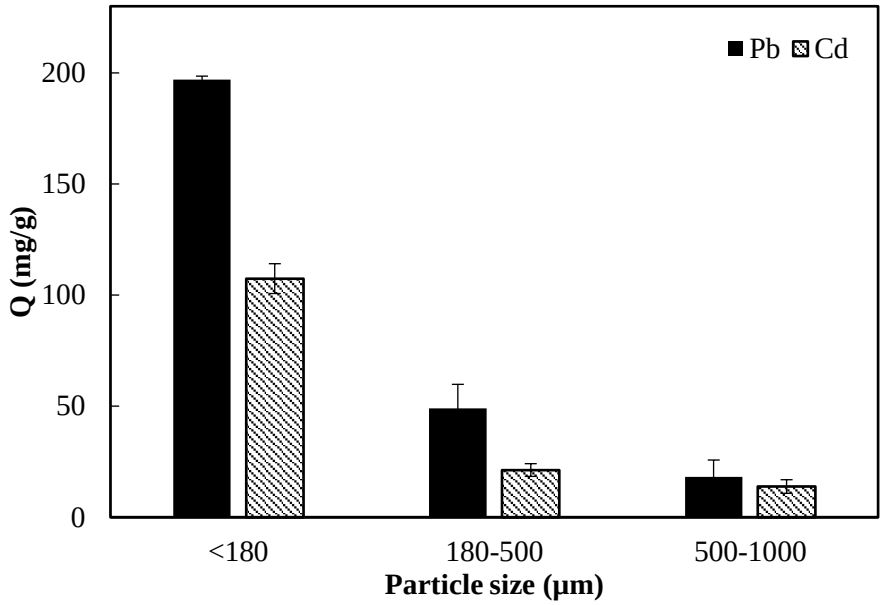

Figure 5.1 Effect of particle size on Pb(II) and Cd(II) biosorption by MS.

[Initial metal concentrations of 500 ppm, pH 5.0 for Pb(II) and 7.5 for Cd(II) biosorption, 1.0 g/L MS, 250 rpm, 298 K, 24 h.]

5.2. Effect of pH

Figure 5.2 indicates that the Pb(II) and Cd(II) biosorption capacities of MS elevated along with increasing pH and reached the maximum at pH 6.0 and 8.0, respectively. The positive correlation should be attributed to the less competition from H^+ for binding sites on the MS surface at higher pH. Moreover, the deprotonation of carboxyl groups (dissociation constant pK_a around 3.5) at high pH would provide more binding sites to Pb(II) and Cd(II). The abrupt decreases of Q at high pH, namely pH > 6.0 in Pb(II) biosorption and pH > 8.0 in Cd(II) biosorption, were due to precipitation of Pb(II) and Cd(II) at the alkaline environment. Given that precipitation of Pb(II) and Cd(II) was respectively observed at pH 6.0 and 8.0 in the control groups, pH 5.0 was chosen in Pb(II) biosorption and pH 7.5 in Cd(II) biosorption by MS in the following studies.

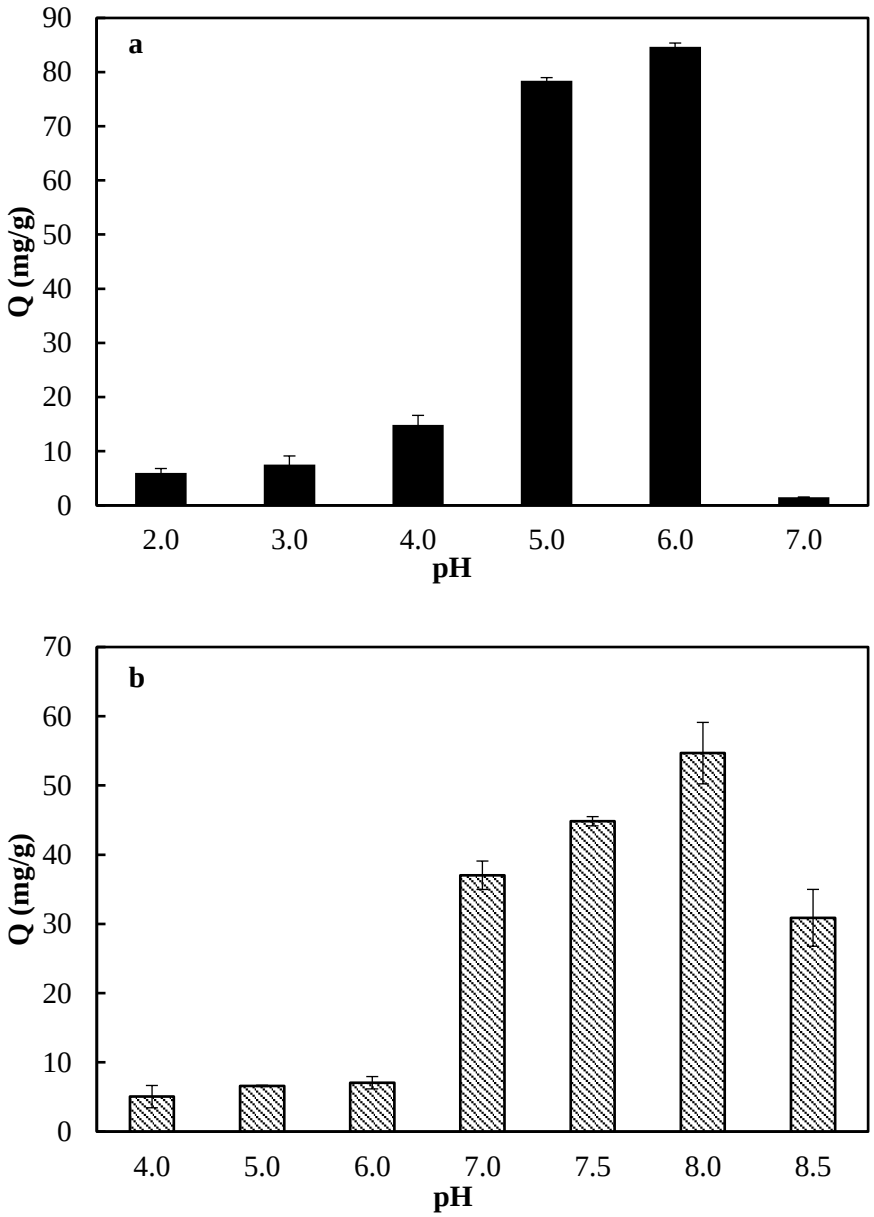

Figure 5.2 Effect of pH on (a) Pb(II) and (b) Cd(II) biosorption by MS.

[Initial metal concentrations of 100 ppm, 1.0 g/L MS, 250 rpm, 298 K, 24 h.]

5.3. Effect of MS dosage

As Figure 5.3 illustrates, higher Pb(II) and Cd(II) biosorption capacities were obtained at the MS dosage of 0.5 and 1.0 g/L. This was because the binding sites available on MS at a low dosage could be easily saturated by the metal ions in the biosorption system. The Pb(II) and Cd(II) biosorption capacities gradually reduced as the MS dosage augmented due to the excessive binding sites provided by a high dosage of MS, resulting in a low metal uptake by a unit mass of MS (i.e., one gram). Although the removal efficiencies of Pb(II) and Cd(II) would increase along with increasing MS dosage, 1.0 g/L was used in the subsequent biosorption studies to achieve a better utilization of MS.

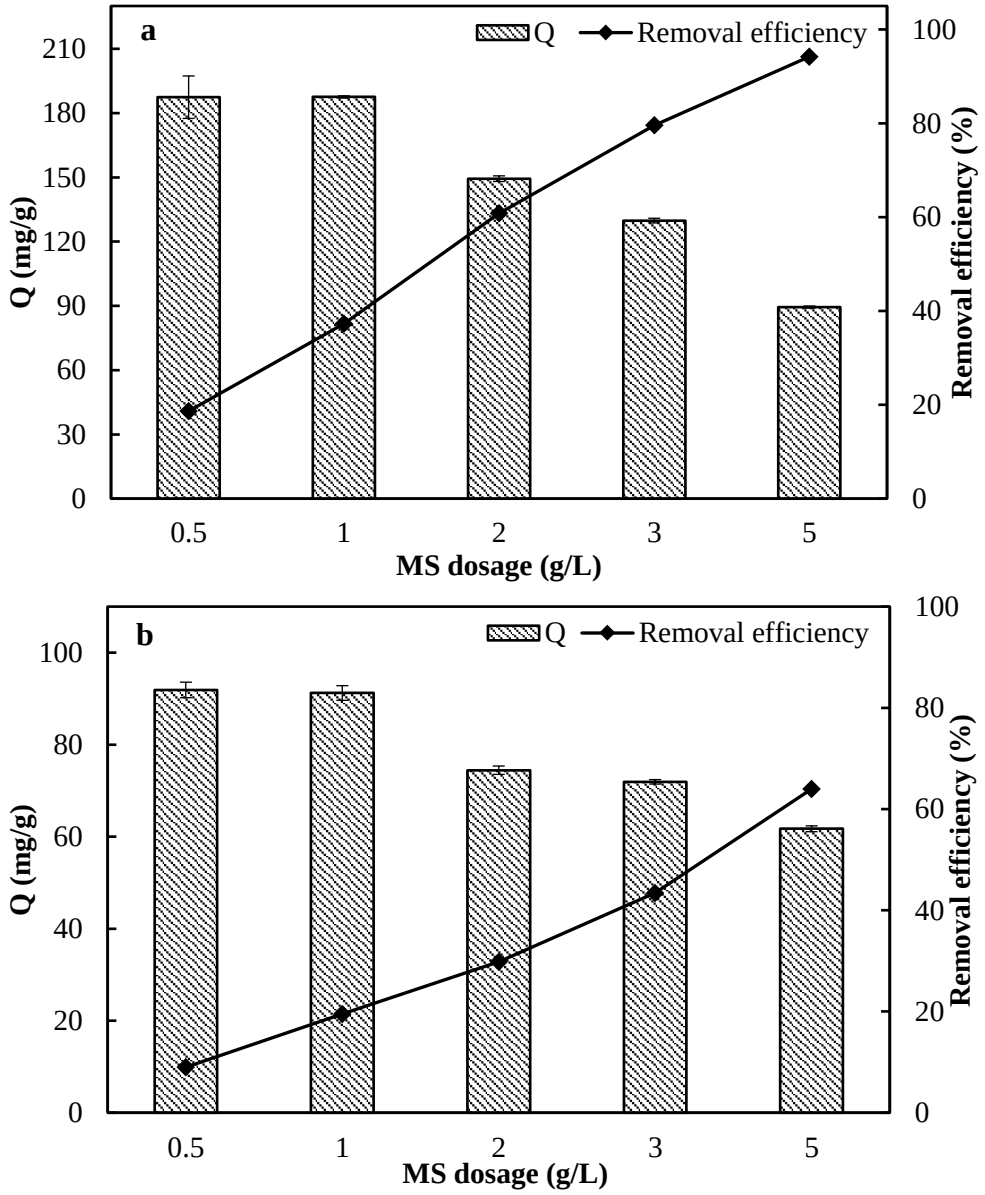

Figure 5.3 Effect of MS dosage on (a) Pb(II) and (b) Cd(II) biosorption.

[Initial metal concentrations of 500 ppm, pH 5.0 for Pb(II) and 7.5 for Cd(II) biosorption, 250 rpm, 298 K, 24 h.]

5.4. Effect of initial metal concentration

As indicated in Figure 5.4, the Pb(II) and Cd(II) biosorption capacities of MS were augmented as the initial metal concentrations increased, and gradually reached a plateau value. This was because a higher concentration of metal ions would exert a more intensive driving force for their mass transport to the binding sites on MS, enhancing the biosorption of Pb(II) and Cd(II) by MS (Aksu and Tezer, 2005). As the amount of metal ions increased to a certain level, binding sites on the MS surface would become saturated, and the biosorption capacity of MS would not increase any more. Decreasing removal efficiencies were observed along with increasing initial metal concentrations given the limited number of binding sites provided by the fixed dosage of MS (i.e., 1.0 g/L) in the biosorption systems (Duan et al., 2010).

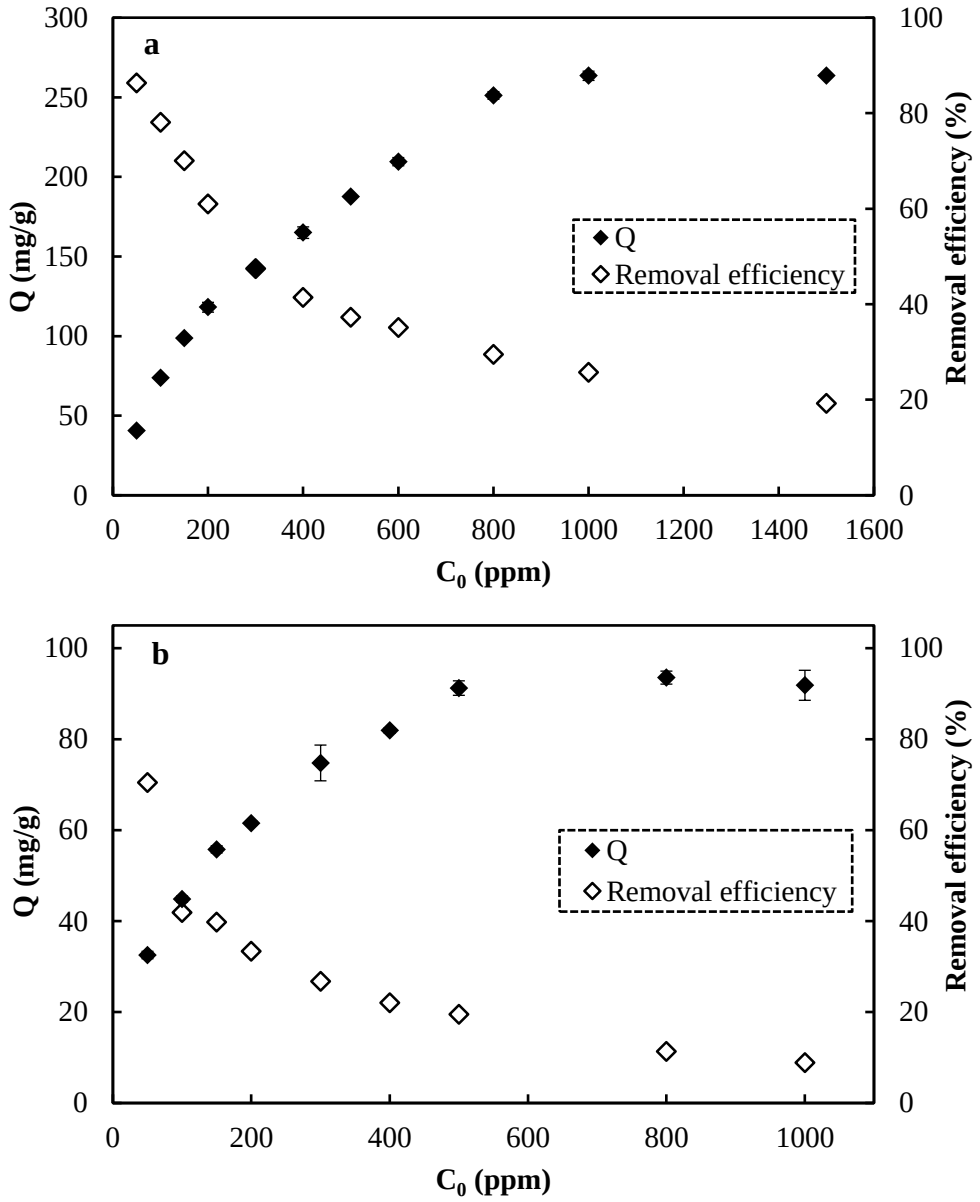

Figure 5.4 Effect of initial metal concentration on (a) Pb(II) and (b) Cd(II) biosorption by MS.

[pH 5.0 for Pb(II) and 7.5 for Cd(II) biosorption, 1.0 g/L MS, 250 rpm, 298 K, 24 h.]

5.5. Effect of ionic strength

As the ionic strength increased from 0 to 0.2 M $NaNO_3$, the Pb(II) biosorption capacity of MS decreased by 22%, and that of Cd(II) decreased by 13% as compared with that of the biosorption systems without $NaNO_3$ (Figure 5.5). This should be caused by the competition from Na^+ for the non-specific binding sites based on electrostatic attraction on the surface of MS (Lv et al., 2012, Wang et al., 2013). The partially impaired biosorption capacities suggested that electrostatic attraction was one of the underlying mechanisms, but not the dominant one, in Pb(II) and Cd(II) biosorption by MS. Other interaction(s) which was(were) not easily influenced by the presence of other ions (especially cationic ones) could contribute to sequestration of Pb(II) and Cd(II) by MS at the same time. Additionally, the small reduction of Pb(II) and Cd(II) biosorption capacities by MS at ionic strength as high as 0.2 M of $NaNO_3$ indicates the application potential of MS in real heavy-metal-bearing wastewater, which usually contains a variety of ions.

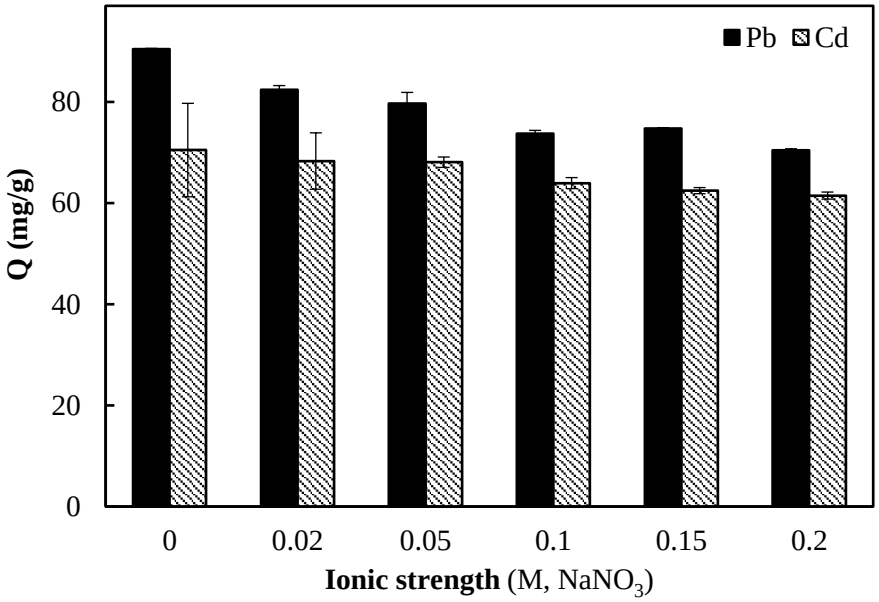

Figure 5.5 Effect of ionic strength on Pb(II) and Cd(II) biosorption by MS.

[Initial metal concentrations of 100 ppm, pH 5.0 for Pb(II) and 7.5 for Cd(II), 1.0 g/L MS, 250 rpm, 298 K, 24 h.]

5.6. Effect of co-metal ions

Figure 5.6 illustrates the effect of different equal molar co-metal ions on Pb(II) and Cd(II) biosorption by MS in binary metal systems. It was indicated that the Pb(II) biosorption capacity of MS was not notably impaired by the presence of co-metal ions (Figure 5.6a). The greatest impact was exerted by Cu(II) and Ni(II), which respectively reduced the Pb(II) biosorption capacity only to 69.6% and 73.1% (the single system without co-metal ions as the control). The influence of co-metal ions on Cd(II) biosorption was more significant (Figure 5.6b). The presence of Zn(II) and Ni(II) respectively decreased the Cd(II) biosorption capacity of MS to 53.1% and 59.6% of that determined in the single Cd(II) system. The high selectivity of MS towards Pb(II) suggests the great potential of MS in Pb(II) removal/recovery from heavy-metal-bearing wastewater. Moreover, biosorption of multiple heavy metals could make a better use of the biosorbent than biosorption of a single heavy metal under certain conditions. For instance, a much higher amount of heavy metal ions was sequestered by MS in the binary system of Pb(II)&Cr(III) as compared with that of the single Pb(II) biosorption system (Figure 5.6a).

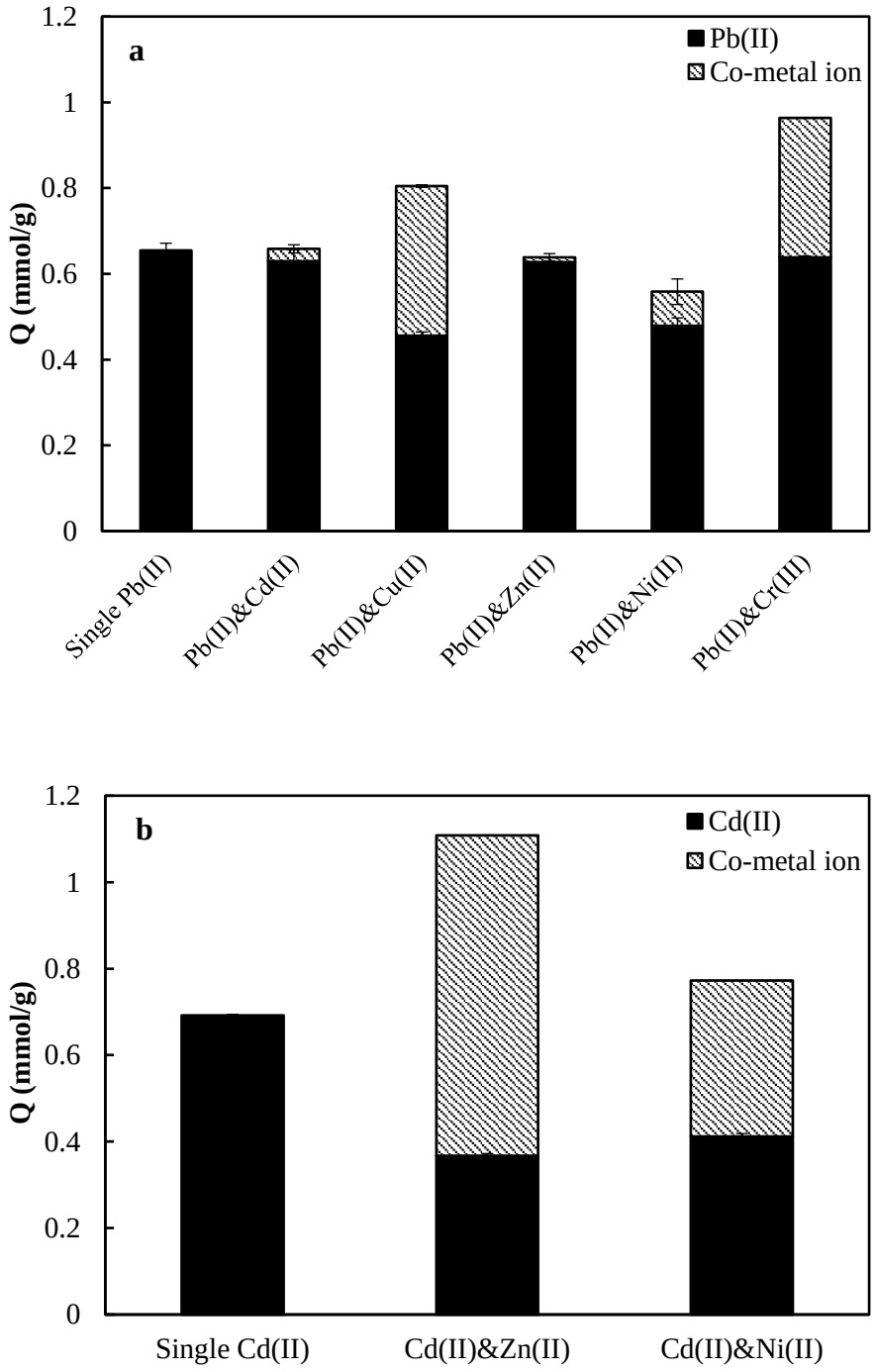

Figure 5.6 Effect of co-metal ions on (a) Pb(II) and (b) Cd(II) biosorption by MS in binary systems.

[Initial metal concentrations of 1.0 mM, pH 5.0 for Pb(II) and 7.5 for Cd(II) biosorption, 1.0 g/L MS, 250 rpm, 298 K, 24 h.]

5.7. Biosorption isotherms of Pb(II) and Cd(II) biosorption by MS

The equilibrium data of Pb(II) and Cd(II) biosorption by MS are plotted in Figure 5.7 with non-linear fitting to a variety of adsorption isotherm models. Table 5.1 summarizes the biosorption isotherm constants derived from the non-linear modeling. The maximum Pb(II) biosorption capacity of MS was experimentally determined as 263.63 ± 0.06 mg/g (1.27 ± 0.0003 mmol/g), and the R-P model provided the best description to the equilibrium data with R^2 of 0.985 and RMSE of 3.564. Both the R^2 and RMSE and the parameters of the different biosorption isotherm models were considered and compared when evaluating the fitting of the models to the biosorption by MS. It is worth mentioning that the Sips model with R^2 of 0.987 and RMSE of 3.353 was not considered due to the much higher predicted Q_m of 541.15 mg/g than the experimental value. The R-P model combines the characteristics of the Langmuir and Freundlich isotherms. It reduces to the Langmuir model when b_R equals 1, and approaches the Freundlich model if the value of $a_R C_e^{bR}$ is much higher than 1 (Jossens et al., 1978, Redlich and Peterson, 1959). In this study, the value of $a_R C_e^{bR}$ ranged from 1.42 to 63.44, suggesting the good fitting of the Freundlich isotherm to Pb(II) biosorption by MS. This was consistent with the higher R^2 (0.981) and lower RMSE (3.986) of the Freundlich model than those of the Langmuir model (R^2 = 0.950; RMSE = 6.493), as shown in Table 5.1. For Cd(II), the Q_m of 93.53 ± 1.43 mg/g (0.83 ± 0.01 mmol/g) was experimentally achieved, and similar non-linear fitting results to those of Pb(II) biosorption by MS were observed. It was concluded that the Cd(II) biosorption by

MS was best described by the R-P isotherm, which also exhibited the properties of the Freundlich isotherm due to its large value of $a_R C_e^{bR}$ (i.e., 2.91-70.93).

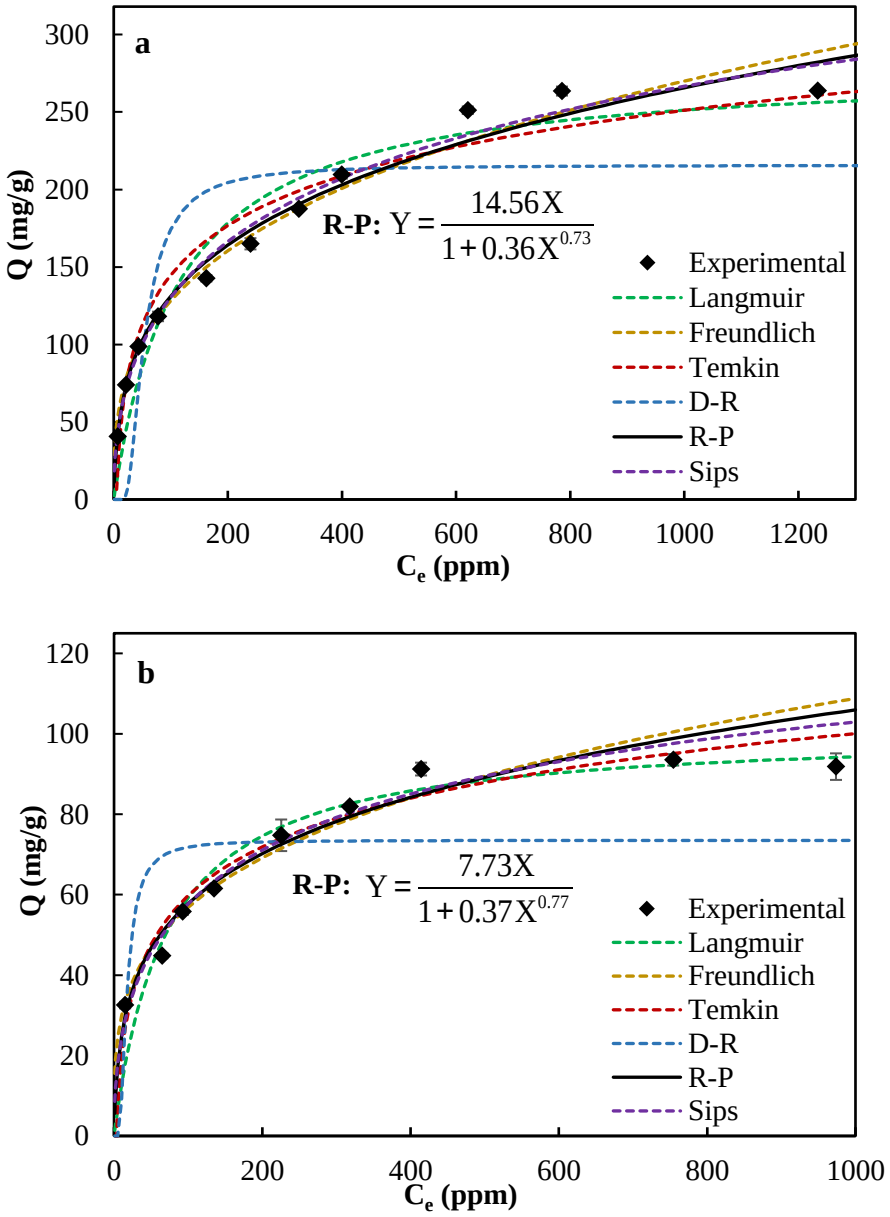

Figure 5.7 Non-linear regression of the equilibrium data of Pb(II) and Cd(II) biosorption by MS.

[pH 5.0 for Pb(II) and 7.5 for Cd(II) biosorption, 1.0 g/L MS, 250 rpm, 298 K, 24 h.]

Table 5.1 Adsorption isotherm constants of Pb(II) and Cd(II) biosorption by MS.

	Parameter	Pb(II)	Cd(II)
Langmuir	Q_m (mg/g)	281.050 ± 4.313	100.900 ± 0.424
	K_L (L/mg)	0.009 ± 0.001	0.014 ± 0.000
	R^2	0.950 ± 0.007	0.959 ± 0.007
	RMSE	6.493 ± 0.399	2.476 ± 0.219
Freundlich	K_F	28.440 ± 1.131	15.565 ± 0.827
	N_F	3.068 ± 0.062	3.554 ± 0.098
	R^2	0.981 ± 0.001	0.980 ± 0.011
	RMSE	3.986 ± 0.177	1.728 ± 0.483
Temkin	A_T (L/mg)	0.224 ± 0.037	0.306 ± 0.033
	B_T (J/mol)	46.465 ± 1.888	17.495 ± 0.276
	R^2	0.965 ± 0.005	0.977 ± 0.009
	RMSE	5.441 ± 0.321	1.852 ± 0.383
D-R	Q_m (mg/g)	215.950 ± 0.778	73.525 ± 0.403
	β (mol^2/kJ^2)	357.450 ± 24.678	38.390 ± 6.152
	R^2	0.761 ± 0.001	0.755 ± 0.007
	RMSE	14.254 ± 0.060	6.081 ± 0.139
R-P	K_r (L/g)	14.555 ± 5.310	7.734 ± 0.298
	a_R (L/mg)	0.359 ± 0.158	0.367 ± 0.042
	b_R	0.727 ± 0.010	0.765 ± 0.011
	R^2	**0.985** ± 0.000	**0.982** ± 0.010
	RMSE	**3.564** ± 0.006	**1.628** ± 0.490
Sips	Q_m (mg/g)	541.150 ± 10.185	164.550 ± 15.627
	b (L/mg)	0.033 ± 0.002	0.056 ± 0.003
	$1/n$	0.491 ± 0.039	0.495 ± 0.027
	R^2	0.987 ± 0.001	0.986 ± 0.009
	RMSE	3.353 ± 0.021	1.444 ± 0.462

5.8. Kinetics of Pb(II) and Cd(II) biosorption by MS

Figure 5.8 reveals that the biosorption of Pb(II) and Cd(II) by MS was very rapid with 93.4% of Pb(II) and 80.6% of Cd(II) biosorption achieved in the first 10 min, and the equilibrium was attained around 180 min. Both the Pb(II) and Cd(II) biosorption processes consisted of three phases: (1) in the first 5 min, Pb(II) and Cd(II) rapidly loaded onto the MS surface because of the wide availability of active binding sites; (2) from 5 to 45 min, the biosorption processes of Pb(II) and Cd(II) became slower; (3) after 45 min, it was the final equilibrium stage with very slow binding of Pb(II) and Cd(II) to MS, due to the decreased concentration of Pb(II)/Cd(II) in the bulk liquid phase as well as the oncoming saturation of binding sites on the MS surface. As shown in Figure 5.8 and Table 5.2, the kinetics of Pb(II) biosorption could be better fitted by the non-linear pseudo-first-order kinetic model, while that of Cd(II) biosorption was better described by the non-linear pseudo-second-order kinetic model.

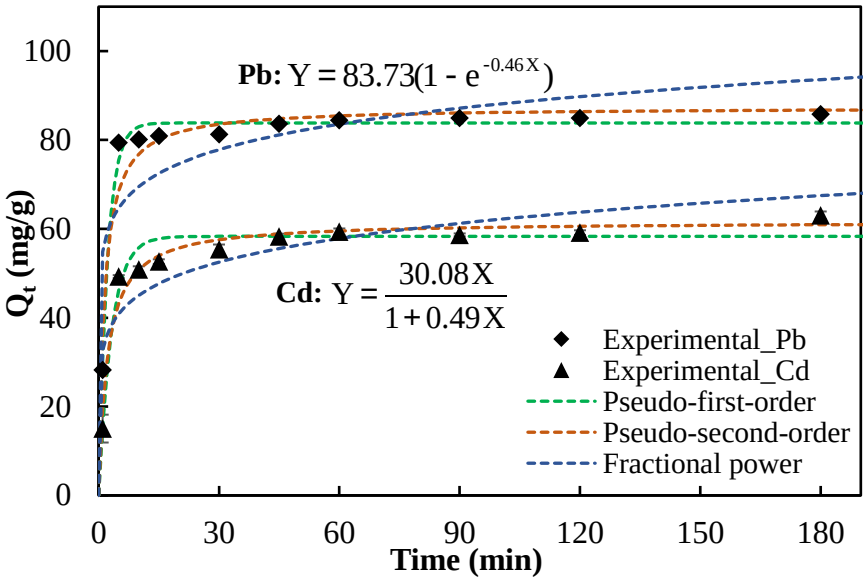

Figure 5.8 Non-linear regression of the kinetic processes of Pb(II) and Cd(II) biosorption by MS.

[Initial metal concentrations of 100 ppm, pH 5.0 for Pb(II) and pH 7.5 for Cd(II) biosorption, 1.0 g/L MS, 250 rpm, 298 K, 24 h.]

Table 5.2 Kinetic constants of Pb(II) and Cd(II) biosorption by MS.

	Parameter	Pb(II)	Cd(II)
Pseudo-first-order	Q_e (mg/g)	83.730 ± 0.014	57.820 ± 0.424
	k_1 (min^{-1})	0.461 ± 0.005	0.324 ± 0.041
	R^2	**0.980** ± 0.000	0.943 ± 0.004
	RMSD	**0.805** ± 0.014	1.088 ± 0.046
Pseudo-second-order	Q_e (mg/g)	87.585 ± 0.021	61.320 ± 0.651
	k_2 (g/mg/min)	0.008 ± 0.000	0.008 ± 0.001
	R^2	0.922 ± 0.003	**0.955** ± 0.006
	RMSD	1.629 ± 0.038	**0.971** ± 0.142
Fractional power	k	54.810 ± 0.156	32.695 ± 1.294
	v	0.103 ± 0.001	0.139 ± 0.010
	R^2	0.554 ± 0.003	0.703 ± 0.007
	RMSD	3.874 ± 0.051	2.497 ± 0.220

5.9. Thermodynamics of Pb(II) and Cd(II) biosorption by MS

The K_D values of Pb(II) biosorption by MS in equilibrium were calculated at different temperatures via Eq. 3.1. By inputting K_D into Eq. 3.2, ΔG^0 of Pb(II) biosorption by MS was calculated to be -5.23 ± 0.013, -6.86 ± 0.205 and -8.43 ± 0.186 kJ/mol at 288, 298 and 308 K, respectively, indicating that Pb(II) biosorption by MS became more spontaneous with increasing temperature. From the slope and intercept of the plot of $\ln K_D$ versus $1/T$ in Eq. 3.3 (Figure 5.9a), ΔH^0 and ΔS^0 were respectively estimated to be 40.94 ± 2.911 kJ/mol and 0.16 ± 0.010 kJ/mol·K, revealing that the biosorption process was endothermic and entropy-driven.

Through the same thermodynamic computation procedures applied in Pb(II) biosorption, the values of ΔG^0 of Cd(II) biosorption by MS were calculated to be -4.06 ± 0.335, -2.59 ± 1.039 and -1.05 ± 0.711 kJ/mol at 288, 298 and 308 K, respectively; ΔH^0 and ΔS^0 were respectively computed to be -47.39 ± 5.243 kJ/mol and -0.15 ± 0.020 kJ/mol·K (Figure 5.9b). The data indicate that the Cd(II) biosorption by MS was more spontaneous at a lower temperature, and it was exothermic and enthalpy-driven. The negative ΔS^0 reveals that the randomness of the solid-liquid interface reduced after Cd(II) loading on the MS surface.

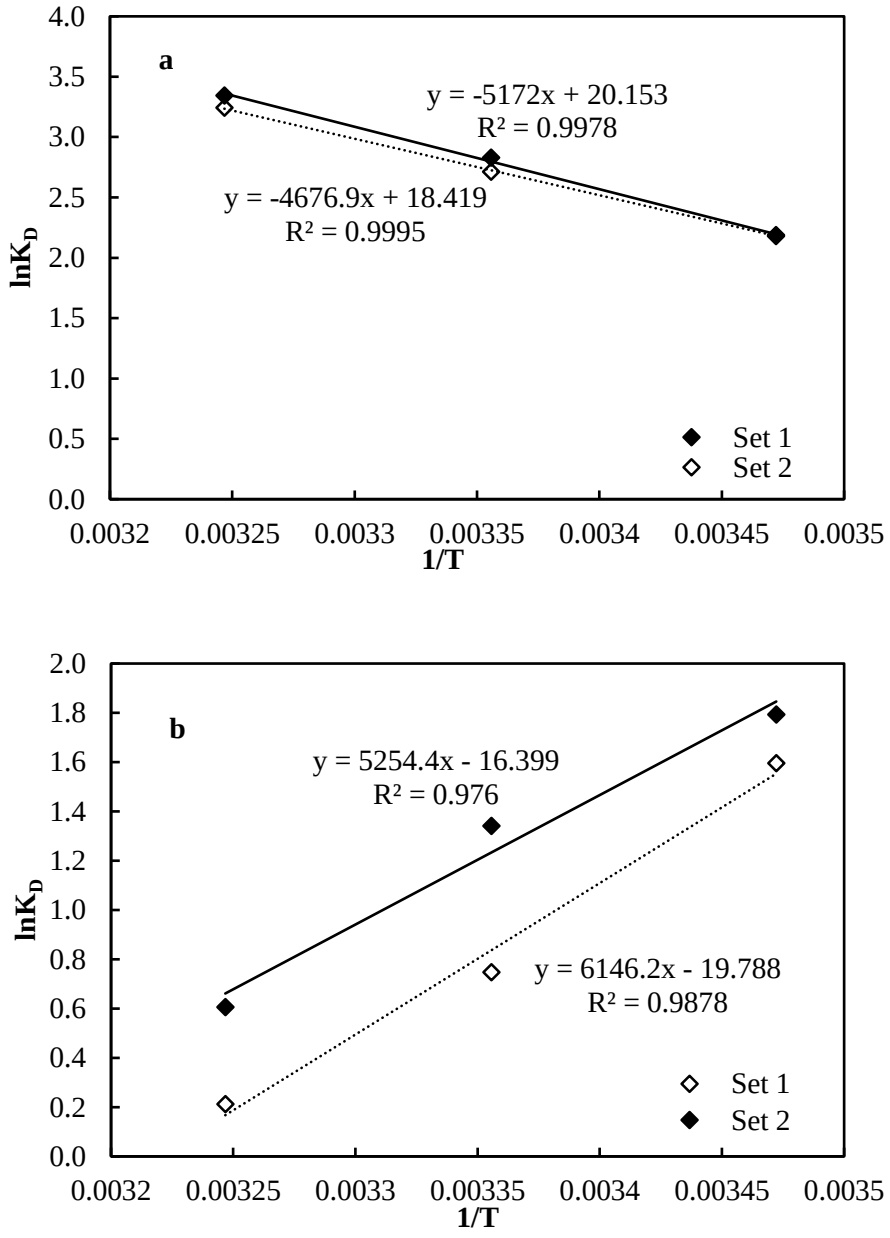

Figure 5.9 Plot of lnK_D versus 1/T for thermodynamic computation of (a) Pb(II) and (b) Cd(II) biosorption by MS in duplicate.

[pH 5.0 for Pb(II) and 7.5 for Cd(II) biosorption.]

5.10. Desorption of Pb(II) and Cd(II) from MS

As Figure 5.10 shows, higher than 98% of Pb(II) sequestered by MS was desorbed by 0.2 M HNO_3, 0.2 M citric acid and 0.1 M EDTA. As for the desorption of Cd(II), desorption efficiencies of 79%-88% were obtained by 0.2 M HNO_3, 0.2 M HCl, 0.2 M citric acid and 0.1 M EDTA. The lower recovery of Cd(II) than Pb(II) was probably caused by Cd(II) loss during the washing of Cd-loaded MS after centrifugation. The binding of Cd(II) to the MS surface might not be as strong as that of Pb(II), given that 10.1% of Cd(II) was desorbed using DDI water as the eluant, whereas only 1.7% of Pb(II) was desorbed in the same condition (Figure 5.10). The resorption experiments (i.e., the second cycle) indicated that 93%, 96%, 99% and 99% of Pb(II) biosorption capacities, and 92%, 97%, 93% and 97% of Cd(II) biosorption capacities remained in the regenerated MS after desorption by 0.2 M HCl, 0.2 M HNO_3, 0.2 M citric acid and 0.1 M EDTA, respectively (details in Table 5.3). Although citric acid and EDTA exhibited comparable desorption capabilities on Pb(II) and Cd(II) and regeneration of MS as compared with HNO_3, they have a higher cost than the mineral acid HNO_3 as aforementioned in Section 2.8. Hence, HNO_3 was selected as a promising desorbing agent for the desorption of Pb(II) and Cd(II) from MS in consideration of the heavy metal desorption efficiency, resorption capability of the treated MS, and the cost of the desorbing agent. It is worth noting that the concentration of a desorbing agent applied in a desorption system should be closely related to the S/L ratio used in the system.

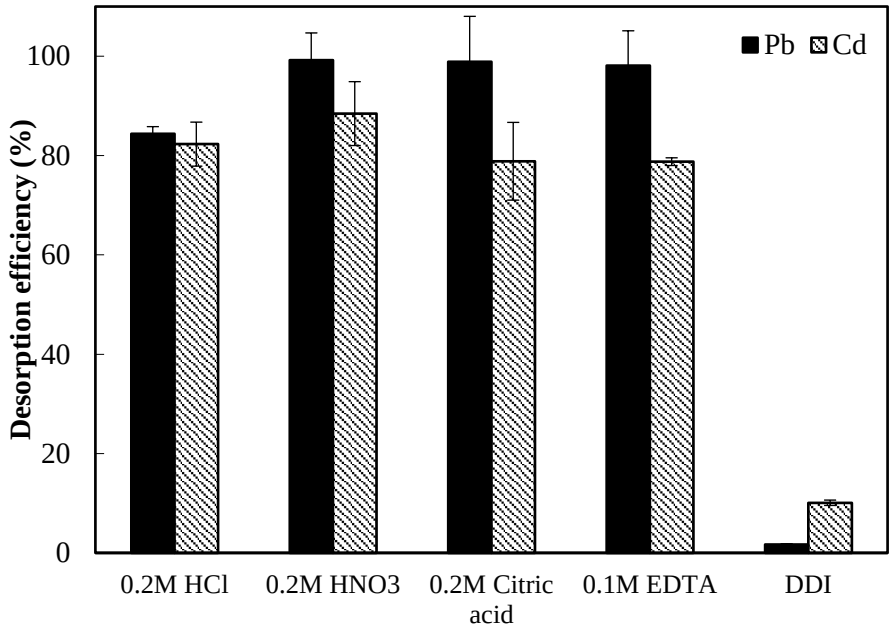

Figure 5.10 Desorption of Pb(II) and Cd(II) from MS by different desorbing agents.

[S/L ratio 2.0 g/L, 3 h, 250 rpm, 298 K.]

Table 5.3 Pb(II) and Cd(II) biosorption capacities of native MS and MS regenerated by different desorbing agents.

	Desorbing agent	*Q*_Pb (mg/g)	*Q*_Cd (mg/g)
1st cycle		142.66 ± 1.32	111.30 ± 1.73
2nd cycle	0.2 M HCl	133.29 ± 7.08	102.53 ± 2.98
	0.2 M HNO_3	136.93 ± 6.21	107.90 ± 1.24
	0.2 M Citric acid	140.66 ± 7.48	103.14 ± 2.02
	0.1 M EDTA	141.87 ± 3.59	107.67 ± 6.88

(**Notes:** NA - Not applicable; Initial metal concentrations of 250 ppm, pH 5.0 for Pb(II) and 7.5 for Cd(II), 1.0 g/L MS and 298 K in the biosorption study.)

5.11. Comparison with other fruit-waste-derived biosorbents

A variety of fruit waste materials have been investigated for Pb(II) and Cd(II) biosorption in aqueous solutions in the literature. Table 5.4 lists a number of fruit-waste-derived biosorbents (pristine biomass without modification) that have been investigated for the removal of Pb(II)/Cd(II) in aqueous solutions. Apparently, WR and MS in this study exhibited much higher Pb(II) biosorption capacities than other fruit waste materials reported in the literature. For Cd(II), the biosorption capacities of WR and MS were relatively high, and next came only to the pectin-abundant peels of *Citrus* fruits such as *Citrus maxima* and orange (Chao and Chang, 2012, Schiewer and Iqbal, 2010). Notably, the MS in this study exhibited a much higher Pb(II) biosorption capacity than the MS reported by Nadeem et al. (2016) (263.6 versus 183.0 mg/g), even when the pH conditions were the same and the particle sizes were similar. This was probably due to the fact that only the shell of the mango seed was used in the biosorption study of Nadeem et al. (2016), whereas both the shell and kernel of the mange seed were ground into the MS biosorbent in this study for better utilization of the fruit waste source. Besides, variations in other operational conditions (e.g., adsorbate concentration range and presence of competing ions) and biosorbents' chemical and physical characteristics (e.g., mineralogy and porosity) could also influence the observed biosorption capacity (Loganathan et al., 2014).

Given the great potential of WR and MS as biosorbents for Pb(II) and Cd(II), further studies are warranted on biosorption of other heavy metals, precious metals, and even radioactive metals. Besides, the high yields of watermelon and mango

among the total fruit production in the world can facilitate the application of WR and MS as promising biosorbents due to their easy availability and low cost.

Table 5.4 Pb(II) and Cd(II) biosorption by various fruit waste materials.

	Biosorbent	Particle size (μm)	Q_m (mg/g)	pH	Reference
Pb(II)	Grape bagasse	< 355	79	3.0	(Farinella et al., 2008)
	Ponkan peel	< 600	112	5.0	(Pavan et al., 2008)
	Mango peel	850-1000	99.1	5.0	(Iqbal et al., 2009a)
	Orange peel	NA	111	5.5	(Feng et al., 2011)
	Pomegranate peel	< 150	166.6	5.5	(Ay et al., 2012)
	Muskmelon waste	< 300	75.4	5.5	(Akar et al., 2012)
	Citrus maxima peel	< 149	145	5.0	(Chao and Chang, 2012)
	Passion fruit peel	< 149	110	5.0	
	Custard apple shell	< 149	90.9	5.0	(Isaac and Sivakumar, 2013)
	Avocado peel		4.9		
	Dragon fruit peel	NA	4.6	NA	(Mallampati et al., 2015)
	Hamimelon peel		7.9		
	Mango seed	< 250	183.0	5.0	(Nadeem et al., 2016)
	WR	< 180	231.6	5.0	This study
	MS	< 180	263.6	5.0	
Cd(II)	Banana peel	< 125	35.5	8.0	(Memon et al., 2008)
	Orange peel	500-1000	107.3	5.0	(Schiewer and Iqbal, 2010)
	Citrus maxima peel	< 149	135.2	5.0	(Chao and Chang, 2012)
	Passion fruit peel	< 149	86.8	5.0	
	Grape bagasse	< 355	87.0	7.0	(Farinella et al., 2008)
	Custard apple shell	< 149	73.3	5.0	(Isaac and Sivakumar, 2013)
	Lemon peel	177-240	52.3	5.0	(Schiewer and Patil, 2008)
	Mango peel	850-1000	67.1	5.0	(Iqbal et al., 2009a)
	WR	< 180	98.5	7.0	This study
	MS	< 180	93.5	7.5	

(**Notes**: NA - Not available.)

5.12. Summary

This chapter presents the results obtained in the macroscopic biosorption studies of Pb(II) and Cd(II) using MS as the biosorbent. The significant findings are summarized as below.

(1) MS in a smaller particle size (< 180 μm) exhibited a much higher biosorption capacity than larger ones (180-500 μm and 500-1000 μm). This could be ascribed to the biosorbent structure and binding mechanism, which will be discussed in the following chapter (see Section 6.2.9).

(2) The biosorption capacities of MS augmented with increasing pH, with optimal pH 5.0 for Pb(II) biosorption and 7.5 for Cd(II) biosorption.

(3) The partially impaired Pb(II) and Cd(II) biosorption capacities of MS at a high ionic strength (i.e., 0.2 M $NaNO_3$) suggested that electrostatic attraction was one of the underlying binding mechanisms governing Pb(II) and Cd(II) biosorption by MS.

(4) The maximum biosorption capacities, 263.63 ± 0.06 mg-Pb/g (1.27 ± 0.0003 mmol/g) and 93.53 ± 1.43 mg-Cd/g (0.83 ± 0.01 mmol/g), of MS were observed at pH 5.0 and 7.5, respectively.

(5) The R-P isotherm provided the best description to Pb(II) and Cd(II) biosorption by MS, implying multilayer loadings of Pb(II) and Cd(II) on the heterogeneous surface of MS.

(6) Pb(II) and Cd(II) were rapidly sequestered by MS, with 93.4% of Pb(II) biosorption and 80.6% of Cd(II) biosorption completed in the first 10 min.

(7) The Pb(II) biosorption by MS was endothermic and entropy-driven, whereas Cd(II) biosorption by MS was exothermic and enthalpy-driven.

(8) Comparable Pb(II) desorption efficiencies (higher than 98%) were achieved with 0.2 M HNO_3, 0.2 M citric acid and 0.1 M EDTA, and higher than 96% of the Pb(II) biosorption capacities remained in the MS after regenerated with 0.2 M HNO_3, 0.2 M citric acid and 0.1 M EDTA. For Cd(II), desorption efficiencies of 79%-88% were obtained by 0.2 M HNO_3, 0.2 M HCl, 0.2 M citric acid and 0.1 M EDTA, and 92%-97% of Cd(II) biosorption capacities remained in the regenerated MS. It seemed that Cd(II) binding to the MS surface was weaker than that of Pb(II).

(9) The biosorption capacity of MS (and also WR as shown in Table 5.4) observed in this study was much higher on Pb(II) and relatively high on Cd(II) as compared with other fruit waste materials reported in the literature.

6. Comprehensive Elucidation of Biosorption Mechanisms

6.1. Characterization of WR and mechanistic studies

A good understanding of the underlying mechanism of a biosorption process will facilitate better process control and provide important insights into the development of commercial (bio)sorbents. In the literature, a series of analytical methods such as SEM-EDX, FTIR and XPS were usually employed for biosorbent characterization and mechanistic elucidation. However, it is not easy to thoroughly decipher the complicated interactions occurring in a biosorption process through these conventional techniques, given the complex composition of a biosorbent. In this study, to the best of my knowledge, it was the first time to employ solid-state NMR spectroscopy to investigate the interactions between biosorbents and heavy metal ions, and QCS to decipher the interactions at a molecular level. The combination of diverse advanced techniques and conventional analytical methods can provide complementary mechanistic information to disclose a biosorption process in a comprehensive way.

6.1.1. Elemental analysis

Elemental analysis indicated that WR comprised 36.89% of C, 6.51% of H, 52.92% of O, 3.30% of N, and 0.38% of S (in dry weight). The atomic ratio of the sum of N and O to C (i.e., (O+N)/C), which is an indicator of polarity with higher ratio suggesting higher polarity (Li et al., 2010), was 1.15 to WR. Besides, the ratio of H to C (i.e., H/C), which indicates higher aromaticity with a lower ratio (Li et al., 2010), was 2.12 to WR.

6.1.2. Zeta potential measurement

Figure 6.1 shows that WR became more negatively charged as pH increased, with the isoelectric point (i.e., pH at which the net charge is zero) at around pH 2.0. This should be caused by the deprotonation of certain organic groups such as carboxyl (from -COOH to $-COO^-$) and protonated amine (from $-NH_3^+$ to $-NH_2$) groups. As pH used in this study was higher than 2.0, electrostatic attraction could be a driving force for Pb(II) and Cd(II) binding to the negatively charged WR. The highly negative zeta potentials of WR at pH 5.0 and 7.0 supported the observations of the highest Pb(II) uptake at pH 5.0 (Pb(II) would precipitate at higher pH) and the highest Cd(II) uptake at pH 7.0 (see Section 4.1). Although the zeta potential could not be measured at pH lower than 2.0 due to the extremely high ionic strength and acidic condition, it was considered to be slightly positive (Ucun et al., 2002).

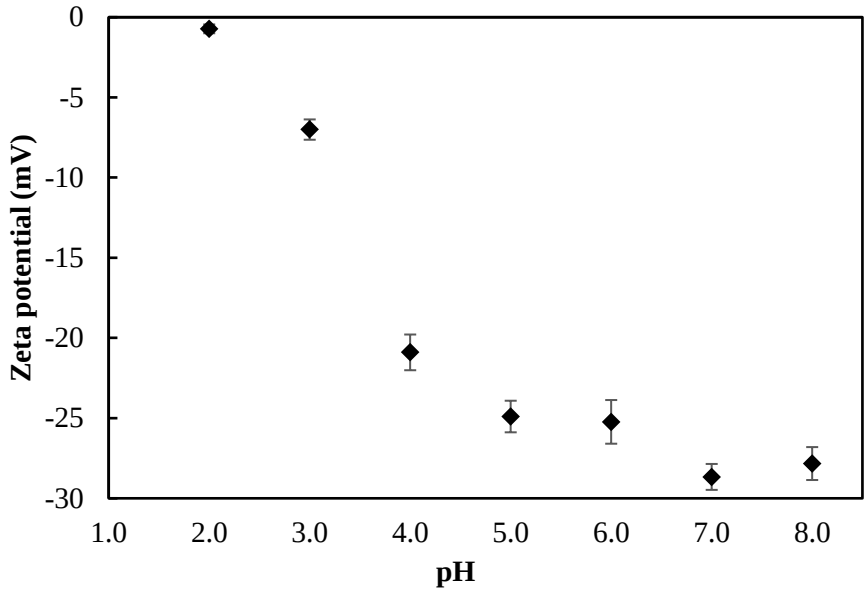

Figure 6.1 Zeta potentials of WR at varying pH.

[0.15 g/L WR in 1 mM KCl.]

6.1.3. PXRD

As illustrated in Figure 6.2, pristine WR exhibited reflections when 2θ was 16.1° and 21.6°, which were typical for the crystalline form of natural cellulose (i.e., cellulose I) (Singha and Guleria, 2014, Tian et al., 2011). The broadness of the peaks indicated the amorphous nature of WR, through which Pb(II) and Cd(II) could easily penetrate and be entrapped since adsorption mainly occurs in amorphous regions (Zhou et al., 2005). The PXRD pattern of Pb-loaded WR (Pb-WR) displayed distinct peaks at 2θ of 27.0° and 30.3°, which could be attributed to the deposition of Pb precipitates in the crystalline state (Lee et al., 1997, Zhou et al., 2005). The PXRD patterns of WR in different particle sizes are shown in Figure 6.3. All of the three WR samples presented reflections at 2θ of 16° and 22°, suggesting similar crystalline structures of WR in different particle sizes.

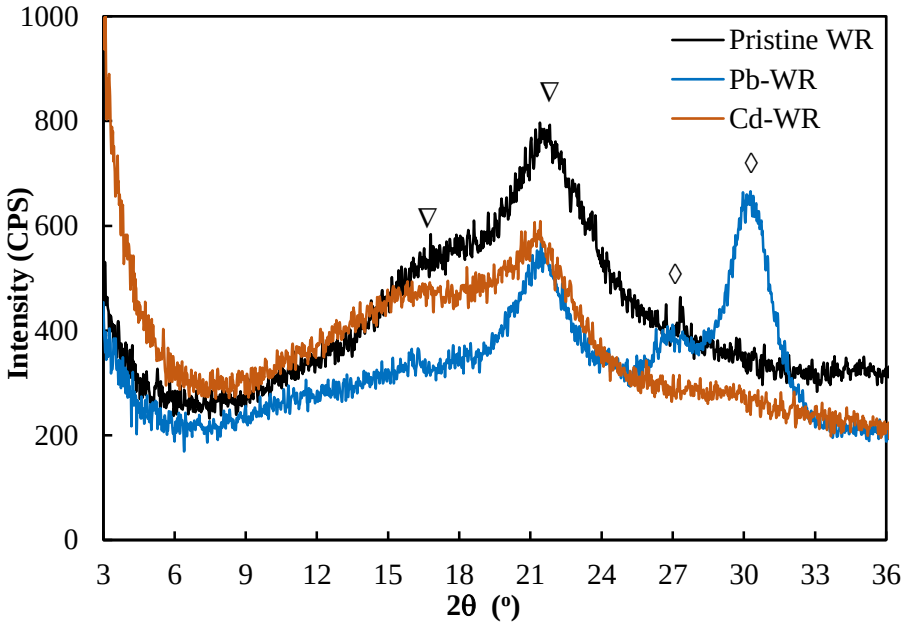

Figure 6.2 PXRD patterns of pristine, Pb-, and Cd-loaded WR.

[∇: Cellulose I; ◊: Pb precipitate.]

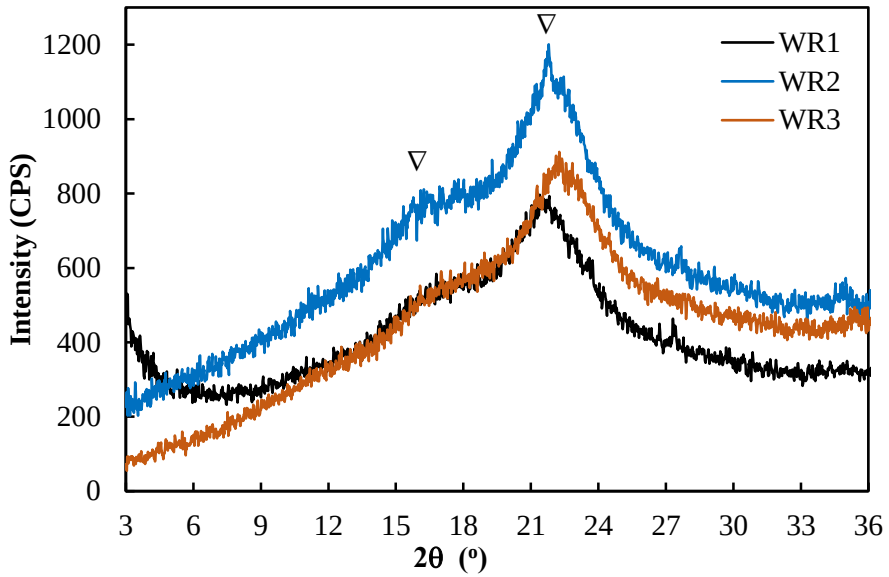

Figure 6.3 PXRD patterns of WR in different particle sizes.

[∇: Cellulose I; WR1: < 180 μm; WR2: 180-500 μm; WR3: 500-1000 μm.]

6.1.4. SEM-EDX

Figure 6.4 shows the SEM micrographs of the WR surface before and after Pb(II) and Cd(II) biosorption. The morphological structure of pristine WR was uneven and irregular (Figure 6.4a), leading to a large surface area for Pb(II) and Cd(II) sequestration. After loadings of Pb(II) and Cd(II), the WR surface became more porous and rougher with some tiny holes (Figures 6.4b & 6.4c), which could be caused by leaching of organic substances (e.g., natural pigments and other impurities) from WR into the liquid phase during biosorption. Distinct precipitates were observed on the surface of Pb- and Cd-loaded WR, indicating that microprecipitation, which refers to the precipitation of metal species due to deviation of the local condition on the biosorbent surface, was involved in Pb(II) and Cd(II) biosorption by WR. Hydrolysis of metal complexes, which were generated from the coordination of Pb(II)/Cd(II) to N and O atoms in the functional groups on WR, could also result in microprecipitation of hydrolysis products on the biosorbent surface (Zhou et al., 2005). Microprecipitation can significantly contribute to metal removal as the metal precipitates are collected by the biosorbent and thus immobilized and separated from the solution (Volesky, 2003). The greater amount of precipitates bound on the surface of Pb-loaded WR than that of Cd-loaded WR revealed greater microprecipitation of Pb(II) than Cd(II) in the biosorption processes.

X-ray elemental mappings indicated that both Pb and Cd were distributed almost everywhere on the WR surface with prominent loadings (Figure 6.5). The intense signals of Pb and Cd detected in the X-ray elemental mappings (highlighted

in circles) were ascribed to Pb(II) and Cd(II) precipitation (Remenarova et al., 2012), given that distinct precipitates were observed at the same sites in the corresponding SEM micrographs. It is noteworthy that Pb/Cd was also mapped in the area where no precipitate was observed in the SEM micrographs, implying the involvement of mechanism(s) other than microprecipitation (e.g., electrostatic attraction and/or complexation) in the biosorption process (Maresova et al., 2011).

The EDX spectra of WR before and after Pb(II) and Cd(II) biosorption are shown in Figure 6.6. It can be observed that light metals, Mg, K and Ca, were present in pristine WR, and they disappeared after the loadings of Pb(II) and Cd(II) onto the WR surface. This was possibly caused by ion exchange between the light metal ions and Pb(II)/Cd(II) for the binding sites on the WR surface.

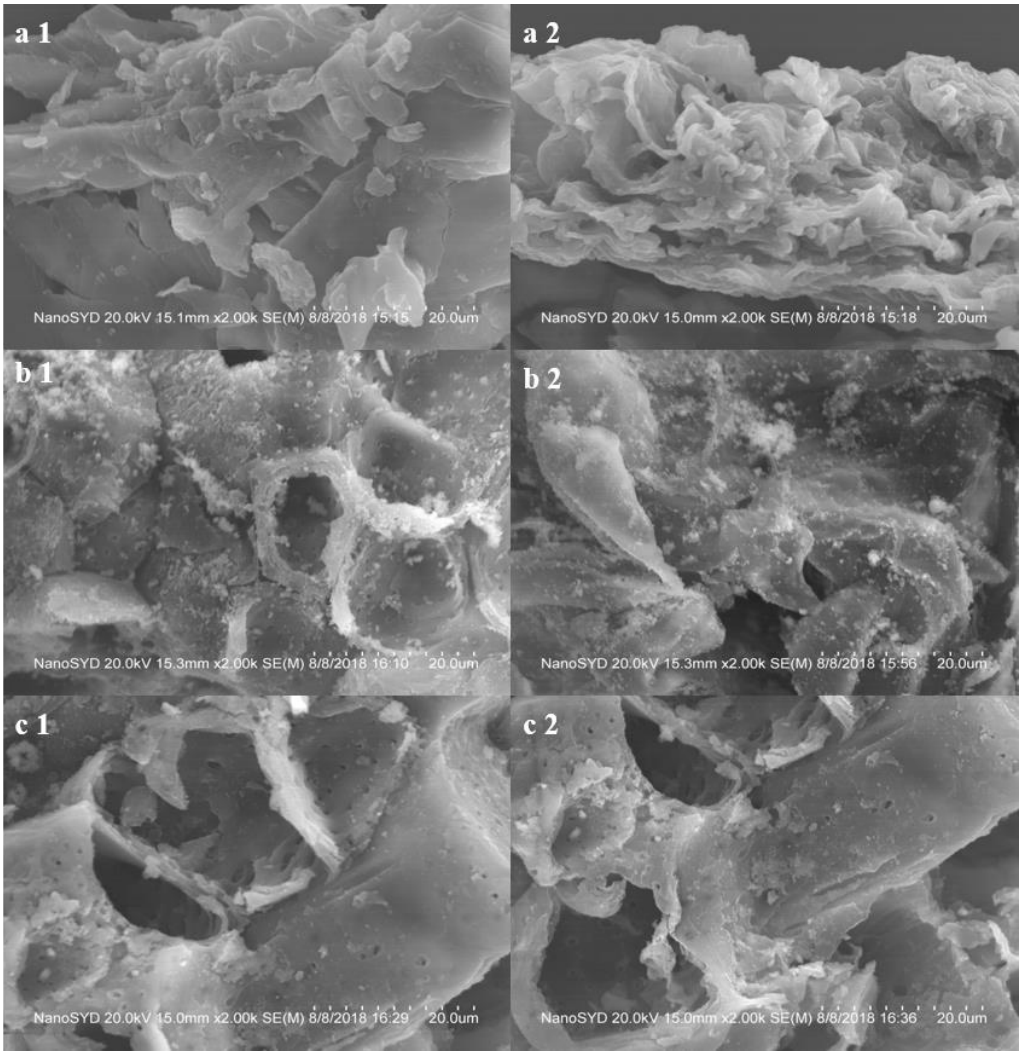

Figure 6.4 SEM micrographs of (a) pristine WR, (b) Pb-, and (c) Cd-loaded WR at two spots on the surface.

[Magnification 2000×.]

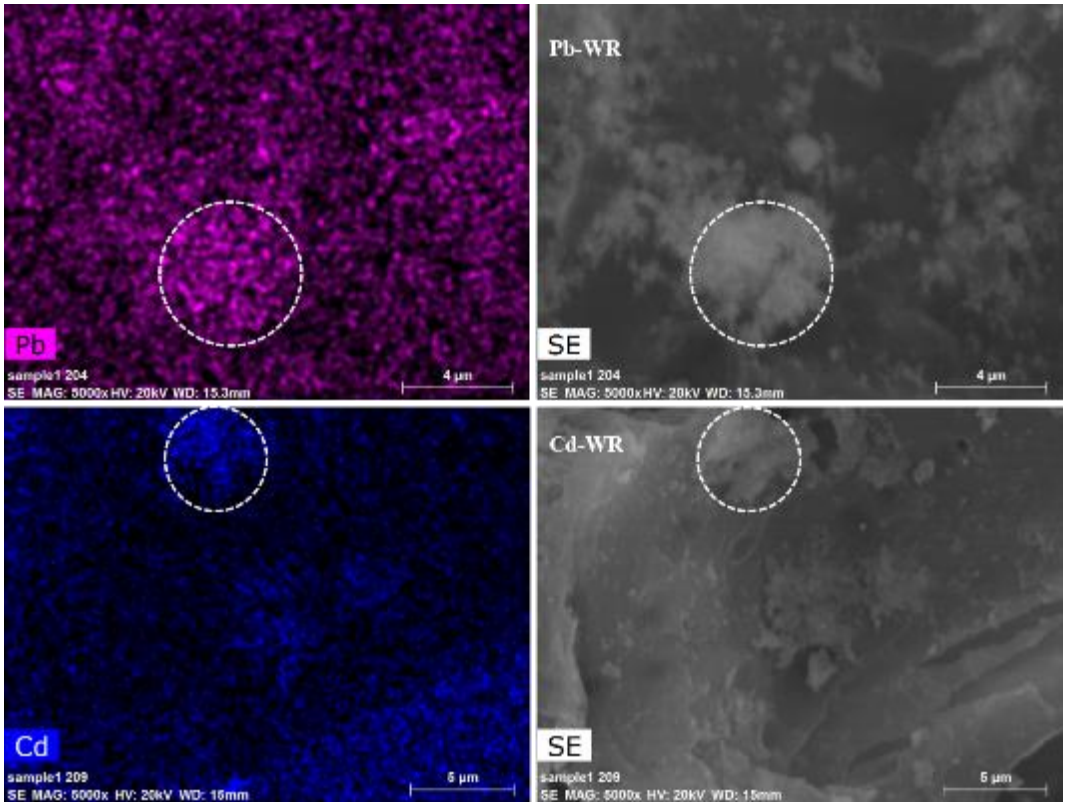

Figure 6.5 X-ray elemental mappings of Pb and Cd on the WR surface and the corresponding SEM micrographs.

[Magnification 5000×.]

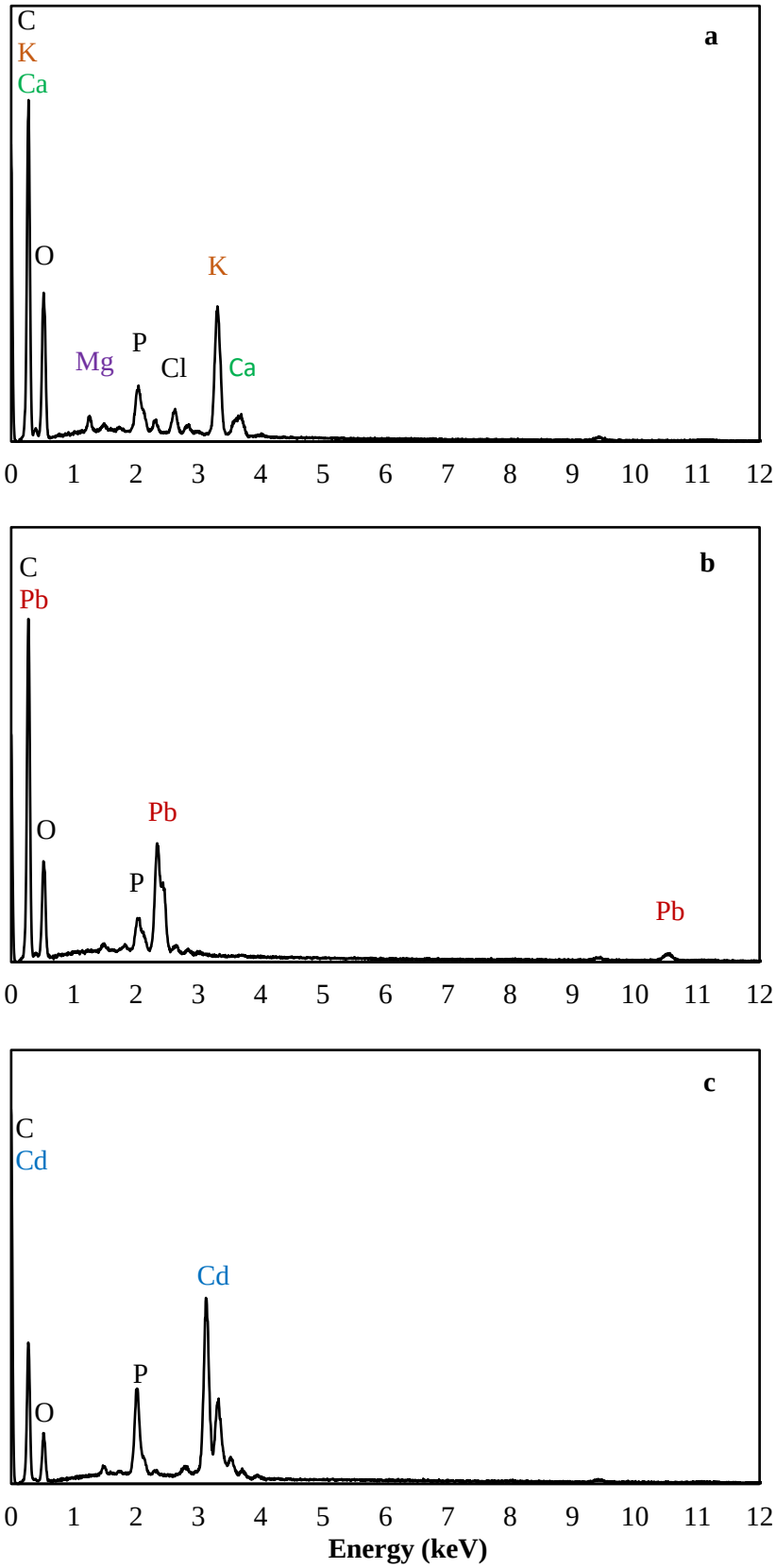

Figure 6.6 EDX spectra of (a) pristine, (b) Pb-, and (c) Cd-loaded MS.

6.1.5. FTIR spectroscopy

The FTIR spectra of WR before and after Pb(II) and Cd(II) biosorption are shown in Figure 6.7. The various absorption bands observed in the FTIR spectra indicated the complicated composition of WR. Bands at 2920 cm^{-1}, 1740 cm^{-1}, and 1632 cm^{-1} respectively represented C-H stretch in alkanes, C=O stretch in esters, and N-H bend in primary amines (R-NH_2). A distinct spectral difference was observed at 1450-1000 cm^{-1} between pristine and heavy metal-loaded WR. The peaks at 1406 cm^{-1} (indicative of symmetric stretch of C=O in carboxylic salts), 1363 cm^{-1} (indicative of C-N stretch in amines), 1259 cm^{-1} (indicative of bending vibration of C-O-H in alcohol), 1149 cm^{-1} (indicative of asymmetric stretch of C-O-C), and 1059 cm^{-1} (indicative of stretching vibration of C-O in primary alcohol) respectively shifted to 1419 cm^{-1}, 1373 cm^{-1}, 1241 cm^{-1}, 1159 cm^{-1}, and 1055 cm^{-1} after Pb(II) biosorption, and to 1437 cm^{-1}, 1369 cm^{-1}, 1248 cm^{-1}, 1159 cm^{-1}, and 1053 cm^{-1} after Cd(II) biosorption (details in Table 6.1). All of the assignments were referred to the absorption information of functional groups reported by Pavia et al. (2008) and Griffiths et al. (2006). Accordingly, Pb(II) and Cd(II) were sequestered by WR via interacting with the surface sites, and hydroxyl (C-O-H), amine (-NH_2), carboxyl (-COOH) and ether (C-O-C) groups were probably involved. Notably, the absorption frequency of a functional group usually locates in a wide range in the infrared region, possibly resulting in its overlap with those of other functional groups (e.g., H-bonded O-H at 3400-3200 cm^{-1} versus N-H stretch at 3500-3100 cm^{-1}, C-O stretch at 1300-1000 cm^{-1} versus C-N stretch at 1350-1000 cm^{-1}). The possible overlap makes the assignment of some bands ambiguous. Other

analytical techniques would be required to complement the FTIR analysis for further clarification.

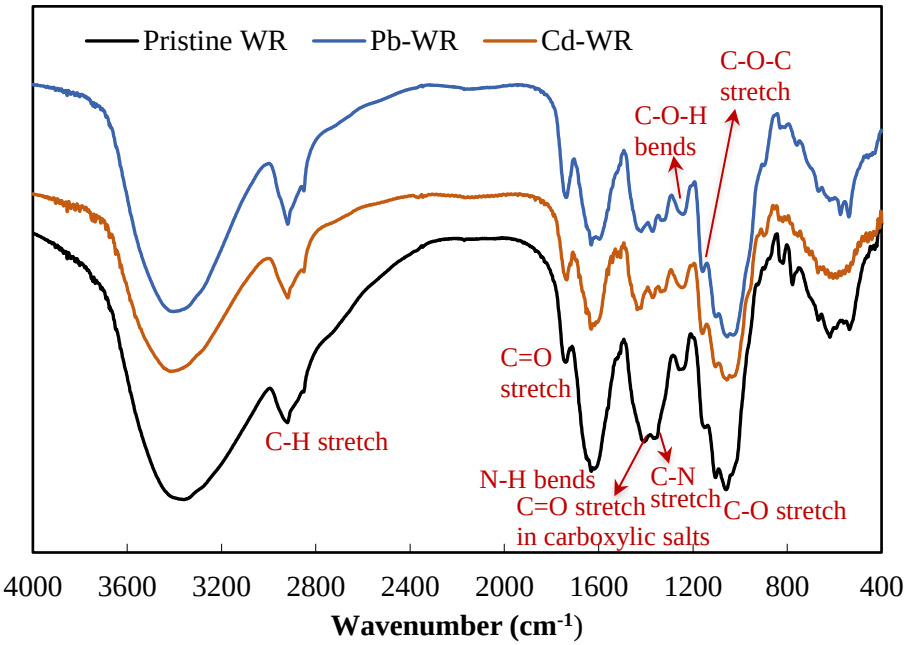

Figure 6.7 FTIR spectra of pristine, Pb-, and Cd-loaded WR.

Table 6.1 Assignments of the functional groups on WR in FTIR analysis.

Wavenumber (cm^{-1})			Shift (cm^{-1})		Assignment
WR	Pb-WR	Cd-WR	Pb-WR	Cd-WR	
2920	2919	2920	-1	0	C-H stretch in alkanes
2850	2850	2850	0	0	Asymmetric stretch of C-H in alkanes
1740	1739	1740	-1	0	C=O stretch in esters
1632	1632	1632	0	0	N-H bend in primary amines
1406	1419	1437	13	31	C=O stretch in carboxylic salts
1363	1373	1369	10	6	C-N stretch in amines
1259	1241	1248	-18	-11	C-O-H bend
1149	1159	1159	10	10	C-O-C stretch
1059	1055	1053	-4	-6	C-O stretch in primary alcohol

6.1.6. XPS

The survey XPS spectra in Figure 6.8 indicate that C and O were the two most predominant elements on the WR surface. Significant signals of Pb and Cd, especially Pb 4f at 138.9 eV (assigned to PbO) and Cd 3d at 405.6 eV (assigned to CdO) (Moulder et al., 1992), were observed in Pb- and Cd-loaded WR, indicating that prominent loadings of Pb(II) and Cd(II) on the WR surface were mainly in the forms of metal oxides. The same phenomena were also observed in Pb(II) and Cd(II) biosorption by biosorbents derived from *Chlorella vulgaris* microalgae (Lalhmunsiama et al., 2017) and *Pinus svlvestris* sawdust (Taty-Costodes et al., 2003). The formation of PbO and CdO should originate from Pb(II) and Cd(II) precipitation and/or heavy metal complexion with O atoms in functional groups on WR. Besides, it was observed that K and Ca almost disappeared from WR after Pb(II)/Cd(II) biosorption (Table 6.2), suggesting the possible occurrence of ion exchange with K^+ and Ca^{2+} for binding sites during Pb(II)/Cd(II) biosorption by WR. The surface sites involved in Pb(II)/Cd(II) biosorption can be further deciphered based on the shifts of binding energies of C 1s, O 1s and N 1s in XPS spectra before and after Pb(II)/Cd(II) biosorption (details in Table 6.3).

C 1s

As illustrated in Figure 6.9a, the C 1s spectrum of pristine WR consisted of four peaks with binding energies of 284.967, 286.404, 287.829 and 288.937 eV, corresponding to the C atoms in C-C, C-O (alcohol and/or ether), C=O and O=C-O, respectively (Lim et al., 2008, Moulder et al., 1992, Ramrakhiani et al., 2017). The peak area distribution indicated that the contents of the four bonds in WR were

in a descending order of C-C > C-O > C=O > O=C-O. This was consistent with the components of WR in which cellulose, hemicellulose, and pectin were the main compositions (see Section 6.1.7; the structures of the three biopolymers are shown in Figure A9). The latter three peaks significantly shifted to 286.583, 288.175 and 289.096 eV after Pb(II) biosorption (Figure 6.9b), and to 286.518, 287.989 and 289.068 eV after Cd(II) biosorption (Figure 6.9c), indicating the participation of hydroxyl (in alcohol), ether and carboxyl groups in Pb(II) and Cd(II) biosorption by WR. The increased binding energies of the C atoms were indicative of the formation of Pb and Cd complexes with the adjacent O atoms in these functional groups (Cid et al., 2018, Ramrakhiani et al., 2017, Sheng et al., 2004). For instance, the O atom in an ether group (C-O-C) donated lone pairs of electrons to the unoccupied orbitals of Pb(II)/Cd(II) to form coordination bonds, resulting in a lower electron density around the two adjacent C atoms and thus a higher binding energy. Besides, the variation of the geometric shape, namely, the change in the C-O-C angle upon its coordination to Pb(II)/Cd(II), could cause a binding energy shift of the C atoms (Chen and Yang, 2006). This angle change was evidenced by the QCS, which indicated that the angle of C-O-C in cellulose enlarged from 112.96° to 115.21° after Pb(II) biosorption (Structure 1 to 1a, Table 6.11). Similarly, the increased binding energies of the C atoms in alcohol and carboxyl groups after Pb(II)/Cd(II) biosorption were also indicative of Pb(II)/Cd(II) complexation with the adjacent O atoms. The increased binding energy of the C atom in the carboxyl group could also be caused by electrostatic binding of Pb(II)/Cd(II) to the deprotonated carboxyl group, i.e., $-COO^-$ (*pKa* 3.5, lower than the pH used in

biosorption); positively charged Pb(II)/Cd(II) would grab electrons and lead to a lower electron density around the C atom.

O 1s

Figure 6.10a indicates that the O 1s spectrum of pristine WR comprised two peaks at 531.077 and 532.700 eV, which were respectively assigned to O atoms in O=C and C-O (hydroxyl and/or ether) groups (Moulder et al., 1992). They shifted to 531.385 eV (+0.308 eV) and 532.961 eV (+0.261 eV) after Pb(II) biosorption (Figure 6.10b), indicating the occurrence of Pb(II) complexation with the O atoms in carboxyl, hydroxyl and ether groups. The donation of lone pairs of electrons to Pb(II) resulted in lower electron densities around the O atoms and thus higher binding energies of themselves (Cid et al., 2018). This was coherent with the increased binding energies of the C atoms in C-O, C=O and O=C-O as aforementioned. Similarly, the two O 1s peaks were also significantly shifted after Cd(II) biosorption (Figure 6.10c), indicating the similar binding mechanisms of Cd(II) to those of Pb(II). Intriguingly, peaks at 530.789 eV and 531.147 eV (assigned to metal oxides) appeared in the O 1s spectra of Pb- and Cd-loaded WR, respectively. The existence of metal oxides on the WR surface after Pb(II) and Cd(II) biosorption was consistent with the intensive Pb signal observed at 138.9 eV (assigned to PbO) on Pb-loaded WR and the Cd one at 405.6 eV (assigned to CdO) on Cd-loaded WR (Figure 6.8). The formation of metal oxides explains why the atomic concentration of O on WR increased from 20.20% to 28.15% and 24.65% after Pb(II) and Cd(II) biosorption, respectively (Table 6.2). In comparison, the more intensive peak of metal oxides observed in Pb-loaded WR than in Cd-loaded

WR was consistent with the observation of more Pb precipitates on the WR surface after Pb(II) biosorption than that of Cd(II) via SEM (Figure 6.4).

N 1s

In Figure 6.11a, two peaks at 399.968 and 401.854 eV, which corresponded to the N atoms in $-NH_2$ and $-NH_3^+$ groups (Gao et al., 2017), were observed in the N 1s spectrum of pristine WR. The peak area indicated a much larger amount of neutral N than the positively charged N on the WR surface (Ren et al., 2016). With Pb(II) and Cd(II) loadings, the former peak shifted to 400.153 and 400.096 eV, respectively. This was probably attributed to complexation in which the N atom in $-NH_2$ donated a lone pair of electrons to the empty orbital of Pb(II)/Cd(II), leading to a lower electron density of itself and thus a higher binding energy (Zhou et al., 2005). Notably, the peak assigned to $-NH_3^+$, which can be formed by protonation of $-NH_2$ at a certain range of pH (Eq. 6.1), vanished in Pb- and Cd-loaded WR. This could be caused by the conversion of $R\text{-}NH_3^+$ groups to $R\text{-}NH_2Pb^{2+}$ (or $R\text{-}NH_2Cd^{2+}$) complexes as indicated in Eq. 6.2 (Jin and Bai, 2002). Compared with C 1s and O 1s (Figures 6.9 and 6.10), the intensity of N 1s was significantly weaker, indicating the much lower content of N-based functional groups and thus their smaller contribution to Pb(II)/Cd(II) biosorption than C- and O-based functional groups.

$$R\text{-}NH_2 + H^+ \leftrightarrow R\text{-}NH_3^+ \quad (6.1)$$

$$R\text{-}NH_3^+ + Pb^{2+} \rightarrow R\text{-}NH_2Pb^{2+} + H^+ \quad (6.2)$$

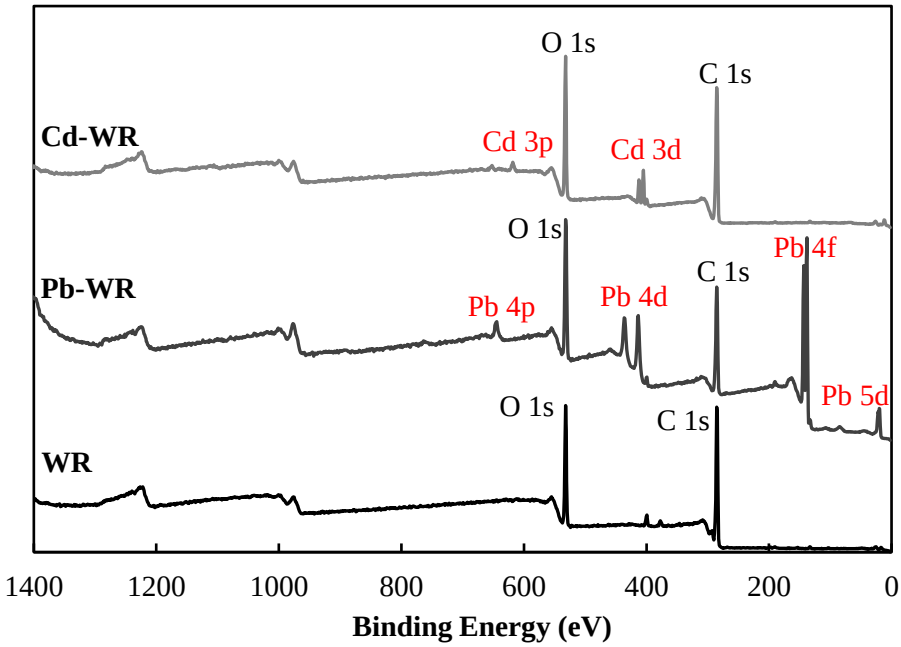

Figure 6.8 XPS survey spectra of pristine, Pb-, and Cd-loaded WR.

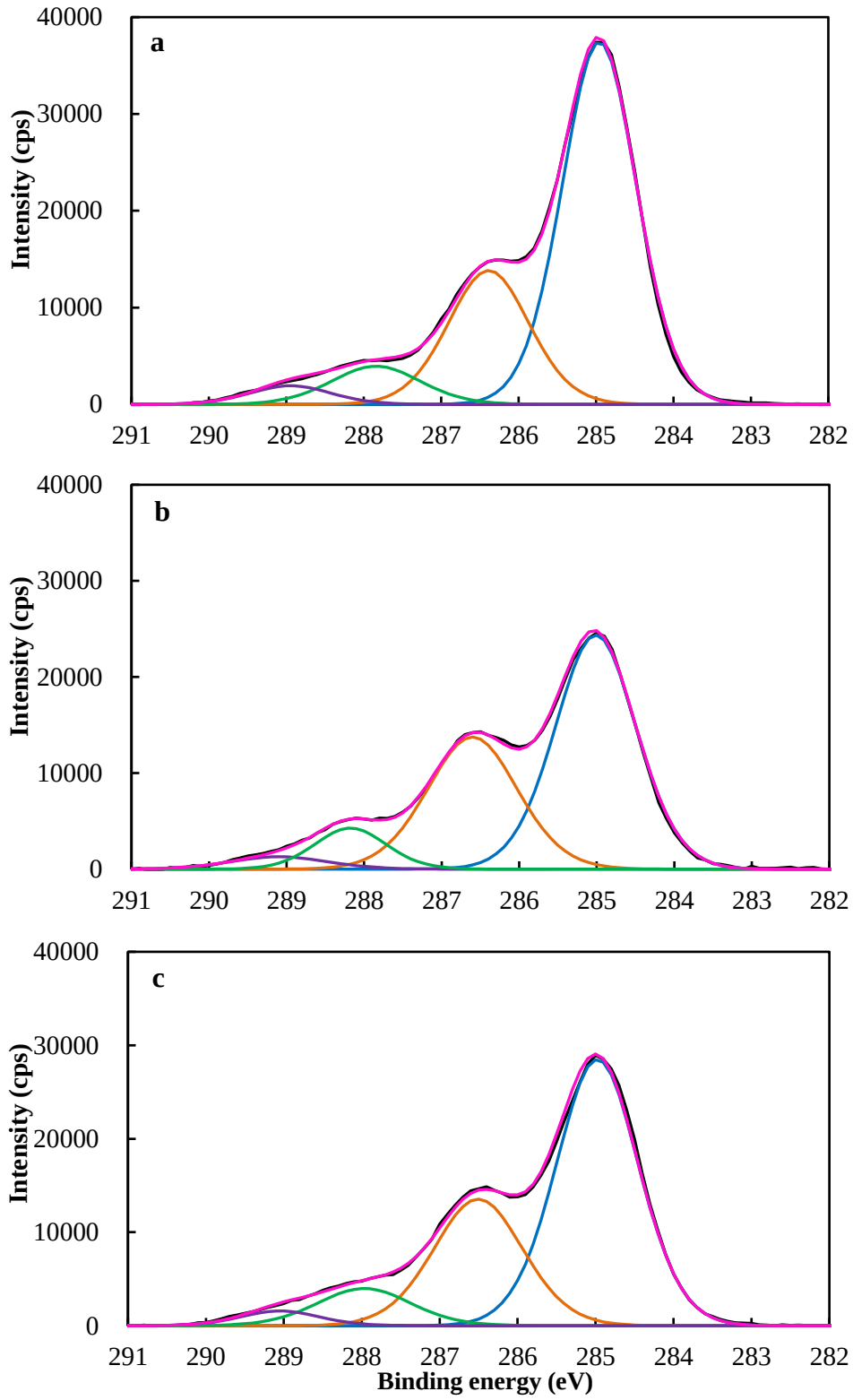

Figure 6.9 XPS spectra of C 1s of (a) pristine, (b) Pb-, and (c) Cd-loaded WR.

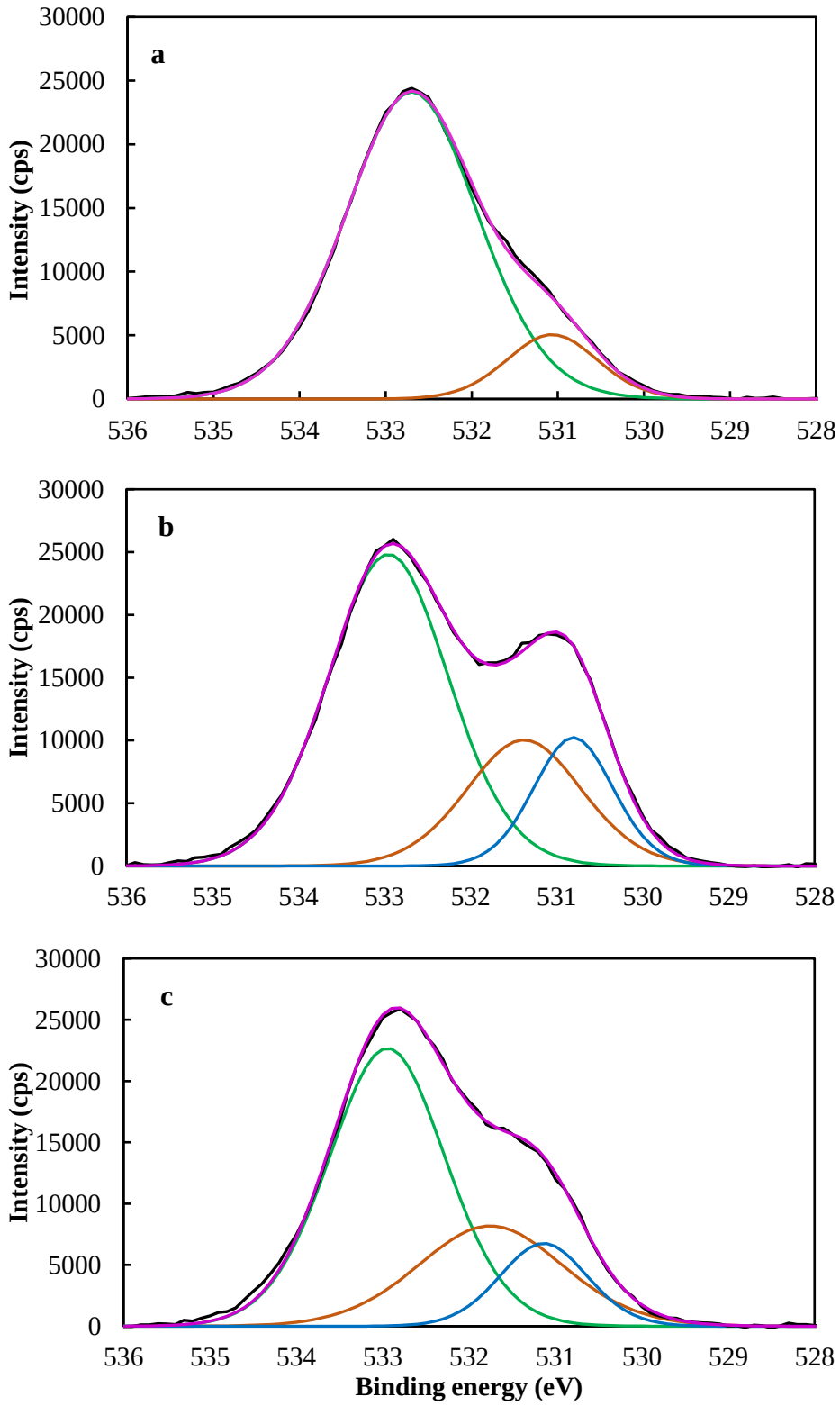

Figure 6.10 XPS spectra of O 1s of (a) pristine, (b) Pb-, and (c) Cd-loaded WR.

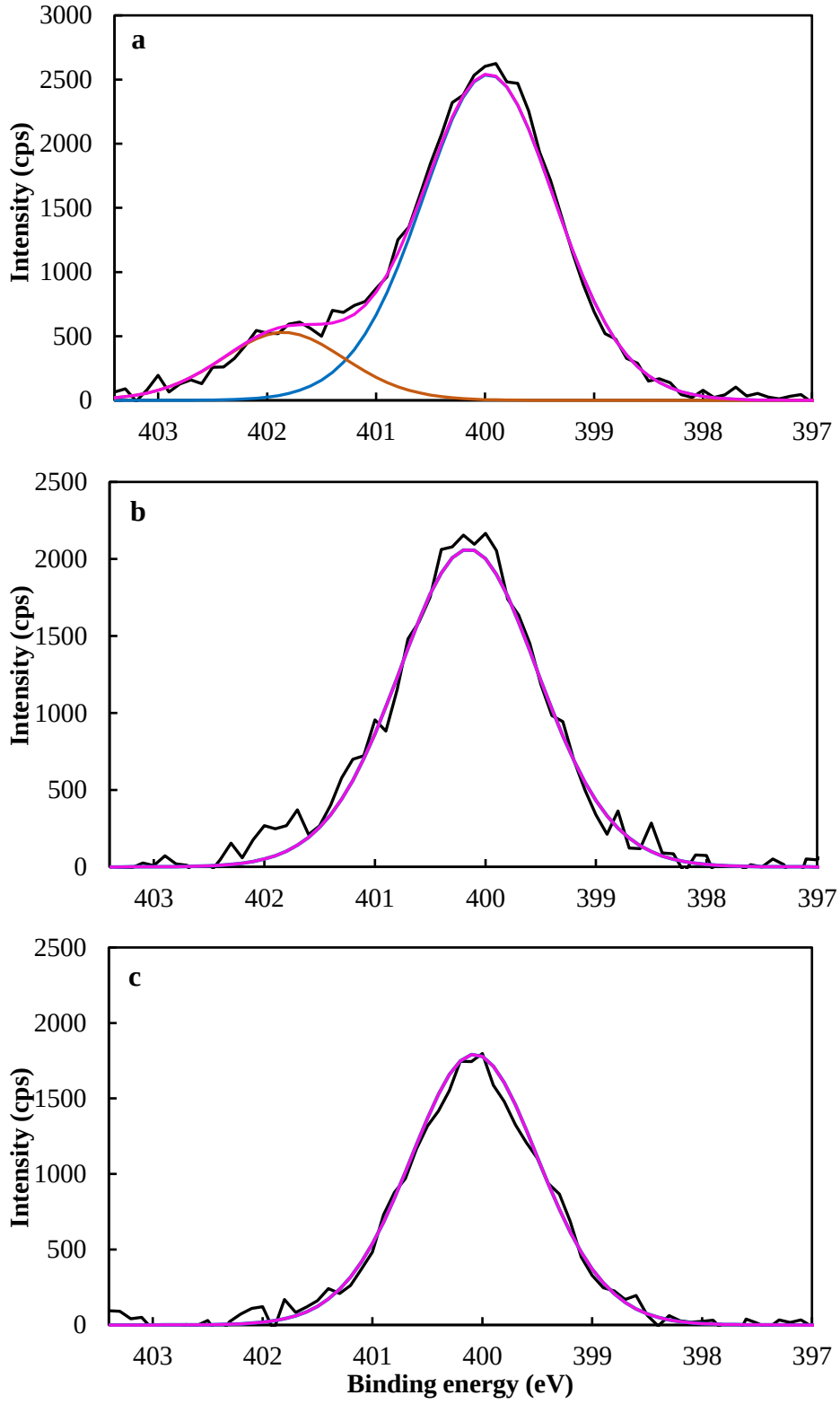

Figure 6.11 XPS spectra of N 1s of (a) pristine, (b) Pb-, and (c) Cd-loaded WR.

Table 6.2 Binding energies and atomic concentrations of different elements on the WR surface.

	Binding energy (eV)			Atomic concentration (%)		
	WR	Pb-WR	Cd-WR	WR	Pb-WR	Cd-WR
C 1s	285.00	285.00	285.00	74.77	63	69.20
O 1s	532.70	532.90	532.80	20.20	28.15	24.65
N 1s	399.90	400.00	400.00	3.02	2.14	1.59
K 2p	293.00	297.40	290.80	1.32	0	0
Ca 2p	346.90	349.10	347.80	0.15	0	0.02
Pb 4f	NA	138.90	NA	NA	4.65	NA
Cd 3d	NA	NA	405.60	NA	NA	2.96

(**Notes:** NA - Not applicable.)

Table 6.3 Bonds in pristine, Pb-, and Cd-loaded WR as identified by XPS.

	Group	Binding energy (eV)					Atomic concentration (%)		
		WR	Pb-WR		Cd-WR		WR	Pb-WR	Cd-WR
			BE	Shift	BE	Shift			
C 1s	C-C	284.967	284.996	0.029	284.975	0.008	63.04	54.25	57.83
	C-O	286.404	286.583	0.179	286.518	0.114	25.44	33.98	29.91
	C=O	287.829	288.175	0.346	287.989	0.16	8.00	8.37	9.19
	O=C-O	288.937	289.096	0.159	289.068	0.131	3.53	3.41	3.06
O 1s	Metal oxide	NA	530.789	NA	531.147	NA	NA	16.42	13.35
	O=C	531.077	531.385	0.308	531.765	0.688	12.63	23.32	26.84
	O-C	532.700	532.961	0.261	532.934	0.234	87.37	60.25	59.81
N 1s	$-NH_2$	399.968	400.153	0.185	400.096	0.128	83.85	100	100
	$-NH_3^+$	401.854	NA	NA	NA	NA	16.15	NA	NA

(**Notes:** BE - Binding energy; NA - Not applicable.)

6.1.7. Solid-state NMR spectroscopy

Solid-state NMR spectroscopy is arguably a powerful approach to provide compositional information with minimal pretreatment. Superior to spectroscopic techniques like FTIR spectroscopy and XPS, it can distinguish magnetically distinct atoms of the functional group being studied. In this sense, it is capable of clarifying the biopolymer source of the binding site, so as to figure out the roles of different biopolymers (e.g., cellulose, hemicellulose and pectin) in Pb(II) and Cd(II) biosorption. This can provide crucial information for developing commercial (bio)sorbents. In this study, the ^{13}C CP-MAS NMR spectra of pristine, Pb-, and Cd-loaded WR were collected to characterize the molecular structure of WR and its change due to Pb(II) and Cd(II) biosorption (Figure 6.12). Spectral deconvolution (not shown in the NMR spectra, details in Figures A10-12) was conducted for better assignment of the broad lines which are characteristic of solid-state NMR spectra, especially for biomaterials with complex compositions (Habets et al., 2013, Ren et al., 2016).

In Figure 6.12, resonances at 179.5 (assigned to ionized carboxyl groups), 174.4 (assigned to carboxyl-C of the acetyl group in hemicellulose), and 171.2 ppm (assigned to carboxyl-C of the ester group in pectin) were observed in pristine WR (Table 6.4). They moved upfield to 177.6, 173.6 and 170.9 ppm after Pb(II) biosorption, and to 175.6, 172.3 and 170.3 ppm after Cd(II) biosorption, respectively. This indicated that carboxyl groups from hemicellulose and pectin were involved in Pb(II) and Cd(II) biosorption by WR. Intriguingly, a resonance at 160.7 ppm (assigned to bicarbonates like $KHCO_3$) was only observed in pristine WR. The bicarbonates were probably produced from the interaction between light

metal ions on WR and CO_2 in the air, and they disappeared from the WR surface due to dissolution into the liquid phase during Pb(II) and Cd(II) biosorption. Moreover, resonances at 105-102 ppm became stronger, while the one at 98.6 ppm (assigned to hemicellulose C-1) significantly weakened after Pb(II)/Cd(II) loading. This could be caused by the downfield shift of the resonance at 98.6 ppm to 105-102 ppm when Pb(II)/Cd(II) bound to the O atom connecting to C-1 in hemicellulose (C-O-C groups). The resonance at 104.8 ppm was assigned to C-1 in (para)crystalline cellulose, and the one at 102.4 ppm could be C-1 of pectin and/or amorphous cellulose (cellulose exposed on the surface). The upfield shift of the latter resonance to 101.6 ppm after Pb(II) biosorption and to 101.2 ppm after Cd(II) biosorption suggested that the ether groups adjacent to C-1 of pectin and/or amorphous cellulose were binding sites. It is worth noting that the two shoulders at 81.8 ppm and 63.9 ppm, which were respectively assigned to C-4 and C-6 in amorphous cellulose, became sharper after Pb(II) and Cd(II) biosorption, indicating a more amorphous structure of the metal-loaded WR. The presence of C-2, 3, 5 in cellulose, C-2, 3, 4, 5 in pectin, and C-2, 3, 4 in hemicellulose resulted in a dominant and broad peak at 80-65 ppm; its precise resonance assignment was difficult due to peak overlap. Still, overall downfield shifts were observed in the NMR spectra of Pd- and Cd-loaded WR compared with that of pristine WR (see Figure 6.12). The downfield shifts could be caused by interactions between Pb(II)/Cd(II) and the hydroxyl and/or ether groups in cellulose, pectin and hemicellulose. Resonances at 54.0 ppm and 20.4 ppm were respectively characteristic of methyl-C of the ester group in pectin and methyl-C of the acetyl group in hemicellulose. No significant changes in the chemical shifts were observed in these groups. Notably, there was

no distinct resonance at 160-100 ppm (characteristic of aromatic C in lignin), indicating that lignin was a negligible constitute in WR used in this study.

Despite the powerfulness of solid-state NMR spectroscopy, the rigidity of solid samples and the intense dipole interactions between proximal nuclei cannot be averaged to zero, resulting in line broadening as observed in this study (Simpson et al., 2011). The considerable overlap rendered identification of components masked by the main resonances difficult, making applications of solid-state NMR spectroscopy limited in environmental studies. For instance, its utilization in biosorption studies has been restricted to the rough compositional characterization of biomaterials (Farinella et al., 2007, Krishnapriya and Kandaswamy, 2010, Perez Marin et al., 2010b, Ren et al., 2016). To this regard, advanced technologies such as chemical shift anisotropy (CSA) filters, dipolar dephasing (DD) filters, and saturation-pulse induced dipolar exchange with recoupling (SPIDER) have been used to obtain more qualified NMR spectra. Yet, these ingenious and "tailored" techniques further restrict the access to solid-state NMR spectroscopy. With aids of spectral deconvolution and references from model components (e.g., cellulose, pectin and lignin), this study indicates that ^{13}C NMR spectra of biomaterials can still provide useful compositional information and help identify the interactions between the contaminant and the sample.

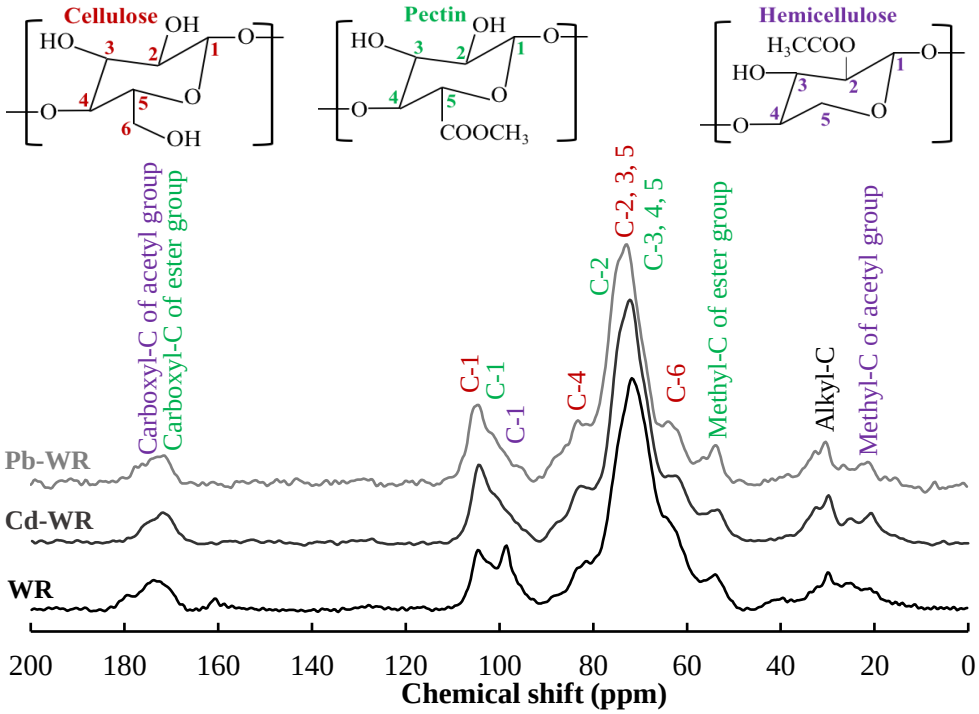

Figure 6.12 ^{13}C CP-MAS NMR spectra of pristine, Pb-, and Cd-loaded WR.

[The typical units of cellulose, hemicellulose and pectin are shown as insets.]

Table 6.4 Assignments of ^{13}C CP-MAS NMR bands in WR.

Chemical shift (ppm)	Functional group	Reference
179.5	Ionized carboxyl groups	(Perez Marin et al., 2010b)
174.4	Carboxyl-C of the acetyl group in hemicellulose	(Freitas et al., 2001, Wawer et al., 2006)
171.2	Carboxyl-C of the ester group in pectin	(Keenan et al., 1985); Table A1
160.7	Bicarbonates	(Perez Marin et al., 2010b)
100-160	Aromatic carbons in lignin	(Farinella et al., 2007); Table A1
104.8	C-1 in (para)crystalline cellulose	(Focher et al., 2001); Table A1
102.4	C-1 in pectin and/or amorphous cellulose on the surface	(Dick-Perez et al., 2011, Focher et al., 2001, Perez Marin et al., 2010b); Table A1
98.6	C-1 in hemicellulose	(Le Brech et al., 2016)
81.8	C-4 in amorphous cellulose	(Jarvis and Apperley, 1990); Table A1
79.7	C-2 in pectin	(Dick-Perez et al., 2011); Table A1
78.5	C-4 in hemicellulose	(Dick-Perez et al., 2011)
75.5	C-3 in hemicellulose	(Dick-Perez et al., 2011)
70-75	C-2, -3, -5 in cellulose	(Focher et al., 2001, Habets et al., 2013); Table A1
72.9	C-4 in pectin	(Dick-Perez et al., 2011); Table A1
72.6	C-2 in hemicellulose	(Dick-Perez et al., 2011)
71.1	C-3 in pectin	(Dick-Perez et al., 2011); Table A1

68.1	C-5 in pectin	(Dick-Perez et al., 2011); Table A1
63.9	C-6 in cellulose	(Jarvis and Apperley, 1990); Table A1
54.0	Methyl-C of the ester group in pectin	(Wang et al., 2015); Table A1
20.4	Methyl-C of the acetyl group in hemicellulose	(Le Brech et al., 2016)

6.1.8. Ion exchange experiment

In the ion exchange experiment, the release of light metal ions (i.e., Mg^{2+}, K^{+} and Ca^{2+}) from WR was determined, with K^{+} at a much higher content than Mg^{2+} and Ca^{2+} (15-20 times higher). However, it was intriguing to note that only Mg^{2+} and Ca^{2+} exhibited more intensive release in the Pb(II)/Cd(II) solution than in DDI water, whereas K^{+} exhibited similar amounts of release no matter with or without the presence of Pb(II)/Cd(II). This revealed that a part of the two naturally occurring divalent light metal ions were squeezed from the binding sites by Pb(II)/Cd(II) ions via ion exchange. Hence, mainly Mg^{2+} and Ca^{2+} participated in the ion exchange with Pb(II)/Cd(II), even though disappearance of K on the WR surface was observed after Pb(II)/Cd(II) biosorption in EDX and XPS measurements. Zheng et al. (2016) also reported the mere release of Mg^{2+} and Ca^{2+} along with Cu(II) and Cd(II) biosorption by water hyacinth roots. Occasionally, participation of a light metal ion in ion exchange was concluded based on spectroscopic observation of its loss from biosorbents (Maresova et al., 2011, Panda et al., 2006), or its release into the liquid phase during biosorption (Girardi et al., 2014). However, the spontaneous dissolution of the light metal ions from the biosorbent into the aqueous solution (e.g., the disappearance of K^{+} from WR in this study) might be overlooked.

In the Pb(II) biosorption system, the Pb(II) biosorption capacity of WR in equilibrium was calculated as 0.492 mmol/g. Compared with the control system (WR in DDI water), 0.0364 mmol of Mg^{2+} and 0.0544 mmol of Ca^{2+} were released in extra from one gram of WR in the Pb(II) system (Table 6.5); it was estimated that ion exchange with divalent light metal ions participated in 18.5% of Pb(II)

biosorption. On the other hand, 0.0847 mmol/g of Mg^{2+} and 0.0783 mmol/g of Ca^{2+} were released in extra from WR in the Cd(II) system, and it was estimated that ion exchange with the two divalent light metal ions was involved in 81.5% of Cd(II) biosorption (Cd uptake of 0.200 mmol/g). Accordingly, it could be inferred that ion exchange played a more important role in Cd(II) biosorption than in Pb(II) biosorption by WR. This should be ascribed to the smaller ionic radius and larger ionic potential of Cd(II) than Pb(II) (see Table 2.1), as ion-exchange materials tend to prefer counter ions of higher valency (ionic potential) and smaller hydrated equivalent volume (Loganathan et al., 2014). Following the step of ion exchange, Pb(II)/Cd(II) ions might interact with the binding sites on WR through electrostatic attraction, as shown in Eqs. 6.3 and 6.4 (M^{2+} represents Pb(II)/Cd(II) ions) (Ahmad et al., 2015). The decrease of pH commonly observed in the Pb(II) and Cd(II) biosorption processes in this study also suggested the occurrence of ion exchange between H^+ and Pb(II)/Cd(II) for the binding sites (taking carboxyl groups as an example in Eq. 6.5).

$$(R\text{-}COO)_2Mg + M^{2+} \leftrightarrow (R\text{-}COO)_2M + Mg^{2+} \quad (6.3)$$

$$R\text{-}O\text{-}Ca\text{-}O\text{-}R + M^{2+} \leftrightarrow R\text{-}O\text{-}M\text{-}O\text{-}R + Ca^{2+} \quad (6.4)$$

$$2(R\text{-}COOH) + M^{2+} \leftrightarrow (R\text{-}COO)_2M + 2H^+ \quad (6.5)$$

Table 6.5 Release of light metal ions during Pb(II) and Cd(II) biosorption by WR.

	Pb(II) biosorption		Cd(II) biosorption	
	Pb solution	Control	Cd solution	Control
Mg^{2+}	0.1313 ± 0.0040	0.0949 ± 0.0005	0.1340 ± 0.0008	0.0493 ± 0.0001
Ca^{2+}	0.0945 ± 0.0001	0.0401 ± 0.0004	0.0871 ± 0.0007	0.0087 ± 0.0002

(**Notes:** Control - WR suspension in DDI water; Unit in mmol/g.)

6.2. Characterization of MS and mechanistic studies

6.2.1. Elemental analysis

Elemental analysis revealed that MS was composed of 43.73% of C, 6.67% of H, 48.81% of O, 0.75% of N and 0.04% of S (in dry weight). The atomic ratios of (O+N)/C and H/C were 0.85 and 1.83, respectively. It was suggested that MS had lower polarity and higher aromaticity than WR (Li et al., 2010). Besides, the amounts of N and S in MS were much lower than those in WR (3.3% of N and 0.38% of S).

6.2.2. Zeta potential measurement

Figure 6.13 reveals that the MS surface was negatively charged, and the zeta potential became more negative with increasing pH, with the isoelectric point at about pH 2.0. As pH increased from 2.0 to 8.0, more and more functional groups such as carboxyl (-COOH) and protonated amine ($-NH_3^+$) groups on the MS surface would deprotonate, resulting in a more negatively charged MS surface. Electrostatic attraction could be a binding force for Pb(II) and Cd(II) ions to MS, since MS would be highly negatively charged in the biosorption systems with pH 5.0 for Pb(II) and 7.5 for Cd(II) biosorption in this study. The most negative zeta potential of MS at pH 7.5 was in consistence with the highest Cd(II) uptake determined at pH 7.5 as reported in Section 5.2.

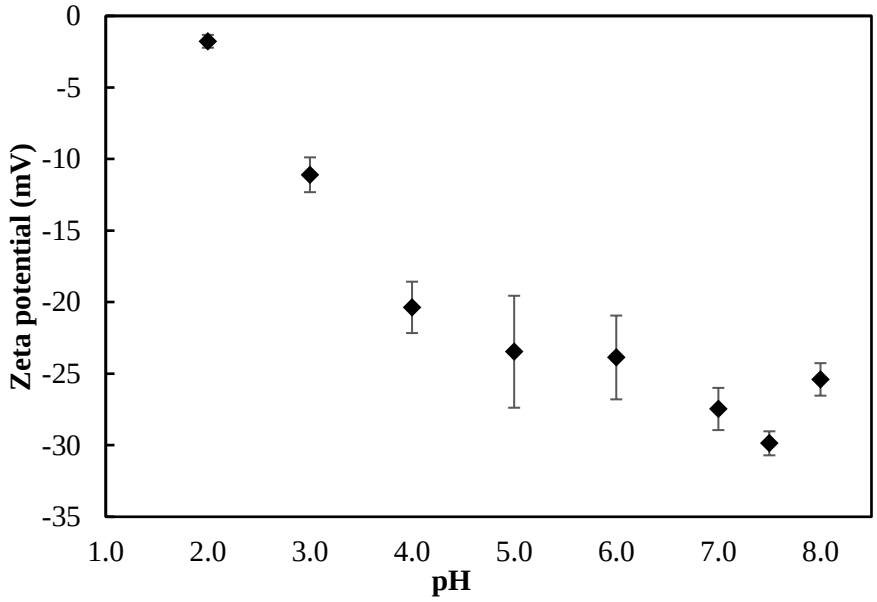

Figure 6.13 Zeta potentials of MS at varying pH.

[0.15 g/L MS in 1 mM KCl.]

6.2.3. PXRD

Distinct reflections at 2θ of 15.3°, 17.0°, 18.0°, 19.5° and 23.0° were detected in the PXRD diffractogram of pristine MS (Figure 6.14). The reflections at 2θ of 15.3°, 23.0°, and the unresolved doublet at 17.0° and 18.0° corresponded to the mango kernel starch (Millan-Testa et al., 2005, Sandhu and Lim, 2008). This indicated the existence of kernel starch in MS. The weaker and broader reflections in the PXRD patterns of Pb- and Cd-loaded MS suggested reduced crystallinity of MS after Pb(II) and Cd(II) biosorption. This should be attributed to the conversion of (para)crystalline regions to disoriented amorphous regions in MS after biosorption. The conversion could be caused by the breakage of hydrogen bonds responsible for maintaining the ordered crystalline regions in MS (Krishnapriya and Kandaswamy, 2010, Moyo et al., 2017).

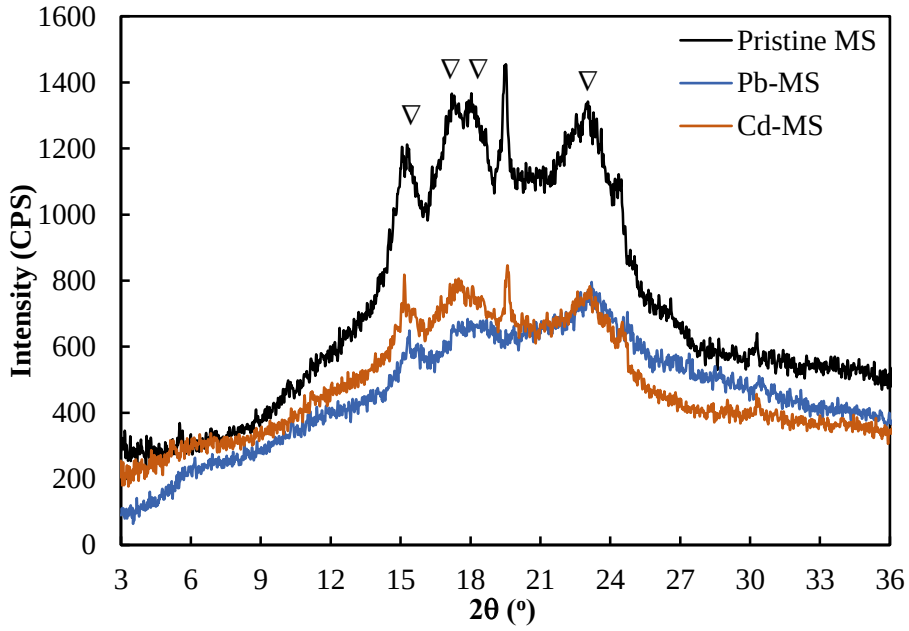

Figure 6.14 PXRD patterns of pristine, Pb-, and Cd-loaded MS.

[∇: Mango kernel starch.]

6.2.4. SEM-EDX

In Figure 6.15a, the SEM micrograph of pristine MS indicates that MS had an irregular and uneven surface, which provided a large surface area for Pb(II) and Cd(II) sequestration. After Pb(II) and Cd(II) biosorption, the MS surface was spread with a number of particles (Figures 6.15b & 6.15c), which should be Pb(II) and Cd(II) precipitates generated during biosorption. This was confirmed by X-ray elemental mappings (Figure 6.16), in which intense Pb and Cd signals were detected at the spots on the MS surface where solid precipitates were exactly observed in the corresponding SEM micrographs (highlighted in circles). The Pb(II) and Cd(II) precipitates on the MS surface could be produced from the microprecipitation of Pb(II) and Cd(II) (Volesky, 2003), and/or conversion of metal complexes which were generated from the coordination of Pb(II)/Cd(II) to N and O atoms in the functional groups on MS (Zhou et al., 2005). Notably, Pb and Cd were mapped over the MS surface even though there was no observation of any solid precipitates in the corresponding SEM micrographs (Figure 6.16), indicating that microprecipitation was not the only mechanism responsible for Pb(II) and Cd(II) biosorption by MS. In Figure 6.17, the EDX spectra reveal the presence of light metals, including Mg, K and Ca, on the surface of the pristine MS, and they vanished after Pb(II) and Cd(II) biosorption. Instead, Pb and Cd were detected on the surface of the Pb- and Cd-loaded MS, respectively. This suggested the occurrence of ion exchange between Pb(II)/Cd(II) and light metal ions at the binding sites on the surface of MS.

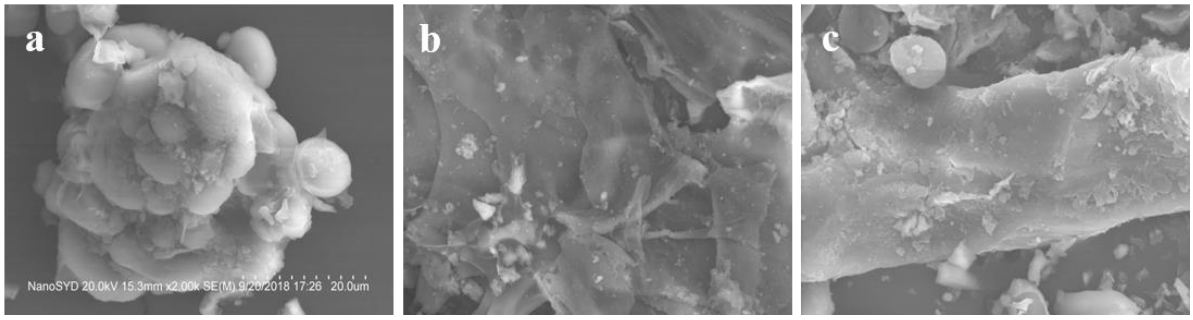

Figure 6.15 SEM micrographs of (a) pristine, (b) Pb-, and (c) Cd-loaded MS.

[Magnification 2000×; Collected by Dr. KIM Tae-Hyun of University of Southern Denmark.]

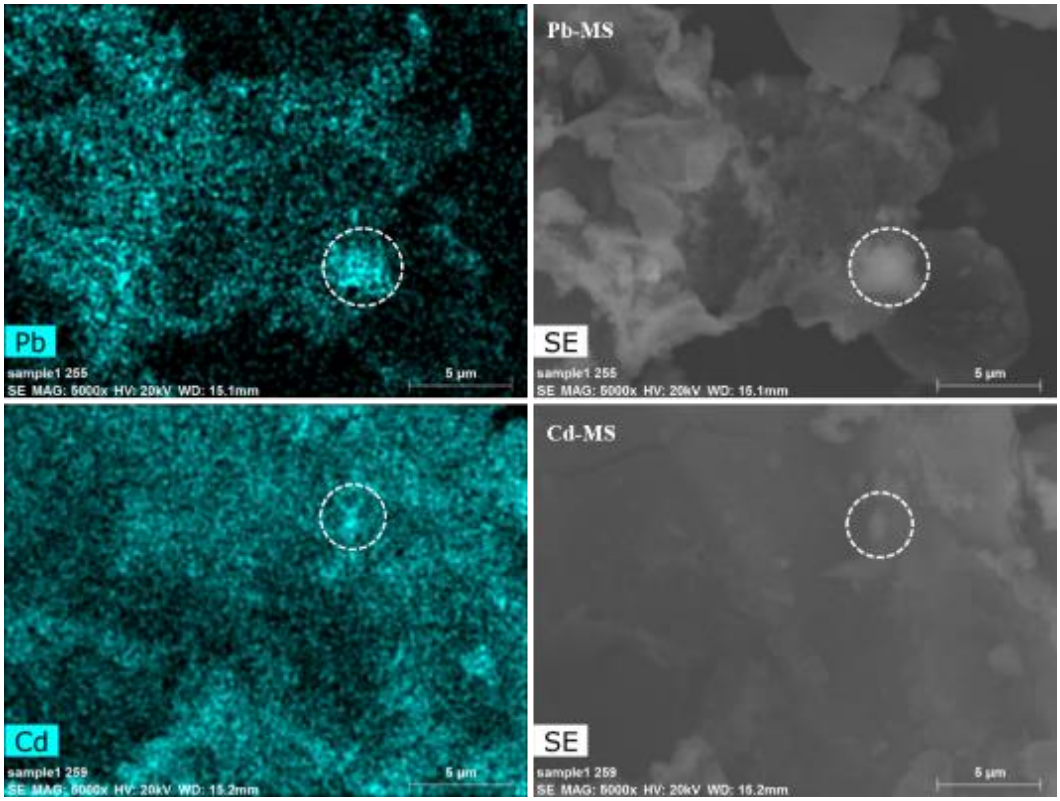

Figure 6.16 X-ray elemental mappings of Pb and Cd on the MS surface and the corresponding SEM micrographs.

[Magnification 5000×; Collected by Dr. KIM Tae-Hyun of University of Southern Denmark.]

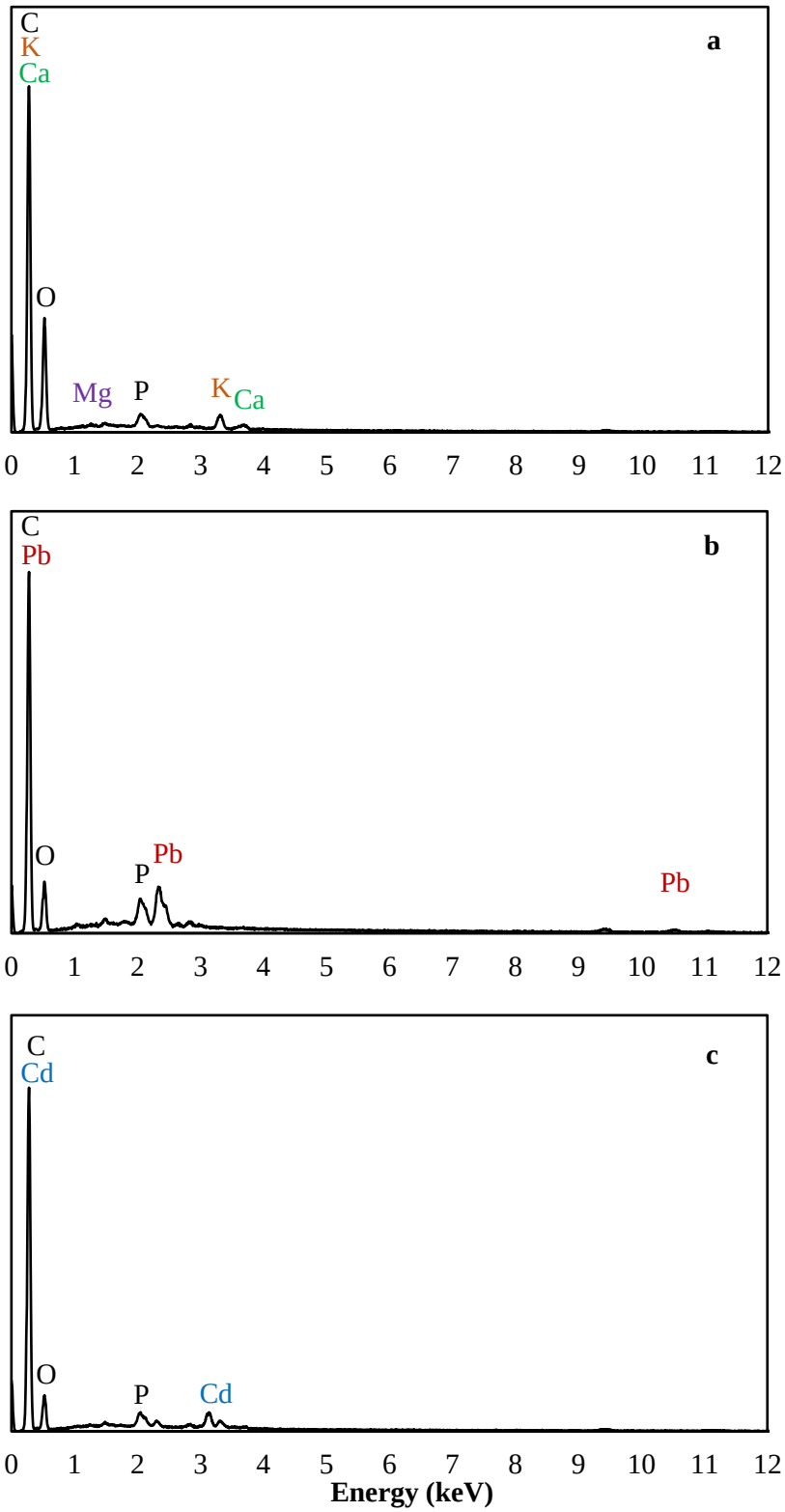

Figure 6.17 EDX spectra of (a) pristine, (b) Pb-, and (c) Cd-loaded MS.

[Collected by Dr. KIM Tae-Hyun of University of Southern Denmark.]

6.2.5. FTIR spectroscopy

In Figure 6.18, a variety of absorption bands were observed in the FTIR spectra of MS, indicating the complicated composition of MS. Specifically, the FTIR spectrum of pristine MS exhibited absorption bands for stretching vibrations of C-H in alkanes (2926 cm^{-1}), C=O in esters (1736 cm^{-1}), C=O in carboxylic salts (1452 cm^{-1}), C-N in amines (1340 cm^{-1}), C-O-C in ethers (1161 cm^{-1}), C-O in primary alcohol (1022 cm^{-1}), and bending vibrations of N-H in primary amines (1618 cm^{-1}) (Griffiths et al. 2006, Pavia et al., 2008). Significant shifts at 1618 cm^{-1} after Pb(II) biosorption, and at 1618 cm^{-1}, 1452 cm^{-1} and 1340 cm^{-1} after Cd(II) biosorption were recorded (details in Table 6.6). This implied the involvement of the corresponding functional groups (e.g., amine and carboxyl groups) in Pb(II) and Cd(II) biosorption by MS. As mentioned before, more analytical techniques were required to support and complement the findings from FTIR analysis in consideration of the wide absorption range of a certain functional group in the infrared region.

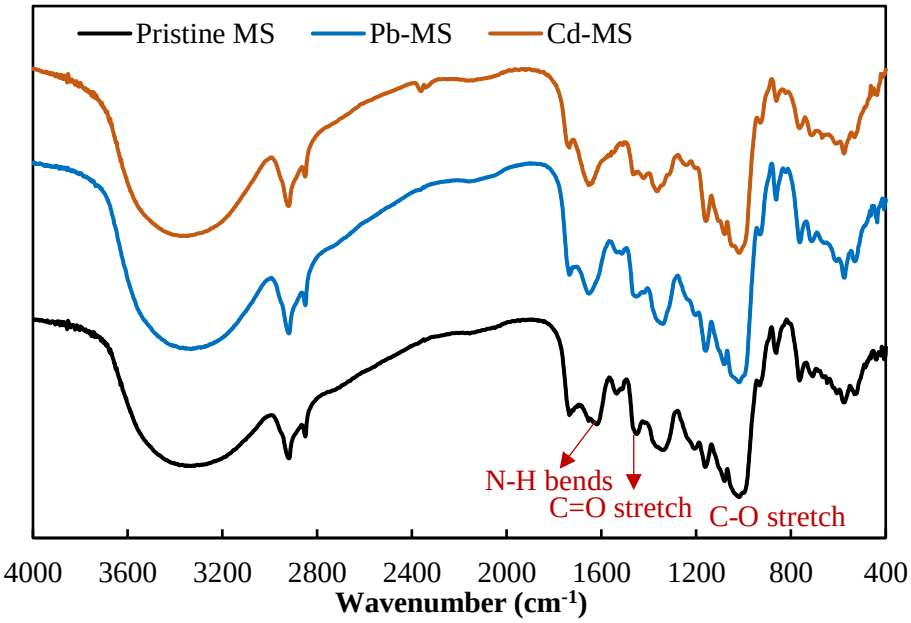

Figure 6.18 FTIR spectra of pristine, Pb-, and Cd-loaded MS.

Table 6.6 Assignments of the functional groups on MS in FTIR analysis.

Wavenumber (cm^{-1})			Shift (cm^{-1})		Assignment
MS	Pb-MS	Cd-MS	Pb-MS	Cd-MS	
2926	2920	2922	-6	-4	C-H stretch in alkanes
2850	2850	2850	0	0	Asymmetric stretch of C-H in alkanes
1736	1736	1736	0	0	C=O stretch in esters
1618	1655	1655	37	37	N-H bend in primary amines
1452	1456	1421	4	-31	C=O stretch in carboxylic salts
1340	1340	1365	0	25	C-N stretch in amines
1161	1161	1159	0	-2	C-O-C stretch
1022	1020	1016	-2	-6	C-O stretch in primary alcohol

6.2.6. XPS

Figure 6.19 shows the XPS survey spectra of pristine, Pb-, and Cd-loaded MS. The strongest signals of C 1s and O 1s revealed that C and O were the two most predominant elements on the MS surface. Distinct signals of Pb and Cd, especially those of Pb 4f and Cd 3d, were observed on the MS surface after exposure of MS to Pb(II) and Cd(II), indicating substantial loadings of Pb(II) and Cd(II) on MS. These findings were consistent with the elemental information summarized in Table 6.7, which indicated that C and O were the two most important elements on the MS surface with atomic concentrations of 76.1-79.6% and 18.6-21.5%, respectively, and distinct amounts of Pb and Cd were detected on MS after Pb(II) and Cd(II) biosorption. It is noteworthy that Ca, which accounted for 0.11% (atomic concentration) on the MS surface, almost vanished after Pb(II) and Cd(II) biosorption. This could be ascribed to the ion exchange between Ca^{2+} and the counter ions Pb(II)/Cd(II) during biosorption. As shown in Table 6.7, Pb and Cd sequestered by MS were mainly detected at 139.0 eV and 405.7 eV, which respectively corresponded to Pb in PbO and Cd in CdO (Moulder et al., 1992). The similar observations were also reported in Pb(II) and Cd(II) biosorption by using biosorbents derived from *Chlorella vulgaris* microalgae (Lalhmunsiama et al., 2017) and *Pinus svlvestris* sawdust (Taty-Costodes et al., 2003). The metal oxides were probably derived from the metal complexes which were formed by Pb(II)/Cd(II) complexation with O atoms in functional groups (e.g., hydroxyl, carboxyl and ether groups) on the MS surface. Besides, the precipitation of metal hydroxides during biosorption could also result in the deposition of metal oxides on the MS surface (Zhou et al., 2005). The binding sites involved in Pb(II) and Cd(II) biosorption

would be disclosed based on the shifts of binding energies of C 1s, O 1s and N 1s in XPS spectra after Pb(II) and Cd(II) biosorption (Table 6.8).

C 1s

Figure 6.20a shows that the C 1s spectrum of pristine MS consisted of four peaks at 284.980, 286.511, 287.941 and 289.160 eV, which agreed with the binding energies of the C atoms in C-C, C-O (alcohol and/or ether), C=O and O=C-O, respectively (Lim et al., 2008, Moulder et al., 1992, Ramrakhiani et al., 2017). The latter three peaks respectively shifted to 286.602, 288.214 and 289.279 eV in the C 1s spectrum of Pb-loaded MS (Figure 6.20b), and to 286.643, 288.419 and 289.396 eV in that of Cd-loaded MS (Figure 6.20c). The relatively significant increases of the binding energies of the C atoms indicated the involvement of hydroxyl (in alcohol), ether, and carboxyl groups in Pb(II) and Cd(II) biosorption by MS. Take an ether group (C-O-C) as an example, the O atom donated lone pairs of electrons to the unoccupied orbitals of Pb(II)/Cd(II) to form metal complexes, resulting in a lower electron density around the two adjacent C atoms and thus a higher binding energy. Similarly, the O atoms in hydroxyl and carboxyl groups could also coordinate to Pb(II)/Cd(II), resulting in lower electron densities of the adjacent C atoms and thus higher binding energies (Cid et al., 2018, Ramrakhiani et al., 2017, Sheng et al., 2004). It is noteworthy that the electrostatic attraction of Pb(II)/Cd(II) to the deprotonated carboxyl groups, i.e., $-COO^-$, might also cause an increase in the binding energy of the C atom as cationic Pb(II)/Cd(II) ions would grab electrons.

O 1s

As Figure 6.21a reveals, the O 1s spectrum of pristine MS comprised two peaks at 531.315 and 532.881 eV, which corresponded to the O atoms in O=C and C-O (hydroxyl and/or ether) groups (Moulder et al., 1992). The two peaks respectively shifted to 531.574 eV and 532.997 eV after Pb(II) biosorption (Figure 6.21b), and to 531.706 eV and 533.001 eV after Cd(II) biosorption (Figure 6.21c). The increased binding energies of the O atoms indicated the occurrence of Pb(II) and Cd(II) complexation with the O atoms in O=C and C-O (e.g., carboxyl, hydroxyl and ether groups). The donation of lone pairs of electrons to the empty orbitals of Pb(II) and Cd(II) to form coordination bonds resulted in lower electron densities around the O atoms and thus higher binding energies (Cid et al., 2018). This observation was consistent with the aforementioned increased binding energies of the C atoms in alcohol, ether and carboxyl groups. Notably, a peak which was assigned to metal oxides emerged in the O 1s spectrum of Pb- (531.097 eV) and Cd-loaded MS (531.143 eV). The formation of PbO and CdO on the MS surface after Pb(II) and Cd(II) biosorption could originate from the metal precipitates as observed in the aforementioned SEM-EDX analysis.

N 1s

In Figure 6.22a, two peaks located at 400.175 eV (assigned to $-NH_2$) and 401.643 eV (assigned to $-NH_3^+$) (Gao et al., 2017), were observed in the N 1s spectrum of pristine MS. The area of the two peaks revealed a much higher content of neutral N than the positively charged N on the MS surface (Ren et al., 2016). The former peak significantly shifted to 400.300 eV and 400.289 eV after the biosorption of Pb(II) and Cd(II), respectively. This was indicative of Pb(II)/Cd(II)

complexation with the N atom in the amine group; the N atom contributed a lone pair of electrons to the empty orbital of Pb(II)/Cd(II), resulting in a lower electron density and thus a higher binding energy of itself (Zhou et al., 2005). Intriguingly, protonated amine groups, $-NH_3^+$, disappeared from the Pb- and Cd-loaded MS (Figures 6.22b & 6.22c). This should be caused by the conversion of $R\text{-}NH_3^+$ to $R\text{-}NH_2Pb^{2+}$ and $R\text{-}NH_2Cd^{2+}$ complexes after Pb(II) and Cd(II) binding to MS, as shown in Eqs. 6.1 & 6.2.

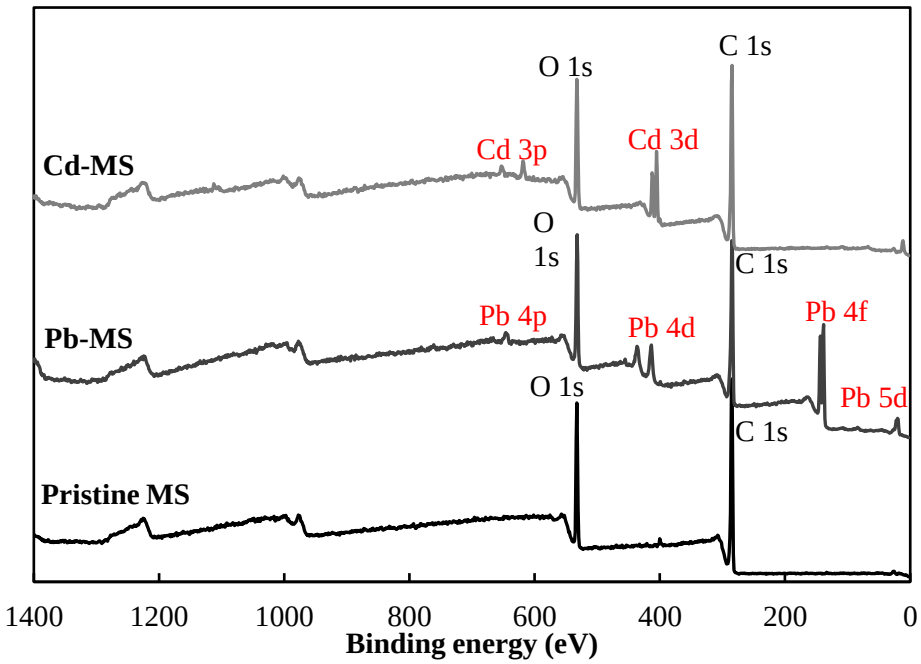

Figure 6.19 XPS survey spectra of pristine, Pb-, and Cd-loaded MS.

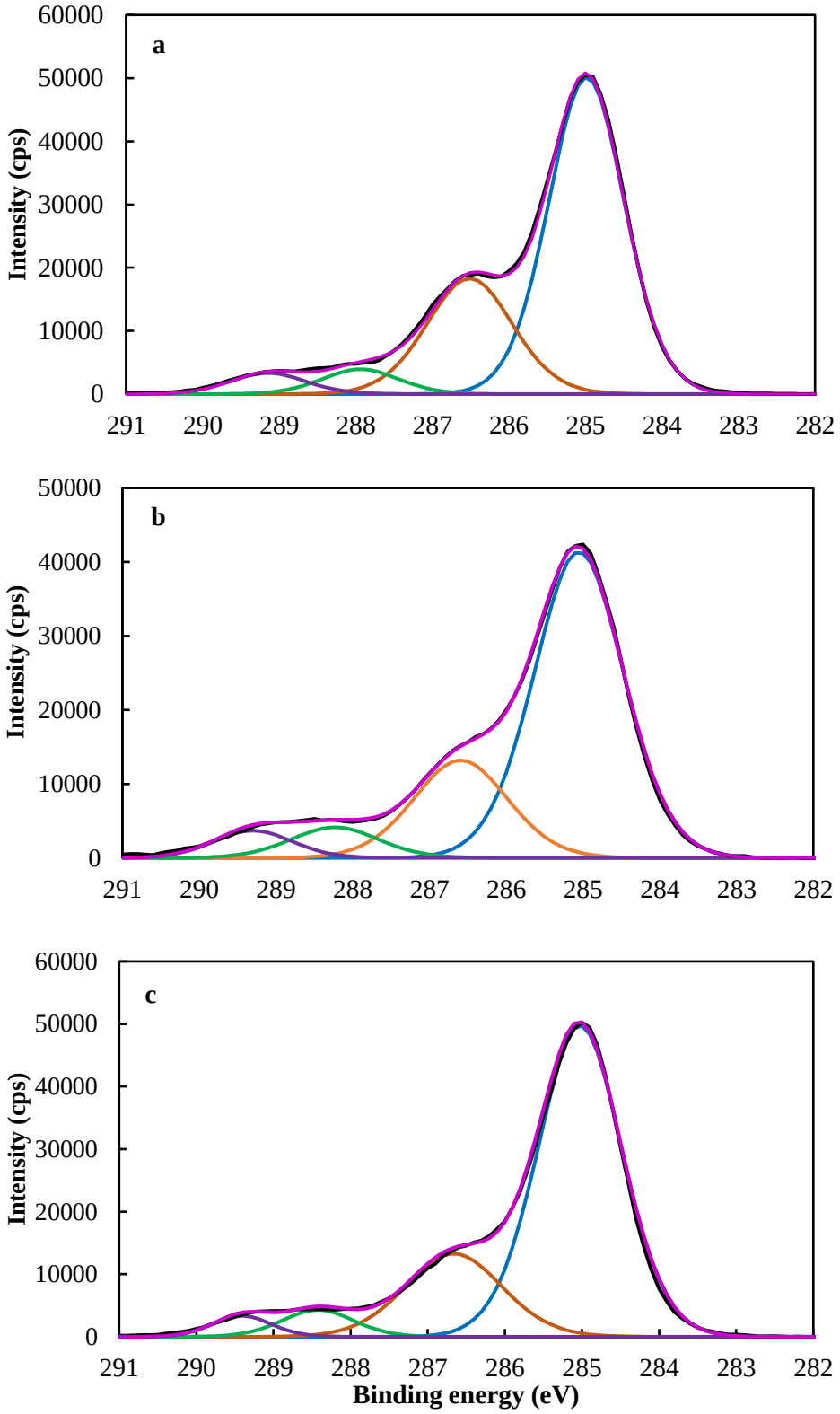

Figure 6.20 XPS spectra of C 1s of (a) pristine, (b) Pb-, and (c) Cd-loaded MS.

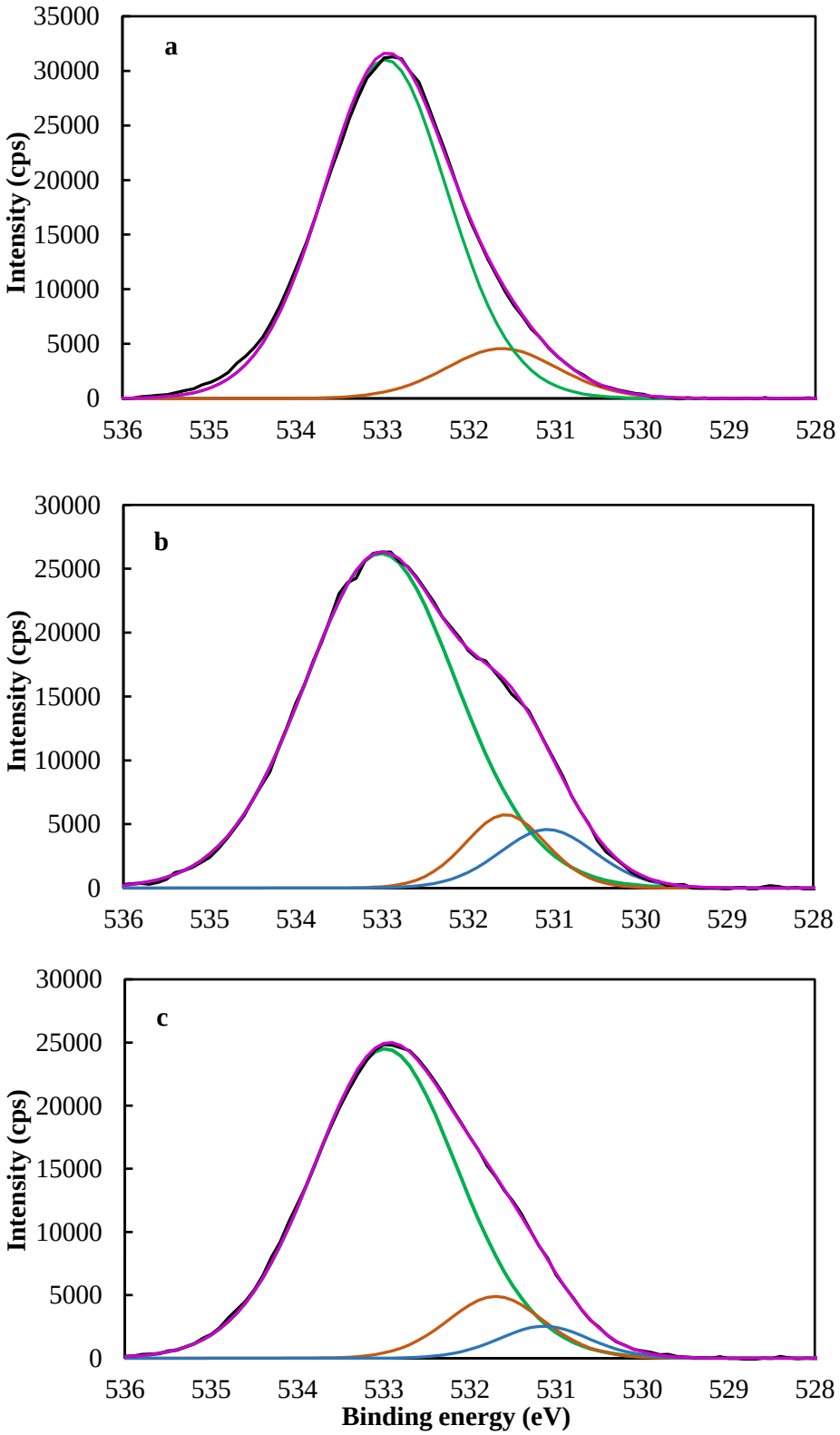

Figure 6.21 XPS spectra of O 1s of (a) pristine, (b) Pb-, and (c) Cd-loaded MS.

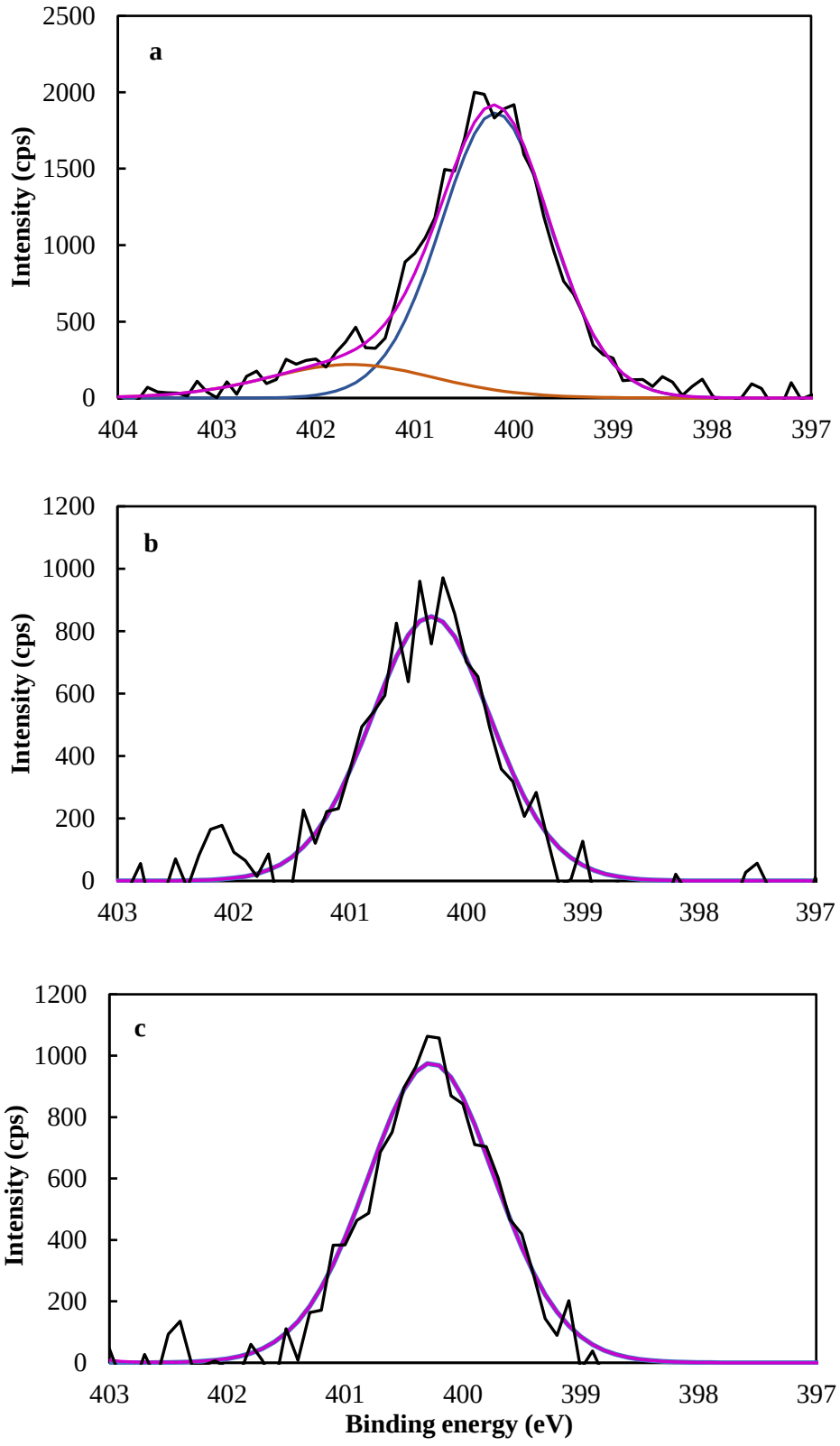

Figure 6.22 XPS spectra of N 1s of (a) pristine, (b) Pb-, and (c) Cd-loaded MS.

Table 6.7 Binding energies and atomic concentrations of different elements on the MS surface.

	Binding energy (eV)			Atomic concentration (%)		
	MS	Pb-MS	Cd-MS	MS	Pb-MS	Cd-MS
C 1s	285.000	285.000	285.000	79.62	76.06	79.1
O 1s	533.000	532.900	533.000	18.64	21.46	18.74
N 1s	400.400	400.200	400.300	1.48	0.48	0.4
Ca 2p	347.400	350.9	347.500	0.11	0.03	0
Pb 4f	NA	139.000	NA	NA	1.96	NA
Cd 3d	NA	NA	405.700	NA	NA	1.59

(**Notes:** NA - Not applicable.)

Table 6.8 Bonds in pristine, Pb-, and Cd-loaded MS as identified by XPS.

	Group	Binding energy (eV)					Atomic concentration (%)		
		MS	Pb-MS		Cd-MS		MS	Pb-MS	Cd-MS
			BE	Shift	BE	Shift			
C 1s	C-C	284.980	285.059	0.079	285.034	0.054	64.16	66.15	70.03
	C-O	286.511	286.602	0.091	286.643	0.134	26.50	22.19	21.50
	C=O	287.941	288.214	0.273	288.419	0.478	5.11	6.50	5.16
	O=C-O	289.160	289.279	0.119	289.396	0.236	4.23	5.16	3.31
O 1s	Metal oxide	NA	531.097	NA	531.143	NA	NA	8.91	5.35
	O=C	531.315	531.574	0.259	531.706	0.391	4.95	9.47	11.02
	O-C	532.881	532.997	0.116	533.001	0.120	95.05	81.62	83.63
N 1s	NH_2	400.175	400.300	0.125	400.289	0.114	84.85	100	100
	NH_3^+	401.643	NA	NA	NA	NA	15.15	NA	NA

(**Notes:** BE - Binding energy; NA - Not applicable.)

6.2.7. Solid-state NMR spectroscopy

To characterize the molecular structure of MS and its change due to Pb(II) and Cd(II) biosorption, the ^{13}C CP-MAS NMR spectra of pristine, Pb-, and Cd-loaded MS were collected (Figure 6.23). Spectral deconvolution was performed for better assignment of the broad lines detected in the spectra (Figures A13-15). In Figure 6.23, a weak resonance at 170.9 ppm (assigned to carboxyl-C of the acetyl group in hemicellulose) was observed in the ^{13}C NMR spectrum of pristine MS, and it moved downfield to 171.6 ppm after Pb(II) and Cd(II) biosorption. The downfield shifts should be attributed to the interaction between Pb(II)/Cd(II) and the O atoms in carboxyl groups, possibly via complexation, which changed the magnetic environment around the C atoms in carboxyl groups. In addition, significant resonances at 143.5 and 137.5 ppm, which corresponded to the C atoms in tannins, were detected in the ^{13}C NMR spectrum of pristine MS; they almost disappeared after Pb(II) and Cd(II) biosorption probably due to the dissolution of tannins in the liquid phase. It has been reported that the mango seed kernel contains a high content of tannins (Maisuthisakul and Gordon, 2009). Besides, the resonances at 102.6 and 99.1 ppm corresponded to C-1 in amorphous cellulose and C in tannins, respectively. The downfield shift of the former to 104.2 ppm after Pb(II) biosorption and to 104.1 ppm after Cd(II) biosorption should be attributed to the binding of Pb(II) and Cd(II) to the O atoms in the ether groups connected to C-1 in cellulose, leading to a change in the magnetic environment around C-1. The latter also moved downfield to 100.1 and 100.0 ppm after Pb(II) and Cd(II) biosorption, respectively, suggesting the involvement of tannins (e.g., hydroxyl and/or carboxyl groups) in biosorption. The dominant resonance was located at about 71.9 ppm,

which might contain C-2, -3, -5 in cellulose and C-2, -3, -4 in hemicellulose. Although precise assignment of the broad lines was difficult due to the overlap, downfield shifts of the peak were observed after Pb(II) and Cd(II) biosorption. This could be caused by the interactions between Pb(II)/Cd(II) and certain functional groups in cellulose and hemicellulose (e.g., hydroxyl, ether and carboxyl groups). Two shoulders at 81.8 and 61.6 ppm, which were respectively assigned to C-4 and C-6 in amorphous cellulose, were located aside the dominant resonance. The resonance at 30.1 ppm might correspond to the lipids in mango kernel, and the one at 21.6 ppm was a characteristic of the methyl carbon of the acetyl group in hemicellulose. As no distinct resonance was observed at around 54.7 ppm, which is a characteristic of the methoxyl-C in lignin (Table A1), it was concluded that lignin was a negligible component in MS used in this test (particle size < 180 μm). All of the ^{13}C spectral assignments of MS are summarized in Table 6.9. Taken together, MS dominantly comprised cellulose, with low contents of hemicellulose, tannins and lipids. In addition to carboxyl groups in hemicellulose, hydroxyl and ether groups in cellulose and hemicellulose were also potential binding sites for Pb(II) and Cd(II). Tannins in MS might also contribute to the sequestration of Pb(II) and Cd(II).

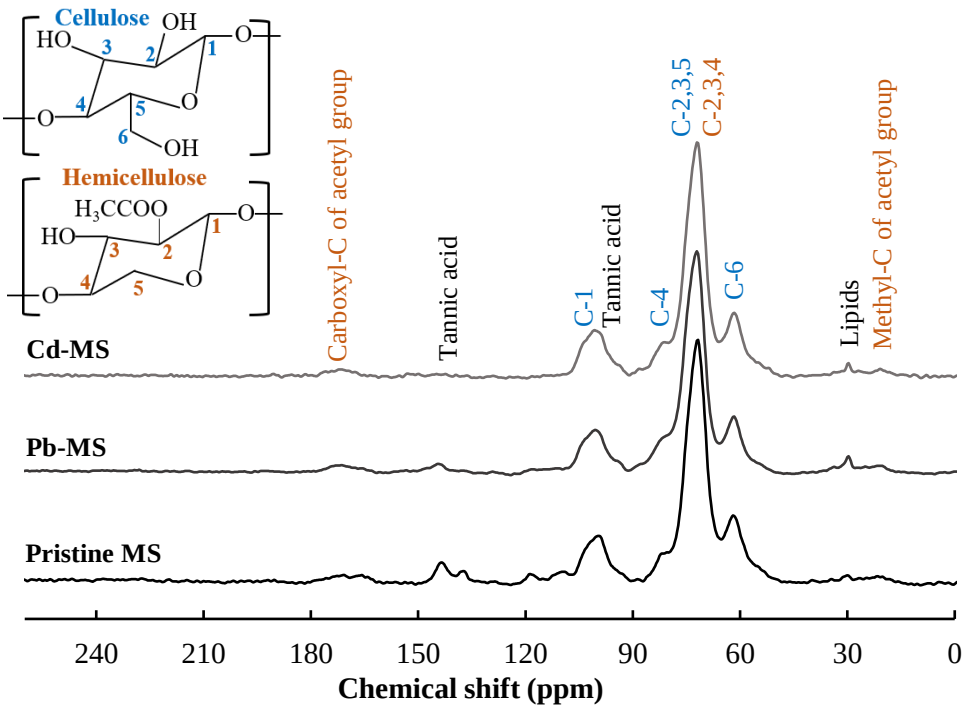

Figure 6.23 ^{13}C solid-state NMR spectra of pristine, Pb-, and Cd-loaded MS.

Table 6.9 Assignments of ^{13}C CP-MAS NMR bands in MS.

Chemical shift (ppm)	Functional group	Reference
170.9	Carboxyl-C of acetyl group in hemicellulose	(Freitas et al., 2001, Wawer et al., 2006)
152.0	Aromatic C-O in lignin	(Habets et al., 2013, Le Brech et al., 2016); Table A1
143.5	Aromatic C-O in lignin	(Le Brech et al., 2016); Table A1
137.5	C in tannic acid	(Gamble et al., 1996)
118.5	Aromatic C in lignin	(Love et al., 1994); Table A1
110	Aromatic C in lignin	(Le Brech et al., 2016); Table A1
104.5	C-1 in (para)crystalline cellulose	(Focher et al., 2001); Table A1
102.6	C-1 in amorphous cellulose	(Focher et al., 2001)
99.11	C in tannic acid	(Gamble et al., 1996)
88.1	C-4 in (para)crystalline cellulose	(Focher et al., 2001); Table A1
81.8	C-4 in amorphous cellulose	(Jarvis and Apperley, 1990); Table A1
79.0-67.0	C-2, -3, -5 in cellulose, C-2, -3, -4 in hemicellulose	(Dick-Perez et al., 2011, Komatsu and Kikuchi, 2013); Table A1
64.0	C-6 in (para)crystalline cellulose	(Wang et al., 2012); Table A1
61.6	C-6 in amorphous cellulose	(Jarvis and Apperley, 1990, Wang et al., 2012); Table A1
56.0	Methoxyl-C in lignin	(Le Brech et al., 2016, Wang et al., 2012); Table A1
30.1	Lipids	(Jarvis and Apperley, 1990)

21.6	Methyl-C of acetyl group in hemicellulose	(Freitas et al., 2001)

6.2.8. Ion exchange experiment

In the ion exchange experiment, it was observed that Mg^{2+}, K^{+} and Ca^{2+} were released from MS during Pb(II) and Cd(II) biosorption, and the amount of K^{+} was 5-20 times higher than those of Mg^{2+} and Ca^{2+}. Only the two divalent light metal ions, Mg^{2+} and Ca^{2+}, were released at distinctly higher amounts in the Pb(II) and Cd(II) biosorption systems as compared with the control groups (MS in DDI water). Therefore, only Mg^{2+} and Ca^{2+} bound to the binding sites significantly exchanged with Pb(II) and Cd(II) in solution. This was probably ascribed to the ease of replacing metal ions with the same valence for the binding sites. The observation in the ion exchange experiment was consistent with the disappearance of Ca in the XPS survey spectra of MS after Pb(II) and Cd(II) biosorption (Table 6.7), as well as the vanishing of Mg and Ca from the EDX spectra of Pb- and Cd-loaded MS (Figure 6.17). Notably, the disappearance of K from MS as observed by EDX spectroscopy should be attributed to the natural dissolution of K^{+} from MS in the solution.

In comparison with the control groups, 0.0107 mmol/g of Mg^{2+} and 0.0069 mmol/g of Ca^{2+} were released in extra in the Pb(II) biosorption system, while 0.0124 mmol/g of Mg^{2+} and 0.0093 mmol/g of Ca^{2+} were released in extra in the Cd(II) system (Table 6.10). As Pb(II) and Cd(II) uptakes were respectively calculated as 0.151 mmol/g and 0.0915 mmol/g, it was estimated that ion exchange with Mg^{2+} and Ca^{2+} was involved in 11.7% of Pb(II) biosorption and 27.1% of Cd(II) biosorption by MS.

Table 6.10 Release of light metal ions during Pb(II) and Cd(II) biosorption by MS.

	Pb(II) biosorption		Cd(II) biosorption	
	Pb solution	Control	Cd solution	Control
Mg^{2+}	0.0565 ± 0.0000	0.0457 ± 0.0005	0.0506 ± 0.0019	0.0382 ± 0.0013
Ca^{2+}	0.0313 ± 0.0003	0.0243 ± 0.0015	0.0168 ± 0.0009	0.0075 ± 0.0002

(**Notes:** Control - MS suspension in DDI water; Unit in mmol/g.)

6.2.9. Further mechanistic studies based on the effect of particle size

As intriguingly observed in Section 5.1, MS in different particle sizes exhibited hugely distinct Pb(II) and Cd(II) biosorption capacities. Deciphering the reason behind would provide important insights into the underlying mechanisms of Pb(II) and Cd(II) biosorption by MS. To this end, the PXRD patterns, ^{13}C solid-state NMR spectra and contents of light metal ions of MS in the three different particle sizes (i.e., MS1: < 180 μm, MS2: 180-500 μm, and MS3: 500-1000 μm) were investigated.

PXRD

As shown in Figure 6.24, the PXRD patterns of MS in larger particle sizes (i.e., MS2 and MS3) presented reflections at 2θ of 16° and 22° (typical for crystalline cellulose I), which were distinctly different from those of MS1 (see Figure 6.14). This indicated that mango kernel starch was negligible in MS2 and MS3, in which cellulose was a crucial constitute. The poor biosorption performance of MS in 180-500 and 500-1000 μm was probably caused by the crystalline structure of MS. The diverse PXRD patterns of MS in different particle sizes lead to a puzzle as to why there was a huge difference in composition between MS < 180 μm and larger MS in 180-500 μm and 500-1000 μm. This should result from the preparation of the MS biosorbent; when grinding MS in an electrical blender, the mango kernel could be ground into fine powders more easily than the mango seed shell. Consequently, the starch-containing mango kernel became the dominant constitute in MS < 180 μm, and the mango seed shell with a high content of cellulose mostly remained in larger MS.

^{13}C solid-state NMR spectra

As the dependence of the biosorption capacity of MS on particle size should be caused by compositional and structural differences of MS in different particle sizes, the ^{13}C CP-MAS NMR spectra of MS1 (< 180 µm), MS2 (180-500 µm) and MS3 (500-1000 µm) were collected (Figure 6.25, deconvolution shown in Figures A13, A16 & A17). It was observed that resonances at 171-172 ppm (assigned to carboxyl-C in hemicellulose) in MS2 and MS3 were stronger than those in MS1. Also, the resonance corresponding to methyl-C of the acetyl group in hemicellulose at 21 ppm exhibited peaks much more intense in MS2 and MS3 than those in MS1, indicating higher contents of hemicellulose in lager MS than smaller MS. Besides, resonances at 152 ppm, which were assigned to carbon atoms in lignin (lignin structure in Figure A9), were observed in MS2 and MS3. Together with the resonances observed at 56 ppm (assigned to methoxyl-C in lignin) in MS2 and MS3, it was concluded that there was lignin in MS2 and MS3, while its content in MS1 was negligible. The resonances corresponding to C atoms in tannins at 143.5 and 137.5 ppm in MS1 almost vanished in MS2 and MS3. This should be ascribed to the much lower amount of mango kernel, which contains tannins, in larger MS. In addition to C-1 (102-103 ppm), C-4 (82-83 ppm) and C-6 (61-62 ppm) in amorphous cellulose (as observed in MS1), C-1 (105 ppm), C-4 (88 ppm) and C-6 (64 ppm) in (para)crystalline cellulose were also observed in MS2 and MS3. This revealed a higher content of cellulose and a more crystalline structure of cellulose in larger MS, which was consistent with the PXRD patterns of MS in different particle sizes (Figure 6.24). It is worth noting that the resonance corresponding to

lipids in mango seed kernel at 30 ppm almost vanished in MS2 and MS3, indicating the insignificant content of mango kernel in MS2 and MS3.

Content of light metal ions

To determine the contents of light metal ion, 0.02 g of MS in different particle sizes was respectively dispersed in 20 mL of 0.05 M HNO_3 and agitated at 250 rpm for 24 h. The light metal ions soaked in the liquid phase were measured. According to Figure 6.26, smaller MS particles had a higher content of Ca^{2+} and Mg^{2+} than the larger ones. As mentioned in Section 6.2.8, Ca^{2+} and Mg^{2+} bound to the binding sites on MS could exchange with Pb(II) and Cd(II) in solution. This was consistent with the negative correlation between the biosorption capacities of MS and its particle size. However, the total molar content of Ca^{2+} and Mg^{2+} in MS was much lower compared with the Pb(II) and Cd(II) biosorption capacities of MS. For example, the Pb(II) biosorption capacity of MS1 was 0.95 ± 0.008 mmol/g, whereas the total content of Ca^{2+} and Mg^{2+} in MS1 was only 0.11 ± 0.001 mmol/g (Figure 6.26). Hence, the total content of Ca^{2+} and Mg^{2+} in MS could not account for the significant effect of MS particle size on Pb(II) and Cd(II) biosorption capacities.

To summarize, there were higher contents of hemicellulose, cellulose and lignin with a more crystalline structure of cellulose in larger MS (i.e., MS2 and MS3). For MS1, the component of mango seed kernel led to a more amorphous structure with the presence of tannins and some lipids. In this sense, the much higher Pb(II) and Cd(II) biosorption capacities of MS1 should be due to its more amorphous structure and the presence of more active binding sites, as tannins contain massive hydroxyl and carboxyl groups (see Figure A9). On the other hand,

the more crystalline structure and higher content of lignin led to lower Pb(II) and Cd(II) biosorption capacities of larger MS. Lignin was assumed to be the main storage medium of organic pollutants, but not to mineral pollutants due to its aromatic structure (high aromaticity) (Tran et al., 2015, Zhang et al., 2016).

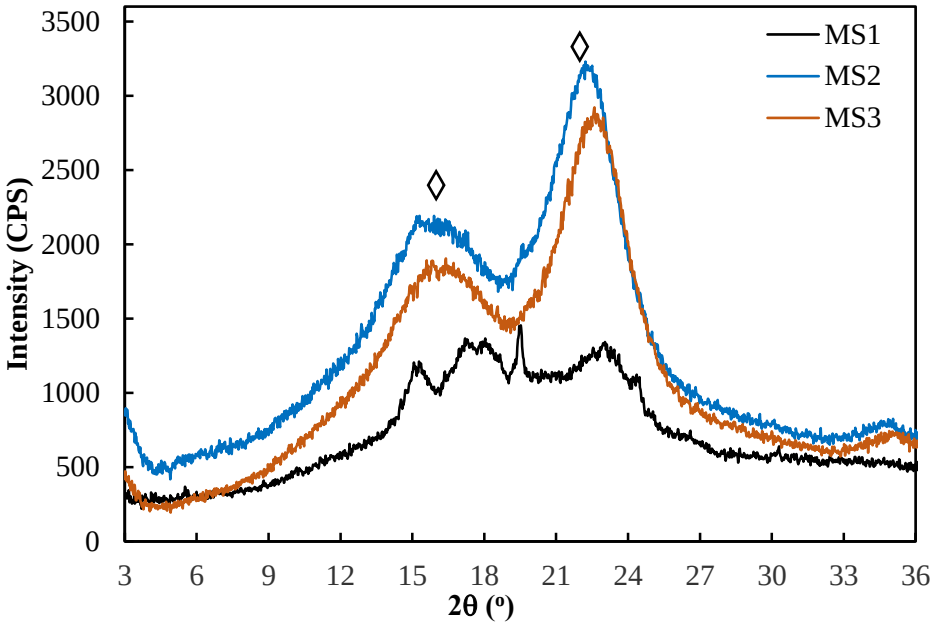

Figure 6.24 PXRD patterns of MS in different particle sizes.

[◊: Cellulose I; MS1: < 180 μm; MS2: 180-500 μm; MS3: 500-1000 μm.]

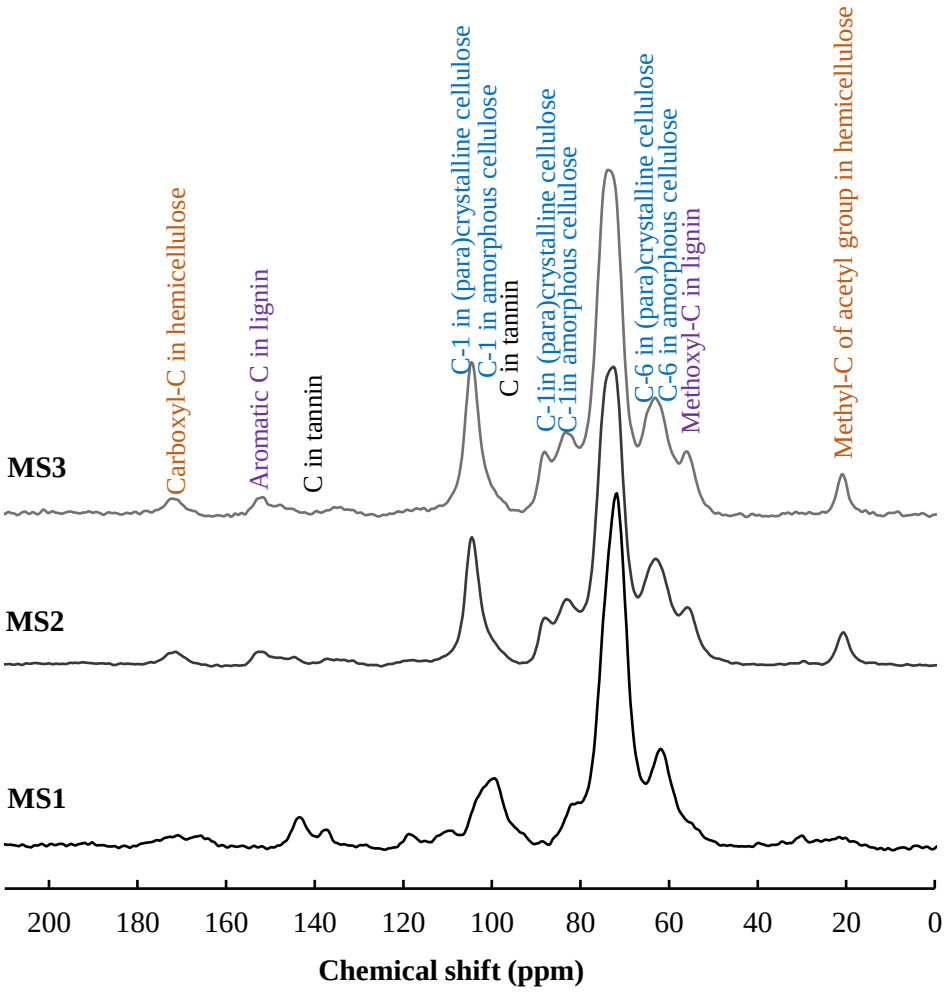

Figure 6.25 ^{13}C solid-state NMR spectra of MS in different particle sizes.

[MS1: < 180 μm; MS2: 180-500 μm; MS3: 500-1000 μm.]

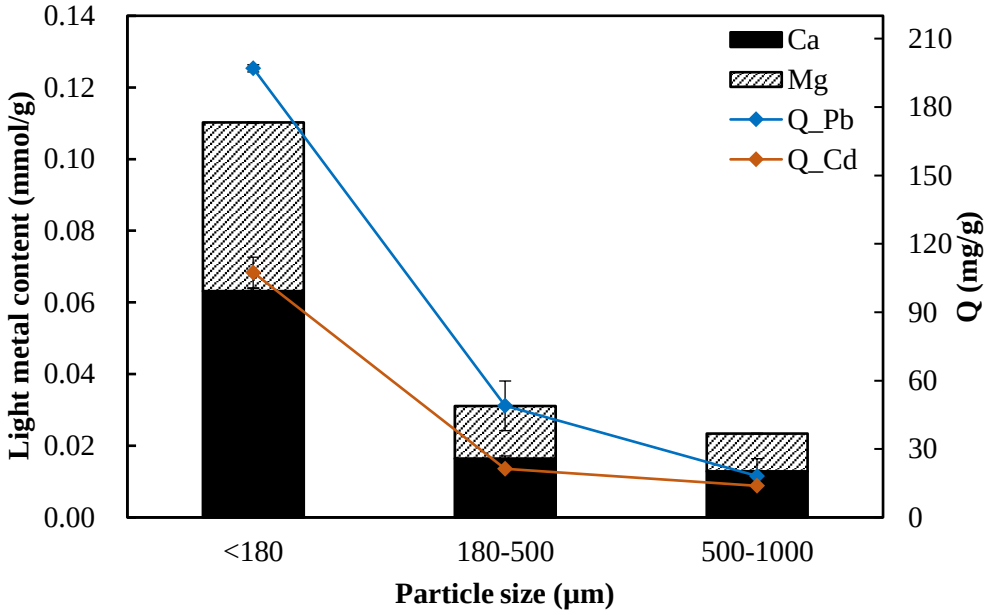

Figure 6.26 Pb(II) and Cd(II) biosorption capacities and light metal ions contents of MS in different particle sizes.

[Initial metal concentrations of 500 ppm, pH 5.0 for Pb and pH 7.5 for Cd, 1.0 g/L MS.]

6.3. Quantum chemistry simulation

As aforementioned, hydroxyl, carboxyl, amine and ether groups in WR and MS were identified as the active functional groups for Pb(II) and Cd(II) biosorption, with the formation of coordination bonds (i.e., complexation) as an important underlying mechanism. But a puzzle remained: how would the heavy metal ions interact with these functional groups *in situ* (i.e., in biopolymers which contain these functional groups)? Also, if the heavy metal ions had any preference to bind to any particular binding sites? To answer these questions, QCS was applied to simulate the microscopic interactions between the heavy metal ions (Pb(II) as the representative, Cd(II) not shown due to similar simulation results) and some typical components of fruit waste materials, such as cellulose, pectin and citrulline (a model of amino acid providing amine groups). This would provide information of the structural and thermodynamic properties of the heavy metal complexes formed in biosorption (Leng et al., 2016).

Table 6.11 lists the optimized structures and thermodynamic properties of a number of Pb-cellulose, Pb-pectin and Pb-citrulline complexes. As hydroxyl groups usually adjoin with ether groups in cellulose (Structure 1 in Table 6.11), three possible reactions, namely Pb(II) complexation with ether and hydroxyl groups (1a), and that with two adjoining hydroxyl groups in different spatial locations (1b and 1c) were simulated. The negative values of ΔG indicated that the reactions were favorable. Given that Pb(II) biosorption was performed at pH 5.0, at which the hydroxyl groups (*pKa* at about pH 10.0) would exist as R-OH without deprotonation, it was still unknown that whether Pb(II) would exchange with H^+ in R-OH and bind to $R\text{-}O^-$. QCS indicated that this process was unfavorable with a

positive ΔG of 21.53 kcal/mol (Structure 1d), implying that the pH decrease during Pb(II) biosorption was mainly due to the deprotonation of carboxyl groups and protonated amine groups (i.e., $-NH_3^+$) rather than hydroxyl groups. Similar to cellulose, carboxyl, hydroxyl and ether groups adjoin with each other in pectin (Structure 2), and the carboxyl groups adjoin amine groups in citrulline (Structure 3). These permutations provide possibilities of forming various Pb complexes. As Table 6.11 shows, the values of ΔG were more negative when carboxyl groups were involved in the reactions (e.g., by comparing 2a, 2b and 2c, to 2d and 2e), revealing that carboxyl groups were more favorable binding sites for Pb(II). This could be attributed to the electrostatic attraction exerted by carboxyl groups as they would stay deprotonated at pH 5.0 (*pKa* around 3.5). Lam (2015) also found that the carboxyl group was the main active site for heavy metal biosorption based on surface complexation modeling, even both hydroxyl and carboxyl groups were abundant on the biosorbent. It is worth noting that the bond length of the coordination bonds in this study was 2.216-2.565 Å, which was comparable to the values reported in Pb-EDTA complexes (Kovács et al., 2010), and Pb complexes formed with aliphatic carboxylates, aliphatic oxoligands and aromatic carboxylates (Davidovich et al., 2009).

Most of the Pb complexes were simulated with two coordination bonds in this study to simplify the simulation. However, real interactions can be more complicated given the composition complexity of fruit waste materials. The favorable formation of Structure 3c and 3d indicated the feasibility of Pb(II) complexation with four or more N/O atoms. The actual coordination number

achieved would be the result of the optimization of the electronic and geometric factors.

Table 6.11 Optimized structures and thermodynamic properties of Pb(II) complexes.

Reaction	Cel + Pb^{2+} → (1a, 1b, or 1c)$^{2+}$;		Cel + Pb^{2+} + $2H_2O$ → 1d + $2H_3O^+$		
No.	Cellulose (Cel): **1**	**1a**	**1b**	**1c**	**1d**
Optimized structure	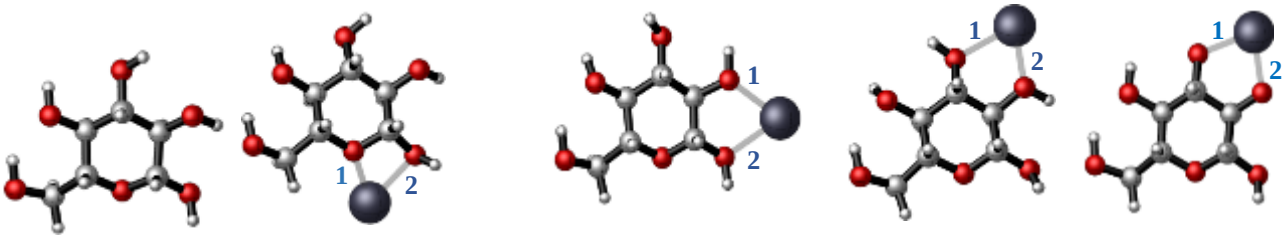				
Bond length (Å)[a]	-	2.426; 2.479	2.404; 2.441	2.408; 2.405	2.189; 2.191
Active groups	-	Ether; Hydroxyl	Hydroxyl	Hydroxyl	Hydroxyl
Δ*G* (kcal/mol)	-	-20.05	-22.56	-25.31	21.53
Reaction	Pec$^-$ + Pb^{2+} → (2a, 2b, or 2c)$^+$ or (2d or 2e)$^{2+}$				
No.	Pectin (Pec): **2**	**2a**	**2b**	**2c**	**2d**	**2e**
Optimized structure	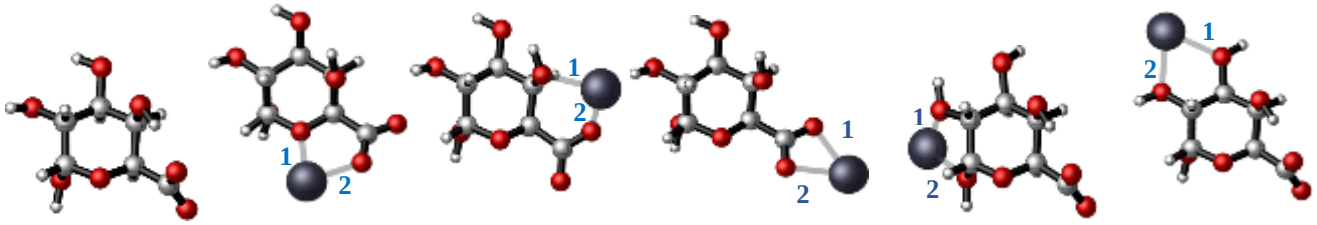					
Bond length (Å)	-	2.388; 2.219	2.393; 2.216	2.370; 2.386	2.395; 2.377	2.388; 2.395
Active groups	-	Ether; Carboxyl	Hydroxyl; Carboxyl	Carboxyl	Hydroxyl	Hydroxyl
Δ*G* (kcal/mol)	-	-46.55	-41.23	-39.86	-29.11	-28.78
Reaction	Cit$^-$ + Pb^{2+} → (3a or 3b)$^+$;		2Cit$^-$ + Pb^{2+} → (3c or 3d)			
No.	Citrulline[b] (Cit): **3**	**3a**	**3b**	**3c**	**3d**
Optimized structure	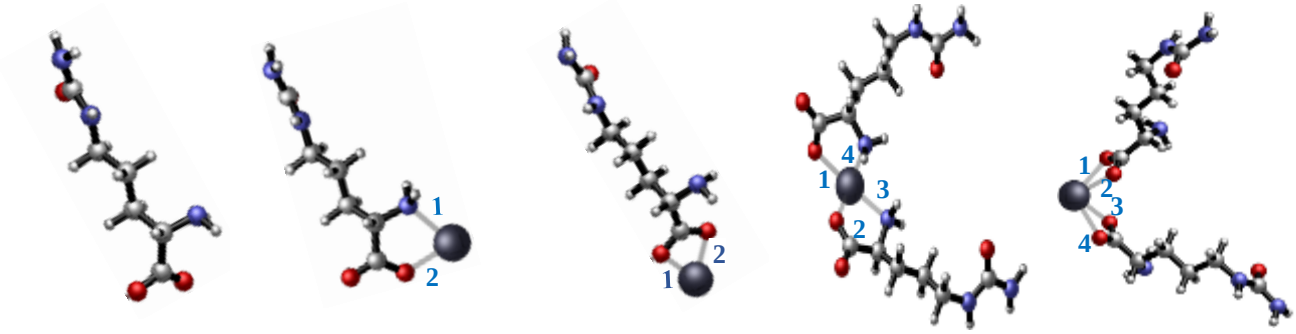				
Bond length (Å)	-	2.416; 2.217	2.362; 2.364	2.455; 2.322; 2.565; 2.469	2.548; 2.386; 2.410; 2.505

Active groups	-	Carboxyl; Amine	Carboxyl	Carboxyl; Amine	Carboxyl
ΔG (kcal/mol)	-	-56.07	-43.03	-76.91	-64.67

(**Notes:** a - Bond length was shown in an order of (1; 2) or (1; 2; 3; 4); b - Citrulline was selected as an amino acid for simulation of Pb-protein complexes given its high concentration in WR (Rimando and Perkins-Veazie, 2005); Monomers of cellulose and pectin were used to simplify the simulation; Pectin monomer and citrulline are charged due to the dissociation of carboxyl at pH 5.0 applied in this study; Numbers in blue show different bonds formed in complexes; Large grey sphere - C atom; Small grey sphere - H atom; Red sphere - O atom; Blue sphere: N atom; Black sphere: Pb atom.)

6.4. Summary

In combination with macroscopic biosorption studies, a variety of spectroscopic techniques (e.g., FTIR, XPS and solid-state NMR), chemical methods (e.g., ion exchange experiment), and some other surface and structure analytical methods (e.g., zeta potential measurement, SEM-EDX and PXRD) were employed to comprehensively elucidate the mechanisms of Pb(II) and Cd(II) biosorption by WR and MS. At last, modeling via QCS at a molecular scale was applied to further disclose the interactions between the heavy metal ions and the surface sites on the biosorbents. The comprehensive mechanistic elucidation via the hybrid methodology established in this study is described in Figure 6.27. The main findings in this chapter are summarized as follows.

(1) Spectroscopic techniques indicated that WR and MS had very complicated compositions, making the biosorbent characterization and mechanistic elucidation challenging.

(2) On both WR and MS, carboxyl, hydroxyl, amine and ether groups were involved in Pb(II) and Cd(II) sequestration via the binding force of complexation, ion exchange (with Ca^{2+} and Mg^{2+}), and electrostatic attraction. Microprecipitation on the surface of WR and MS also contributed to Pb(II) and Cd(II) removal from aqueous solutions. Among the four types of active functional groups, carboxyl groups were more preferable for Pb(II) and Cd(II) binding.

(3) Specifically, Pb(II) and Cd(II) could be bound to the negatively charged surface of WR and MS via electrostatic attraction according to the zeta

potential measurements. Pb(II) and Cd(II) also acquired binding sites through the ion exchange with naturally occurring Ca^{2+} and Mg^{2+} in the biosorbents. Besides, complexation with O and N atoms from carboxyl, hydroxyl, amine and ether groups provided a stronger force for Pb(II) and Cd(II) sequestration. In addition, a part of Pb(II) and Cd(II) ions deposited on the biosorbent surface due to microprecipitation.

(4) Solid-state NMR analysis indicated that the three main constitutes of WR, i.e., cellulose, pectin and hemicellulose, were all capable of providing binding sites to Pb(II) and Cd(II). For MS, it was found that cellulose, hemicellulose and tannins were responsible for supplying binding sites to Pb(II) and Cd(II). Additionally, significant differences were found in the compositions of MS in different particle sizes; the drastically reduced biosorption capacity of larger MS should be mainly caused by its more crystalline structure and higher content of lignin.

(5) Despite the same underlying mechanisms in Pb(II) and Cd(II) biosorption processes, the contributions of different mechanisms to Pb(II) and Cd(II) biosorption were different. For instance, microprecipitation of Pb(II) was more intense than that of Cd(II) as observed by SEM-EDX and XPS (O 1s spectra), whereas ion exchange played a more important role in Cd(II) biosorption than in Pb(II) biosorption.

(6) For developing commercial (bio)sorbents, amorphous cellulose, pectin and hemicellulose which contain carboxyl groups and other active functional groups (e.g., hydroxyl, ether and amine groups) could be promising

matrices, whereas lignin and (para)crystalline cellulose seemed not preferable.

(7) Neither spectroscopic techniques nor other analytical methods can stand alone for complete mechanistic elucidation. For example, it is not easy to identify microprecipitation through FTIR, XPS or solid-state NMR analysis, whereas SEM-EDX can give a distinct micrograph of the surface precipitates. Superior to FTIR and XPS, solid-state NMR spectroscopy can identify atoms or organic groups in different chemical environments, e.g., distinguishing carboxyl groups from pectin or hemicellulose. Yet, ^{13}C spectra give no information about O and N based functional groups. FTIR and XPS can complement information in this respect, and the latter can also examine the binding force of complexation. On the other hand, chemical methods can further disclose a biosorption process. For example, EDX spectra and XPS elemental analysis suggested the occurrence of ion exchange given the disappearance of light metal ions (e.g., K, Ca and Mg) after Pb(II) and Cd(II) biosorption in this study. The ion exchange experiment further indicated that only Mg^{2+} and Ca^{2+} bound to the binding sites on WR and MS significantly exchanged with Pb(II)/Cd(II) in solution, and the disappearance of K from the surfaces of WR and MS was due to natural dissolution. Also, the ion exchange experiment was capable of quantifying the significance of ion exchange in the Pb(II) and Cd(II) biosorption processes. Integrated investigations using different methods can achieve a more reliable conclusion. For example, the peak at 287.829 ppm in the XPS C 1s spectrum of WR and the peak at 287.941 ppm in the XPS

C 1s spectrum of MS were assigned to C=O, which could be the carbonyl group in aldehydes and ketones, or the carboxyl group in carboxylic acids and carboxylates (Moulder et al., 1992). However, the ^{13}C solid-state NMR spectra indicated the presence of cellulose, hemicellulose and pectin in WR, and cellulose, tannins and hemicellulose in MS, in which the carbonyl groups were negligible. Therefore, the C=O bonds in WR and MS were assigned to carboxyl groups.

Accordingly, the complementary techniques and methods employed in this mechanistic study presented a comprehensive and reliable elucidation of Pb(II) and Cd(II) biosorption by fruit-waste-derived biosorbents. The findings will facilitate the better process control and development of commercial (bio)sorbents.

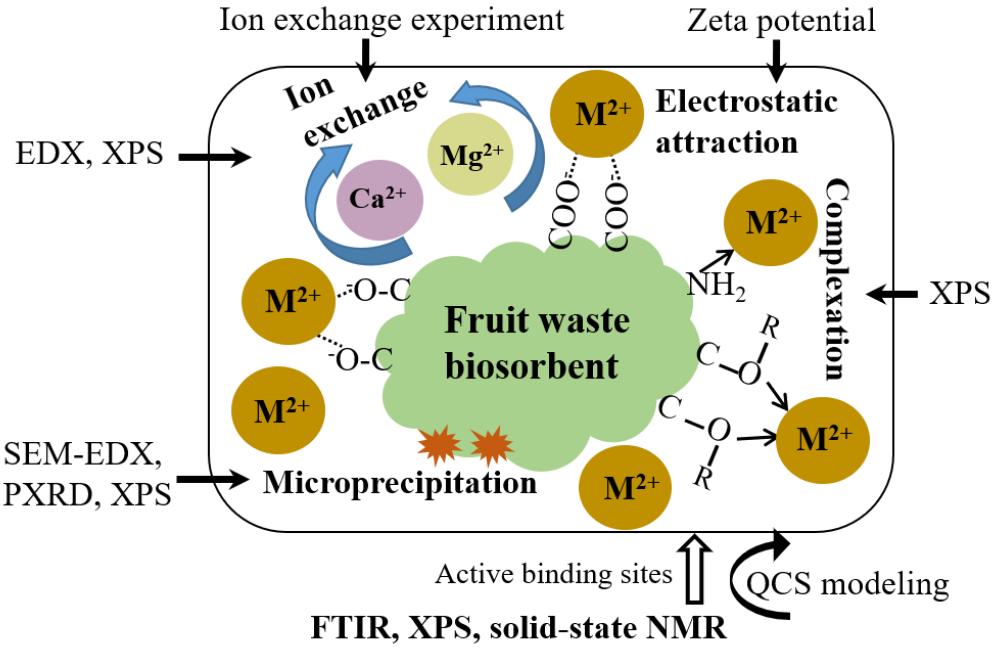

Figure 6.27 Comprehensive mechanistic elucidation of Pb(II) and Cd(II) biosorption by fruit-waste-derived biosorbents via the established methodology.

[M^{2+}: Pb^{2+}/Cd^{2+}.]

7. Conclusions and Future Perspectives

Low-cost fruit waste materials are promising biosorbents for heavy metal removal from wastewater. In this study, WR and MS exhibited highly efficient biosorption of Pb(II) and Cd(II), with much higher Pb(II) biosorption capacities and comparable Cd(II) biosorption capacities as compared with other fruit waste materials reported in the literature. Column studies indicated that the WR-packed bed column reactor maintained excellent biosorption performance on Pb(II) over 10 biosorption-desorption cycles, and the sequestered Pb(II) was rapidly eluted by 0.05 M HCl with the achievement of excellent Pb(II) recovery in concentrated solutions. Mechanistic studies revealed the involvement of carboxyl, hydroxyl, amine and ether groups from cellulose, pectin and hemicellulose in WR, and cellulose, hemicellulose and tannins in MS in Pb(II) and Cd(II) biosorption, with electrostatic attraction, complexation, ion exchange (with Ca^{2+} and Mg^{2+}), and microprecipitation as the underlying mechanisms. The modeling method, QCS, further interpreted the biosorption nature at a molecular level, verifying the feasibility of heavy metal complexation with the active functional groups and indicating the preference of heavy metal binding to carboxyl groups. It is inferred that pectin, hemicellulose and amorphous cellulose are promising matrices for developing commercial (bio)sorbents for heavy metal removal.

Findings in this study provided important insights into the potential of WR and MS for scale-up Pb(II) and Cd(II) biosorption from (waste)water, especially the practicability of Pb(II) removal/recovery by WR. Furthermore, the hybrid mechanistic methodology developed in this study not only shed light on the mechanisms of Pb(II) and Cd(II) biosorption by fruit waste materials, it should also be helpful to other relevant environmental studies as interactions between an

adsorbate and a biological surface is involved in most natural and environmental processes.

Last but not least, there are a number of blind spots in this study and further research efforts are required.

(1) This study exhaustively deciphered the active binding sites for Pb(II) and Cd(II) biosorption, as well as the biosorption mechanisms involved. However, some specifics of the interactions between Pb(II)/Cd(II) and the biosorbent surface are still ambiguous. For example, the XPS O 1s spectra identified the solid precipitates on the biosorbent surface, which were also observed by SEM, as metal oxides (PbO/CdO). It remains ambiguous what the precursors (e.g., metal hydroxides and/or metal carbonates) of the metal oxides are. Furthermore, how did the precursors convert to metal oxides?

(2) Extended X-ray absorption fine structure (EXAFS) measurement could be a useful analytical technique to further disclose the details of the complexation mechanisms in this study. It may provide crucial information about the structures of the Pb and Cd complexes (e.g., coordination number and bond length) generated in biosorption (Dithmer et al., 2016).

(3) As an advanced spectroscopic technique, solid-state NMR spectroscopy has the potential to provide more useful information about the structures of the biosorbents, their interactions with heavy metal ions, and even the dynamics of the interaction. More specialized knowledge and analytical technologies in solid-state NMR spectroscopy are required to be developed for better biomass characterization and mechanistic elucidation.

(4) To further evaluate the biosorption performance of WR and MS, real heavy-metal-bearing wastewater, e.g., electroplating effluents and landfill leachate, needs to be used.

(5) Life cycle assessment can be used to assess the environmental impact associated with all the stages of the life of WR and MS, so as to evaluate the competitiveness of fruit-waste-derived biosorbents in comparison with commercial ion-exchangers and adsorbents for pollutants removal.

Appendices

Table A1 Assignments of ^{13}C CP-MAS NMR bands of model biopolymers.

Chemical shift (ppm)	Assignment
181.58	Carboxyl-C in lignin
146.82 (154-140)	Aromatic C-O in lignin
140-100	Aromatic C in lignin
54.74	Methoxyl-C in lignin
104.57	(Para)crystalline cellulose C-1
88.23	(Para)crystalline cellulose C-4
83.39	Amorphous cellulose C-4
76-70	Cellulose C-2, 3, 5
64.72	(Para)crystalline cellulose C-6
62.04	Amorphous cellulose C-6
170.54	Carboxyl-C of acetyl group in pectin
100.01	Pectin C-1
79.35	Pectin C-2
73-68	Pectin C-3, 4, 5
52.96	Methyl ester-C in pectin

Table A2 Experimental design derived from CCD of RSM.

Run	Code values			Real values			DE_e	DE_p	Residual	Categorical factor level
	x1	x2	x3	X1	X2	X3	(%)	(%)		
1	-1	-1	-1	4	0.2	1	89.45	90.19	-0.74	Factorial points (2^k=8)
2	1	-1	-1	8	0.2	1	73.01	76.89	-3.88	
3	-1	1	-1	4	0.6	1	97.22	98.87	-1.65	
4	1	1	-1	8	0.6	1	93.64	93.56	0.08	
5	-1	-1	1	4	0.2	3	95.18	96.07	-0.89	
6	1	-1	1	8	0.2	3	91.70	90.86	0.84	
7	-1	1	1	4	0.6	3	97.06	94.00	3.06	
8	1	1	1	8	0.6	3	96.70	96.78	-0.08	
9	-1.682	0	0	2.64	0.4	2	98.86	99.12	-0.26	Star points (6)
10	1.682	0	0	9.36	0.4	2	91.70	90.27	1.43	
11	0	-1.682	0	6	0.064	2	87.56	85.16	2.40	
12	0	1.682	0	6	0.74	2	96.22	97.44	-1.22	
13	0	0	-1.682	6	0.4	0.32	90.45	87.16	3.29	
14	0	0	1.682	6	0.4	3.68	92.70	94.81	-2.11	
15	0	0	0	6	0.4	2	92.31	95.19	-2.88	Central points (6)
16	0	0	0	6	0.4	2	96.62	95.19	1.43	
17	0	0	0	6	0.4	2	95.21	95.19	0.02	
18	0	0	0	6	0.4	2	95.38	95.19	0.19	
19	0	0	0	6	0.4	2	95.77	95.19	0.58	
20	0	0	0	6	0.4	2	95.69	95.19	0.50	

(**Notes**: DE_e - Experimental desorption efficiency; DE_P - Predicted desorption efficiency.)

Table A3 ANOVA for RSM analysis.

Source	Sum of squares	df.	Mean Square	F-value	*p*-value Prob>F	
Model	523.57	9	58.17	8.98	0.0010	Significant
A-S/L	94.38	1	94.38	14.57	0.0034	
B-Acid conc.	181.92	1	181.92	28.08	0.0003	
C-Time	70.84	1	70.84	10.93	0.0079	
AB	31.92	1	31.92	4.93	0.0507	
AC	32.72	1	32.72	5.05	0.0484	
BC	57.89	1	57.89	8.93	0.0136	
A^2	0.45	1	0.45	0.070	0.7973	
B^2	27.26	1	27.26	4.21	0.0674	
C^2	31.86	1	31.86	4.92	0.0509	
Lack of Fit	53.84	5	10.77	4.91	0.0527	Not significant
Std. Dev.				2.55		
Mean				93.12		
C.V.%				2.73		
R^2				0.89		
Adj. R^2				0.79		
Pred. R^2				0.25		

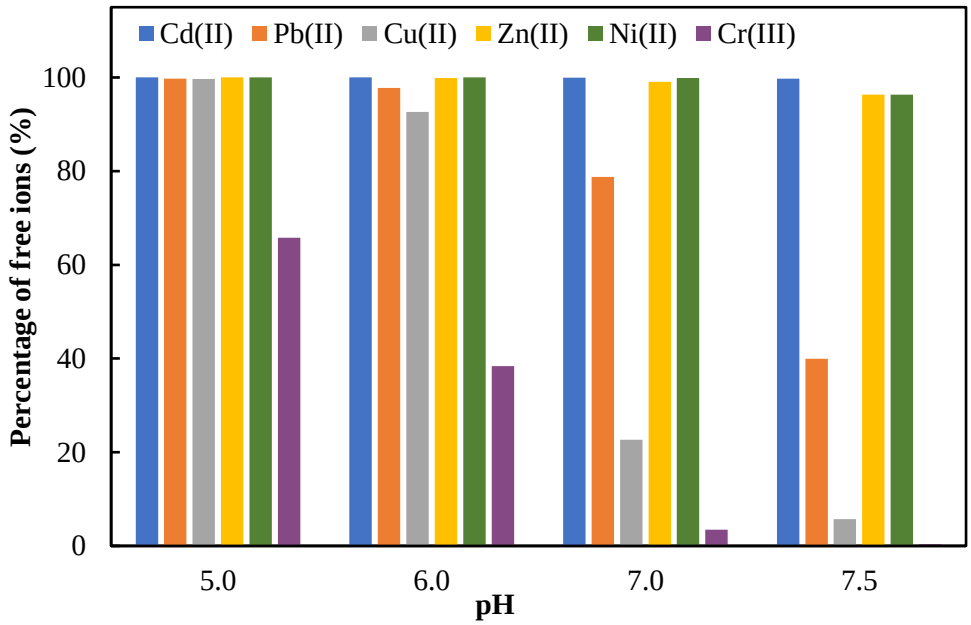

Figure A1 Speciation of heavy metal ions at different pH.

[Initial metal concentrations of 1 mM, simulated by *Visual MINTEQ* 3.1.]

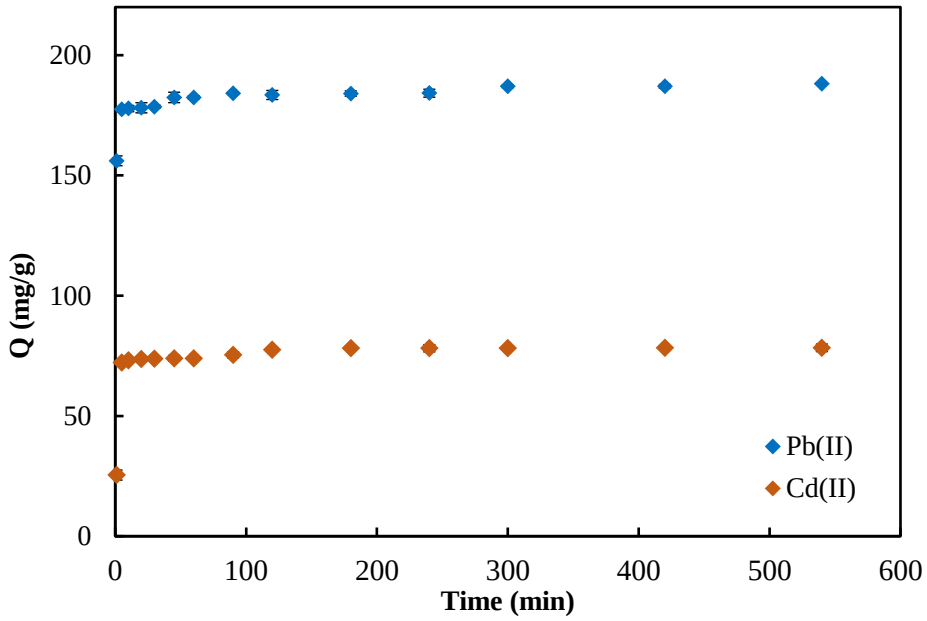

Figure A2 Kinetics of Pb(II) and Cd(II) biosorption by WR.

[Initial metal concentration of 500 ppm, pH 5.0 for Pb(II) and 7.0 for Cd(II) biosorption, 1.0 g/L WR, 250 rpm, 298 K.]

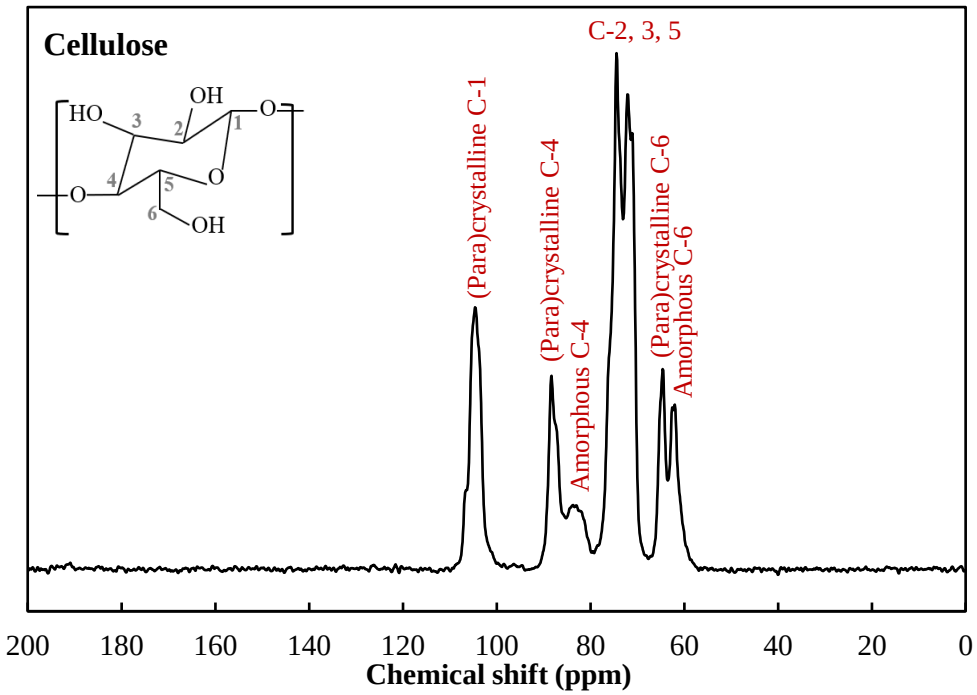

Figure A3 ^{13}C CP-MAS NMR spectrum of cellulose.

[Collected by Prof. Nielsen and Mr. Anders Bruhn Arndal Andersen of University of Southern Denmark.]

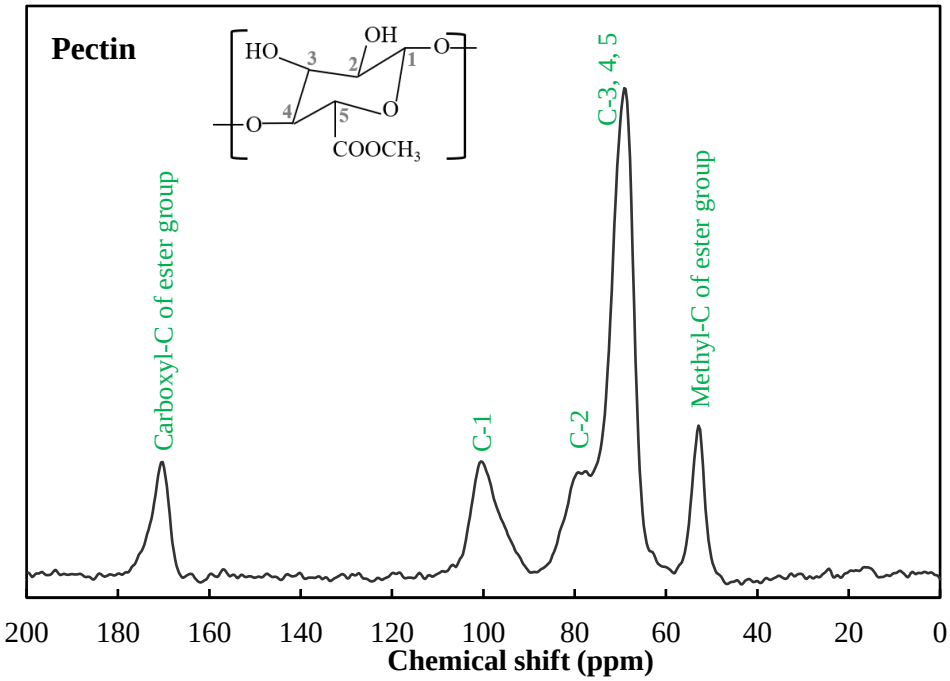

Figure A4 ^{13}C CP-MAS NMR spectrum of pectin.

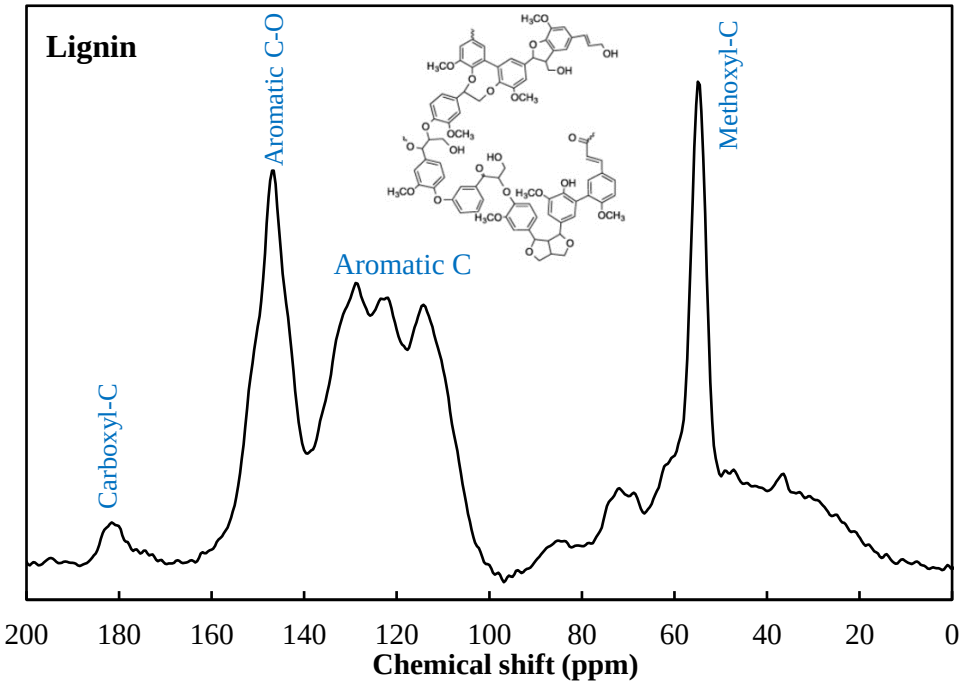

Figure A5 ^{13}C CP-MAS NMR spectrum of lignin.

[Collected by Prof. Nielsen and Mr. Anders Bruhn Arndal Andersen of University of Southern Denmark.]

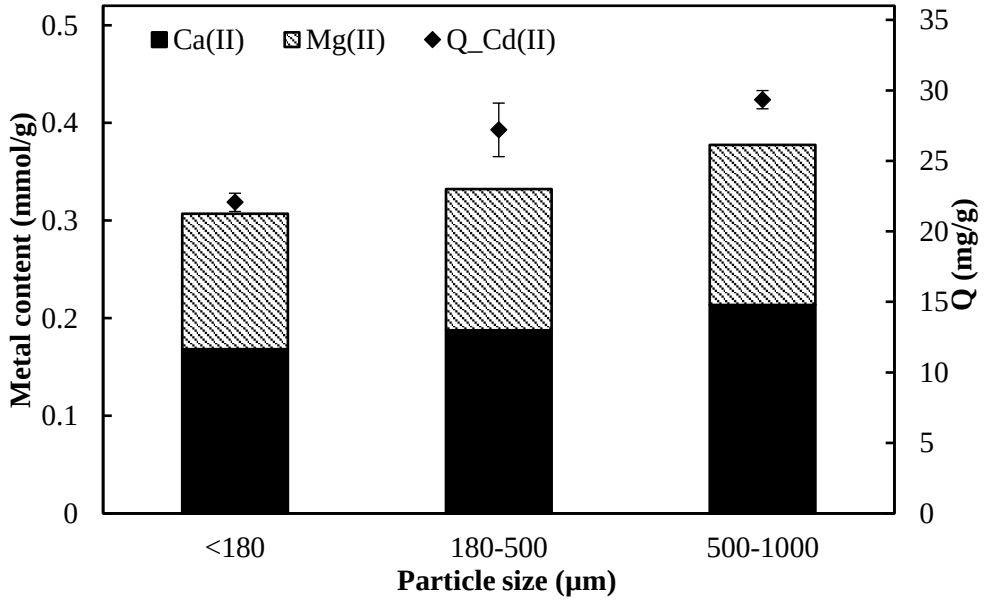

Figure A6 Cd(II) biosorption capacities and light metal ion contents of WR in different particle sizes.

[Initial Cd(II) concentration of 50 ppm, 0.5 g/L WR, pH 7.0, 1.0 g/L WR in 0.05 M HNO_3 for 24 h for the light metal ion release.]

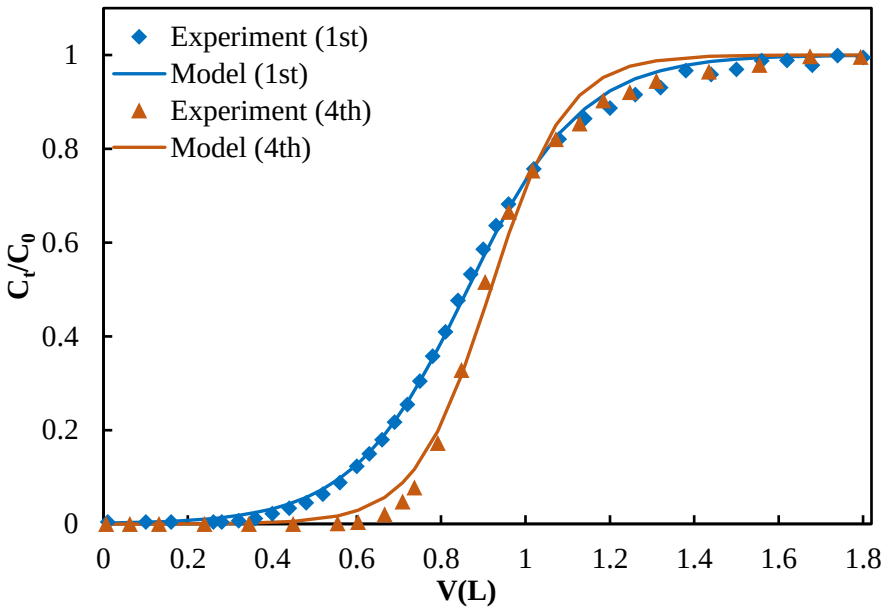

Figure A7 Simulation of the breakthrough curves of Pb(II) biosorption in the WR-packed bed column reactor by the Thomas model.

[The first and fourth cycle were selected as the representatives to avoid overlap.]

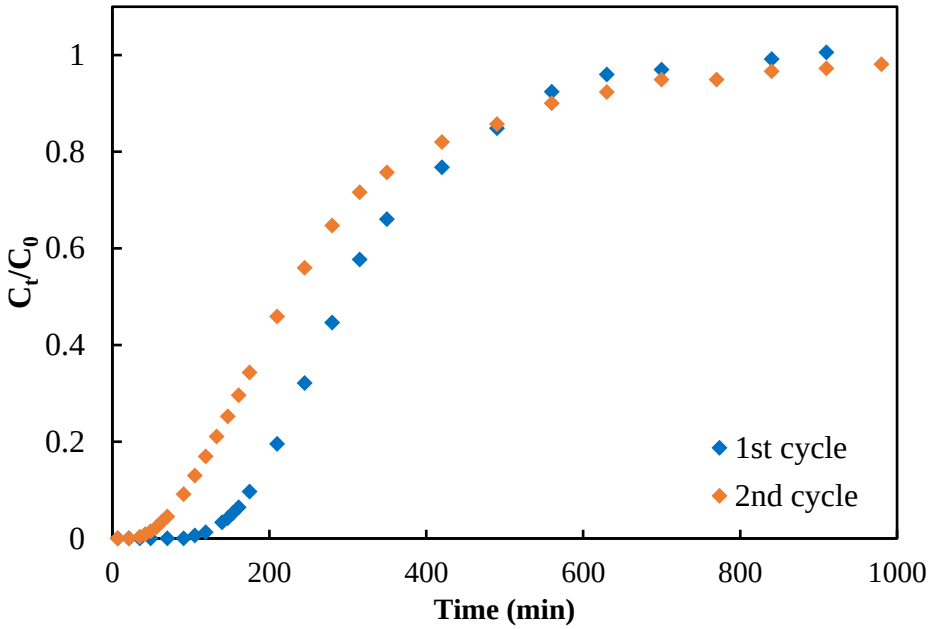

Figure A8 Breakthrough curves of Cd(II) biosorption in the WR-packed bed column reactor.

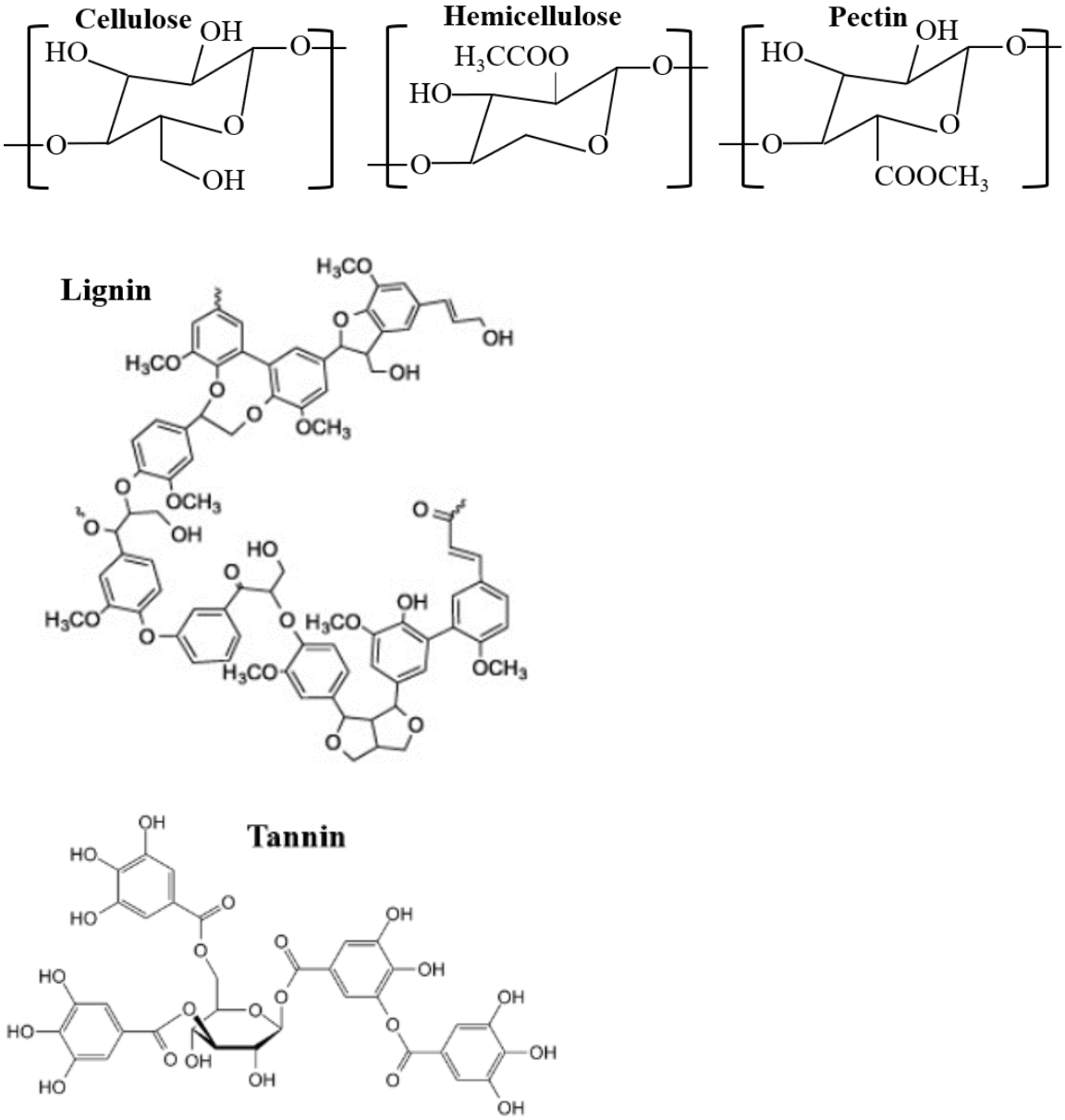

Figure A9 Structures of the main biopolymers contained in WR and MS.

[Lignin structure from (Fu et al., 2016) and tannin structure from (Sionkowska et al., 2014).]

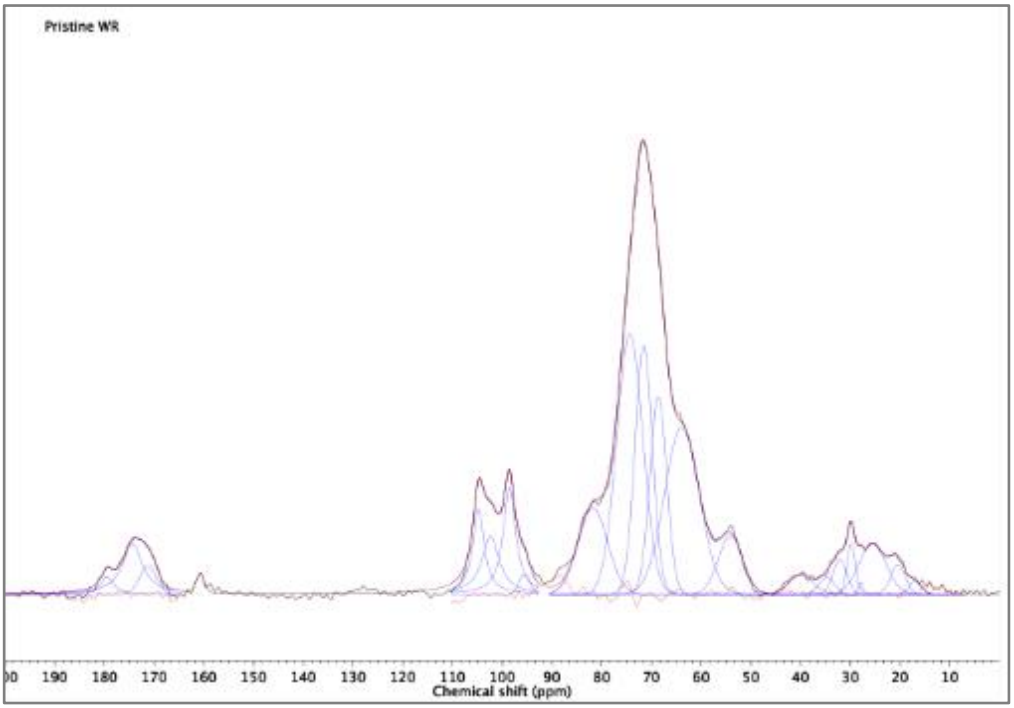

Figure A10 ^{13}C CP-MAS NMR spectrum of pristine WR with spectral deconvolution.

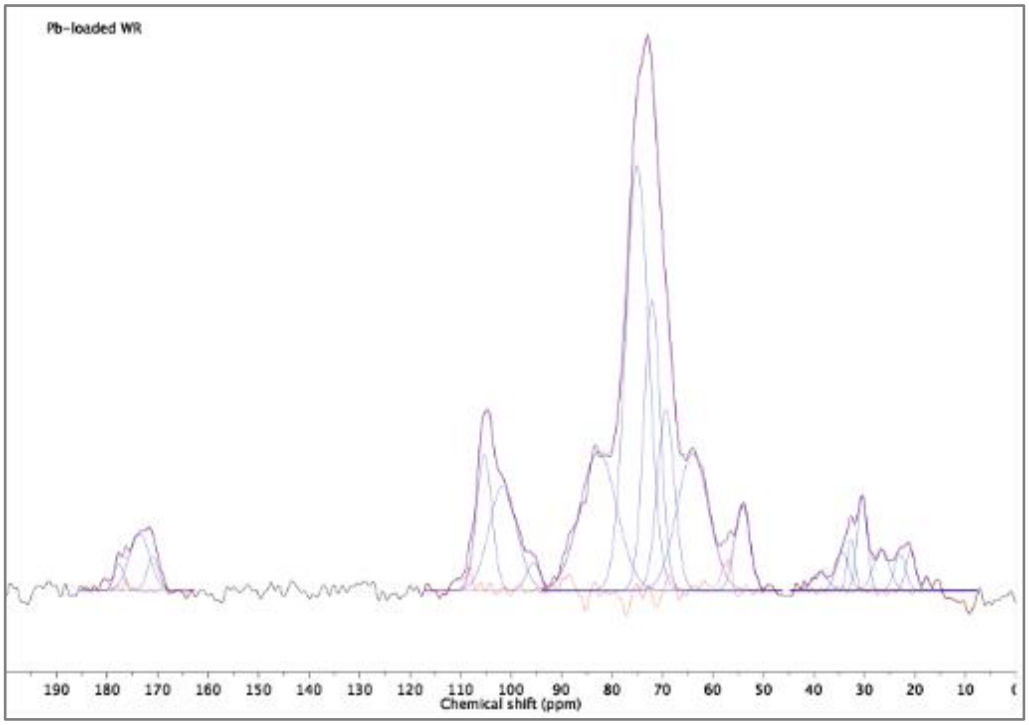

Figure A11 ^{13}C CP-MAS NMR spectrum of Pb-loaded WR with spectral deconvolution.

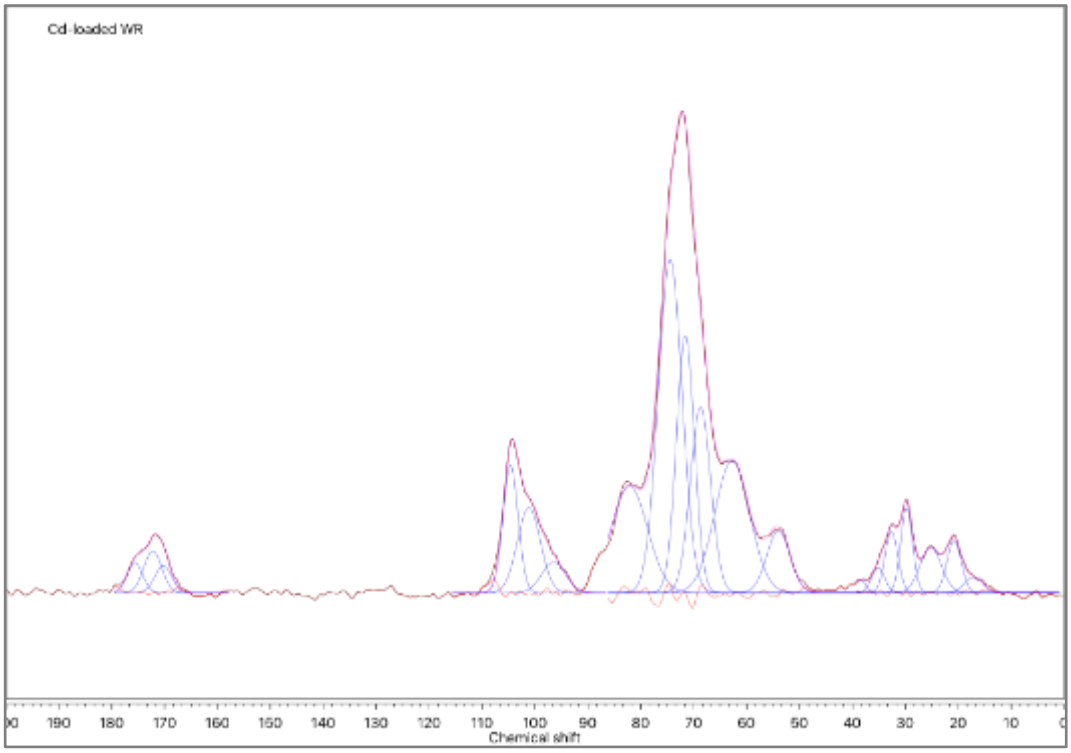

Figure A12 ^{13}C CP-MAS NMR spectrum of Cd-loaded WR with spectral deconvolution.

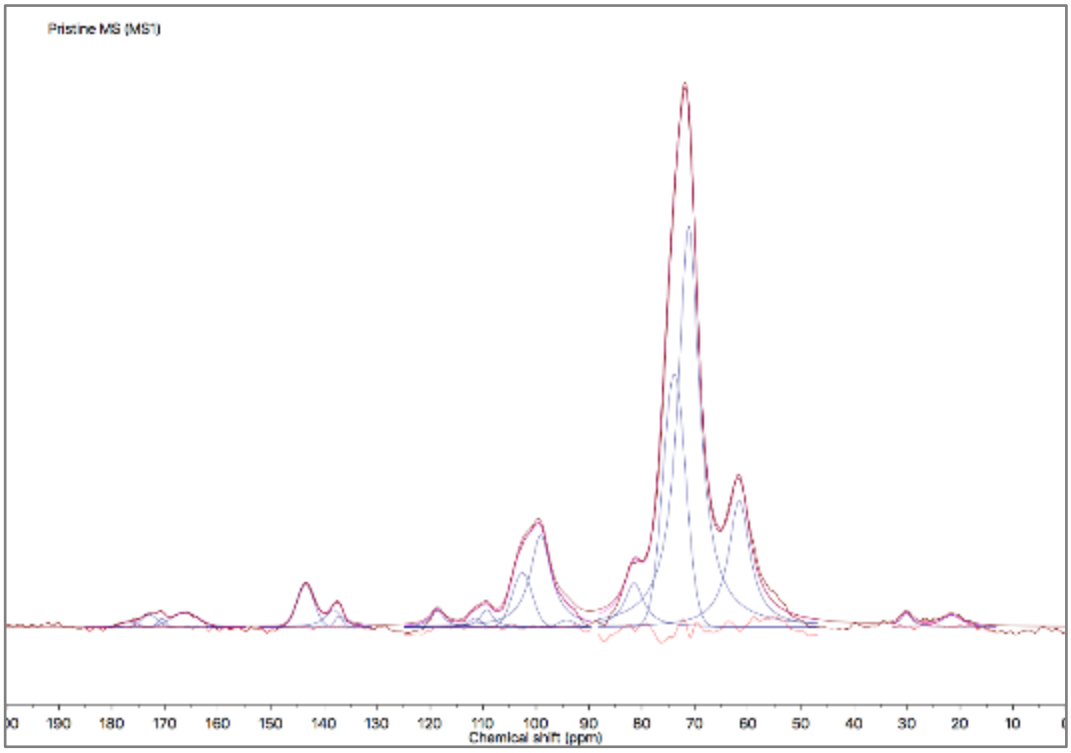

Figure A13 ^{13}C CP-MAS NMR spectrum of pristine MS (MS1) with spectral deconvolution.

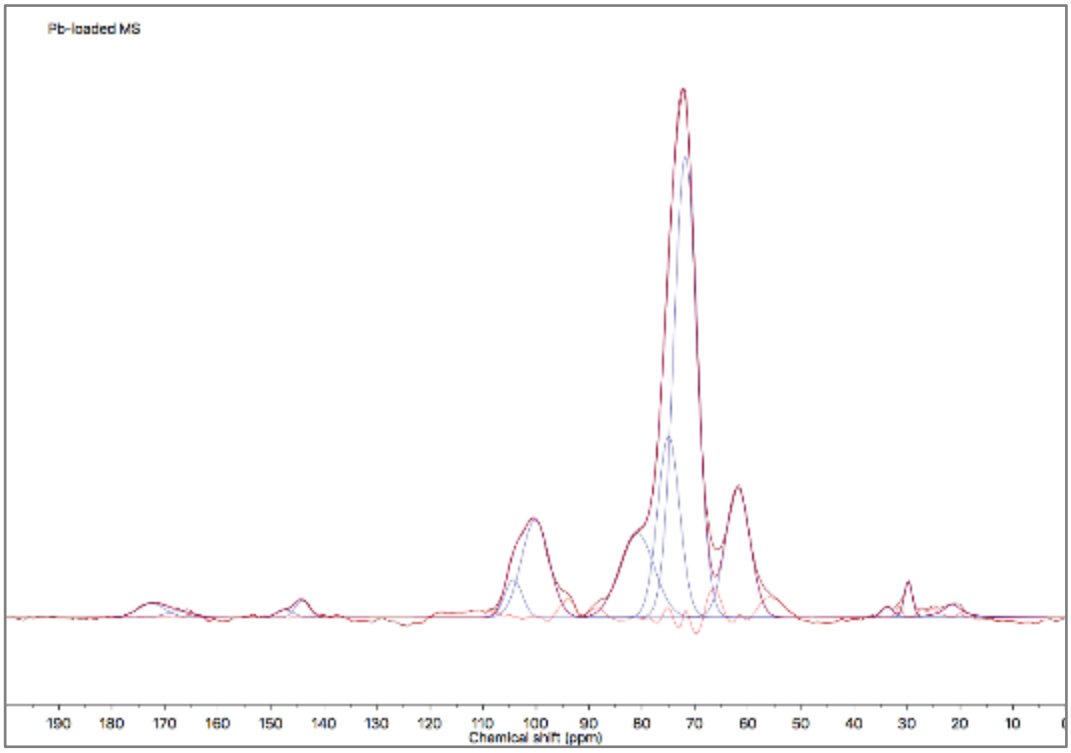

Figure A14 ^{13}C CP-MAS NMR spectrum of Pb-loaded MS with spectral deconvolution.

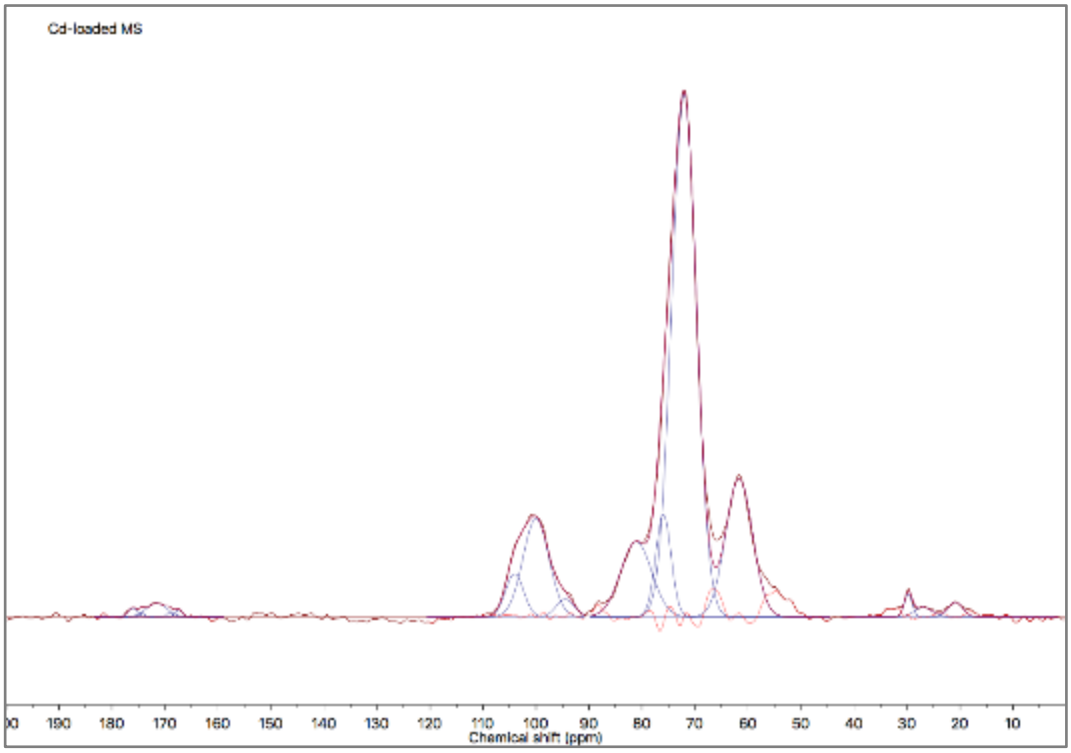

Figure A15 ^{13}C CP-MAS NMR spectrum of Cd-loaded MS with spectral deconvolution.

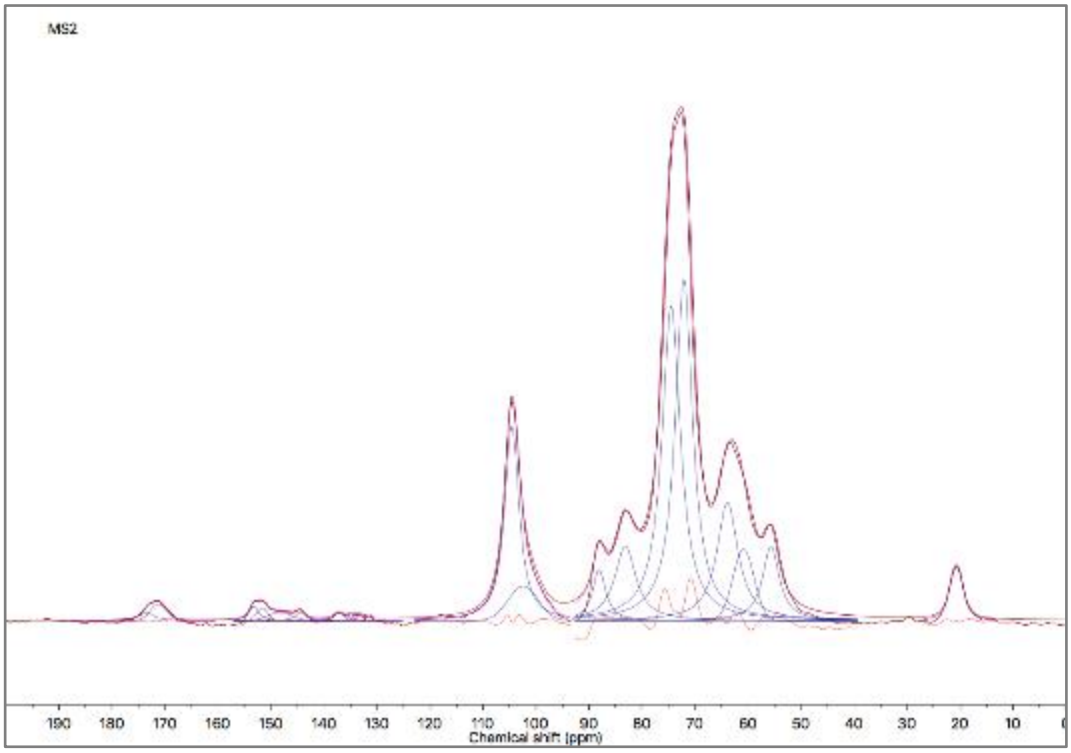

Figure A16 ^{13}C CP-MAS NMR spectrum of MS2 (180-500 µm) with spectral deconvolution.

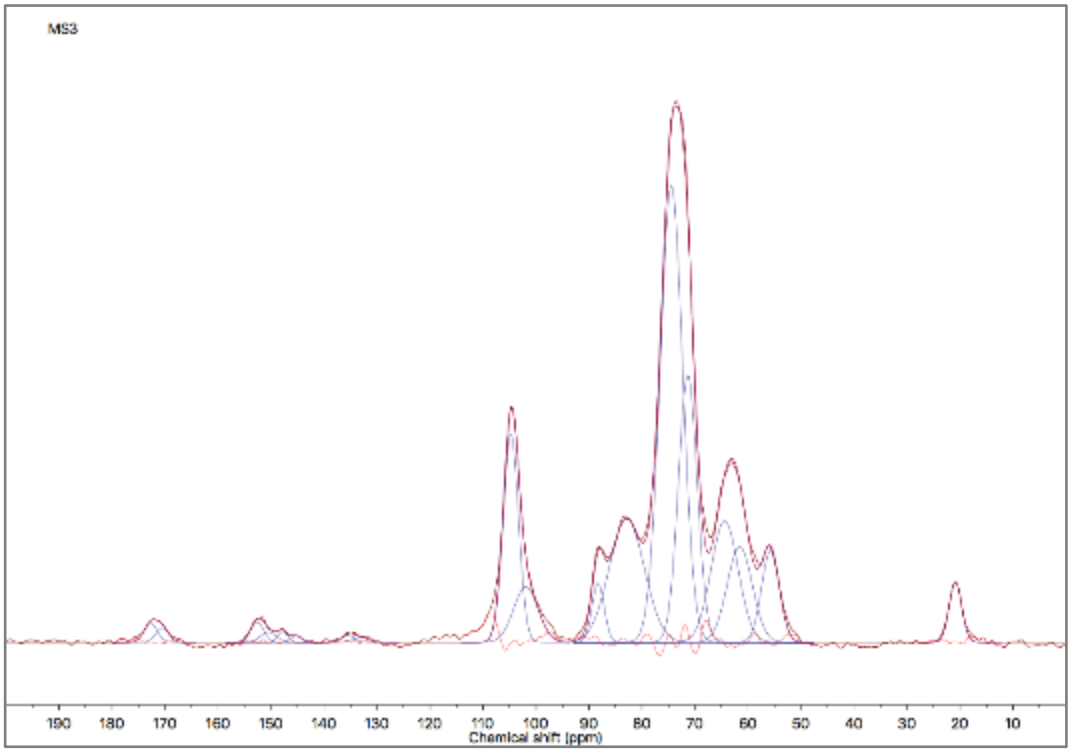

Figure A17 ^{13}C CP-MAS NMR spectrum of MS3 (500-1000 µm) with spectral deconvolution.

References

Abdolali, A., Ngo, H.H., Guo, W.S., Zhou, J.L., Du, B., Wei, Q., Wang, X.C.C. and Nguyen, P.D. (2015) Characterization of a multi-metal binding biosorbent: Chemical modification and desorption studies. Bioresource Technology 193, 477-487.

Abidin, M.A.Z., Jalil, A.A., Triwahyono, S., Adam, S.H. and Kamarudin, N.H.N. (2011) Recovery of gold(III) from an aqueous solution onto a durio zibethinus husk. Biochemical Engineering Journal 54(2), 124-131.

Abo-Farha, S.A., Abdel-Aal, A.Y., Ashour, I.A. and Garamon, S.E. (2009) Removal of some heavy metal cations by synthetic resin purolite C100. Journal of Hazardous Materials 169(1-3), 190-194.

Aharoni, C. and Sparks, D.L. (1991) Kinetics of soil chemical reactions-A theoretical treatment. Research, 1-18.

Aharoni, C. and Ungarish, M. (1977) Kinetics of activated chemisorption. Part 2-Theoretical models. Journal of the Chemical Society, Faraday Transactions 1: Physical Chemistry in Condensed Phases 73, 456-464.

Ahmad, A., Bhat, A.H. and Buang, A. (2018) Biosorption of transition metals by freely suspended and Ca-alginate immobilised with Chlorella vulgaris: Kinetic and equilibrium modeling. Journal of Cleaner Production 171, 1361-1375.

Ahmad, A., Khatoon, A., Mohd-Setapar, S.-H., Kumar, R. and Rafatullah, M. (2015) Chemically oxidized pineapple fruit peel for the biosorption of heavy metals from aqueous solutions. Desalination and Water Treatment 57(14), 1-11.

Akar, S.T., Arslan, S., Alp, T., Arslan, D. and Akar, T. (2012) Biosorption potential of the waste biomaterial obtained from Cucumis melo for the removal of Pb^{2+} ions from aqueous media: Equilibrium, kinetic, thermodynamic and mechanism analysis. Chemical Engineering Journal 185, 82-90.

Aksu, Z. and Tezer, S. (2005) Biosorption of reactive dyes on the green alga Chlorella vulgaris. Process Biochemistry 40(3-4), 1347-1361.

Albadarin, A.B., Al-Muhtaseb, A.a.H., Al-laqtah, N.A., Walker, G.M., Allen, S.J. and Ahmad, M.N.M. (2011) Biosorption of toxic chromium from aqueous phase by lignin: mechanism, effect of other metal ions and salts. Chemical Engineering Journal 169(1-3), 20-30.

Alencar, W.S., Acayanka, E., Lima, E.C., Royer, B., de Souza, F.E., Lameira, J. and Alves, C.N. (2012) Application of Mangifera indica (mango) seeds as a

biosorbent for removal of Victazol Orange 3R dye from aqueous solution and study of the biosorption mechanism. Chemical Engineering Journal 209, 577-588.

Ali, R.M., Hamad, H.A., Hussein, M.M. and Malash, G.F. (2016) Potential of using green adsorbent of heavy metal removal from aqueous solutions: Adsorption kinetics, isotherm, thermodynamic, mechanism and economic analysis. Ecological Engineering 91, 317-332.

Allen, L.C. (1989) Electronegativity is the average one-electron energy of the valence-shell electrons in ground-state free atoms. Journal of the American Chemical Society 111(25), 9003-9014.

Asgher, M. and Bhatti, H.N. (2010) Mechanistic and kinetic evaluation of biosorption of reactive azo dyes by free, immobilized and chemically treated Citrus sinensis waste biomass. Ecological Engineering 36(12), 1660-1665.

Assamoi, B. and Lawryshyn, Y. (2012) The environmental comparison of landfilling vs. incineration of MSW accounting for waste diversion. Waste Management 32(5), 1019-1030.

Ay, C.O., Ozcan, A.S., Erdogan, Y. and Ozcan, A. (2012) Characterization of Punica granatum L. peels and quantitatively determination of its biosorption behavior towards lead(II) ions and Acid Blue 40. Colloids and Surfaces B-Biointerfaces 100, 197-204.

Banerjee, K., Ramesh, S., Gandhimathi, R., Nidheesh, P. and Bharathi, K. (2012) A novel agricultural waste adsorbent, watermelon shell for the removal of copper from aqueous solutions. Iranica Journal of Energy and Environment 3(2), 143-156.

Ben-Ali, S., Jaouali, I., Souissi-Najar, S. and Ouederni, A. (2017) Characterization and adsorption capacity of raw pomegranate peel biosorbent for copper removal. Journal of Cleaner Production 142, 3809-3821.

Bhatnagar, A., Minocha, A.K., Kumar, E., Sillanpaa, M. and Jeon, B.H. (2009) Removal of phenolic pollutants from water utilizing Mangifera indica (Mango) seed waste and cement fixation. Separation Science and Technology 44(13), 3150-3169.

Bohart, G. and Adams, E. (1920) Some aspects of the behavior of charcoal with respect to chlorine. Journal of the Franklin Institute 189(5), 669.

Calero, M., Hernáinz, F., Blázquez, G., Tenorio, G. and Martín-Lara, M. (2009) Study of Cr (III) biosorption in a fixed-bed column. Journal of Hazardous Materials 171(1-3), 886-893.

Camarillo, R., Llanos, J., Garcia-Fernandez, L., Perez, A. and Canizares, P. (2010) Treatment of copper (II)-loaded aqueous nitrate solutions by polymer

enhanced ultrafiltration and electrodeposition. Separation and Purification Technology 70(3), 320-328.

Castro, R.S.D., Caetano, L., Ferreira, G., Padilha, P.M., Saeki, M.J., Zara, L.F., Martines, M.A.U. and Castro, G.R. (2011) Banana peel applied to the solid phase extraction of copper and lead from river water: Preconcentration of metal ions with a fruit waste. Industrial & Engineering Chemistry Research 50(6), 3446-3451.

Chand, P., Shil, A.K., Sharma, M. and Pakade, Y.B. (2014) Improved adsorption of cadmium ions from aqueous solution using chemically modified apple pomace: Mechanism, kinetics, and thermodynamics. International Biodeterioration & Biodegradation. 90, 8-16.

Chand, R., Narimura, K., Kawakita, H., Ohto, K., Watari, T. and Inoue, K. (2009) Grape waste as a biosorbent for removing Cr(VI) from aqueous solution. Journal of Hazardous Materials 163(1), 245-250.

Chang, J.H., Ellis, A.V., Yan, C.T. and Tung, C.H. (2009a) The electrochemical phenomena and kinetics of EDTA-copper wastewater reclamation by electrodeposition and ultrasound. Separation and Purification Technology 68(2), 216-221.

Chang, Q. and Wang, G. (2007) Study on the macromolecular coagulant PEX which traps heavy metals. Chemical Engineering Science 62(17), 4636-4643.

Chang, Q., Zhang, M. and Wang, J.X. (2009b) Removal of Cu^{2+} and turbidity from wastewater by mercaptoacetyl chitosan. Journal of Hazardous Materials 169(1-3), 621-625.

Chao, H.P. and Chang, C.C. (2012) Adsorption of copper(II), cadmium(II), nickel(II) and lead(II) from aqueous solution using biosorbents. Adsorption-Journal of the International Adsorption Society 18(5-6), 395-401.

Chao, H.P., Chang, C.C. and Nieva, A. (2014) Biosorption of heavy metals on Citrus maxima peel, passion fruit shell, and sugarcane bagasse in a fixed-bed column. Journal of Industrial and Engineering Chemistry 20(5), 3408-3414.

Charerntanyarak, L. (1999) Heavy metals removal by chemical coagulation and precipitation. Water Science and Technology 39(10-11), 135-138.

Chatterjee, A. and Schiewer, S. (2011) Biosorption of cadmium(II) ions by citrus peels in a packed bed column: Effect of process parameters and comparison of different breakthrough curve models. Clean-Soil Air Water 39(9), 874-881.

Chaudhari, S.A. and Singhal, R.S. (2015) Cutin from watermelon peels: A novel inducer for cutinase production and its physicochemical characterization. International Journal of Biological Macromolecules 79, 398-404.

Chen, J.P. and Yang, L. (2006) Study of a heavy metal biosorption onto raw and chemically modified Sargassum sp via spectroscopic and modeling analysis. Langmuir 22(21), 8906-8914.

Chen, Q.Y., Luo, Z., Hills, C., Xue, G. and Tyrer, M. (2009) Precipitation of heavy metals from wastewater using simulated flue gas: Sequent additions of fly ash, lime and carbon dioxide. Water Research 43(10), 2605-2614.

Cheng, H.F. and Hu, Y.A. (2010) Lead (Pb) isotopic fingerprinting and its applications in lead pollution studies in China: A review. Environmental Pollution 158(5), 1134-1146.

Choinska-Pulit, A., Sobolczyk-Bednarek, J. and Laba, W. (2018) Optimization of copper, lead and cadmium biosorption onto newly isolated bacterium using a Box-Behnken design. Ecotoxicology and Environmental Safety 149, 275-283.

Chong, K. and Volesky, B. (1996) Metal biosorption equilibria in a ternary system. Biotechnology and Bioengineering 49(6), 629-638.

Cid, H.A., Flores, M.I., Pizarro, J.F., Castillo, X.A., Barros, D.E., Moreno-Pirajan, J.C. and Ortiz, C.A. (2018) Mechanisms of Cu^{2+} biosorption on Lessonia nigrescens dead biomass: Functional groups interactions and morphological characterization. Journal of Environmental Chemical Engineering 6(2), 2696-2704.

Dalal, R. (1974) Desorption of soil phosphate by anion - exchange resin. Communications in Soil Science & Plant Analysis 5(6), 531-538.

Davidovich, R.L., Stavila, V., Marinin, D.V., Voit, E.I. and Whitmire, K.H. (2009) Stereochemistry of lead(II) complexes with oxygen donor ligands. Coordination Chemistry Reviews 253(9-10), 1316-1352.

Deniz, F. and Karabulut, A. (2017) Biosorption of heavy metal ions by chemically modified biomass of coastal seaweed community: Studies on phycoremediation system modeling and design. Ecological Engineering 106, 101-108.

Desai, K.M., Survase, S.A., Saudagar, P.S., Lele, S.S. and Singhal, R.S. (2008) Comparison of artificial neural network (ANN) and response surface methodology (RSM) in fermentation media optimization: Case study of fermentative production of scleroglucan. Biochemical Engineering Journal 41(3), 266-273.

Dias, J.M., Alvim-Ferraz, M.C.M., Almeida, M.F., Rivera-Utrilla, J. and Sanchez-Polo, M. (2007) Waste materials for activated carbon preparation and its use in aqueous-phase treatment: A review. Journal of Environmental Management 85(4), 833-846.

Dick-Perez, M., Zhang, Y.A., Hayes, J., Salazar, A., Zabotina, O.A. and Hong, M. (2011) Structure and interactions of plant cell-wall polysaccharides by two- and three-dimensional magic-angle-spinning solid-state NMR. Biochemistry 50(6), 989-1000.

Dithmer, L., Lipton, A. S., Reitzel, K., Warner, T. E., Lundberg, D. and Nielsen, U. G. (2015) Characterization of phosphate sequestration by a lanthanum modified bentonite clay: a solid-state NMR, EXAFS, and PXRD study. Environmental Science and Technology 49(7), 4559-4566.

Duan, J.C., Lu, Q., Chen, R.W., Duan, Y.Q., Wang, L.F., Gao, L. and Pan, S.Y. (2010) Synthesis of a novel flocculant on the basis of crosslinked Konjac glucomannan-graft-polyacrylamide-co-sodium xanthate and its application in removal of Cu^{2+} ion. Carbohydrate Polymers 80(2), 436-441.

Dubinin, M.M. and Radushkevich, L.V. (1947) Equation of the characteristic curve of activated charcoal. Proceedings of the Academy of Sciences of the USSR, Physical Chemistry Section 55, 331-333.

FAOSTAT (2016) Food and agricultural commodities production, Food and Agricultural Organization of United Nations: Economic and Social Department: The Statistical Division.

Farinella, N.V., Matos, G.D. and Arruda, M.A.Z. (2007) Grape bagasse as a potential biosorbent of metals in effluent treatments. Bioresource Technology 98(10), 1940-1946.

Farinella, N.V., Matos, G.D., Lehmann, E.L. and Arruda, M.A.Z. (2008) Grape bagasse as an alternative natural adsorbent of cadmium and lead for effluent treatment. Journal of Hazardous Materials 154(1-3), 1007-1012.

Feng, N., Guo, X., Liang, S., Zhu, Y. and Liu, J. (2011) Biosorption of heavy metals from aqueous solutions by chemically modified orange peel. Journal of Hazardous Materials 185(1), 49-54.

Focher, B., Palma, M.T., Canetti, M., Torri, G., Cosentino, C. and Gastaldi, G. (2001) Structural differences between non-wood plant celluloses: evidence from solid state NMR, vibrational spectroscopy and X-ray diffractometry. Industrial Crops & Products 13(3), 193-208.

Fomina, M. and Gadd, G.M. (2014) Biosorption: Current perspectives on concept, definition and application. Bioresource Technology 160, 3-14.

Fontana, I.B., Peterson, M. and Cechinel, M.A.P. (2018) Application of brewing waste as biosorbent for the removal of metallic ions present in groundwater and surface waters from coal regions. Journal of Environmental Chemical Engineering.

Franca, A.S., Oliveira, L.S., Saldanha, S.A., Santos, P.I.A. and Salum, S.S. (2010) Malachite green adsorption by mango (Mangifera indica L.) seed husks: Kinetic, equilibrium and thermodynamic studies. Desalination and Water Treatment 19(1-3), 241-248.

Freitas, J.C.C., Bonagamba, T.J. and Emmerich, F.G. (2001) Investigation of biomass- and polymer-based carbon materials using ^{13}C high-resolution solid-state NMR. Carbon 39(4), 535-545.

Freundlich, H. (1906) Over the adsorption in solution. The Journal of Physical Chemistry 57(385), e470.

Friis, N. and Myerskeith, P. (1986) Biosorption of uranium and lead by streptomyces longwoodensis. Biotechnology and Bioengineering 28(1), 21-28.

Frisch, M.J., Trucks, G. W., Schlegel, H. B., Scuseria, G. E., Robb, M. A., Cheeseman, J. R., Scalmani, G., Barone,V., Mennucci, B., Petersson, G. A., Nakatsuji, H., Caricato, M., Li, X., Hratchian, H. P., Izmaylov, A. F., Bloino, J., Zheng, G., Sonnenberg, J. L., Hada, M., Ehara, M., Toyota, K., Fukuda, R., Hasegawa, J., Ishida, M., Nakajima, T., Honda, Y., Kitao, O., Nakai, H., Vreven, T., Montgomery Jr, J. A., Peralta, J. E., Ogliaro, F., Bearpark, M., Heyd, J. J., Brothers, E., Kudin, K. N., Staroverov, V. N., Keith, T., Kobayashi, R., Normand, J., Raghavachari, K., Rendell, A., Burant, J. C.,Iyengar, S. S., Tomasi, J., Cossi, M., Rega, N., Millam, J. M., Klene, M., Knox, J. E., Cross, J. B., Bakken, V., Adamo, C., Jaramillo, J., Gomperts, R., Stratmann, R. E., Yazyev, O., Austin, A. J., Cammi, R., Pomelli, C., Ochterski, J. W., Martin, R. L., Morokuma, K., Zakrzewski, V. G., Voth, G. A., Salvador, P., Dannenberg, J. J., Dapprich, S., Daniels, A. D., Farkas,O., Foresman, J. B., Ortiz, J. V., Cioslowski, J. and Fox, D. J. (2009) Gaussian 09, Revision D.01.

Fu, F. and Wang, Q. (2011) Removal of heavy metal ions from wastewaters: A review. Journal of Environmental Management 92(3), 407-418.

Fu, L., McCallum, S., Miao, J.J., Hart, C., Tudryn, G., Zhang, F.M. and Linhardt, R. (2016) Rapid and accurate determination of the lignin content of lignocellulosic biomass by solid-state NMR. Fuel 141, 39-45.

Gamble, G.R., Akin, D.E., Makkar, H.P.S. and Becker, K. (1996) Biological degradation of tannins in sericea lespedeza (Lespedeza cuneta) by the white rot fungi Ceriporiopsis subvermispora and Cyathus stercoreus analyzed by solid-state C-13 nuclear magnetic resonance spectroscopy. Applied and Environmental Microbiology 62(10), 3600-3604.

Gao, X.P., Zhang, Y. and Zhao, Y.M. (2017) Biosorption and reduction of Au (III) to gold nanoparticles by thiourea modified alginate. Carbohydrate Polymers 159, 108-115.

Gerola, G.P., Boas, N.V., Caetano, J., Tarley, C.R.T., Goncalves, A.C. and Dragunski, D.C. (2013) Utilization of passion fruit skin by-product as lead(II) ion biosorbent. Water Air and Soil Pollution 224(2).

Girardi, F., Hackbarth, F.V., de Souza, S., de Souza, A.A.U., Boaventura, R.A.R. and Vilar, V.J.P. (2014) Marine macroalgae Pelvetia canaliculata (Linnaeus) as natural cation exchanger for metal ions separation: A case study on copper and zinc ions removal. Chemical Engineering Journal 247, 320-329.

Goel, J., Kadirvelu, K., Rajagopal, C. and Garg, V.K. (2005) Removal of lead(II) by adsorption using treated granular activated carbon: Batch and column studies. Journal of Hazardous Materials 125(1-3), 211-220.

Goldstein, J.I., Newbury, D.E., Michael, J.R., Ritchie, N.W., Scott, J.H.J. and Joy, D.C. (2017) Scanning Electron Microscopy and X-ray Microanalysis. New York: Springer New York.

Gonzalez-Munoz, M.J., Rodriguez, M.A., Luque, S. and Alvarez, J.R. (2006) Recovery of heavy metals from metal industry waste waters by chemical precipitation and nanofiltration. Desalination 200(1-3), 742-744.

Greene, K.L. and Tonjes, D.J. (2014) Quantitative assessments of municipal waste management systems: Using different indicators to compare and rank programs in New York State. Waste Management 34(4), 825-836.

Griffiths, P.R. and De Haseth, J.A. (2006) Fourier Transform Infrared Spectrometry. Second Edition. New York: John Wiley & Sons.

Gunay, A., Arslankaya, E. and Tosun, I. (2007) Lead removal from aqueous solution by natural and pretreated clinoptilolite: Adsorption equilibrium and kinetics. Journal of Hazardous Materials 146(1-2), 362-371.

Gupta, V.K. and Rastogi, A. (2008) Biosorption of lead from aqueous solutions by green algae Spirogyra species: Kinetics and equilibrium studies. Journal of Hazardous Materials 152(1), 407-414.

Gupta, V.K. and Rastogi, A. (2009) Biosorption of hexavalent chromium by raw and acid-treated green alga Oedogonium hatei from aqueous solutions. Journal of Hazardous Materials 163(1), 396-402.

Habets, S., de Wild, P.J., Huijgen, W.J.J. and van Eck, E.R.H. (2013) The influence of thermochemical treatments on the lignocellulosic structure of wheat straw as studied by natural abundance ^{13}C NMR. Bioresource Technology 146, 585-590.

Hackbarth, F.V., Girardi, F., Santos, J.C., de Souza, A.A.U., Boaventura, R.A.R., de Souza, S. and Vilar, V.J.P. (2015) Ion-exchange breakthrough curves for single and multi-metal systems using marine macroalgae Pelvetia canaliculata as a natural cation exchanger. Chemical Engineering Journal 269, 359-370.

He, J. and Chen, J.P. (2014) A comprehensive review on biosorption of heavy metals by algal biomass: Materials, performances, chemistry, and modeling simulation tools. Bioresource Technology 160, 67-78.

Heidmann, I. and Calmano, W. (2008) Removal of Zn(II), Cu(II), Ni(II), Ag(I) and Cr(VI) present in aqueous solutions by aluminium electrocoagulation. Journal of Hazardous Materials 152(3), 934-941.

Henrique, M.A., Silverio, H.A., Neto, W.P.F. and Pasquini, D. (2013) Valorization of an agro-industrial waste, mango characterization of its cellulose nanocrystals. Journal of Environmental Management 121, 202-209.

HK, G. (2015) Report of the task force on investigation of excessive lead content in drinking water, Hong Kong SAR Government.

Ho, Y., Porter, J. and McKay, G. (2002) Equilibrium isotherm studies for the sorption of divalent metal ions onto peat: copper, nickel and lead single component systems. Water, Air, and Soil Pollution 141(1-4), 1-33.

Ho, Y.S. (2006) Isotherms for the sorption of lead onto peat: Comparison of linear and non-linear methods. Polish Journal of Environmental Studies 15(1), 81-86.

Ho, Y.S., Chiu, W.T. and Wang, C.C. (2005) Regression analysis for the sorption isotherms of basic dyes on sugarcane dust. Bioresource Technology 96(11), 1285-1291.

Ho, Y.S. and McKay, G. (1999) Pseudo-second order model for sorption processes. Process biochemistry 34(5), 451-465.

Ho, Y.S. and McKay, G. (2002) Application of kinetic models to the sorption of copper(II) on to peat. Adsorption Science & Technology 20(8), 797-815.

Hui, K.S., Chao, C.Y.H. and Kot, S.C. (2005) Removal of mixed heavy metal ions in wastewater by zeolite 4A and residual products from recycled coal fly ash. Journal of Hazardous Materials 127(1-3), 89-101.

Iqbal, M., Saeed, A. and Zafar, S.I. (2009a) FTIR spectrophotometry, kinetics and adsorption isotherms modeling, ion exchange, and EDX analysis for understanding the mechanism of Cd^{2+} and Pb^{2+} removal by mango peel waste. Journal of Hazardous Materials 164(1), 161-171.

Iqbal, M., Schiewer, S. and Cameron, R. (2009b) Mechanistic elucidation and evaluation of biosorption of metal ions by grapefruit peel using FTIR spectroscopy, kinetics and isotherms modeling, cations displacement and EDX analysis. Journal of Chemical Technology and Biotechnology 84(10), 1516-1526.

Isaac, C.P.J. and Sivakumar, A. (2013) Removal of lead and cadmium ions from water using Annona squamosa shell: Kinetic and equilibrium studies. Desalination and Water Treatment 51(40-42), 7700-7709.

Jacques, R.A., Lima, E.C., Dias, S.L.R., Mazzocato, A.C. and Pavan, F.A. (2007) Yellow passion-fruit shell as biosorbent to remove Cr(III) and Pb(II) from aqueous solution. Separation and Purification Technology 57(1), 193-198.

Jalil, A.A., Triwahyono, S., Yaakob, M.R., Azmi, Z.Z.A., Sapawe, N., Kamarudin, N.H.N., Setiabudi, H.D., Jaafar, N.F., Sidik, S.M., Adam, S.H. and Hameed, B.H. (2012) Utilization of bivalve shell-treated Zea mays L. (maize) husk leaf as a low-cost biosorbent for enhanced adsorption of malachite green. Bioresource Technology 120, 218-224.

Järup, L. (2003) Hazards of heavy metal contamination. British medical bulletin 68(1), 167-182.

Jarvis, M.C. and Apperley, D.C. (1990) Direct observation of cell-wall structure in living plant-tissues by solid-state C-13 NMR spectroscopy. Plant Physiology 92(1), 61-65.

Jenkins, R. and Snyder, R.L. (1996) Introduction to X-ray Powder Diffractometry (Volume 138), Wiley Online Library.

Jin, L. and Bai, R.B. (2002) Mechanisms of lead adsorption on chitosan/PVA hydrogel beads. Langmuir 18(25), 9765-9770.

Jin, Y., Teng, C.Y., Yu, S.M., Song, T., Dong, L.Y., Liang, J.S., Bai, X., Liu, X.S., Hu, X.J. and Qu, J.J. (2018) Batch and fixed-bed biosorption of Cd(II) from aqueous solution using immobilized Pleurotus ostreatus spent substrate. Chemosphere 191, 799-808.

Jing, Y.D., He, Z.L. and Yang, X.E. (2007) Effects of pH, organic acids, and competitive cations on mercury desorption in soils. Chemosphere 69(10), 1662-1669.

Jossens, L., Prausnitz, J.M., Fritz, W., Schlunder, E.U. and Myers, A.L. (1978) Thermodynamics of multi-solute adsorption from dilute aqueous-solutions. Chemical Engineering Science 33(8), 1097-1106.

Jusoh, A., Shiung, L.S., Ali, N. and Noor, M. (2007) A simulation study of the removal efficiency of granular activated carbon on cadmium and lead. Desalination 206(1-3), 9-16.

Kalmykova, Y., Stromvall, A.M. and Steenari, B.M. (2008) Adsorption of Cd, Cu, Ni, Pb and Zn on Sphagnum peat from solutions with low metal concentrations. Journal of Hazardous Materials 152(2), 885-891.

Kamala, C.T., Chu, K.H., Chary, N.S., Pandey, P.K., Ramesh, S.L., Sastry, A.R.K. and Sekhar, K.C. (2005) Removal of arsenic(III) from aqueous solutions using fresh and immobilized plant biomass. Water Research 39(13), 2815-2826.

Kang, K.C., Kim, S.S., Choi, J.W. and Kwon, S.H. (2008) Sorption of Cu2+ and Cd^{2+} onto acid- and base-pretreated granular activated carbon and activated carbon fiber samples. Journal of Industrial and Engineering Chemistry 14(1), 131-135.

Keenan, M.H., Belton, P.S., Matthew, J.A. and Howson, S.J. (1985) A 13C-nmr study of sugar-beet pectin. Carbohydrate Research 138(1), 168-170.

Khambhaty, Y., Mody, K., Basha, S. and Jha, B. (2009) Kinetics, equilibrium and thermodynamic studies on biosorption of hexavalent chromium by dead fungal biomass of marine Aspergillus niger. Chemical Engineering Journal 145(3), 489-495.

Khan, S., Shahnaz, M., Jehan, N., Rehman, S., Shah, M.T. and Din, I. (2013) Drinking water quality and human health risk in Charsadda district, Pakistan. Journal of Cleaner Production 60, 93-101.

Khani, M.H., Keshtkar, A.R., Ghannadi, M. and Pahlavanzadeh, H. (2008) Equilibrium, kinetic and thermodynamic study of the biosorption of uranium onto Cystoseria indica algae. Journal of Hazardous Materials 150(3), 612-618.

Khaskheli, M.I., Memon, S.Q., Siyal, A.N. and Khuhawar, M.Y. (2011) Use of orange peel waste for arsenic remediation of drinking water. Waste and Biomass Valorization 2(4), 423-433.

Khormaei, M., Nasernejad, B., Edrisi, M. and Eslamzadeh, T. (2007) Copper biosorption from aqueous solutions by sour orange residue. Journal of Hazardous Materials 149(2), 269-274.

Koduru, J.R., Chang, Y.Y., Yang, J.K. and Kim, I.S. (2013) Iron oxide impregnated Morus alba L. fruit peel for biosorption of Co(II): Biosorption properties and mechanism. The Scientific World Journal 2013, 1-14.

Komatsu, T. and Kikuchi, J. (2013) Comprehensive signal assignment of ^{13}C-labeled lignocellulose using multidimensional solution NMR and ^{13}C chemical shift comparison with solid-state NMR. Analytical chemistry 85(18), 8857-8865.

Komatsu, T., Kobayashi, T., Hatanaka, M. and Kikuchi, J. (2015) Profiling planktonic biomass using element-specific, multicomponent nuclear

magnetic resonance spectroscopy. Environmental Science & Technology 49(11), 7056-7062.

Kousi, P., Rernoudaki, E., Hatzkoseyian, A. and Tsezos, M. (2007) A study of the operating parameters of a sulphate-reducing fixed-bed reactor for the treatment of metal-bearing wastewater. Advanced Materials Research 20-21, 230-234.

Kovács, A., Nemcsok, D.S. and Kocsis, T. (2010) Bonding interactions in EDTA complexes. Journal of Molecular Structure: THEOCHEM 950(1), 93-97.

Krika, F., Azzouz, N. and Ncibi, M.C. (2016) Adsorptive removal of cadmium from aqueous solution by cork biomass: Equilibrium, dynamic and thermodynamic studies. Arabian Journal of Chemistry 9, S1077-S1083.

Krishnapriya, K.R. and Kandaswamy, M. (2010) A new chitosan biopolymer derivative as metal-complexing agent: synthesis, characterization, and metal(II) ion adsorption studies. Carbohydrate Research 345(14), 2013-2022.

Kumar, K.V. (2007) Optimum sorption isotherm by linear and non-linear methods for malachite green onto lemon peel. Dyes and Pigments 74(3), 595-597.

Kurniawan, T.A., Chan, G.Y.S., Lo, W.H. and Babel, S. (2006a) Comparisons of low-cost adsorbents for treating wastewaters laden with heavy metals. Science of the Total Environment 366(2-3), 409-426.

Kurniawan, T.A., Chan, G.Y.S., Lo, W.H. and Babel, S. (2006b) Physico-chemical treatment techniques for wastewater laden with heavy metals. Chemical Engineering Journal 118(1-2), 83-98.

Kuyucak, N. and Volesky, B. (1989) The mechanism of cobalt biosorption. Biotechnology and bioengineering 33(7), 823-831.

Lagergren, S. (1898) About the theory of so-called adsorption of soluble substances. Kungliga Svenska Vetenskapsakademiens Handlingar 24(4), 1-39.

Lakshmipathy, R. and Sarada, N.C. (2013) Application of watermelon rind as sorbent for removal of nickel and cobalt from aqueous solution. International Journal of Mineral Processing 122, 63-65.

Lakshmipathy, R. and Sarada, N.C. (2016) Metal ion free watermelon (Citrullus lanatus) rind as adsorbent for the removal of lead and copper ions from aqueous solution. Desalination and Water Treatment 57(33), 15362-15372.

Lakshmipathy, R., Vinod, A. and Sarada, N. (2013) Watermelon rind as biosorbent for removal of Cd^{2+} from aqueous solution: FTIR, EDX and kinetic studies. Journal of the Indian Chemical Society 90 (8), 1147-1154.

Lalhmunsiama, Gupta, P.L., Jung, H., Tiwari, D., Kong, S.H. and Lee, S.M. (2017) Insight into the mechanism of Cd(II) and Pb(II) removal by sustainable

magnetic biosorbent precursor to Chlorella vulgaris. Journal of the Taiwan Institute of Chemical Engineers 71, 206-213.

Lam, Y.Y. (2015) Utilization of fruit waste materials for Cr(III) biosorption and fungal biomass for As(V) biosorption, The Hong Kong Polytechnic University.

Landaburu-Aguirre, J., Pongracz, E., Peramaki, P. and Keiski, R.L. (2010) Micellar-enhanced ultrafiltration for the removal of cadmium and zinc: Use of response surface methodology to improve understanding of process performance and optimisation. Journal of Hazardous Materials 180(1-3), 524-534.

Langmuir, I. (1918) The adsorption of gases on plane surfaces of glass, mica and platinum. Journal of the American Chemical society 40(9), 1361-1403.

Le Brech, Y., Raya, J., Delmotte, L., Brosse, N., Gadiou, R. and Dufour, A. (2016) Characterization of biomass char formation investigated by advanced solid state NMR. Carbon 108, 165-177.

Le Troedec, M., Sedan, D., Peyratout, C., Bonnet, J.P., Smith, A., Guinebretiere, R., Gloaguen, V. and Krausz, P. (2008) Influence of various chemical treatments on the composition and structure of hemp fibres. Composites Part a-Applied Science and Manufacturing 39(3), 514-522.

Lee, M.Y., Park, J.M. and Yang, J.W. (1997) Micro precipitation of lead on the surface of crab shell particles. Process Biochemistry 32(8), 671-677.

Leng, L., Wang, J., Qiu, X.X., Zhao, Y.X., Yip, Y.W., Law, G.L., Shih, K., Zhou, Z.Y. and Lee, P.H. (2016) Thermodynamic selectivity of functional agents on zeolite for sodium dodecyl sulfate sequestration. Journal of Hazardous Materials 318, 41-47.

Leusch, A. and Volesky, B. (1995) The influence of film diffusion on cadmium biosorption by marine biomass. Journal of Biotechnology 43(1), 1-10.

Li, X.H., Xu, H.X., Gao, B., Shi, X.Q., Sun, Y.Y. and Wu, J.C. (2018) Efficient biosorption of Pb(II) from aqueous solutions by a PAH-degrading strain Herbaspirillum chlorophenolicum FA1. Journal of Industrial and Engineering Chemistry 57, 64-71.

Li, Y.G., Chen, B.L. and Zhu, L.Z. (2010) Enhanced sorption of polycyclic aromatic hydrocarbons from aqueous solution by modified pine bark. Bioresource Technology 101(19), 7307-7313.

Li, Z.Y., Ma, Z.W., van der Kuijp, T.J., Yuan, Z.W. and Huang, L. (2014) A review of soil heavy metal pollution from mines in China: Pollution and health risk assessment. Science of the Total Environment 468, 843-853.

Liang, S., Guo, X.Y., Feng, N.C. and Tian, Q.H. (2010) Effective removal of heavy metals from aqueous solutions by orange peel xanthate. Transactions of Nonferrous Metals Society of China 20, S187-S191.

Lim, S.F., Zheng, Y.M., Zou, S.W. and Chen, J.P. (2008) Characterization of copper adsorption onto an alginate encapsulated magnetic sorbent by a combined FT-IR, XPS and mathematical modeling study. Environmental Science & Technology 42(7), 2551-2556.

Liu, C., Ngo, H.H. and Guo, W. (2012a) Watermelon rind: Agro-waste or superior biosorbent? Applied biochemistry and biotechnology 167(6), 1699-1715.

Liu, C., Ngo, H.H., Guo, W.S. and Tung, K.L. (2012b) Optimal conditions for preparation of banana peels, sugarcane bagasse and watermelon rind in removing copper from water. Bioresource Technology 119, 349-354.

Liu, Y. and Liu, Y.J. (2008) Biosorption isotherms, kinetics and thermodynamics. Separation and Purification Technology 61(3), 229-242.

Loganathan, P., Vigneswaran, S., Kandasamy, J. and Bolan, N.S. (2014) Removal and recovery of phosphate from water using sorption. Critical Reviews in Environmental Science and Technology 44(8), 847-907.

Long, Y., Lei, D., Ni, J., Ren, Z., Chen, C. and Xu, H. (2014) Packed bed column studies on lead(II) removal from industrial wastewater by modified Agaricus bisporus. Bioresource Technology 152, 457-463.

Lopez-Garcia, M., Lodeiro, P., Herrero, R., Barriada, J.L., Rey-Castro, C., David, C. and de Vicente, M.E.S. (2013) Experimental evidences for a new model in the description of the adsorption-coupled reduction of Cr(VI) by protonated banana skin. Bioresource Technology 139, 181-189.

Lopicic, Z.R., Stojanovic, M.D., Radoicic, T.S.K., Milojkovic, J.V., Petrovic, M.S., Mihajlovic, M.L. and Kijevcanin, M.L.J. (2017) Optimization of the process of Cu(II) sorption by mechanically treated Prunus persica L. - Contribution to sustainability in food processing industry. Journal of Cleaner Production 156, 95-105.

Love, G.D., Snape, C.E., Jarvis, M.C. and Morrison, I.M. (1994) Determination of phenolics structures in flax fiber by solid-state ^{13}C NMR. Phytochemistry 35(2), 489-491.

Lv, J., Luo, L., Zhang, J., Christie, P. and Zhang, S. (2012) Adsorption of mercury on lignin: Combined surface complexation modeling and X-ray absorption spectroscopy studies. Environmental Pollution 162, 255-261.

Mahamadi, C. and Nharingo, T. (2010) Competitive adsorption of Pb^{2+}, Cd^{2+} and Zn^{2+} ions onto Eichhornia crassipes in binary and ternary systems. Bioresource Technology 101(3), 859-864.

Maisuthisakul, P. and Gordon, M.H. (2009) Antioxidant and tyrosinase inhibitory activity of mango seed kernel by product. Food Chemistry 117(2), 332-341.

Mallampati, R., Li, X., Adin, A. and Vaiyaveettil, S. (2015) Fruit peels as efficient renewable adsorbents for removal of dissolved heavy metals and dyes from water. ACS Sustainable Chemistry & Engineering 3(6), 1117-1124.

Maresova, J., Pipiska, M., Rozloznik, M., Hornik, M., Remenarova, L. and Augustin, J. (2011) Cobalt and strontium sorption by moss biosorbent: Modeling of single and binary metal systems. Desalination 266(1-3), 134-141.

Martin-Lara, M.A., Blazquez, G., Ronda, A., Rodriguez, I.L. and Calero, M. (2012) Multiple biosorption-desorption cycles in a fixed-bed column for Pb(II) removal by acid-treated olive stone. Journal of Industrial and Engineering Chemistry 18(3), 1006-1012.

McKay, G. (1984) The adsorption of basic dye onto silica from aqueous solution-solid diffusion model. Chemical Engineering Science 39(1), 129-138.

Meireles, C.D., Rodrigues, G., Ferreira, M.F., Cerqueira, D.A., Assuncao, R.M.N., Ribeiro, E.A.M., Poletto, P. and Zeni, M. (2010) Characterization of asymmetric membranes of cellulose acetate from biomass: Newspaper and mango seed. Carbohydrate Polymers 80(3), 954-961.

Memon, J.R., Memon, S.Q., Bhanger, M.I., Memon, G.Z., El-Turki, A. and Allen, G.C. (2008) Characterization of banana peel by scanning electron microscopy and FT-IR spectroscopy and its use for cadmium removal. Colloids and Surfaces B-Biointerfaces 66(2), 260-265.

Mende, M., Schwarz, D., Steinbach, C., Boldt, R. and Schwarz, S. (2016) Simultaneous adsorption of heavy metal ions and anions from aqueous solutions on chitosan Investigated by spectrophotometry and SEM-EDX analysis. Colloids and Surfaces A: Physicochemical and Engineering Aspects 510, 275-282.

Michalak, I., Chojnacka, K. and Witek-Krowiak, A. (2013) State of the art for the biosorption process-a review. Applied Biochemistry and Biotechnology 170(6), 1389-1416.

Millan-Testa, C.E., Mendez-Montealvo, M.G., Ottenhof, M.A., Farhat, I.A. and Bello-Perez, L.A. (2005) Determination of the molecular and structural characteristics of Okenia, Mango, and banana starches. Journal of Agricultural and Food Chemistry 53(3), 495-501.

Moubarik, A. and Grimi, N. (2015) Valorization of olive stone and sugar cane bagasse by-products as biosorbents for the removal of cadmium from aqueous solution. Food Research International 73, 169-175.

Moulder, J.F., Stickle, W.F., Sobol, P.E. and Bombe, K., D. (1992) Handbook of X-ray Photoelectron Spectroscopy: A Reference Book of Standard Spectra for Identification and Interpretation of XPS Data. Physical Electronics Division, Perkin-Elmer Corporation, Eden Prairie, MN.

Moyo, M., Pakade, V.E. and Modise, S.J. (2017) Biosorption of lead(II) by chemically modified Mangifera indica seed shells: Adsorbent preparation, characterization and performance assessment. Process Safety and Environmental Protection 111, 40-51.

Muralidhar, R.V., Chirumamila, R.R., Marchant, R. and Nigam, P. (2001) A response surface approach for the comparison of lipase production by Candida cylindracea using two different carbon sources. Biochemical Engineering Journal 9(1), 17-23.

Nadeem, R., Manzoor, Q., Iqbal, M. and Nisar, J. (2016) Biosorption of Pb(II) onto immobilized and native Mangifera indica waste biomass. Journal of Industrial and Engineering Chemistry 35, 185-194.

Nguyen, T.A.H., Ngo, H.H., Guo, W.S., Zhang, J., Liang, S., Yue, Q.Y., Li, Q. and Nguyen, T.V. (2013) Applicability of agricultural waste and by-products for adsorptive removal of heavy metals from wastewater. Bioresource Technology 148, 574-585.

Njikam, E. and Schiewer, S. (2012) Optimization and kinetic modeling of cadmium desorption from citrus peels: A process for biosorbent regeneration. Journal of Hazardous Materials 213, 242-248.

Ofomaja, A.E. (2010) Intraparticle diffusion process for lead(II) biosorption onto mansonia wood sawdust. Bioresource Technology 101(15), 5868-5876.

Ogi, T., Makino, T., Iskandar, F., Tanabe, E. and Okuyama, K. (2016) Heat-treated Escherichia coli as a high-capacity biosorbent for tungsten anions. Bioresource Technology 218, 140-145.

Ok, Y.S., Kim, S.C., Kim, D.K., Skousen, J.G., Lee, J.S., Cheong, Y.W., Kim, S.J. and Yang, J.E. (2011) Ameliorants to immobilize Cd in rice paddy soils contaminated by abandoned metal mines in Korea. Environmental Geochemistry and Health 33, 23-30.

Oliveira, R.C., Hammer, P., Guibal, E., Taulemesse, J.-M. and Garcia, O., Jr. (2014) Characterization of metal-biomass interactions in the lanthanum(III) biosorption on Sargassum sp using SEM/EDX, FTIR, and XPS: Preliminary studies. Chemical Engineering Journal 239, 381-391.

Oztekin, Y. and Yazicigil, Z. (2006) Recovery of metals from complexed solutions by electrodeposition. Desalination 190(1-3), 79-88.

Özverdi, A. and Erdem, M. (2006) Cu^{2+}, Cd^{2+} and Pb^{2+} adsorption from aqueous solutions by pyrite and synthetic iron sulphide. Journal of Hazardous Materials 137(1), 626-632.

Padmavathy, V. (2008) Biosorption of nickel(II) ions by baker's yeast: Kinetic, thermodynamic and desorption studies. Bioresource Technology 99(8), 3100-3109.

Panda, G.C., Das, S.K., Chatterjee, S., Maity, P.B., Bandopadhyay, T.S. and Guha, A.K. (2006) Adsorption of cadmium on husk of Lathyrus sativus: Physico-chemical study. Colloids and Surfaces B-Biointerfaces 50(1), 49-54.

Papadopoulos, A., Fatta, D., Parperis, K., Mentzis, A., Haralambous, K.J. and Loizidou, M. (2004) Nickel uptake from a wastewater stream produced in a metal finishing industry by combination of ion-exchange and precipitation methods. Separation and Purification Technology 39(3), 181-188.

Papageorgiou, S.K., Katsaros, F.K., Kouvelos, E.P., Nolan, J.W., Le Deit, H. and Kanellopoulos, N.K. (2006) Heavy metal sorption by calcium alginate beads from Laminaria digitata. Journal of Hazardous Materials 137(3), 1765-1772.

Park, D., Lim, S.R., Yun, Y.S. and Park, J.M. (2008) Development of a new Cr(VI)-biosorbent from agricultural biowaste. Bioresource Technology 99(18), 8810-8818.

Pavan, F.A., Lima, I.S., Lima, E.C., Airoldi, C. and Gushikem, Y. (2006) Use of Ponkan mandarin peels as biosorbent for toxic metals uptake from aqueous solutions. Journal of Hazardous Materials 137(1), 527-533.

Pavan, F.A., Mazzocato, A.C., Jacques, R.A. and Dias, S.L.P. (2008) Ponkan peel: A potential biosorbent for removal of Pb(II) ions from aqueous solution. Biochemical Engineering Journal 40(2), 357-362.

Pavia, D.L., Lampman, G.M., Kriz, G.S. and Vyvyan, J.A. (2008) Introduction to spectroscopy, Cengage Learning.

Pearson, R.G. (1963) Hard and soft acids and bases. Journal of the American Chemical Society 85(22), 3533-3539.

Pehlivan, E. and Kahraman, H.T. (2012) Hexavalent chromium removal by Osage Orange. Food Chemistry 133(4), 1478-1484.

Perez Marin, A.B., Isabel Aguilar, M., Francisco Ortuno, J., Francisco Meseguer, V., Saez, J. and Llorens, A. (2010a) Biosorption of Zn(II) by orange waste in batch and packed-bed systems. Journal of Chemical Technology and Biotechnology 85(10), 1310-1318.

Perez Marin, A.B., Ortuno, J.F., Aguilar, M.I., Meseguer, V.F., Saez, J. and Llorens, M. (2010b) Use of chemical modification to determine the binding of Cd(II),

Zn(II) and Cr(III) ions by orange waste. Biochemical Engineering Journal 53(1), 2-6.

Pozdniakova, T.A., Mazur, L.P., Boaventura, R.A.R. and Vilar, V.J.P. (2016) Brown macro-algae as natural cation exchangers for the treatment of zinc containing wastewaters generated in the galvanizing process. Journal of Cleaner Production 119, 38-49.

Pugazhendhi, A., Boovaragamoorthy, G.M., Ranganathan, K., Naushad, M. and Kaliannan, T. (2018) New insight into effective biosorption of lead from aqueous solution using Ralstonia solanacearum: Characterization and mechanism studies. Journal of Cleaner Production 174, 1234-1239.

Qu, X., Alvarez, P.J. and Li, Q. (2013) Applications of nanotechnology in water and wastewater treatment. Water Research 47(12), 3931-3946.

Ramrakhiani, L., Halder, A., Majumder, A., Mandal, A.K., Majumdar, S. and Ghosh, S. (2017) Industrial waste derived biosorbent for toxic metal remediation: Mechanism studies and spent biosorbent management. Chemical Engineering Journal 308, 1048-1064.

Rao, R.A.K. and Ikram, S. (2011) Sorption studies of Cu(II) on gooseberry fruit (emblica officinalis) and its removal from electroplating wastewater. Desalination 277(1-3), 390-398.

Reddy, D.H.K., Ramana, D., Seshaiah, K. and Reddy, A. (2011) Biosorption of Ni(II) from aqueous phase by Moringa oleifera bark, a low cost biosorbent. Desalination 268(1-3), 150-157.

Reddy, N.A., Lakshmipathy, R. and Sarada, N. (2014) Application of Citrullus lanatus rind as biosorbent for removal of trivalent chromium from aqueous solution. Alexandria Engineering Journal 53(4), 969-975.

Redlich, O. and Peterson, D.L. (1959) A useful adsorption isotherm. Journal of Physical Chemistry 63(6), 1024-1024.

Remenarova, L., Pipiska, M., Hornik, M., Rozloznik, M., Augustin, J. and Lesny, J. (2012) Biosorption of cadmium and zinc by activated sludge from single and binary solutions: Mechanism, equilibrium and experimental design study. Journal of the Taiwan Institute of Chemical Engineers 43(3), 433-443.

Ren, Z.F., Xu, X., Wang, X., Gao, B.Y., Yue, Q.Y., Song, W., Zhang, L. and Wang, H.T. (2016) FTIR, Raman, and XPS analysis during phosphate, nitrate and Cr(VI) removal by amine cross-linking biosorbent. Journal of Colloid and Interface Science 468, 313-323.

Rimando, A.M. and Perkins-Veazie, P.M. (2005) Determination of citrulline in watermelon rind. Journal of Chromatography A 1078(1-2), 196-200.

RoHS3 (2015) Restriction of Hazardous Substances, Directive 2015/863. Union, E. (ed).

Ruthven, D.M. (1984) Principles of Adsorption and Adsorption Processes. New York: John Wiley & Sons.

Saeed, A., Sharif, M. and Iqbal, M. (2010) Application potential of grapefruit peel as dye sorbent: Kinetics, equilibrium and mechanism of crystal violet adsorption. Journal of Hazardous Materials 179(1-3), 564-572.

Saleem, N. and Bhatti, H.N. (2011) Adsorptive removal and recovery of U(VI) by citrus waste biomass. Bioresources 6(3), 2522-2538.

Sandhu, K.S. and Lim, S.T. (2008) Structural characteristics and in vitro digestibility of mango kernel starches (Mangifera indica L.). Food Chemistry 107(1), 92-97.

Sari, A. and Tuzen, M. (2008) Biosorption of Pb(II) and Cd(II) from aqueous solution using green alga (Ulva lactuca) biomass. Journal of Hazardous Materials 152(1), 302-308.

Schiewer, S. and Balaria, A. (2009) Biosorption of Pb^{2+} by original and protonated citrus peels: Equilibrium, kinetics, and mechanism. Chemical Engineering Journal 146(2), 211-219.

Schiewer, S. and Iqbal, M. (2010) The role of pectin in Cd binding by orange peel biosorbents: A comparison of peels, depectinated peels and pectic acid. Journal of Hazardous Materials 177(1-3), 899-907.

Schiewer, S. and Iqbal, M. (2014) Physicochemical characterization and mechanism analysis of native and protonated grapefruit peels adsorbing cadmium. Desalination and Water Treatment 52(31-33), 5900-5911.

Schiewer, S. and Patil, S.B. (2008) Pectin-rich fruit wastes as biosorbents for heavy metal removal: Equilibrium and kinetics. Bioresource Technology 99(6), 1896-1903.

Shen, Y.S., Wang, S.L., Huang, S.T., Tzou, Y.M. and Huang, J.H. (2010) Biosorption of Cr(VI) by coconut coir: Spectroscopic investigation on the reaction mechanism of Cr(VI) with lignocellulosic material. Journal of Hazardous Materials 179(1-3), 160-165.

Sheng, P.X., Ting, Y.P., Chen, J.P. and Hong, L. (2004) Sorption of lead, copper, cadmium, zinc, and nickel by marine algal biomass: characterization of biosorptive capacity and investigation of mechanisms. Journal of Colloid and Interface Science 275(1), 131-141.

Simpson, A.J., McNally, D.J. and Simpson, M.J. (2011) NMR spectroscopy in environmental research: From molecular interactions to global processes. Progress in Nuclear Magnetic Resonance Spectroscopy 58(3-4), 97-175.

Singh, R., Kumar, J. and Nandpuri, K. (1975) A Study on the influence of the structural chemical constituents of the skin of water melon (Citrullus Lanatus Sch.) fruit on the incidence of its blossom-end-rot and cracking. Indian Journal of Horticulture 32, 98-101.

Singh, S. and Shukla, S.R. (2017) Theoretical studies on adsorption of Ni(II) from aqueous solution using Citrus limetta peels. Environmental Progress & Sustainable Energy 36(3), 864-872.

Singha, A.S. and Guleria, A. (2014) Chemical modification of cellulosic biopolymer and its use in removal of heavy metal ions from wastewater. International Journal of Biological Macromolecules 67, 409-417.

Sionkowska, A., Kaczmarek, B. and Lewandowska, K. (2014) Modification of collagen and chitosan mixtures by the addition of tannic acid. Journal of Molecular Liquids 199, 318-323.

Sips, R. (1948) On the structure of a catalyst surface. The Journal of Chemical Physics 16(5), 490-495.

Sivasankara, V., Ramachandramoorthy, T. and Chandramohan, A. (2010) Fluoride removal from water using activated and MnO_2-coated Tamarind Fruit (Tamarindus indica) shell: Batch and column studies. Journal of Hazardous Materials 177(1-3), 719-729.

Sostaric, T.D., Petrovic, M.S., Pastor, F.T., Loncarevic, D.R., Petrovic, J.T., Milojkovic, J.V. and Stojanovic, M.D. (2018) Study of heavy metals biosorption on native and alkali-treated apricot shells and its application in wastewater treatment. Journal of Molecular Liquids 259, 340-349.

Stirk, W.A. and van Staden, J. (2002) Desorption of cadmium and the reuse of brown seaweed derived products as biosorbents. Botanica Marina 45(1), 9-16.

Stokes, D. (2008) Principles and Practice of Variable Pressure: Environmental Scanning Electron Microscopy (VP-ESEM). Chichester, UK: John Wiley & Sons.

Tarley, C.R.T. and Arruda, M.A.Z. (2004) Biosorption of heavy metals using rice milling by-products. Characterisation and application for removal of metals from aqueous effluents. Chemosphere 54(7), 987-995.

Taty-Costodes, V.C., Fauduet, H., Porte, C. and Delacroix, A. (2003) Removal of Cd(II) and Pb(II) ions, from aqueous solutions, by adsorption onto sawdust of Pinus sylvestris. Journal of Hazardous Materials 105(1-3), 121-142.

Thomas, H.C. (1948) Chromatography: a problem in kinetics. Annals of the New York Academy of Sciences 49(2), 161-182.

Tian, Y., Wu, M., Lin, X.B., Huang, P. and Huang, Y. (2011) Synthesis of magnetic wheat straw for arsenic adsorption. Journal of Hazardous Materials 193, 10-16.

Torab-Mostaedi, M. (2013) Biosorption of lanthanum and cerium from aqueous solutions using tangerine (Citrus reticulata) peel: Equilibrium, kinetic and thermodynamic studies. Chemical Industry and Chemical Engineering Quarterly 19(1), 79-88.

Tran, V.S., Ngo, H.H., Guo, W.S., Zhang, J., Liang, S., Ton-That, C. and Zhang, X.B. (2015) Typical low cost biosorbents for adsorptive removal of specific organic pollutants from water. Bioresource Technology 182, 353-363.

Tsezos, M. and Volesky, B. (1981) Biosorption of uranium and thorium. Biotechnology and Bioengineering 23(3), 583-604.

Tsezos, M. and Volesky, B. (1982) The mechanism of uranium biosorption by rhizopus-arrhizus. Biotechnology and Bioengineering 24(2), 385-401.

Ucun, H., Bayhan, Y.K., Kaya, Y., Cakici, A. and Algur, O.F. (2002) Biosorption of chromium(VI) from aqueous solution by cone biomass of Pinus sylvestris. Bioresource Technology 85(2), 155-158.

Unuabonah, E.I., Adebowale, K.O., Olu-Owolabi, B.I., Yang, L.Z. and Kong, L.X. (2008) Adsorption of Pb(II) and Cd(II) from aqueous solutions onto sodium tetraborate-modified Kaolinite clay: Equilibrium and thermodynamic studies. Hydrometallurgy 93(1-2), 1-9.

USDA (2004) National Nutrient Database for Standard Reference.

Vafajoo, L., Cheraghi, R., Dabbagh, R. and McKay, G. (2018) Removal of cobalt (II) ions from aqueous solutions utilizing the pre-treated 2-Hypnea Valentiae algae: Equilibrium, thermodynamic, and dynamic studies. Chemical Engineering Journal 331, 39-47.

Vasanth Kumar, K. (2006) Comparative analysis of linear and non-linear method of estimating the sorption isotherm parameters for malachite green onto activated carbon. Journal of Hazardous Materials 136(2), 197-202.

Vigneswaran, S., Ngo, H.H., Chaudhary, D.S. and Hung, Y.T. (2005) Physicochemical treatment processes for water reuse. In Physicochemical Treatment Processes (pp. 635-676). Totowa, NJ: Humana Press.

Volesky, B. (1990) Biosorption of Heavy Metals. Boca Raton, Fla.: CRC Press.

Volesky, B. (1994) Advances in biosorption of metals: Selection of biomass types. FEMS Microbiology Reviews 14(4), 291-302.

Volesky, B. (2001) Detoxification of metal-bearing effluents: biosorption for the next century. Hydrometallurgy 59(2-3), 203-216.

Volesky, B. (2003) Sorption and Biosorption. BV Sorbex, Inc.

Wang, T., Liu, W., Xiong, L., Xu, N. and Ni, J.R. (2013) Influence of pH, ionic strength and humic acid on competitive adsorption of Pb(II), Cd(II) and Cr(III) onto titanate nanotubes. Chemical Engineering Journal 215, 366-374.

Wang, T., Park, Y.B., Cosgrove, D.J. and Hong, M. (2015) Cellulose-pectin spatial contacts are inherent to never-dried arabidopsis primary cell walls: Evidence from solid-state nuclear magnetic resonance. Plant Physiology 168(3), 871-884.

Wang, T., Zabotina, O. and Hong, M. (2012) Pectin-cellulose interactions in the arabidopsis primary cell wall from two-dimensional magic-angle-spinning solid-state nuclear magnetic resonance. Biochemistry 51(49), 9846-9856.

Wawer, I., Wolniak, M. and Paradowska, K. (2006) Solid state NMR study of dietary fiber powders from aronia, bilberry, black currant and apple. Solid State Nuclear Magnetic Resonance 30(2), 106-113.

Weber, W.J. and Morris, J.C. (1963) Kinetics of adsorption on carbon from solution. Journal of the Sanitary Engineering Division 89(2), 31-60.

Wei, D., Ngo, H.H., Guo, W.S., Xu, W.Y., Du, B., Khan, M.S. and Wei, Q. (2018) Biosorption performance evaluation of heavy metal onto aerobic granular sludge-derived biochar in the presence of effluent organic matter via batch and fluorescence approaches. Bioresource Technology 249, 410-416.

WHO (2010) Exposure to lead: A major public health concern, World Health Organization, Geneva.

WHO (2011a) Cadmium in drinking-water. Background document for preparation of WHO Guidelines for drinking-water quality, World Health Organization, Geneva.

WHO (2011b) Guidelines for drinking water quality, World Health Organization, Geneva.

WHO (2011c) Lead in drinking water. World Health Organization, Geneva.

Widsten, P., Cruz, C.D., Fletcher, G.C., Pajak, M.A. and McGhie, T.K. (2014) Tannins and extracts of fruit byproducts: antibacterial activity against foodborne bacteria and antioxidant capacity. Journal of Agricultural and Food Chemistry 62(46), 11146-11156.

Wu, F.C., Tseng, R.L. and Juang, R.S. (2009) Initial behavior of intraparticle diffusion model used in the description of adsorption kinetics. Chemical Engineering Journal 153(1-3), 1-8.

Wulfsberg, G. (2000) Inorganic Chemistry. Sausalito, Calif.: University Science Books, USA.

Xie, M., Lee, J., Nghiem, L.D. and Elimelech, M. (2015) Role of pressure in organic fouling in forward osmosis and reverse osmosis. Journal of Membrane Science 493, 748-754.

Yan, G., Viraraghavan, T. and Chen, M. (2001) A new model for heavy metal removal in a biosorption column. Adsorption Science & Technology 19(1), 25-43.

Yang, K.B., Peng, J.H., Srinivasakannan, C., Zhang, L.B., Xia, H.Y. and Duan, X.H. (2010) Preparation of high surface area activated carbon from coconut shells using microwave heating. Bioresource Technology 101(15), 6163-6169.

Yuan, X.Z., Meng, Y.T., Zeng, G.M., Fang, Y.Y. and Shi, J.G. (2008) Evaluation of tea-derived biosurfactant on removing heavy metal ions from dilute wastewater by ion flotation. Colloids and Surfaces A-Physicochemical and Engineering Aspects 317(1-3), 256-261.

Yuvaraja, G., Krishnaiah, N., Subbaiah, M.V. and Krishnaiah, A. (2014) Biosorption of Pb(II) from aqueous solution by Solanum melongena leaf powder as a low-cost biosorbent prepared from agricultural waste. Colloids and Surfaces B-Biointerfaces 114, 75-81.

Zein, R., Suhaili, R., Earnestly, F., Indrawati and Munaf, E. (2010) Removal of Pb(II), Cd(II) and Co(II) from aqueous solution using Garcinia mangostana L. fruit shell. Journal of Hazardous Materials 181(1-3), 52-56.

Zhang, D.N., Duan, D.D., Huang, Y.D., Yang, Y. and Ran, Y. (2016) Novel phenanthrene sorption mechanism by two pollens and their fractions. Environmental Science & Technology 50(14), 7305-7314.

Zheng, J.C., Liu, H.Q., Feng, H.M., Li, W.W., Lam, M.H.W., Lam, P.K.S. and Yu, H.Q. (2016) Competitive sorption of heavy metals by water hyacinth roots. Environmental Pollution 219, 837-845.

Zhou, D., Zhang, L. and Guo, S.L. (2005) Mechanisms of lead biosorption on cellulose/chitin beads. Water Research 39(16), 3755-3762.